Modulation of tight junction composition by the ERK pathway

Bryant, Christopher

Award date:
2015

Awarding institution:
University of Bath

Modulation of tight junction composition by the ERK pathway

Christopher Bryant

A thesis submitted for the degree of Doctor of Philosophy

University of Bath

Department of Biology and Biochemistry

March 2015

Acknowledgments

I would like to thank my supervisors Dr. Jim Caunt, Dr. Andrew Chalmers and Dr. Paul Whitley for their continual patience and support throughout my PhD. I could not have hoped for a more supportive and friendly environment in which to work.

I would also like to thank the University of Bath, the Biotechnology and Biological Sciences Research Council (BBSRC) and Cancer Research at Bath (CR@B) for funding this project. Special thanks are for Adrian Rogers of the University of Bath Microscopy and Analysis Suite and Val Millar of GE Healthcare for their expertise in microscopy and technical assistance regarding image acquisition and data analysis.

Thanks also go to project students who have contributed to this thesis, and in particular Heather Reay, who generated several adenoviral constructs. I would also like thank all present and past members of the Caunt, Chalmers, Whitley, Williams, Wood and Licchesi laboratories who have made my PhD a memorable and enjoyable experience.

I would finally like to thank my friends and family who have supported me throughout my PhD.

Abstract

Epithelia are an essential organising feature of multicellular organisms and the selective permeability of these barriers is regulated by the junctional repertoire of tight junction proteins. The regulation of epithelial permeability is essential for the physiological function of various organs and is often pathologically deregulated, for example in inflammatory disease and cancer. Tight junctions are dynamically regulated in response to diverse stimuli through multiple signalling pathways. The RAF/MEK/ERK pathway has been reported to mediate junctional remodelling in response to various growth factors and hormones, although the unique contribution of this pathway and the mechanisms of reorganisation remain unclear**.** To address this, specific activation of the RAF/MEK/ERK pathway was achieved through the expression of $BRAF^{WT}$ or oncogenic $BRAF^{V600E}$ in Madin-Darby Canine Kidney (MDCK) II cells, a model epithelial cell line used to study tight junctions.

Specific activation of the RAF/MEK/ERK pathway generated a transient increase in transepithelial resistance, which occurred concurrently with the differential regulation of tight junction protein expression levels and subcellular distribution. Claudin-2 protein levels were decreased, while junctional levels of claudin-4 were increased. Total levels of claudin-1, occludin and ZO-1 were unchanged and were retained at areas of cell contact although showing varying degrees of cytoplasmic accumulation.

Conditionally active CRAF:ER fusion proteins were expressed to provide increased control of RAF/MEK/ERK signal duration and to study the rates of TJ protein synthesis, degradation and localisation. RAF-mediated downregulation of *CLDN2* mRNA caused subsequent claudin-2 protein depletion without influencing rates of internalisation or degradation. In contrast, RAF activation caused the redistribution of claudin-1 and -4 from the lateral membrane to the apical junction. This junctional accumulation could not be attributed to changes in claudin protein levels, stability or endocytic trafficking. Taken together, these data reveal surprising diversity in RAF/MEK/ERK-mediated TJ control, where distinct combinations of claudin-specific regulatory mechanisms act in concert to regulate epithelial permeability.

Abbreviations

16-HBE	Epithelial cells of the human bronchiole
4HT	4-hydroxytamoxifen
94D	Renal epithelial cells of the mouse collecting duct
Ad	Adenovirus
AJ	Adherens junction
AMPS	Ammonium persulphate
AP-1	Activator protein 1
aPKC	Atypical protein kinase C
APMSF	4-amidinophenylmethanesulphonyl fluoride hydrochloride
APT	Acyl-protein thioesterase
ATP	Adenosine-5'-triphosphate
BCA	Bicinchoninic acid
BSA	Bovine serum albumin
CA	Constitutively active
Caco-2	Human colon carcinoma cell line
CAR	Coxsackie adenovirus receptor
Cdx1/2	Caudal-related homeobox 1/2
CHMP3	Charged multivesicular body protein 3
CHX	Cycloheximide
CK2	Casein kinase 2
CNS	Central nervous system
CQ	Chloroquine
CREB	cAMP response element binding protein
DAPI	4', 6'-diamino-2-phenylindole
DBPS/CM	Phosphate-buffered saline supplemented with calcium and magnesium
ddH_2O	Double distilled water
DHHC PAT	His-Asp-Asp-Cys protein acyl-transferases
DMEM	Dulbecco's modified Eagle's medium
DMSO	Dimethyl sulphoxide
DN	Dominant negative
DNA	Deoxyribonucleic acid
DTT	Diothiothreitol
E box	Enhancer box
ECL	Enhanced chemiluminescence substrate
EDTA	Diaminoethanetetra-acetic acid disodium salt
EDTA	Ethylenediaminetetraacetic acid
EEA1	Early endosomal auto-antigen 1
EGF	Epidermal growth factor
EGFR	Epidermal growth factor receptor
ELF3	E74-like transcription factor 3
EMT	Epithelial-mesenchymal transition
EphA2	Ephrin type-A receptor 2
ER	Estrogen receptor
ERK	Extracellular signal-regulated kinase
ESCRT	Endosomal sorting complexes required for transport
FBS	Fetal bovine serum
FFEM	Freeze-fracture electron microscopy
FLIP	Fluorescence loss in photobleaching
FRAP	Fluorescence recovery after photobleaching
FYVE	(Domain found in) Fab1, YOTB, Vac1, EEA1
g	gram
GAP	GTPase-activating protein

GATA-4	GATA-motif recognising transcription factor 4
GDP	Guanosine diphosphate
GEF	Guanine exchange factor
GFP	Green fluorescent protein
GJ	Gap junction
GTP	Guanosine-5'- triphosphate
GUK	Guanylate kinase domain
HBSS	Hank's buffered salt solution
HECT	Homologous to the E6AP carboxyl terminus protein domain
HEPES	4-(2-hydroxyethyl)-1-piperazineethanesulphonic acid
HGF	Hepatocyte growth factor
HNF-1α	Hepatocyte nuclear factor 1 alpha
hr	Hour
HRAS	Harvey rat sarcoma GTPase
HRP	Horseradish peroxidase
IF	Immunofluorescence
IFNɣ	Interferon gamma
JAK	Janus kinase
JAM	Junction adhesion molecule
JNK	c-Jun N-terminal kinase
JRAB/MICAL-L2	Junctional Rab13-binding protein/molecules interacting with CasL-like 2
kb	Kilobase
kDa	Kilodaltons
KRAS	Kirsten rat sarcoma GTPase
LB	Lysogeny broth
LLC-PK1	Renal epithelial cells of the porcine proximal tubule
LNX1p80	Ligand-of-Numb splice variant
MAGUK	Membrane-associated guanylate kinase
MAPK	Mitogen-activated protein kinase
MARVEL	Mal and related proteins for vesicle trafficking and membrane link domain
MDCK	Madin-Darby canine kidney
MEIS	Homeodomain factor expressed in myeloid leukemia
MEK	MAPK/ERK kinase
MEKi	MEK inhibitor
MESNA	2-mercaptoethane sulphate
MET	Mesenchymal-epithelial transition
min	Minutes
MLCK	Myosin light chain kinase
MMP	Matrix metalloproteinase
MOKF	Mouse Krueppel-like factor
mRNA	Messenger ribonucleic acid
MTD-1A	Mouse mammary epithelial cell line
NGS	Normal goat serum
Par	Partitioning defective polarity protein
PBS	Phosphate-buffered saline
PCR	Polymerase chain reaction
PD	PD0325901, MEK inhibitor
PDZ	Post-synaptic density 95/Discs large/Zonula occludens 1 domain
PFA	Paraformaldehyde
PI3K	Phosphoinositide 3-kinase
PIK	Peptide inhibitor of myosin light chain kinase
PIKfyve	Phosphoinositide kinase, FYVE finger containing
PKA	Protein kinase A
PKC	Protein kinase C

RAF	Rapidly accelerated fibrosarcoma
RAS	Rat sarcoma GTPase
RCCD2	Rat cortical collecting duct cell line
RNA	Ribonucleic acid
RNAi	RNA interference
rpm	Revolutions per minute
RSK	Ribosomal S6 kinase
RTK	Receptor tyrosine kinase
RT-qPCR	Reverse transcription quantitative polymerase chain reaction
RUNX3	Runt-related transcription factor 3
SDS	Sodium dodecylsulphate
SDS-PAGE	Sodium dodecylsulphate polyacrylamide gel electrophoresis
SOC	Super optimal broth with catabolite repression
SH2	Src homology 2 domain
SH3	Src homology 3 domain
siRNA	Short interfering RNA
Src	Sarcoma GTPase
STAT3	Signal transducer and activator of transcription 3
SUMO	Small ubiquitin-like modifier
TALE	Three amino acid loop extension transcription factor
TALEN	Transcription activator-like effector nuclease
TAMP	Tight junction-associated MARVEL protein
TBE	Tris/Borate/EDTA buffer
TBS	Tris-buffered saline
TBS/CM	Tris-buffered saline supplemented with calcium and magnesium
TBS-T	Tris-buffered saline with Tween-20
TEMED	N,N,N',N-tetramethylethylenediamine
TER	Transepithelial electrical resistance
TfR	Transferrin receptor
TGFB	Transforming growth factor beta
TGN	*trans*-Golgi network
TJ	Tight junction
TNFα	Tumour necrosis factor alpha
Tween-20	Polyoxyethylene sorbitan monolaureate
UTR	Untranslated region
WNK	With no lysine kinase
WT	Wild-type
ZA	Zonula adherens
ZEB1	Zinc finger E-box binding homeobox 1
ZO	Zonula occludens

Table of contents

Table of figures

Table of tables

Chapter 1: Introduction

1.1 Epithelial structure

Epithelial cells form multicellular sheets, which compartmentalise the body by lining external and internal surfaces, cavities and organs. Epithelia are characterised by a highly polarised structure, with an apical plasma membrane that faces the central lumen, a lateral domain that contacts neighbouring cells and a basal membrane that interacts with the underlying extracellular matrix through focal adhesions (Figure 1.1). These membrane domains are distinct in terms of their lipid and protein composition and the maintenance of this polarised structure is essential for the directional transport of water, ions and other molecules across the monolayer.

Individual cells are connected by four junctional complexes; the tight junction (TJ) or *zonula occludens*, the Adherens junction (AJ) or *zonula adherens*, desmosomes or *macula adherens* and gap junctions (GJ), which succeed each other in an apical to basal direction along the lateral plasma membrane and have distinct biological functions (Figure 1.1). Gap junctions are composed of pannexins and connexins, which form intercellular pores that allow intercellular communication through the transfer of ions, secondary messengers and metabolites between cells (Meşe et al., 2007). The cadherin-based AJ and desmosomes form strong intercellular adhesions and provide structural integrity to the cell monolayer (Green et al., 2010). The TJ is a specialised structure that is generally confined to the apical-most tip of the lateral plasma membrane and defines the boundary between the apical and basolateral plasma membrane domains (Shin et al., 2006). The TJ plays a minor role in cell adhesion, but confers a number of properties that are essential for physiological epithelial function (Steed et al., 2010).

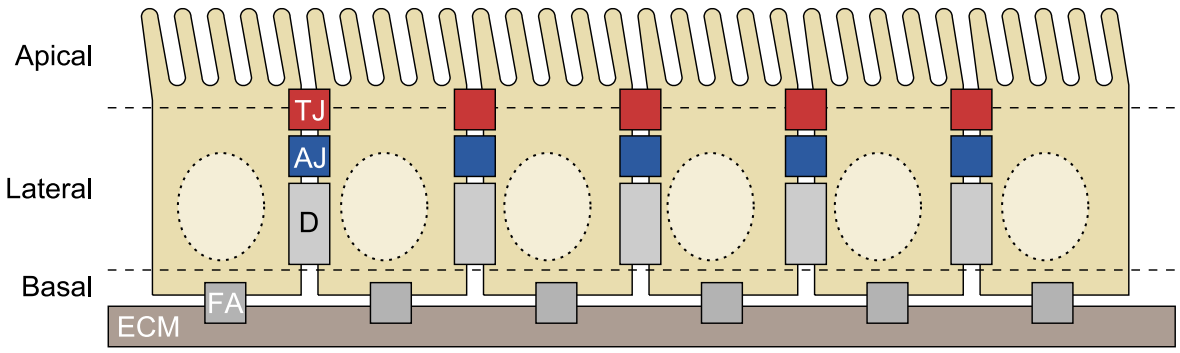

Figure 1.1: A schematic of cell-cell junctions present in an epithelial monolayer. Individual epithelial cells form multicellular sheets that line body organs and cavities. These epithelia are characterised by a highly polarised structure, with an apical membrane facing the central lumen, and a basolateral surface that interacts with neighbouring cells and underlying tissues. Cell-cell adhesion is primarily mediated through cadherin-based Adherens junctions (AJ) and desmosomes (D), while the monolayer is anchored to the extracellular matrix (ECM) through focal adhesions (FA). The tight junction (TJ) is confined to the apex of the lateral membrane and has a key role in regulating paracellular permeability, apicobasal polarity and intracellular signalling cascades.

The TJ initially appears as an area where the intercellular space becomes extremely narrow, and at higher magnifications as a series of “kissing points” where neighbouring plasma membranes appear to fuse (Figure 1.2A) (Farquhar and Palade, 1963). As epithelial cell membranes are relatively impermeable, solutes more readily traverse the epithelium by moving between, rather than through cells (Cereijido et al., 1983). The TJ regulates the permeability of this paracellular route by sealing the intercellular space, hence its designation as the “*zonula occludens”,* Latin for “closing belt”, with “tight junction” used as descriptive term for its structural features (Claude and Goodenough, 1973; Farquhar and Palade, 1963).

1.2 Functions of the tight junction

1.2.1 Paracellular permeability

Further characterisation of the TJ by freeze-fracture electron microscopy (FFEM) revealed that the TJ forms a complex meshwork of branching and anastomosing strands (Figure 1.2A) (Claude and Goodenough, 1973). The number of strands varies in TJs from different tissues and roughly correlates with the “tightness” of epithelial permeability (Claude and Goodenough, 1973). Highly permeable, or “leaky” epithelia, such as those in the proximal renal tubule, have a single TJ strand, whereas “tight” epithelia, like those found in the essentially leak-proof urinary bladder, consist of 5 or more TJ strands arranged in series (Claude and Goodenough, 1973). Conductance is not distributed evenly along each strand, suggesting that otherwise impermeable belts are studded with conducting channels (Figure 1.2A) (Cereijido et al., 1983).

The overall electrical resistance of the TJ is dependent on the probability of these channels being found in an open, rather than closed state, as well as the number of strands constituting the TJ, and is described by the equation, $R_T \propto {P_O}^{-n}$, where R_T is transepithelial resistance, P_O is the probability of a channel being open and n is the number of TJ strands (Figure 1.2B). As each TJ strand has numerous channels, there is a high probability that at least one channel is “open” at any given time, allowing current to flow. In this scenario, resistance increases in a linear fashion with increasing strand number (Figure 1.2C). However, experimental observations show that by doubling the strand number, resistance is actually increased four-fold (Cereijido et al., 1989). The frequent anastomoses between strands observed by FFEM act to segment these flickering ion channels and maintain the exponential relationship between strand number and overall resistance (Figure 1.2D) (Cereijido et al., 1989; Tsukita et al., 2001).

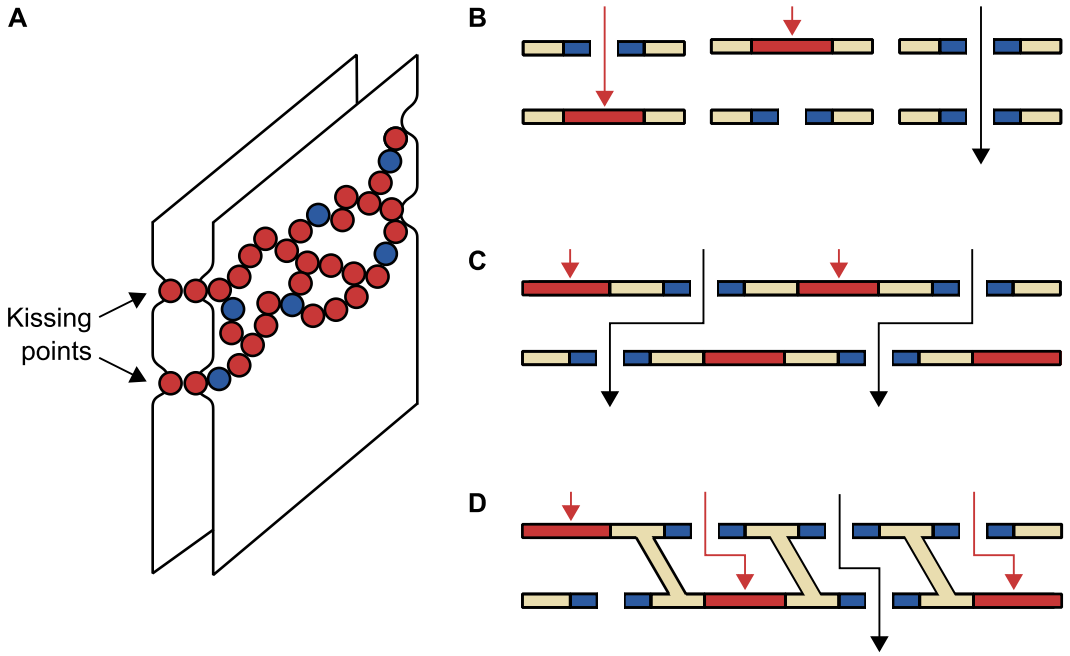

Figure 1.2: **The complex branched structure of the tight junction determines paracellular permeability.** (A) In cross-section, the TJ appears as a series of kissing points where neighbouring membranes are tightly apposed. *En face*, the TJ consists of multiple branching and anastomosing strands. These impermeable strands (red) seal the intercellular space and limit paracellular diffusion to dynamically opening and closing channels (blue). Paracellular permeability is determined by strand number and the probability of channels being in an open state. (B) To traverse the TJ, an ion must pass through multiple channels. In the case of single channels arranged in series, resistance increases linearly with strand number. (C) This relationship is maintained for multichannel strands arranged in parallel, as only a single channel needs to be open in each strand for ionic transport to proceed. (D) Segregation of ion channels by strand branching is required to model the exponential increase in epithelial electrical resistance observed with increasing strand number. Images adapted from Tsukita (2001).

Paracellular permeability, or “gate” function, is comprised of two complimentary pore and leak pathways (Figure 1.3A and B). The pore pathway is a high-capacity, charge and size-selective route and its specific properties are determined by the specific subset constituent claudin proteins that are expressed (Table 1.1) (Shen et al., 2011). Ionic permeability is mediated by the dynamic opening and closing of claudin-based pores within the TJ (Figure 1.3A) (Weber, 2012). In contrast, zonula occludens (ZO) and occludin proteins are the molecular determinants of leak pathway permeability, a low-capacity paracellular route that does not discriminate between solutes based on charge and allows the limited flux of larger molecules across the epithelium (Figure 1.3B and Table 1.1) (Shen et al., 2011). This paracellular leak is thought to be mediated by infrequent openings that are large enough to allow macromolecules to pass, but are rare enough in frequency to maintain the overall ion selectivity of the tissue (Weber, 2012). These “leak events” may be due to transient breaking and resealing of individual TJ strands, allowing the gradual movement of molecules through the multistrand structure (Figure 1.3B) (Sasaki et al., 2003). The relatively high

frequency of pore opening compared to leak events may explain the relative conductance of the two pathways (summarised in Table 1.1).

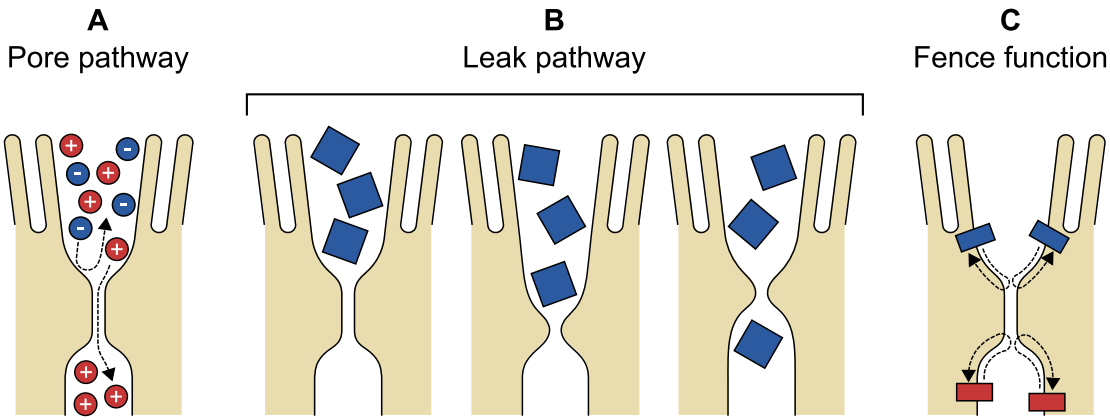

Figure 1.3: The TJ regulates paracellular permeability and membrane protein distribution. Paracellular permeability is comprised of distinct pore and leak pathways. (A) The pore pathway determines ionic conductance through charge- and size-selective claudin-based pores. (B) The leak pathway permits the passage of larger uncharged solutes and is thought to proceed via transient and infrequent breaking and resealing of the TJ, allowing solutes to gradually progress across the junction, while maintaining the overall ionic specificity of the tissue barrier. (C) The tight apposition of neighbouring membranes is also thought to prevent the free diffusion of membrane proteins and lipids between apical and basolateral plasma membrane domains, therefore contributing to the characteristic polarised structure of the epithelium.

Paracellular pathway	**Pore**	**Leak**
Charge-selective?	Yes	No
Size-selective?	Yes (radii less than ~4Å)	Yes - permeability is inversely correlated with increasing molecular weight
Capacity	High	Low
Molecular determinants	Claudins	Occludin, ZO-1
Techniques for measurement	Transepithelial resistance Dilution potential Bi-ionic substitution	Permeability to fluorescently tagged, radiolabelled or biotinylated carbohydrates or tracers of varying molecular weights

Table 1.1: Properties of paracellular pore and leak pathways. The claudin-based pore pathway allows rapid, bulk transport of ions in a charge- and size-selective manner. The leak pathway, regulated by occludin and ZO-1, permits the relatively slow passage of large solutes, independently of their charge. Information obtained from Shen (2011).

1.2.3 Apicobasal polarity

Epithelial cells are polarised into apical and basolateral membranes with distinct lipid and protein compositions (St Johnston and Ahringer, 2010). Several cues combine to initiate the formation of this polarised structure, with important signals generated by initial cell-cell and cell-matrix interactions (St Johnston and Ahringer, 2010). Mechanistically, epithelial polarisation is regulated by three main polarity complexes; the Crumbs complex (Crb1-3, PALS1, PATJ) is crucial for forming the apical domain and TJs, the Par3/Par6/aPKC complex establishes the boundary between apical and basolateral domains and the Scribble complex (Scribble, Lgl, Dlg) localises to the lateral membrane and excludes apical proteins from the basolateral domain (St Johnston and Ahringer, 2010). Mutual antagonism of these apical and basolateral determinants maintains the polarised distribution of target proteins within the cell (Shin et al., 2006; St Johnston and Ahringer, 2010). The evolutionarily conserved Crumbs and Par complexes localise to the apical junction and are important both for TJ formation and epithelial polarisation (Shin et al., 2006). The mechanism through which the Par3/Par6/aPKC complex mediates TJ assembly is poorly understood (Matter and Balda, 2003); aPKC appears to be dispensable for initial cell adhesion, but is required for the maturation of primitive junctions into distinct TJ and AJ regions (Suzuki et al., 2002). Therefore, there is extensive and complex crosstalk between the TJ and key polarity regulators; Crumbs and Par complexes mediate TJ maturation and the TJ is important for the proper localisation of these complexes.

The tight apposition of neighbouring membranes is also thought to generate a molecular “fence”, which prevents the free diffusion of membrane proteins and lipids between apical and basolateral plasma membrane domains, therefore contributing to the characteristic polarised structure of the epithelium (Figure 1.3C) (Tsukita et al., 2001).

Additionally, epithelial cells use endocytic sorting and trafficking machinery to generate and maintain the unique compositions of the apical and basolateral plasma membrane domains (Köhler and Zahraoui, 2005). The TJ plays a key role in membrane transport as it appears to be a preferred site for the initial delivery of plasma membrane proteins, before they diffuse into the correct domain (Zahraoui et al., 2000). Small GTPases, including Rab3b, Rab8 and Rab13 are localised to the TJ (Zahraoui et al., 2000). Rab8 is implicated in trafficking vesicles from the *trans*-Golgi network to the basolateral membrane (Zahraoui et al., 2000). Furthermore, the exocyst, a multiprotein complex that mediates the docking of transport vesicles to their target membrane, closely associates with the TJ (Zahraoui et al., 2000). Therefore, the TJ appears to acts as a

"switching station", which coordinates cell signalling, membrane trafficking and the orientation of polarised membrane protein distribution (Köhler and Zahraoui, 2005; Zahraoui et al., 2000).

1.2.4 Tissue morphogenesis

The presence of claudins that promote paracellular permeability is essential for normal lumen formation, both *in vitro* and *in vivo* (Lu et al., 2014). For example, in zebrafish, knockdown of claudin-15 disrupts the normal development of the gut, leading to the formation of multiple lumens (Bagnat et al., 2007). Similarly, MDCK cells depleted of claudin-2 also form multiluminal cysts (Gálvez-Santisteban et al., 2012). This may be driven by luminal fluid accumulation, and highlights the importance of the TJ in regulating the overall architecture of the epithelium (Bagnat et al., 2007).

1.2.5 Intracellular signalling

Different types of signalling proteins and transduction pathways are associated with the TJ. This signalling is bidirectional; TJs receive signals from the cell interior to modulate epithelial permeability and transmit signals to modulate gene expression and behaviour (Matter and Balda, 2003). Various signalling pathways, including those mediated by protein kinase A, protein kinase C, heterotrimeric G proteins, Rho family GTPases and mitogen-activated protein (MAP) kinases can influence TJ formation, disassembly or properties (Matter and Balda, 2003; Zihni and Terry, 2015). Studies involving the fusion of biotin ligase to junctional components, including ZO-1, occludin and claudin-4 have identified a huge number of cytoskeletal, signalling and endocytic trafficking proteins that are associated with the TJ (Fredriksson et al., 2015; Van Itallie et al., 2013; Van Itallie et al., 2014). There are also a growing number of dual residence proteins that appear to function in the nucleus as well as localising to the TJ (Keon et al., 1996; Matter and Balda, 2003). For example, the Y-box transcription factor, ZO-1-associated nucleic acid-binding protein (ZONAB), is sequestered at the TJ and plays a role in regulating cell proliferation in a cell density-dependent manner (Balda et al., 2003), while symplekin is associated with the machinery involved in 3'-end processing of pre-mRNA and polyadenylation (Keon et al., 1996; McCrea et al., 2009). Furthermore, claudin-2 knockdown increases the rate of recovery in an MDCKII scratch wound migration assay, in a manner dependent on the transcriptional upregulation of proteases involved in extracellular matrix remodelling (Ikari et al., 2011a). Therefore, in addition to its interactions with mediators of polarity and trafficking, these studies implicate the TJ in regulating gene expression, mRNA processing, cell proliferation and migration.

1.3 The nature of tight junction strands: lipid, protein and hybrid models

FFEM observations revealed a series of raised TJ ridges and complementary grooves on the corresponding fascia, suggesting that intramembranous strands can bind laterally with paired strands in the adjacent cell, forming discrete areas of membrane fusion. Lipid-based models involve the formation of lipid "tunnels" that essentially form a continuous membrane between neighbouring cells (Figure 1.4A) (Lee et al., 2008). Alternative protein-based models involve the polymerisation of individual proteins into TJ strands, which interact in trans to form a paired TJ strand between neighbouring cells (Figure 1.4B) (Furuse et al., 1999; Lee et al., 2008). Following the initial discovery of the peripheral TJ-associated protein, ZO-1, and subsequent identification of integral transmembrane proteins including occludin and the extensive family of claudins, support for the lipid-based model has waned and attention has focussed on a protein-centric model (Lee et al., 2008). However, a protein-only model is disputed as the close apposition of hydrophobic membranes requires the displacement of water, which is a thermodynamically unfavourable process. The energy required would have to be accounted for by strong membrane-bridging contacts, which cannot currently be accounted for by relatively weak claudin- or occludin-mediated interactions (Lee et al., 2008). Furthermore, lipid probes can readily diffuse, depending on their size, between neighbouring cells via an intact TJ, suggesting some degree of lipid membrane continuity (Lee et al., 2008). Although a critical role for proteins, including claudins and occludin, is not disputed, lipid-protein hybrid models may more accurately reflect the composition of the TJ (Lee et al., 2008). Although TJ membranes are widely recognised as cholesterol-enriched, raft-like microdomains (Nusrat et al., 2000), the exact conformation of proteins and lipids in the junctional complex is not well-defined.

The width of a TJ strand is approximately 10nm and similar to the diameter of a connexin hexamer, the basic unit of the gap junction (Furuse et al., 1998a; Markov et al., 2015; Tsukita et al., 2001). Like most conventional ion channels, connexins oligomerise to form a channel with a central pore, through which ions can pass (Meşe et al., 2007). The diameter of the pore, together with the electrostatic properties of residues that line it, determines the ion selectivity (Yu et al., 2009). Connexins and claudins are both tetraspan integral membrane proteins, and *in vitro* claudins have been shown to form various oligomers, including dimers, hexamers and higher order linear polymers (Krause et al., 2008). It is conceivable that the basic unit of the TJ strand may be a hexamer or other oligomer of claudins, which form ion channels comparable to those of connexin-based gap junctions (Krause et al., 2008). Current models suggest that transcellular ion transport, for example via gap junctions, is likely to be very different to paracellular ion transport across the TJ (Yu et al., 2009).

Conventional transcellular channels mediate the movement of ions in the plane perpendicular to that of the lipid membrane, with the pore consisting of the transmembrane domains of the pore protein. In contrast, for paracellular transport, ions move in a plane parallel and extracellular to that of the lipid membrane, where the pore would presumably consist of residues belonging to the extracellular loops of claudins interacting in trans (Yu et al., 2009). It is tempting to speculate that a lipid-protein hybrid model may facilitate the organisation of claudins into a more conventional ion channel, where ions would pass through a central pore (Figure 1.4C) (Lee et al., 2008). It is unclear how such a model would be consistent with the organisation of claudins into continuous belt-like strands, though it is possible that higher order complex strands contain lower order oligomers that form discrete pores (Günzel and Yu, 2013), with the specific composition of these claudin "clusters" determining epithelial barrier properties (Markov et al., 2015). The opening and closing of ion channels could then be achieved through the dynamic assembly and disassembly of these pore-like structures from the TJ strand pool.

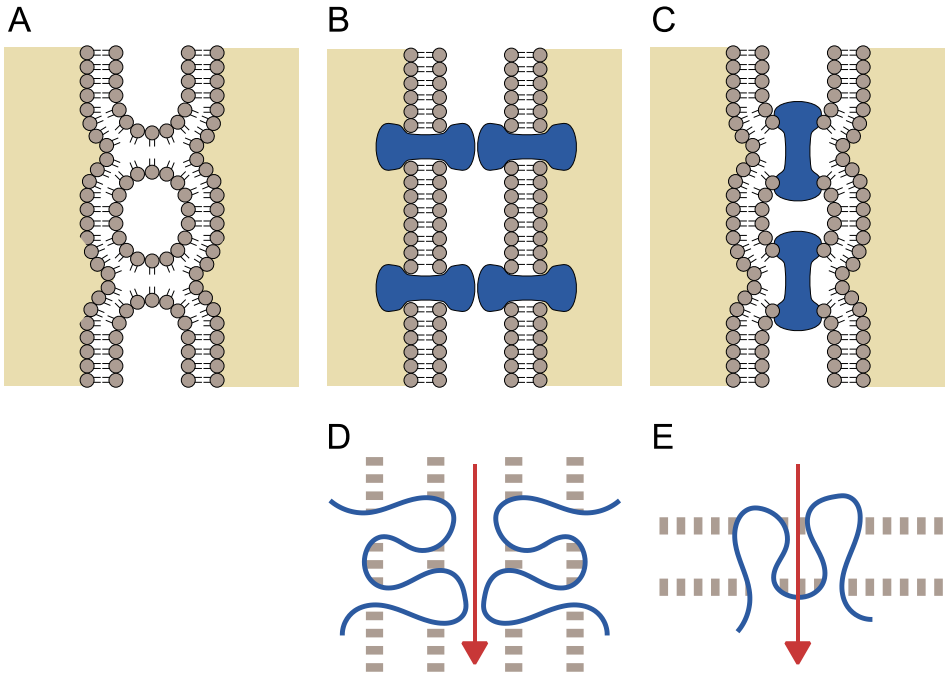

Figure 1.4: Lipid-, protein- or lipid-protein hybrid models of TJ strand formation. (A) Lipid-based models were proposed following the early observation that the outer leaflets of tightly apposed membranes appear to physically fuse and form a continuous membrane. (B) Protein-based models explain the detergent-insoluble nature of the TJ and found favour following the identification of TJ-associated ZO, occludin and claudin family proteins. Recent observations, including the TJ-facilitated diffusion of lipids between neighbouring plasma membranes, may be explained by lipid-protein hybrid models (C). (D) In the current protein-based TJ model, paracellular movement of ions proceeds in the plane parallel and extracellular to the lipid membrane. The ion pore consists of residues of the transmembrane domains of the pore proteins. (E) A lipid-protein hybrid model could generate a pore more akin to conventional ion channels, which facilitate ion movement perpendicular to the plane of the lipid membrane. Images adapted from Lee (2008) and Yu (2009).

1.4 Tight junction proteins

Protein-based models of TJ strand formation were initially proposed on the basis that TER development is prevented by inhibition of protein synthesis and that TJ structure is maintained when cells are treated with detergents that would disrupt normal lipid environments (Cereijido et al., 1983; Furuse et al., 1993). However, this does not necessarily exclude a lipid-based structure as TJ-associated lipid rafts may be detergent-resistant (Nusrat et al., 2000). A critical role for proteins has been established since the discovery of the first TJ-associated protein, zonula occludens (ZO)-1 (Stevenson et al., 1986) and the subsequent identification of integral transmembrane proteins belonging to three families: i) claudins, ii) tight junction-associated MARVEL proteins (TAMPs) and iii) junction adhesion molecules (JAMs) (Figure 1.5) (Furuse et al., 1993; Furuse et al., 1998b; Martìn-Padura et al., 1998).

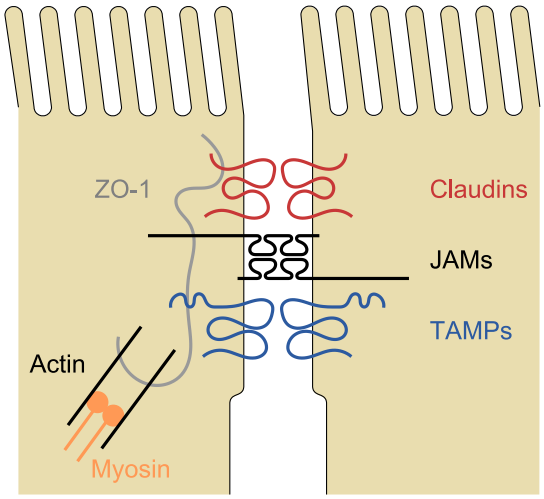

Figure 1.5: Core proteins of epithelial tight junctions. The TJ is composed of transmembrane proteins belonging to three families: i) claudins, ii) tight junction-associated MARVEL proteins (TAMPs) and iii) junction adhesion molecules (JAMs). These transmembrane proteins bind to ZO family scaffold proteins, which regulate their stability at the TJ, partially through mediating interaction with the perijunctional actin cytoskeleton. ZO proteins act as scaffolds, which mediate the attachment of various adaptor and signalling plaque proteins. Image adapted from Shen (2011).

These proteins form oligomeric TJ strands within the plasma membrane, which then dimerise between adjacent cells to form paired TJ strands (Furuse et al., 1999). The transmembrane proteins interact with cytoplasmic scaffold proteins such as ZO-1, -2 and -3, which regulate their polymerisation into strands, couple the TJ to the actin cytoskeleton and act as platforms that mediate the formation of “cytoplasmic plaques”. These plaques are large multiprotein complexes composed of an extensive number of diverse TJ-associated proteins including signalling proteins, transcriptional and post-

transcriptional regulators and complex-forming proteins (Balda and Matter, 2009; Traweger et al., 2013). The overall properties of the TJ are determined by the specific repertoire of proteins that are expressed and incorporated into this structure.

Experiments described in this thesis will utilise Madin-Darby canine kidney (MDCK) type II cells, an immortalised renal cell line that is widely used as a model for studying epithelial TJs *in vitro* (Dukes et al., 2011a). The cell line used in this thesis is a verified MDCKII strain sourced from the European Collection of Cell Cultures (ECACC). However, several low-resistance MDCK "type II like" strains have been independently isolated on separate occasions (Dukes et al., 2011a); when previously published work is cited in this thesis, the nomenclature used is consistent with the source literature. The MDCKII cell line used in this study endogenously express ZO proteins, occludin and claudin-1, -2, -3, -4 and -7. The specific roles of these TJ proteins are discussed below.

1.4.1 Zonula occludens (ZO) proteins

Zonula occludens (ZO)-1 was the first TJ protein to be identified from a junction-enriched membrane fraction (Stevenson et al., 1986). ZO-1 appears to be a ubiquitous component of all mammalian tight junctions, although it is at least partially redundant in function with other subsequently identified isoforms, ZO-2 and -3 (Jesaitis and Goodenough, 1994; Umeda et al., 2006). ZO proteins belong to the family of membrane-associated guanylate kinases (MAGUKs), which have a core structure consisting of PDZ, SH3 and GUK domains and mediate the interaction between transmembrane TJ proteins and the actin cytoskeleton (Shin et al., 2006). Additionally, the modular composition of ZO proteins allows them to act as scaffolds, which mediate the accumulation of a diverse array of plaque proteins (Balda and Matter, 2008; Traweger et al., 2013). ZO-1 is a peripheral membrane-associated protein that does not span the lipid bilayer, but specifically localises to the cytoplasmic face of TJ strands. Therefore, ZO proteins alone cannot account for the close association of neighbouring proteins at the TJ, but appear to be essential in organising a series of integral transmembrane proteins.

Specifically, TJ formation is completely abrogated in cells lacking all three ZO protein isoforms, as claudins fail to oligomerise into functional strands (Umeda et al., 2006). This phenotype is rescued by the re-expression of ZO-1 or -2, but not -3, indicating that the individual isoforms have overlapping but distinct functions (Umeda et al., 2006). This is reinforced by observations of ZO protein knockout mice (Tsukita et al., 2001). ZO-1 knockout is embryonic lethal, due to defective yolk sac angiogenesis and

apoptosis of embryonic cells (Katsuno et al., 2008). Embryos deficient for ZO-2 die shortly after implantation due to an arrest early in gastrulation (Xu et al., 2008), while ZO-3$^{-/-}$ mice lack an obvious phenotype (Xu et al., 2008). Therefore, while ZO-3 appears to be dispensable for viability and TJ formation, ZO-1 and -2 have overlapping and essential roles in the generation of a functional paracellular barrier.

Mouse mammary Eph4 cells lacking ZO proteins fail to form TJs, and monolayers exhibit negligible TER and high permeability to biotin (Umeda et al., 2006), indicating a crucial role for ZO-mediated TJ formation in determining pore and leak pathway permeability. However, these cells maintain functional segregation of apical and basolateral membrane proteins, suggesting that TJ strands are not necessarily required to provide a molecular fence to maintain the asymmetric distribution of membrane proteins (Umeda et al., 2006). Other mechanisms, involving external cues from the microenvironment, and the signalling of key polarity regulators such as the Par3/Par6/aPKC complex are thought to maintain overall apicobasal polarity in the absence of TJ strands, which may have a fine-tuning, rather than essential role (Shin et al., 2006; Tsukita et al., 2009).

In MDCK cells, TALEN-mediated knockout of ZO-1, but not ZO-2/-3, induces dramatic changes in myosin organisation and disrupts the localisation, but not the expression, of TJ proteins; junctional levels of claudin-2 decrease, while those of claudin-1 and -7 increase (Tokuda et al., 2014). ZO-1$^{-/-}$ clones tend towards increased TER values, decreased Na^+ permeability, and increased permeability to Cl^- and 4kDa dextran (Tokuda et al., 2014). The specific roles of each isoform will need to be fully addressed using knockout studies, as re-expression of trace amounts of ZO-1 was sufficient to rescue these diverse phenotypic changes (Tokuda et al., 2014).

There are also emerging roles for ZO proteins in the regulation of transcription and cell proliferation (Bauer et al., 2010; McCrea et al., 2009; Traweger et al., 2013). ZO-1 is observed in the nuclei of sparse proliferating cells, while it is sequestered at the TJ once cultures become confluent (Gottardi et al., 1996). This suggests that ZO-1 may regulate cell growth and TJ formation in coordination with cell density and contact, possibly through the regulation of the Y-box transcription factor ZONAB, which promotes cell proliferation in a manner dependent on its nuclear localisation (Balda et al., 2003). Furthermore, ZO-1/ZONAB may influence the nuclear accumulation of Cdk4, a key regulator of the G1/S transition (Balda et al., 2003).

1.4.2 Occludin

Using monoclonal antibodies raised against the junctional fraction of the chick liver, occludin was the first identified transmembrane protein that localised exclusively to the tight junction of epithelial and endothelial cells (Furuse et al., 1993). Occludin is a 65kDa tetraspan membrane protein, with cytoplasmic N- and C-termini and two extracellular loops. As occludin was predicted to seal the paracellular space, its name was derived from the Latin word “occlude” meaning “to shut or close” (Furuse et al., 1993). The consequences of occludin knockout are complex; mice are born without any gross phenotype but exhibit postnatal growth retardation (Saitou et al., 2000). Surprisingly, TJ morphology is largely unaffected and intestinal barrier function appears to be uncompromised, but occludin$^{-/-}$ mice exhibit several abnormalities including chronic inflammation of the gastric epithelium, brain calcification and testicular atrophy (Saitou et al., 2000). These phenotypes may be manifestations of altered barrier functions in gastric and testicular epithelia and brain endothelia (Yu et al., 2005).

Although occludin can form adhesions when expressed in fibroblasts that normally lack TJs (Van Itallie and Anderson, 1997), its expression alone is not sufficient to drive TJ strand formation (Furuse et al., 1998a). Furthermore, occludin is not strictly required for TJ formation or maintenance, as intact TJs were formed in the absence of occludin (Saitou et al., 1998). Taken together, these studies suggest that although occludin may be dispensable for TJ formation, it appears to have additional uncharacterised yet indispensable physiological functions.

RNAi-mediated occludin knockdown also has diverse effects in MDCK cells (Yu et al., 2005). Although TER is unaffected, permeability to mono- and divalent inorganic cations, and to larger molecular weight tracers, is increased, without affecting ion selectivity (Yu et al., 2005). Occludin-null cells also exhibit a reduced ability to extrude apoptosing cells from the monolayer. Occludin overexpression increases the TER of MDCK cells, which occurs with a concurrent increase in TJ strand number from 3 to 4, and an increase in mean TJ width (McCarthy et al., 1996). This suggests that occludin may regulate TJ strand organisation and resulting barrier properties (Balda et al., 1996). Increased mannitol flux was also observed in cells overexpressing occludin, suggesting that occludin may serve to promote electrical barrier function while increasing permeability to larger, uncharged molecules through differential regulation of pore and leak pathway permeability (Shen et al., 2011).

These observations were corroborated by studies involving the stable expression of either full-length or C-terminally truncated occludin in MDCKII cells (Balda et al., 1996).

Expression of either increases TER and the paracellular flux of small molecular weight tracers (Balda et al., 1996). Cation selectivity is not affected, suggesting that occludin expression correlates with increased paracellular permeability to uncharged solutes, while an electrical seal is maintained. This study also identified an apparent fence function for occludin, as expression of C-terminally truncated occludin rendered MDCKII cells incapable of maintaining a fluorescent lipid in a specifically labelled domain. C-terminally truncated occludin localises to the TJ, but does not form a continuous band like full-length protein. However, the TJ strands themselves are complete, suggesting that the "gaps" in occludin staining are filled by other TJ components. The first members of the claudin family, claudin-1 and -2 were subsequently identified in 1998 (Furuse et al., 1998b).

1.4.3 Claudins

Two distinct peptides of ~22kDa were detected by silver-staining of the previously described junctional fraction of chicken liver (Furuse et al., 1998b). These proteins were named claudin-1 and claudin-2 from the Latin word "claudere" meaning "to close". Claudin-1 and -2 are both tetraspan transmembrane proteins, although they bear no sequence similarity with occludin (Furuse et al., 1998b). Expression of claudin-1 or -2 is sufficient to drive the formation of TJ-like strands in fibroblasts that lack endogenous TJs, suggesting that claudins are the major protein component of TJ strands (Furuse et al., 1998b; Sasaki et al., 2003). Since the initial discovery of claudin-1 and -2, further family members have been identified. There are currently 24 identified mammalian claudin family members, which are all expressed in humans, with the exception of claudin-13 (Kwon, 2013). These claudins are expressed to different extents and ratios to tailor the function and properties of the TJ in a tissue-dependent manner. MDCKII cells express claudin-1, -2, -3, -4 and -7 and various studies have begun to elucidate the specific properties that they each confer to the TJ. For example, claudin-2, -10b and -16 form cation-selective channels (Hou et al., 2013; Li et al., 2013), whereas claudin-7, -10a and -17 form anion-selective channels (Hou et al., 2013). The recent solving of the crystal structure of the claudin-15 protomer has provided key insights into how ion selectivity may be regulated in different claudin species (Suzuki et al., 2014).

The first claudin crystal structure

Sequence analysis suggests that claudin family proteins have four transmembrane (TM) segments, a large extracellular loop (ECL1) joining TM1 and TM2 via a short extracellular helix (ECH), and a second shorter extracellular loop (ECL2) between TM3 and TM4 (Figure 1.6) (Suzuki et al., 2014). The four transmembrane segments form a left-handed four-helix bundle while the extracellular loops form a β-sheet structure

(Figure 1.6) (Suzuki et al., 2014). The length of the TM segments is consistent with the width of the lipid bilayer, and tight helical packing is possible due to the presence of residues with small side chains (Suzuki et al., 2014). The β-sheet is comprised of five β-strands, with four contributed from ECL1 and one from ECL2, and is stabilised by a disulphide bond formed between β3 and β4. The two cysteine residues involved are conserved amongst all claudins and may be necessary for proper claudin function (Suzuki et al., 2014). The sequences of ECL1 and ECL2 are relatively diverse and may be crucial for the ion selectivity of pores formed by different claudins. The β-sheet forms a "palm", which is negatively charged in cation-selective claudins (claudin-2 and -15) and positively charged in the anion-selective claudin-10a (Suzuki et al., 2014). Specific charged residues in ECL1 are thought regulate ion specificity of different claudins (Hou et al., 2013). For example, cation-selective, pore-forming claudins have an acidic residue at position 65 or 66, which is proposed to form part of an electrostatic cation-binding interface (Yu et al., 2009). Variable regions, V1 and V2 in ECL1 and ECL2 respectively, may be involved in subtype-specific compatibility of different claudins (Suzuki et al., 2014). The ECH between β5 and TM2 has a conserved hydrophobic residue that snugly fits into a hydrophobic pocket between TM3 and ECL2 of adjacent claudin-15 protomers to form a linear polymer in the crystal lattice (Suzuki et al., 2014). These sites also have complementary electrostatic potentials and their relative positions on opposite sides of the protomer may permit claudin polymerisation into oligomeric pores and/or strands. FFEM revealed that mutation of the corresponding hydrophobic methionine residue prevented the formation of TJ strands in the plasma membrane, suggesting a molecular basis for the polymerisation of claudins into linear TJ strands (Suzuki et al., 2014).

Additional structural features that are likely to be common to claudin family proteins have been identified independently of the crystal structure. For crystallisation studies, the C-terminal was truncated, but a conserved YV motif on the C-terminal tail of claudins is involved in their association with the PDZ domain of ZO-1, which may be essential for the polymerisation of claudins into functional TJ strands (Umeda et al., 2006). Additionally, membrane proximal cysteine residues were mutated to avoid heterogeneous palmitoylation. Palmitoylation of these two additional cysteine residues at the cytoplasmic terminus of TM2 and TM3 increases the efficiency with which claudins are incorporated into the TJ (Van Itallie et al., 2005). The conserved disulphide bond immediately precedes residues involved in ion selectivity, suggesting it may function to orientate the relevant side group to protrude into the pore lumen (Yu et al., 2009).

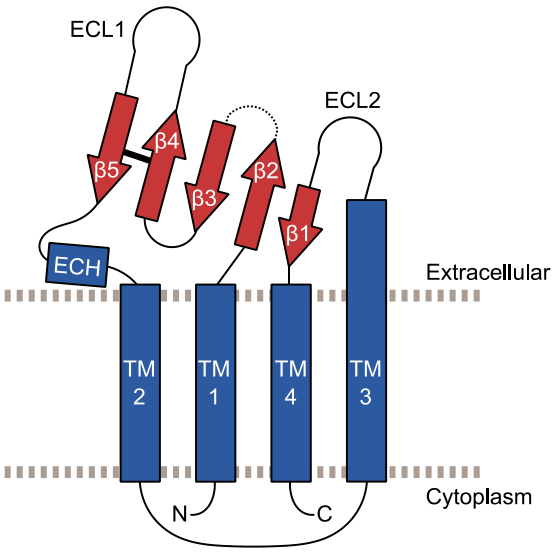

Figure 1.6: The overall secondary structure of the claudin-15 protomer. Claudin-15 has 4 transmembrane helical segments (TM1 – 4) and an antiparallel β-sheet (β1 – 5), which forms two extracellular loops (ECL1 and 2) that protrude from the plasma membrane. β3 and β4 strands are joined by a conserved disulphide bond, which may orientate residues required for ion selectivity. Dotted grey lines indicate suggested boundaries of the plasma membrane. Based on sequence conservation, the claudin-15 structure has provided key insights into the structural basis of membrane packing, TJ strand formation, claudin compatibility and ion selectivity that are likely to be common between claudin family proteins. (ECH) extracellular helix, (blue) α-helices, (red) β-strands. Image adapted from Suzuki *et al* (2014).

The first claudin crystal structure has provided crucial insights into the structural basis for membrane insertion and packing, oligomeric strand formation via cis-interactions, subtype compatibility via trans-interactions and ion selectivity. The specific roles of different claudins have been further investigated using mouse knockout models, in combination with overexpression and RNAi-mediated knockdown studies in cultured cells.

Claudin-1

CLDN1 knockout mice are viable, but die within one day of birth due to transepidermal water loss through the skin (Furuse et al., 2002). This was initially surprising as the TJ was thought to regulate the barrier function of simple epithelia, but not necessarily stratified epithelia like the epidermis. As with most TJ proteins, conditional or tissue-specific knockout of claudin-1 has not been attempted. Claudin-1 expression increases TER in MDCKII cells by approximately 4-fold and decreases paracellular flux to dextran tracers of 4 – 40kDa, indicating that claudin-1 has a general barrier-promoting role when overexpressed (Inai et al., 1999). However, RNAi-mediated knockdown of claudin-1 has no discernible effect on MDCK TER or paracellular permeability (Hou et al., 2006). Considering the ability of claudin-1 to form recognisable TJ strands in fibroblasts and the functional consequences of overexpression, it appears that claudin-1 is likely to have a genuine role in increasing epithelial barrier function, although this may be redundant with other expressed claudins or TJ proteins.

Claudin-2

In contrast to claudin-1, claudin-2 expression is associated with a decrease in TER and an increase in selective permeability to Na^+ and water (Hou et al., 2006). Type I and II MDCK cells have contrasting barrier properties; MDCKI cells lack claudin-2 expression and have a high TER of ~4000Ω.cm^2, while claudin-2-positive MDCKII cells have a low TER of <300 Ω.cm^2 (Dukes et al., 2011a). The expression of claudin-2 in MDCKI cells mediates the conversion from a highly resistant to highly permeable phenotype (Furuse et al., 2001). RNAi-mediated knockdown of claudin-2 in MDCKII cells causes a three-fold increase in TER and decrease in cation permeation (Hou et al., 2006). The TALEN-mediated knockout of claudin-2 has more severe effects, increasing TER by approximately fifty-fold to levels of 3000 – 4000Ω.cm^2, comparable to the high-resistance MDCKI strain (Tokuda and Furuse, 2015). Claudin-2 overexpression increases TER by increasing the number of cation pores, without increasing permeability to non-charged solutes larger than the pore (~ 6 – 7Å in radius) (Van Itallie et al., 2008). Claudin-2 knockout mice are viable and exhibit normal appearance, growth and behaviour (Muto et al., 2010). In the kidney, claudin-2 expression is confined to the areas of high epithelial permeability, such as the proximal tubule and descending limb of Henle (Hou et al., 2013). Although renal proximal tubules of *CLDN2*$^{-/-}$ mice appear normal, there is a significant decrease in the net reabsorption of Na^+, Cl^- and water, suggesting a key role for claudin-2 in ionic homeostasis in the kidney.

Claudin-3

Claudin-3 is expressed in a number of epithelia including skin, lung, kidney and intestine as well as in endothelia (Milatz et al., 2010). Claudin-3 is generally considered to be a barrier-forming protein as it seals the paracellular pathway to the passage of small cations, anions and uncharged solutes (Milatz et al., 2010) and is expressed in the “tighter” distal tubule in the kidney (Rahner et al., 2001). MDCKII cells only weakly express claudin-3 and its overexpression increases the TER of two MDCKII clones, expressing either high or low levels of claudin-2, indicating an intrinsic role for claudin-3 in forming an electrical barrier (Milatz et al., 2010). The increase in TER was accompanied by decreased permeability to both positively and negatively charged ions as well as larger uncharged solutes (Milatz et al., 2010). Claudin-3 overexpression did not alter ion selectivity, indicating that ionic permeability was still governed by claudin-2 based channels, although their number was reduced (Milatz et al., 2010).

Claudin-4

Claudin-3 and -4 resemble each other in many ways (Milatz et al., 2010). Both seal the TJ to the passage of ions and macromolecules and overexpression of either causes the formation of increasingly curved looping TJ strands (Milatz et al., 2010; Van Itallie et al., 2001). They have high sequence homology (67% of amino acids are identical, while ECL1 and 2 are 94% and 68% identical, respectively) and both are located on chromosome 7, suggesting possible gene duplication (Milatz et al., 2010). Claudin-3 and -4 are commonly transcriptionally co-regulated (Milatz et al., 2010), although not by the RAF/MEK/ERK pathway (Doehn et al., 2009). Claudin-3 and -4 have non-homologous C-termini, which are thought to be important for intracellular signalling, and vary in their ability to interact with other claudins. For example claudin-3, but not claudin-4, has been shown to interact in trans with claudin-1, -2 and -5 (Milatz et al., 2010). In the kidney, claudin-4 is expressed in the high-resistance ascending limb of Henle and collecting duct, indicating that its expression correlates with low paracellular permeability (Hou et al., 2013).

The functions of claudin-4 have been studied using RNAi in MDCKII and LLC-PK1 cells (Hou et al., 2006). Knockdown of claudin-4 decreases MDCKII TER by increasing permeability to Na^+, but not Cl^- ions (Hou et al., 2006). In contrast, claudin-4 knockdown depresses paracellular permeability to Cl^- ions in LLC-PK1 cells. Therefore, claudin-4 can act as either a Na^+ barrier or Cl^- channel depending on the cellular background. LLC-PK1 cells do not endogenously express claudin-2, and the observed increase in Na^+ permeability following claudin-4 knockdown in MDCKII cells may potentially be explained by the ability of MDCKII, but not LLC-PK1 cells, to form claudin-2 based cation channels when claudin-4 is depleted (Hou et al., 2013). It has been proposed that differences in TJ protein composition, or pathways regulating its function, may explain why claudin-4 forms Cl^- channels in LLC-PK1, but not in MDCKII cells (Hou et al., 2006). Consistent with these RNAi studies, overexpression of claudin-4 in MDCKII cells increases TER by decreasing permeability to Na^+, but not Cl^- ions or mannitol. Therefore, in the MDCKII cell line relevant to this thesis, both knockdown and overexpression studies indicate that claudin-4 acts to seal the epithelial barrier by reducing Na^+ permeability, although this function may be dependent on direct or indirect interactions with other TJ components.

Claudin-7

Claudin-7 is highly expressed in the high-resistance distal convoluted tubules and collecting duct of the kidney (Hou et al., 2013). Although, claudin-7 knockout mice are viable, they die within 12 days of birth, exhibiting severe salt wasting, chronic

dehydration and growth retardation (Tatum et al., 2010). This study concluded that claudin-7 was essential for NaCl homeostasis in distal nephrons of the kidney. *CLDN7*$^{-/-}$ mice also exhibit high levels of inflammation and defective architecture in the intestine (Ding et al., 2012). RNAi-mediated knockdown studies revealed that claudin-7 has similar functions to that of claudin-4 (Hou et al., 2006). Claudin-7 depletion significantly decreases MDCKII TER by increasing paracellular permeability to Na^+ but not Cl^- ions (Hou et al., 2006). Furthermore, knockdown of claudin-7 decreases paracellular Cl^- permeability in LLC-PK1 cells, indicating that both claudin-4 and -7 can act as either Na^+ barriers or Cl^- channels depending on cell background (Alexandre et al., 2005). This effect is likely to be mediated by the difference in TJ composition between the cell types, and regulatory pathways, which may vary in different contexts.

1.4.4 Additional TJ proteins

The TAMP family of integral transmembrane TJ proteins includes tricellulin and MARVELD3 in addition to occludin. These proteins have distinct but overlapping functions (Raleigh et al., 2010). In contrast to occludin, ZO and claudin family proteins, tricellulin appears to accumulate specifically at tricellular (rather than bicellular) cell-cell contacts, forming a peculiar tightly sealed tube that is aligned parallel with (rather than perpendicular to) the apicobasal axis (Ikenouchi et al., 2005). Stable suppression of tricellulin decreases the TER of Eph4 mouse mammary epithelial cells and increases paracellular permeability to small molecular weight dextran tracers (Ikenouchi et al., 2005). Therefore, tricellulin appears to constitute a novel TJ subdomain, which specifically mediates paracellular permeability where multiple plasma membranes meet. However, tricellulin can redistribute to bicellular membranes to compensate for the loss of occludin (Ikenouchi et al., 2008). Relatively little is known about the biological functions of MARVELD3. Although it appears to partially compensate for the loss of occludin or tricellulin, its expression alone is insufficient to restore barrier function (Raleigh et al., 2010). RNAi-based studies in Caco-2 intestinal epithelial cells indicate that MARVELD3 is not required for TJ formation, but that its depletion results in monolayers with increased TER (Steed et al., 2009).

In contrast to the tetraspan TAMP and claudin family proteins, junction adhesion molecules (JAMs) are single-pass integral membrane proteins belonging to the immunoglobulin superfamily (Van Itallie and Anderson, 2014). The JAM family includes JAM-A, -B, -C, -4, -L and the coxsackie adenovirus receptor (CAR) (Luissint et al., 2014). This family of proteins has not been studied as extensively as other TJ proteins. JAM-A concentrates to epithelial and endothelial TJs and lateral membranes, and is also expressed in immune cells. Therefore, JAM proteins may play a role in

mediating the transmigration of immune cells across epithelial and endothelial monolayers (Martìn-Padura et al., 1998). JAMs do not appear to be essential for TJ formation, but do contribute to adhesion and signalling (Van Itallie and Anderson, 2014).

In summary, the TJ is an important subcellular structural feature that has key roles in determining paracellular permeability, apicobasal polarity and epithelial architecture. It also has emerging signalling functions, allowing it to regulate cell proliferation and migration. For these reasons, the study of TJ regulation is important in understanding how normal epithelia are generated during development and maintained in a physiological setting. Furthermore, the TJ and epithelial barrier properties are often deregulated in disease settings, such as inflammatory bowel disease and cancer. Therefore, understanding the mechanisms of TJ disruption has important therapeutic relevance.

1.5 Regulation of the tight junction

1.5.1 Transcriptional regulation of individual TJ proteins

The overall properties of the TJ are regulated by its specific protein composition, which varies between different tissues and can be regulated by a variety of different extracellular signals. These compositional changes are often achieved through the transcriptional regulation of individual TJ proteins (Kwon, 2013).

Colonic claudin-1 expression is regulated by Cdx1, Cdx2 and GATA4 transcription factors (Bhat et al., 2012). The E-box transcription family proteins, Slug and Snail, which are associated with epithelial-mesenchymal transition, have been show to bind to and inhibit the promoter activity of claudin-1, as well as occludin, claudin-3, -4 and -7 (Ikenouchi et al., 2003; Martínez-Estrada et al., 2006). Claudin-1 expression is also regulated by RUNX3 in gastric epithelial cells (Chang et al., 2010) and the microRNA miR-155 in ovarian tissues (Qin et al., 2013).

Molecular cloning of the 5' flanking region of claudin-2 revealed a series of transcription factor binding sites that are conserved between mouse and human, suggesting that claudin-2 expression may be regulated by AP-1, NFκB, E-box, GATA, HNF-1 and Cdx transcription factors (Sakaguchi et al., 2002). Furthermore, LEF-1, a nuclear effector of the Wnt signalling pathway, directly binds to the claudin-2 promoter to enhance transcription, and also acts indirectly through the transactivation of Cdx2 (Mankertz et al., 2004). However, claudin-2 expression appears to be regulated in a highly tissue-specific manner. HNF-1 is expressed in various tissues, including the liver, intestine,

pancreas, stomach and kidneys, and is required for claudin-2 expression in the intestine and liver (Sakaguchi et al., 2002). However, renal claudin-2 expression is not affected in HNF-1α deficient mice (Sakaguchi et al., 2002). In addition, the expression of Cdx1 and Cdx2 is confined to the intestine, where they cooperate with GATA-4 and HNF-1α to regulate the regional expression of claudin-2 (Escaffit et al., 2005). In renal MDCKII cells, the expression of claudin-2, as well as claudin-3 and ZO-3, is regulated by GATA-4 (Guillemot et al., 2013) and the epidermal growth factor (EGF)-mediated downregulation of claudin-2 is mediated by STAT3 (García-Hernández et al., 2015).

Although the expression of claudin-3 is decreased following GATA-4 knockdown, the claudin-3 promoter lacks the GATA consensus binding sequence. Therefore, this is likely to be an indirect consequence of transcriptional downregulation of claudin-2 and ZO-3 (Guillemot et al., 2013). The expression of claudin-3 and -4 is dependent on Sp1 expression and specific epigenetic modifications (Honda et al., 2006). Furthermore, the EGF-mediated upregulation of claudin-4 is mediated through Sp1 (Ikari et al., 2009) and STAT3 (García-Hernández et al., 2015). In colonic crypts, claudin-7 expression is suppressed by TCF-4 and Sox9 (Darido et al., 2008). E74-like factor 3 (ELF3) is an ETS family transcription factor, which binds to and increases the activity of the claudin-7 promoter (Kohno et al., 2006). In addition, hypermethylation of the claudin-7 promoter is associated with its reduced expression in breast cancer (Nakayama et al., 2008).

Cloning of the occludin promoter from human genomic DNA revealed putative transcription factor binding sites for TCF, NF-IL6 and AP2, and occludin expression was downregulated by TNFα and IFNɣ (Mankertz et al., 2000). By computational analysis, the ZO-1 promoter contains several potential AP-1 and CREB sites, suggesting it may be a target of JunD. Consecutive promoter deletions revealed that JunD suppresses ZO-1 by binding CREB sites, but also inhibits translation, possibly by mediating interactions between the 3'UTR and RNA-binding proteins (Chen et al., 2008). ZO-1 promoter activity is also regulated by E-box, MEIS, MOKF and TALE transcription factors (Cohen et al., 2006).

Taken together, these studies illustrate that the transcriptional regulation of individual claudins is highly complex. Diverse transcription factors, epigenetic modifications and microRNA regulation act in concert to generate tissue-specific expression patterns. Additionally, the expression of individual claudins is differentially and diversely regulated in different cancer types (see Section 1.6.2).

1.5.2 Dynamic regulation of tight junction proteins

Due to the extensive interaction of different TJ proteins with each other and the actin cytoskeleton via ZO protein mediated interactions, the TJ was initially considered to be a stable heavily cross-linked complex (Shen et al., 2011). However, the molecular structure of the TJ exhibits a surprising degree of plasticity and undergoes constant remodelling (Turner et al., 2014). Individual TJ components are dynamic, both in terms of their movement within the plasma membrane and in exchange with cytoplasmic or vesicular protein pools (Shen et al., 2008). Functionally, constant TJ disassembly and reformation may provide a mechanism to regulate the probability of paracellular channels being found in an open state, and therefore form the molecular basis of experimental observations of paracellular permeability. Furthermore, the constant exchange of proteins between vesicular and junctional pools would allow rapid TJ remodelling. TJs require rapid assembly and disassembly in tissues that undergo continuous dynamic remodelling, for example, in the mammalian intestine where epithelial cells are replaced every 4 – 5 days (Chalmers and Whitley, 2012; Vereecke et al., 2011). These dynamic properties would also maintain barrier function during cell division or the extrusion of apoptosing cells from the monolayer.

Although bulk internalisation of the TJ can be induced by non-physiological means, such as the depletion of extracellular calcium (Ivanov et al., 2004), individual TJ proteins exhibit distinct dynamic properties and are subject to differential modes of regulation (Shen et al., 2008). Protein dynamics within the TJ can be assessed by expressing fluorescently-tagged proteins and using time-lapse microscopy for fluorescence recovery after photobleaching (FRAP) experiments. The fluorescent signal is “bleached” by destroying the fluorophore with the beam of a laser scanning microscope. The fluorescent signal within the bleached region then recovers through the diffusion of intact fluorescently-tagged proteins from adjacent regions. The percentage and speed of fluorescence recovery reflects the overall mobility of the tagged-protein.

The nature of recovery can be studied by photobleaching a length of plasma membrane and monitoring fluorescence recovery in the centre and edges of this region. Exchange with an intracellular pool is exhibited by uniform recovery across the length of the bleached region, whereas intramembrane diffusion is indicated by recovery at the edges prior to at the centre (Figure 1.7A and B) (Shen et al., 2011). Initial FRAP studies revealed that claudin-1, occludin and ZO-1 display distinct dynamic properties; claudin-1 is relatively stable at the TJ and exchange is mediated by diffusion within the plasma membrane, occludin is more mobile but still recovers via

intramembrane diffusion, whereas junctional ZO-1 primarily exchanges with an intracellular pool (Shen et al., 2011). Furthermore, FRAP studies have been used to determine changes in TJ protein dynamics caused by different stimuli. For example, treatment of Caco-2 intestinal epithelial cells with PIK, a highly-specific peptide inhibitor of MLCK, increases TER by stabilising ZO-1 within the TJ, without affecting the dynamic behaviour of claudin-1, occludin or actin (Yu et al., 2010).

Fluorescence loss in photobleaching (FLIP) involves photobleaching the cytoplasmic area. If claudin exchange is primarily through intramembrane diffusion, the fluorescence intensity of the junctional pool will remain constant, while exchange of junctional and cytoplasmic pools through endocytic exchange will lead to the depletion of junctional fluorescence (Figure 1.7C and D) (Shen et al., 2008). For example, continuous photobleaching of the intracellular region only slightly diminished the TJ-associated fluorescence of occludin and claudin-1, suggesting minimal endocytic exchange (Shen et al., 2008). In contrast, photobleaching of cytoplasmic ZO-1 leads to the progressive decrease of junctional ZO-1 fluorescence (Shen et al., 2008). Photoactivatable tags allow fluorescence to be “switched on” in specific subcellular areas, allowing the movement of photoactivated proteins to be assessed independently of newly synthesised protein (Figure 1.7E and F) (Lippincott-Schwartz et al., 2003). Following photoactivation of occludin within the TJ, fluorescence within the area of activation progressively decreased but increased in adjacent regions of the TJ, indicating movement by intramembrane diffusion (Shen et al., 2008). The lack of fluorescent intracellular vesicles following junctional photoactivation suggests that, at steady-state, occludin does not exchange rapidly with an intracellular pool (Shen et al., 2008).

These reports indicate that dynamic regulation is a common regulatory feature of diverse TJ proteins. Furthermore, the combination of FRAP, FLIP and photoactivation studies indicate that individual proteins are characterised by distinct kinetics of endocytic exchange and intramembrane diffusion. This suggests that despite extensively characterised molecular interactions between ZO-1, occludin and claudin family proteins, the TJ is not a static cross-linked structure, but undergoes continuous dynamic remodelling. An important caveat of these studies is that the fusion of GFP to the C-terminal of different claudins is thought to interfere with the PDZ-domain mediated interaction with ZO-1/-2 (Sasaki et al., 2003). This is likely to affect the polymerisation of claudins into TJ strands (Umeda et al., 2006). Although these fusion proteins accurately target to the TJ, colocalise with their corresponding endogenous proteins and do not disrupt normal epithelial function, they may still display dynamic

properties that are not truly reflective of endogenous claudins. The work in this thesis will instead focus on studying the endocytic trafficking of endogenous TJ proteins, which can be measured using alternative biochemical trafficking assays (Dukes et al., 2011b; Dukes et al., 2012; Nishimura and Sasaki, 2008).

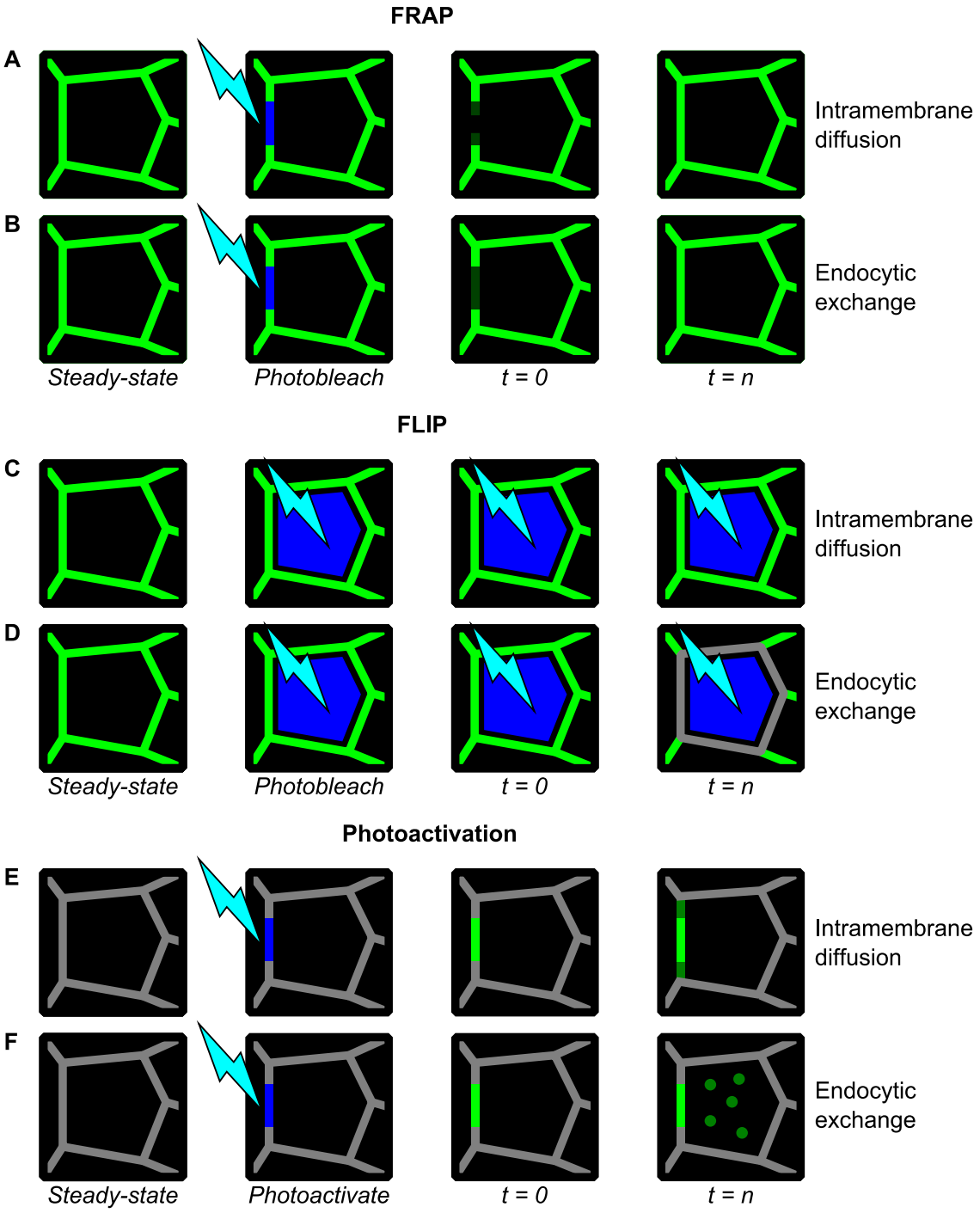

Figure 1.7: Intramembrane diffusion and endocytic exchange can be distinguished using fluorescently tagged junction proteins in combination with photobleaching and photoactivation experiments. Predicted outcomes of protein dynamic experiments for intramembrane diffusion and endocytic trafficking models of claudin-1 and -4 redistribution. Various fluorescently tagged TJ proteins localise normally to areas of cell-cell contact (shown in red). (A and B) Fluorescence recovery after photobleaching (FRAP) involves localised fluorophore destruction by photobleaching (blue bolt). Fluorescence in the photobleached area is recovered by movement of fluorescently tagged proteins from adjacent regions. (A) Intramembrane diffusion would result in gradual recovery of fluorescence, initially at the periphery of the photobleached area. (B) Endocytic trafficking would result in uniform recovery of fluorescence across the photobleached area. (C and D) Fluorescence loss in photobleaching (FLIP) involves photobleaching the cytoplasmic area. (C) If claudin exchange is primarily through intramembrane diffusion, the fluorescence intensity of the junctional pool will remain constant. (D) Exchange of junctional and cytoplasmic pools through endocytic exchange will lead to the depletion of junctional fluorescence. (E and F) Photoactivatable tags allow fluorescence to be “switched on” in specific subcellular areas, allowing the movement of photoactivated proteins to be assessed. (E) Intramembrane diffusion would lead to increased fluorescence in the adjacent plasma membrane. (F) Endocytic exchange would result in an increase in cytoplasmic fluorescence. Image adapted from Shen et al (2011).

1.5.3 Endocytic trafficking of TJ proteins

Selective sorting of proteins through biosynthetic, internalisation, recycling and degradative pathways is a common feature of epithelial cells (Mostov et al., 2003). In MDCKII cells, 50% of the entire cell surface is endocytosed per hour and is largely replenished through recycling of internalised protein back to the cell surface (Mostov et al., 2003). Furthermore, mislocalised proteins can be endocytosed specifically from either the apical or basolateral plasma membrane domains into distinct endosomal compartments. From here, they can either be degraded or transported to the correct surface in a process called transcytosis (Mostov et al., 2003). Therefore, the polarised delivery of transmembrane proteins and their selective removal results in localised cell surface expression patterns, indicating a key role for endocytic sorting in maintaining steady-state polarity (Köhler and Zahraoui, 2005; Mostov et al., 2003; Zahraoui et al., 2000).

TJ proteins can undergo internalisation via clathrin-mediated endocytosis (Ikari et al., 2011c) macropinocytosis (Bruewer et al., 2005) and caveolar endocytosis (Shen and Turner, 2005). They are initially trafficked into early endosomes, and from here they can either proceed along the degradative pathway, culminating in lysosomal degradation, or be recycled back to the plasma membrane (Figure 1.8A) (Chalmers and Whitley, 2012). This can proceed either directly via recycling endosomes or after additional sorting following retrograde transport to the *trans*-Golgi network (Figure 1.8A) (De Matteis and Luini, 2008).

Surface-biotinylation techniques have been utilised to establish that constitutive endocytosis and recycling of endogenous TJ proteins is a common in various epithelial cell lines (Chalmers and Whitley, 2012; Dukes et al., 2011b; Dukes et al., 2012; Nishimura and Sasaki, 2008). These assays rely on the ability to label proteins specifically at the cell surface, using a membrane-impermeable and cleavable biotin moiety that forms a covalent bond with accessible lysine residue side chains (Figure 1.8B). These biotin moieties can be cleaved from proteins remaining at the cell surface using membrane-impermeable reducing agents. Endocytosed protein is protected from this “surface strip” by an intact plasma membrane. Following cell lysis, biotinylated proteins can be retrieved using neutravidin beads, and the relative extent of protein internalisation can be assessed by SDS-PAGE and immunoblotting for proteins of interest. This assay can be extended to study endocytic recycling as, following the first surface strip, endocytosed protein is recycled back to the membrane and again becomes prone to stripping (Figure 1.8B).

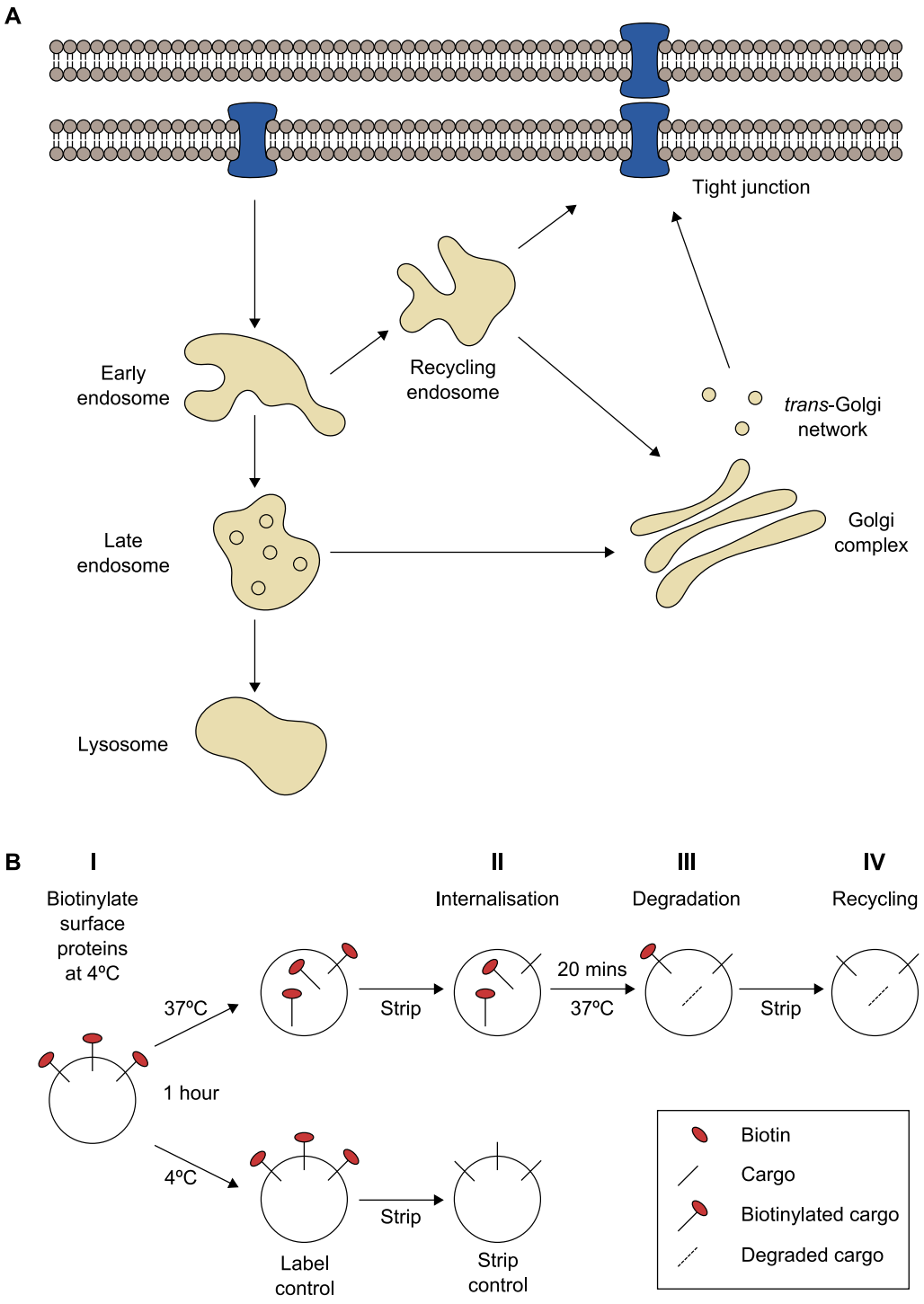

Figure 1.8: Tight junction proteins undergo constitutive endocytic recycling in epithelial cells. (A) Newly synthesised transmembrane TJ proteins are trafficked to the cell surface via the Golgi complex and *trans*-Golgi network (TGN), where they form extensive interactions with other proteins, both within the same and adjacent membranes. Despite these complex interactions, individual TJ proteins are highly dynamic in nature and are constitutively endocytosed from the plasma membrane into early endosomes. From here, they can either be trafficked through late endosomes towards the lysosome for degradation, or recycled back to the plasma membrane, either directly via recycling endosomes or after retrograde sorting in the Golgi/TGN. This allows rapid TJ remodelling in response during physiological processes that involve cell movement, but require epithelial barrier maintenance. (B) TJ protein trafficking can be assessed using a surface-biotinylation based biochemical trafficking assay. (I) Cell-surface proteins are labelled with a membrane-impermeant biotin moiety. Cooling cells effectively blocks endocytic trafficking as membranes become viscous at low temperatures. Surface biotin is effectively stripped with a membrane-impermeant reducing agent. (II) Endocytosed protein is protected from the surface strip by an intact plasma membrane. Biotinylated proteins are retrieved by neutravidin pulldown, allowing rates of internalisation to be established by SDS-PAGE and immunoblot. Recycled biotinylated protein again becomes amenable to surface-stripping. Lysing cells before and after the second surface-strip reveals the proportion of endocytosed protein that is degraded and recycled over the duration of the second incubation (III and IV).

These biochemical trafficking assays have identified the constitutive endocytosis and recycling of occludin in MTD-1A mouse mammary epithelial cells (Morimoto et al., 2005), claudin-2 in MDCKII cells (Dukes et al., 2012) and claudin-1 in MDCKII, Caco-2 and 16-HBE human lung epithelial cells (summarised in Table 1.2) (Dukes et al., 2011b), Therefore, the constitutive endocytosis and trafficking of TJ proteins is a common feature of diverse epithelial cell lines, although the specific trafficking rates of different components vary in a cell line-specific manner (Table 1.2). The ability to differentially regulate the trafficking of individual TJ components permits cells to alter the molecular composition of the TJ to fine-tune paracellular permeability properties under different conditions (Chalmers and Whitley, 2012).

Tight junction protein	MDCKII	Caco-2	16-HBE	MTD-1A
Claudin-1	Recycled	Recycled	Recycled	Not endocytosed
Claudin-2	Recycled	-	-	-
Claudin-4	Not endocytosed	-	-	-
Occludin	Not endocytosed	Degraded and recycled	Degraded and recycled	Recycled

Table 1.2: Continuous recycling of tight junction proteins is a common feature in diverse epithelial cell lines. Individual TJ proteins are constitutively endocytosed with distinct kinetics in epithelial cell lines derived from different tissues and species. (MDCKII) Madin-Darby canine kidney type II, (Caco-2) human colorectal carcinoma, (16-HBE) human bronchial epithelium, (MTD-1A) mouse mammary epithelium, (-) trafficking rates have not been determined. Table adapted from Chalmers and Whitley (2012).

Various proteins have been implicated in regulating the internalisation and post-endocytic trafficking of TJ proteins. The constitutive recycling of claudin-1 and -2 can be blocked by the expression of a dominant-negative CHMP3 ESCRT protein, which results in the internal accumulation of these claudins in discrete cytoplasmic compartments, potentially by mediating interactions with deubiquitination enzymes (Dukes et al., 2011b). YM201636 is an inhibitor of PIKfyve (FYVE finger-containing phosphoinositide kinase), which also blocks the constitutive recycling of claudin-1 and -2. PIKfyve inhibition may alter the phospholipid composition of endosomes, influencing their interactions with the ESCRT trafficking machinery (Chalmers and Whitley, 2012; Dukes et al., 2012).

The polarised targeting and recycling of TJ proteins is regulated by the Rab family of small GTPases, which act as molecular switches, alternating between GTP- and GDP-bound states to mediate various aspects of vesicular trafficking (Bhuin and Roy, 2014; Kitt et al., 2008; Lu et al., 2015). For example, the endocytosis and recycling of E-cadherin is regulated by Rab5 and Rab11, respectively (Desclozeaux et al., 2008; Kimura et al., 2006; Lock and Stow, 2005). Furthermore, the constitutive endocytic recycling of occludin is dependent on Rab13 function and its binding partner JRAB/MICAL-L2 (Morimoto et al., 2005; Yamamura et al., 2008).

Rab14 is involved in the trafficking of molecules to the apical plasma membrane (Kitt et al., 2008) and colocalises with claudin-1, -2 and -4, but not occludin, mainly in intracellular punctae (Lu et al., 2014). Rab14 interacts with endotubin, a constituent apical endosome protein, to mediate junction formation and recycling of internalised TJ proteins back to the apical junction (McCarter et al., 2010). Rab14 knockdown results in increased TER, which coincides with the specific depletion of claudin-2 and altered endocytic trafficking of claudin-1 and occludin (Lu et al., 2014). Rab14 is proposed to sort claudin-2 out of the degradative pathway by regulating its trafficking out of the recycling endosome (Lu et al., 2014). Claudin-1 and occludin are also recycled significantly faster in Rab14-KD cells (Lu et al., 2014), suggesting that altered TJ protein trafficking may also play a role in mediating epithelial barrier changes (Lu et al., 2014).

As with Rab14, PKCι protects claudin-2 from lysosomal degradation and its depletion causes an increase in TER and decrease in dextran permeability (Lu et al., 2015). PKCι binds to Rab14, which mediates its apical distribution in MDCKII cells (Lu et al., 2015). Therefore, PKCι and Rab14 appear to function in a coordinated manner to regulate tight junction composition through the regulation of claudin-2 trafficking (Lu et al., 2015). PKCι knockdown significantly deceases claudin-2, and increases claudin-4, protein levels, without altering levels of claudin-1, occludin, ZO-1 or E-cadherin (Lu et al., 2015). The current model involves the PKCι-mediated phosphorylation of claudin-2 on S208, which functions to retain claudin-2 in a Rab14-mediated membrane recycling pathway. Taken together, these studies indicate that membrane trafficking and cell polarity pathways intersect at the endosomal compartment to regulate TJ protein trafficking through the interaction of Rab14 and PKCι (Lu et al., 2015).

Interestingly, altered claudin-2 trafficking through depletion of Rab14 or PKCι is also associated with decreased claudin-2 transcription (Lu et al., 2014; Lu et al., 2015). A similar observation has been made regarding Rab25 knockdown and integrin

transcription (Krishnan et al., 2013), suggesting that trafficking of adhesive proteins and receptors may provide signals that regulate their own transcription (Lu et al., 2015). In summary, various trafficking mediators, including ESCRT proteins, protein kinases and Rab GTPases, are required for TJ protein trafficking. However, the specific signalling pathways and post-translational modifications involved in specific cargo selection and the dynamic regulation of these processes during TJ remodelling are poorly understood.

1.5.4 Post-translational modifications

The C-terminal tail of claudins is recognised as an effector of claudin stability and a key site of post-translational modification. (Van Itallie et al., 2004). Yeast two-hybrid studies have been used to identify numerous interactions between TJ proteins and modifying enzymes and various modifications have been shown to occur *in vitro*. However, the majority of these reactions have not been demonstrated *in vivo* and how these modifications are dynamically regulated is poorly understood.

Palmitoylation

Palmitoylation is a lipid modification involving the acylation of cysteine residues with palmitic acid. These “lipid tethers” are thought to promote the association of proteins with lipid membranes (Conibear and Davis, 2010). Claudin family proteins contain conserved membrane-proximal cysteine residues after the second and fourth transmembrane domains (Suzuki et al., 2014; Van Itallie et al., 2005). Cysteine palmitoylation influences the behaviour of claudin-14; mutation of these residues to serine decreases junctional localisation and increases the amount of claudin-14 found in lysosomes (Van Itallie et al., 2005). Other than inefficiently targeting to the junction, palmitoylation-deficient claudin-14 appeared to behave normally, in terms of its ability to organise into TJ strands and regulate barrier function (Van Itallie et al., 2005). The reduced efficiency, rather than failure, in localising to the TJ suggests that palmitoylation is not a strict requirement for normal claudin distribution.

In comparison to prenylation and myristoylation, which are considered to be essentially irreversible, palmitoylation is a reversible process (Conibear and Davis, 2010). Palmitic acid is added to His-Asp-Asp-Cys motifs by protein acyl-transferases (DHHC PATs). There are currently 23 identified mammalian DHHC PATs, which are antagonised by depalmitoylation enzymes called acyl-protein thioesterases (APT1, APT2 and APTL1) (Conibear and Davis, 2010). For example, H-Ras and N-Ras are regulated by reversible palmitoylation allowing them to shuttle between a membrane-bound and cytoplasmic state (Conibear and Davis, 2010). Research into claudin palmitoylation is

in its infancy; the specific enzymes involved in claudin palmitoylation have yet to be identified and it has not been established if claudins are dynamically regulated by rounds of palmitoylation and depalmitoylation.

Ubiquitination

Ubiquitin is a small 8.5kDa protein that is covalently conjugated to target lysine residues of other proteins (Cohen and Tcherpakov, 2010). Although initially associated with protein degradation, ubiquitination is increasingly recognised as a series of complex and diverse modifications that influence various protein properties (Cohen and Tcherpakov, 2010). A yeast two-hybrid screen identified the E3 ubiquitin ligase LNX1p80 as a novel binding partner of claudin-1. Overexpression of LNX1p80 decreased the concentration of claudin-1, -2 and -4 at the TJ. Of note, the localisation of occludin, ZO-1 and E-cadherin were largely unaffected by LNX1p80 overexpression, suggesting claudins may be selectively targeted by specific ubiquitin ligases. LNX1p80 promoted claudin-1 ubiquitination and colocalised with claudins in lysosomes, suggesting that LNX1p80-mediated ubiquitination may drive claudin endocytosis and lysosomal degradation (Takahashi et al., 2009).

Another yeast two-hybrid study found that the HECT E3 ubiquitin ligase Itch could bind to and polyubiquitinate the N-terminal domain of occludin (Traweger et al., 2002). Itch overexpression increased the relative amount of occludin in the soluble fraction, suggesting that it may regulate the stability of occludin at the TJ, potentially by inducing its internalisation or by blocking its recycling (Traweger et al., 2002).

SUMOylation

The addition SUMO-1 (small ubiquitin-like modifier 1) can regulate a number of protein functions including protein-protein interactions, subcellular localisation and trafficking (Van Itallie et al., 2012a). A yeast two-hybrid screen identified ubiquitin-conjugating enzyme E21 (SUMO ligase-1) and E3 SUMO-protein ligase PIAS (protein inhibitors of activated STATs) as binding partners of the C-terminal of claudin-2 (Van Itallie et al., 2012a). Further study showed that claudin-2 is SUMOylated on K218. Interestingly, SUMO-1 overexpression selectively decreases claudin-2 levels along the lateral membrane, while TJ intensity is unaffected. This suggests that SUMOylation of claudin-2 may selectively target lateral membrane-associated claudin-2 for degradation. However, modification of K218 was undetectable in basal conditions and physiological mechanisms that may induce claudin-2 SUMOylation have not been identified (Van Itallie et al., 2012a)

The consensus peri-lysine sequence for SUMOylation is not conserved between all claudins (Van Itallie et al., 2012a). For example, claudin-4 lacks the sequence, suggesting SUMOylation is one potential mechanism for differentially regulating claudin proteins at the post-translational level. Claudin SUMOylation has yet to be demonstrated *in vivo* and the physiological relevance remains unclear. Claudin SUMOylation studies are at a very early stage and further work is required to establish if claudins are dynamically modified and how this may influence their function, localisation or stability.

Phosphorylation

Claudin phosphorylation by WNK kinases

Mutations in the serine/threonine kinases WNK1 and 4 (with no lysine) are associated with pseudohypoaldosteronism type II, or Gordon's syndrome, which is characterised by hypertension, hyperkalemia and hyperchloremic acidosis (Ohta et al., 2006). Large deletions of the first intron of WNK1 increase its mRNA expression levels, while missense mutations that cluster around a putative coiled-coil domain are observed in WNK4. There are two proposed pathogenesis models; a transcellular model where WNK kinases target thioazide-sensitive NaCl transporters and a paracellular model where claudin phosphorylation increases the chloride shunt (Ohta et al., 2006).

Disease-causing WNK mutants have been shown to bind and phosphorylate claudin-1, -2, -3, -4 and -7 (Kahle et al., 2004; Ohta et al., 2006; Tatum et al., 2007; Yamauchi et al., 2004). WNK4 localises to the TJ, while WNK1 is mainly cytosolic (Ohta et al., 2006). WNK kinases phosphorylate claudins on both serine (Tatum et al., 2007) and threonine residues (Ohta et al., 2006), with S206 of claudin-7 identified as a putative WNK phosphorylation site in mutagenesis studies (Tatum et al., 2007). Hyperphosphorylation of claudin C-terminal domains mediated by WNK overexpression or mutation is associated with increased paracellular Cl^- permeability (Kahle et al., 2004; Ohta et al., 2006; Tatum et al., 2007; Yamauchi et al., 2004). The mechanism by which these epithelial barrier changes proceed is not clear; WNK4 phosphorylation of claudin C-terminal residues may induce a conformational change to alter the ionic permeability of the extracellular claudin loops, or could affect claudin interactions with other proteins that bind via their cytoplasmic domains. Furthermore, although WNK kinases appear to be able to bind and phosphorylate many claudins, it is not clear which are the pathologically relevant targets, or how WNK kinases regulate physiological barrier function.

S208 phosphorylation of claudin-2

Phosphorylation of claudin-2 on S208 promotes its membrane retention and reduces its trafficking to lysosomes (Van Itallie et al., 2012b). This site is constitutively phosphorylated in MDCKII cells, with up to 50% of the total claudin-2 pool being phosphorylated at any given time (Van Itallie et al., 2012b). Various localisation-deficient mutants that do not fully localise to the tight junction all show reduced phosphorylation at S208, suggesting that plasma membrane-associated kinases, for example PKCι (Lu et al., 2015), may phosphorylate claudin-2 to augment its function or enhance its retention at the cell surface.

Both S208A and S208E mutants of claudin-2 are targeted to some extent to the plasma membrane, suggesting that a small amount of claudin-2 can localise to the TJ independently of S208 phosphorylation status. More recently, studies have implicated S208 phosphorylation of claudin-2 with its Rab14-mediated recycling (Lu et al., 2015). Claudin-2 is also phosphorylated at a number of other serine, threonine and tyrosine residues on the cytoplasmic C-terminal domain, suggesting that its regulation by phosphorylation is probably highly complex (Van Itallie et al., 2012b).

CK2-mediated phosphorylation of occludin S408

Barrier function can also be regulated through the phosphorylation of occludin. The C-terminus of occludin appears to be heavily phosphorylated, although the functional consequences of phosphorylation of individual sites are highly variable. T403/404 phosphorylation enhances trafficking of occludin to the TJ (Suzuki et al., 2009), whereas Y398/402 phosphorylation reduces trafficking to the TJ by interfering with occludin-ZO-1 interactions (Elias et al., 2009). Of note, occludin is phosphorylated on S408 by casein kinase 2 (CK2). Inhibition of CK2 increases TER and decreases paracellular cation permeability, in a claudin- and ZO-1-dependent manner (Raleigh et al., 2011). Phosphorylated occludin self-associates, allowing claudin-2 to form cation channels through homotypic trans-interactions (Raleigh et al., 2011). In its dephosphorylated state, occludin interacts with claudin-2 via ZO-1 to disrupt claudin-2 pore formation (Raleigh et al., 2011). Thus, the phosphorylation states of several residues in the C-terminal of occludin appear to regulate its interaction with ZO-1, allowing it to modulate epithelial barrier properties by directly influencing claudin interactions.

MAP kinase phosphorylation of claudin-1 T203

The phosphorylation of claudin-1 on T203, a putative MAP kinase phosphorylation site, has been reported to be required for epithelial barrier formation (Fujibe et al., 2004).

However, T203 is only conserved between mouse and rat, with an alanine present in this position in the corresponding chicken, cow, dog and human sequences. Furthermore, this threonine residue is not conserved in any other human claudin. The lack of conservation implies that phosphorylation of this site is not physiologically essential and unlikely to be relevant to studies in canine MDCKII cells.

EphA2 phosphorylation of claudin-4 Y208

Eph receptors and their ephrin ligands are widely expressed in epithelia and mediate cell-cell interaction. Upon cell contact, EphA2 is activated by binding of its cognate ephrin to modulate claudin-4 expression and localisation (Tanaka et al., 2005). EphA2 expression increases phosphorylation of claudin-4 on Y208, part of the C-terminal YV motif involved in binding the PDZ domains of ZO-1/-2. Phosphorylation of this motif attenuates the interaction between claudin-4 and ZO-1 and decreases the incorporation of claudin-4 into the TJ. Furthermore, claudin-4 can restrain the oncogenic activity of EphA2, suggesting that they may reciprocally regulate one another (Shang et al., 2014). Given that the YV motif is highly conserved between claudins (Itoh et al., 1999) its phosphorylation by EphA2, other Eph receptors or other unrelated kinases, may represent a widely applicable mechanism that regulates the incorporation of claudins into TJ strands.

Aldosterone-induced threonine phosphorylation of claudin-4

RCCD2 (rat cortical collecting duct) cells exhibit a “tight” phenotype with basal TER of ~5000Ω.cm^2 (Le Moellic et al., 2005). Treatment of RCCD2 cells with aldosterone specifically increases threonine phosphorylation of claudin-4, without affecting its overall expression level or subcellular localisation (Le Moellic et al., 2005). This occurs concurrently with a decrease in TER and increase in paracellular permeability to iodine, but decreased permeability to mannitol. However, the kinase responsible and specific residues targeted were not identified.

The C-terminal tails of claudins are heavily phosphorylated and the functional consequences of specific site modifications are beginning to be unravelled. Phosphorylation can alter protein stability, localisation, protein-protein interactions and incorporation into the TJ and possibly induce conformational changes to alter pore permeability. Therefore, direct phosphorylation of claudins, occludin or other TJ proteins is becoming increasingly recognised as a mechanism that will permit the dynamic regulation of TJ structure, composition and function.

1.6 Emerging roles for tight junction proteins in cancer

1.6.1 Epithelial-mesenchymal transition

The epithelial-mesenchymal transition (EMT) is involved in developmental morphogenesis, regenerative processes like wound healing, and in diseases including fibrosis and carcinoma (Doehn et al., 2009; Kalluri and Weinberg, 2009). Although EMT exists as three distinct subtypes, these processes share common features: i) the loss of cell junctions, ii) the loss of apicobasal polarity, iii) the adoption of mesenchymal, or front-rear, polarity and iv) the increased ability to migrate and invade. TJs are implicated in all of these processes; they are intrinsic components of cell-cell junctions, regulate apicobasal polarity through fence and gate functions and by interacting with the Par3/aPKC complex, and also have pro- and antimigratory roles (see Section 1.2).

Cells that have undergone EMT can revert to an epithelial state via a mesenchymal-epithelial transition (MET). However EMT and MET do not represent committed one-way processes; cells exhibit high levels of plasticity to adopt increasingly epithelial or mesenchymal characteristics (Huang et al., 2012). The gradual progression of an epithelial cell into a motile mesenchymal state proceeds through the gradual disassembly of epithelial junctions, from the apical to basal side of the cell. Early stages of TJ breakdown and the accompanying disruption of apicobasal polarity (Figure 1.9A) are followed by early intermediate stage AJ and desmosome disassembly, initially through post-translational mechanisms (Figure 1.9B) (Huang et al., 2012). Late intermediate stages are characterised by the transcriptional downregulation of junction proteins by master transcriptional regulators (Figure 1.9C). EMT is only “complete” when TJ, AJ and desmosomes proteins are fully transcriptionally downregulated and the cell has adopted mesenchymal traits, which promote an invasive phenotype to favour metastasis (Figure 1.9D) (Huang et al., 2012). These discrete stages of EMT serve only to highlight that the transition is gradual, but do not necessarily reflect the degree of phenotypic plasticity and reversibility that actually exists. However, TJ disruption and the loss of polarity is considered a relatively early event in the transformation of growth-arrested and organised epithelial cells into mesenchymal-like cells with increased capacity for migration, invasion and metastasis (Huang et al., 2012) (Martin 2014).

EMT is governed by a set of master regulators including Snail, Twist and Zeb transcription factors (Savagner, 2010). Snail binds to E-box elements in the promoter regions of E-cadherin, occludin and claudin-3, -4 and -7 to repress their activity (Ikenouchi et al., 2003). In contrast, Snail does not affect the mRNA or protein levels of ZO-1, although it is lost from areas of cell-cell contact and accumulates in the

cytoplasm (Ikenouchi et al., 2003). This suggests that TJs are disassembled during EMT through the transcriptional downregulation of specific TJ components.

In a similar fashion, Snail and Slug repress claudin-1 expression in MDCK cells by binding to E-box promoter elements, causing a complete loss of TER (Martínez-Estrada et al., 2006). Furthermore, Snail/Slug levels are inversely correlated with claudin-1 expression in invasive human breast tumours (Martínez-Estrada et al., 2006). Snail expression also induces the loss of MDCKII TER and increases paracellular permeability to Na^+ and Cl^- through the downregulation of claudin-4 and -7, and to a lesser extent claudin-2 (Carrozzino et al., 2005). These studies suggest that during EMT, TJs are disassembled through the direct transcriptional repression of occludin and claudin family proteins. Additionally, altered endocytosis and recycling of E-cadherin have emerged as alternative mechanisms allowing cells to undergo dynamic morphological changes (Bryant and Stow, 2004; Palacios et al., 2001; Palacios et al., 2005). Endocytic circuitries are frequently “rewired” in physiological transition states to impart phenotypic plasticity by modulating adhesive junctions, the distribution of polarity regulators and actomyosin dynamics, allowing rapid adaption to dynamically changing microenvironments (Corallino et al., 2015). Although structural alterations to TJs and increased epithelial leakiness have been observed in preneoplastic growths and in adenocarcinoma (Mullin et al., 2005), little is known about the role of TJ protein trafficking during tumourigenesis, possibly due to the paucity of *in vitro* cell lines that form functional TJs (Huang et al., 2012).

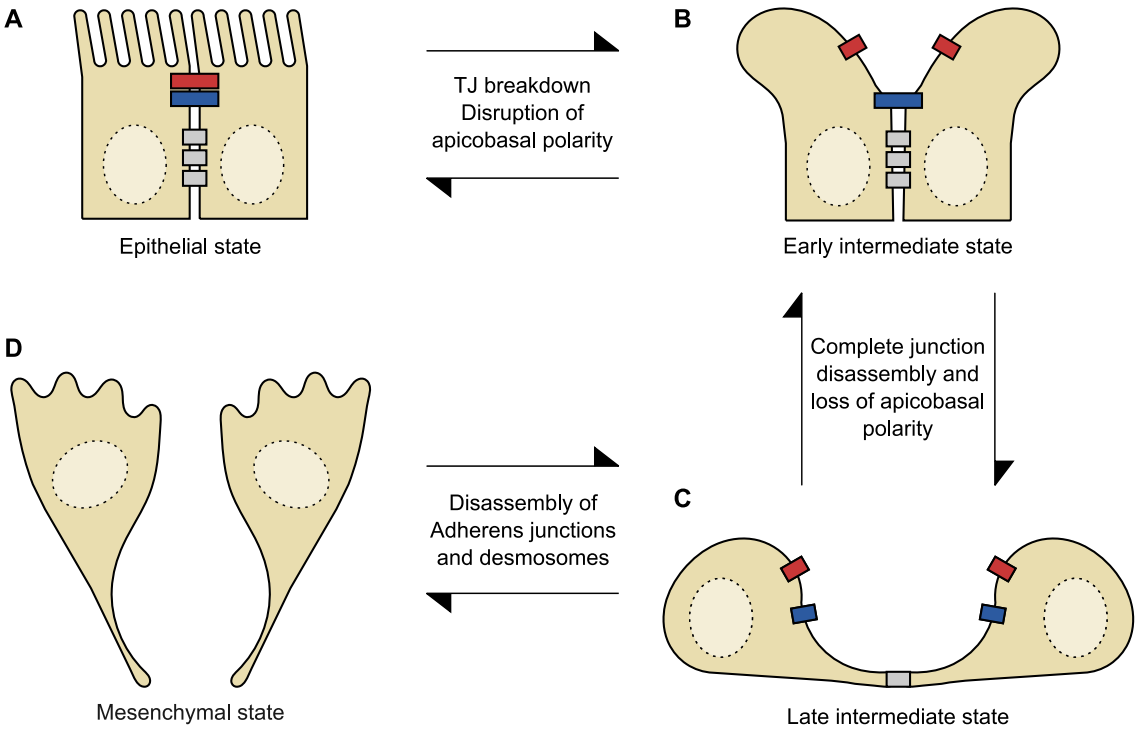

Figure 1.9: Alterations in adhesive cell-cell junctions and cell polarity during epithelial-mesenchymal transition. (A) Epithelial cells are characterised by a highly polarised structure and a series of cell-cell junctions, including the TJ (red), AJ (blue) and desmosomes (grey). During the epithelial-mesenchymal transition, these cell-cell contacts loosen and “unzip” through the sequential loss of the TJ (B), AJ (C) and desmosomes (D). This transition proceeds via intermediate stages with a high degree of plasticity and reversibility. Dynamic regulation of junction protein trafficking may be involved in TJ and AJ remodelling during these transitions. Image adapted from Huang (2012).

1.6.2 Differential claudin expression in cancer

Although there is no systematic sequence data on claudin mutations in any tumour type (Turksen and Troy, 2011), their expression is differentially regulated in a huge number of tumours (Table 1.3) (Ding et al., 2013; Kwon, 2013). However, there is no overriding pattern, with the specific claudins being either up or downregulated depending on tumour type and stage (Turksen and Troy, 2011). Therefore, it would be an oversimplification to state that epithelial barrier function is simply "lost" during tumourigenesis, when more complex changes in the expression and localisation of individual TJ components are clearly evident in diverse tumour types.

Although many studies implicate TJ proteins in tumour suppression by providing a barrier to uncontrolled tumour growth and increased migration (Royer and Lu, 2011), various TJ components are actually upregulated in some tumour types. For example, claudin-4 is not normally expressed in ovarian epithelia, but was found to be highly expressed in pancreatic, ovarian and primary breast tumours (Boylan et al., 2011; Jiwa et al., 2014; Neesse et al., 2012). Increased claudin-4 expression generally favours prognosis, but is also associated with cancer progression in some contexts (Neesse et al., 2012). Claudin-4 expression may inhibit primary tumour growth but promote the cohesion of established metastases, conferring a survival advantage in the host tissue (Jiwa et al., 2014; Lin et al., 2013; Shang et al., 2012; Shang et al., 2014).

Furthermore, claudin-2 expression is significantly upregulated in colorectal cancer and correlates with cancer progression (Dhawan et al., 2011). Claudin-2 expression increases colorectal cancer cell proliferation, anchorage-independent growth and tumour growth *in vivo*. Mechanistically, this may be mediated through increased paracellular permeability to luminal carcinogens, as well as growth factors, which would gain increased access to activate basolateral receptors and promote neoplastic transformation and growth (Dhawan et al., 2011).

Taken together, these studies indicate that the regulation of claudins in cancer is highly complex, with context-dependent consequences. Claudin expression can correlate positively or negatively with prognosis, depending on whether they are expressed in primary or metastatic tumours. Furthermore, the effect of specific changes in TJ composition on paracellular permeability may gain functional significance depending on the tissue microenvironment in which they are situated.

While complex and differential claudin expression is widely observed in cancers of many origins, there is currently a lack of data regarding relevant claudin mutations

(Turksen and Troy, 2011). Claudin-1 mutations cause neonatal sclerosing cholangitis associated with ichthyosis, claudin-14 mutations are associated with nonsyndromic recessive deafness (Wilcox et al., 2001) and mutations to either claudin-16 or -19 underlie hereditary hypomagnesia (Kang et al., 2005). While these specific disease-causing claudin mutations have been identified, no corresponding mutations have been observed in cancer. Future studies will be required to determine whether and how claudins or other TJ-associated proteins are mutated in cancer, as well as how claudin expression is regulated by epigenetic mechanisms, EMT-associated transcription factors, specific oncogenes and related signalling pathways.

Tissue	Claudin-1	Claudin-2	Claudin-3	Claudin-4	Claudin-7
Breast	↓	↓	↓	↑↓	↓
Cervical	↑	↑	-	↑	↑
Colorectal	↑	-	↑	↑	
Oesophageal	-	-	↑	↑	↓
Kidney	↑↓	-	↑	↑↓	↑
Gastric	-	-	-	-	-
Liver	↓	-	-	-	-
Melanoma	↑	-	-	-	-
Ovarian	-	-	↑↓	↑↓	-
Prostate	↓	↓	↑	↑	↓
Pancreatic	-	-	-	↑	-
Uterine	-	-	↑	↑	-

Table 1.3: Differential regulation of claudin expression levels is frequently observed in cancers of diverse origins. (↑) Upregulated, (↓) Downregulated, (↑↓) Up- or downregulated, (-) No reported changes in expression. Data combined from Ding et al (2013) and Kwon (2013).

1.6.3 Paracellular permeability in tumourigenesis

Many growth factor receptors are largely confined to the basolateral surface of epithelial cells, where they are functionally segregated from relatively high luminal ligand concentrations by an intact TJ. This has been demonstrated *in vitro*, where apical heregulin-α only activates basolateral erbB2 receptors following epithelial damage or when TJs are disassembled by depleting extracellular calcium (Vermeer et al., 2003). This suggests that the loss of epithelial barrier function may result in the constitutive exposure of growth factor receptors to ligands, driving aberrant downstream signalling and proliferation. It has also been suggested that changes in

intercellular pH and electrical cues influence cell proliferation, although these suggestions are largely speculative in nature (Tsukita et al., 2008).

1.6.4 Cell Migration

Increased junctional levels of claudins generally impair cell migration in MDCKII cells (Ikari et al., 2011a; Ikari et al., 2012b). In addition to increasing TER, claudin-2 knockdown increases the rate of recovery in an MDCKII scratch wound migration assay (Ikari et al., 2011a). This proceeds without any significant increase in cell proliferation, and is dependent on the increased expression of matrix metalloproteinase (MMP9), at both the mRNA and protein level (Ikari et al., 2011a). Furthermore, the forced expression of claudin-2 effectively blocks the induction of MMP9 and reduces cell migration to basal levels (Ikari et al., 2011a). This suggests that the loss of claudin-2 expression leads to the transcriptional upregulation of proteinases that enhance cell migration through the degradation and remodelling of the extracellular matrix (Ikari et al., 2011a). Claudin-4 overexpression decreases cell migration in an MDCKII scratch-wound assay and also increases the extent of cell-cell contact and adhesion, by increasing the proportion of claudin-1, -3 and -4 associated with ZO-1 at the apical junction (Ikari et al., 2012b).

The expression of individual claudin proteins is frequently deregulated in various cancers. While EMT is generally associated with TJ loss and the transcriptional downregulation of its components, individual TJ proteins can be up- or downregulated in different tissues and cancers. TJ deregulation may contribute to tumourigenesis through changes in paracellular permeability and apicobasal polarity in addition to emerging roles in regulating cell migration. However, the specific impact of different oncogenes and their associated signalling pathways on individual TJ proteins is poorly understood.

1.7 The RAF/MEK/ERK pathway

Mitogen-activated protein kinases form functional signalling modules that relay messages from the cell surface to nuclear and cytoplasmic effectors, which determine a cell's response to diverse stimuli (Figure 1.10A) (Santarpia et al., 2012). Growth factor receptors expressed at the cell surface, including the receptor tyrosine kinases (RTKs) epidermal growth factor receptor (EGFR) and Met, are activated upon binding of their cognate growth factor ligands (Wortzel and Seger, 2011). Ligand-binding normally induces RTK dimerisation and autophosphorylation of the corresponding dimer partner through the intrinsic tyrosine kinase activity of each RTK (Roskoski, 2012). Various phosphotyrosine residues on the cytosolic RTK domain then serve as docking sites for adaptor proteins that contain SH2 or PTB domains (Roskoski, 2012). GRB2 is an adaptor protein that binds to activated receptors and recruits Sos, a guanine exchange factor (GEF), which converts GDP-bound Ras into its active GTP-bound form (Sturm et al., 2010). Active Ras activates a plethora of downstream signalling pathways including PI3 kinase, Rac, Rho and RAF/MEK/ERK pathways (Santarpia et al., 2012).

In its inactive state, RAF protein exists in a closed conformation, where the N-terminal region sterically inhibits the catalytic region of the C-terminal kinase domain (Matallanas et al., 2011). The RAF activation mechanism is complex and proceeds via the following steps: i) the dephosphorylation of CRAF to unmask the RBD and CRD domains, enabling Ras interaction and membrane recruitment, ii) direct molecular interaction of CRAF with Ras, iii) phosphorylation of the CRAF activation segment in the CR3 domain and N-region, by proteins including Src and JAK family kinases, iv) homo- and heterodimerisation of RAF monomers, which enhances the kinase activity and signalling of RAF and v) deactivation initiated by binding of protein phosphatases that return CRAF to its inactive state (Matallanas et al., 2011).

In their active phosphorylated state, RAF proteins specifically bind and phosphorylate MEK1/2 kinases on neighbouring serine residues, leading to their catalytic activation (Figure 1.10A) (McMahon, 2001). MEK1/2 are dual specificity kinases that activate ERK1/2 by phosphorylating threonine and tyrosine residues in a conserved TEY motif (Figure 1.10A) (Butch and Guan, 1996). This facilitates the translocation of ERK1/2 to the nucleus, where they interact with a huge number of transcriptional activators and repressors to modulate gene expression (Figure 1.10A). ERK1/2 also have a large number of substrates in the cytoplasm and other subcellular organelles (Wortzel and Seger, 2011), allowing the RAF/MEK/ERK pathway to mediate a diverse range of

cellular processes, including proliferation, differentiation and apoptosis, in a stimulus-dependent manner (O'Neill and Kolch, 2004).

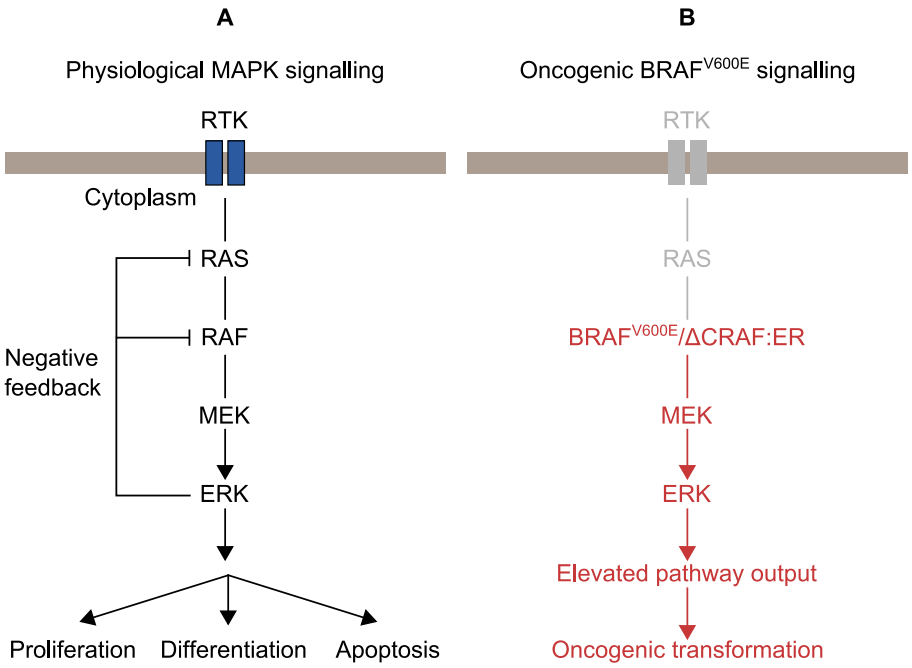

Figure 1.10: Physiological and pathological RAF/MEK/ERK pathway signalling. The RAF/MEK/ERK pathway is involved in the transduction of extracellular signals from cell surface receptors, including receptor tyrosine kinases (RTKs), to the cell interior, and participates in the regulation of diverse responses to a number of stimuli. (A) In a physiological setting, RTK activation leads to activation of the GTPase, Ras, which recruits RAF kinase for activation at the plasma membrane. RAF is activated in a complex process involving phosphorylation, dephosphorylation, dimerisation and transactivation. RAF is the first member of a three-tiered kinase cascade and phosphorylates MEK, which in turn phosphorylates and activates ERK. ERK has many substrates in the nucleus and throughout the cell and can regulate various processes in stimulus-dependent manner. Activated ERK also provides negative feedback at various levels of the cascade to inhibit its own activation. (B) BRAF is frequently mutated in cancer, with an activating V600E mutation being particularly prevalent. Activating mutations generate a constitutively active BRAF kinase, the activity of which is independent of upstream activation by RTKs or Ras. BRAF^{V600E} is also insensitive to ERK-mediated negative feedback, resulting in elevated pathway output and ERK-dependent transformation. Experimentally, this can be mimicked by expression of oncogenic BRAF variants or non-physiological inducible-activity RAF constructs, for example ΔCRAF:ER.

Stimuli that activate the RAF/MEK/ERK pathway through the activation of RTKs and Ras will also lead to the simultaneous activation of other parallel signalling pathways. Various studies have implicated the RAF/MEK/ERK pathway in the regulation of TJ permeability, and have involved the use of growth factors in combination with small molecule inhibitors to independently block downstream pathways. As a result, it is difficult to elucidate the exact contribution of the RAF/MEK/ERK signalling pathway, when other pathways will inevitably be activated. By contrast, a limited number of studies have activated the pathway at the level of RAF or MEK. The expression of oncogenic or non-physiological constitutively active RAF proteins provides the ability to

specifically activate the RAF/MEK/ERK pathway due to the highly specific nature of RAF/MEK and MEK/ERK interactions (Figure 1.10B).

1.7.1 RAF, MEK and ERK kinases

ERK kinases appear to be the only physiological substrates of MEK (Roberts and Der, 2007; Shaul and Seger, 2007). In contrast ERK has more than 150 identified nuclear and cytoplasmic substrates (Yoon and Seger, 2006). The ability of a common pathway to mediate different outcomes is thought to be achieved through a combination of differential signal strength and duration, crosstalk with other signalling cascades and scaffolding complexes that connect activators and effectors and target them to different subcellular locations (O'Neill and Kolch, 2004; Shaul and Seger, 2007). Although the effects of RAF/MEK/ERK activation are often due to changes in gene expression, ERK has numerous cytoplasmic substrates and has been implicated in regulating clathrin-independent membrane trafficking at the apical recycling endosome by interacting with the GTPase Arf6 (Robertson et al., 2006).

MEK kinases are the only widely accepted RAF substrates (Matallanas et al., 2011). However, MAP kinase-independent roles of RAF kinases have also emerged (Ehrenreiter et al., 2005; Hindley and Kolch, 2002; Matallanas et al., 2011). These include the suppression of proapoptotic kinases, ASK1 and MST2, the regulation of cell motility by modulating Rho activity (Ehrenreiter et al., 2005) and the induction of aneuploidy (Kamata et al., 2010). Notwithstanding, activation at the level of RAF still permits activation of the pathway in a far more specific manner than through growth factor stimulation, which will simultaneously activate other RTK- and Ras-dependent pathways. MEK-dependent and -independent effects can be further distinguished through the use of small molecule inhibitors of RAF, MEK and ERK.

The first *raf* gene (rapidly accelerated fibrosarcoma) identified was a retroviral oncogene, *v-raf*, which is transduced by the murine sarcoma virus (Bonner et al., 1985; Matallanas et al., 2011). Raf-1, or CRAF, the protein encoded by the corresponding cellular proto-oncogene *c-raf*, was shown to mediate the cellular effects of growth factors by acting as an effector of Ras, and an activator of MEK (Matallanas et al., 2011). Two additional RAF isoforms, ARAF and BRAF, were subsequently identified (Beck et al., 1987; Ikawa et al., 1988). The three RAF isoforms, encoded by independent genes, share MEK1/2 kinases as substrates, but can elicit distinct biological outcomes (Matallanas et al., 2011). BRAF, CRAF and ARAF have similar structures with three conserved regions (CR1 – 3) (Figure 1.11A) (Matallanas et al., 2011). CR1 contains a Ras-binding domain (RBD) and cysteine-rich domain (CRD),

which mediate the interaction with Ras at the plasma membrane. CR2 contains inhibitory phosphorylation sites that participate in the negative regulation of Ras-binding and RAF activation. CR3 features the kinase domain, including the activation loop, the phosphorylation of which is crucial for kinase activation (Matallanas et al., 2011). Functionally, the RAF structure can be considered as a regulatory N-terminal domain consisting of the RBD, CRD and inhibitory phosphorylation sites, and a C-terminal catalytic domain, which includes the active site and phosphorylation sites that are necessary for kinase activation (Matallanas et al., 2011). The regulatory domain acts to restrain the activity of the catalytic domain, and its removal generates truncated and constitutively active kinases, referred to as ΔARAF, ΔBRAF and ΔCRAF (Figure 1.11) (Stanton et al., 1989).

The three RAF isoforms exhibit distinct biochemical properties; BRAF exhibits greater kinase activity than CRAF, and in turn ARAF. This is explained by differences in their modes of activation. RAF activation requires phosphorylation of at least two sites, the N-terminal acidic motif (NtA) and the activation loop (Hu et al., 2013). In ARAF and CRAF, the NtA motif is comprised of SSYY residues (S = serine, Y =tyrosine) (Figure 1.11). For full activation, all four sites must be negatively charged (Emuss et al., 2005). At the plasma membrane, tyrosine residues are phosphorylated by Src and serine residues by PAK or PKC family kinases (Hu et al., 2013). Following NtA phosphorylation, RAF monomers form asymmetric dimers, with one partner acting as the activator, and the other as a receiver (Hu et al., 2013). NtA phosphorylation is required for the activator to allosterically induce cis-autophosphorylation of the receiver kinase, which is required for its full activation (Hu et al., 2013). In contrast to ARAF and CRAF, the NtA motif of BRAF is comprised of SSDD residues (S = serine, D = aspartic acid) (Figure 1.11). Therefore, the N-region is exhibits a constitutive negative charge due to the presence of the two aspartic acid residues combined with constitutive serine phosphorylation (Emuss et al., 2005). As a result, activation of BRAF is relatively simple, requiring activation loop phosphorylation induced by Ras activation, while ARAF and CRAF require additional tyrosine and serine phosphorylation events (Marais et al., 1997). Figure 1.11 illustrates the structural similarities and differences between RAF isoforms.

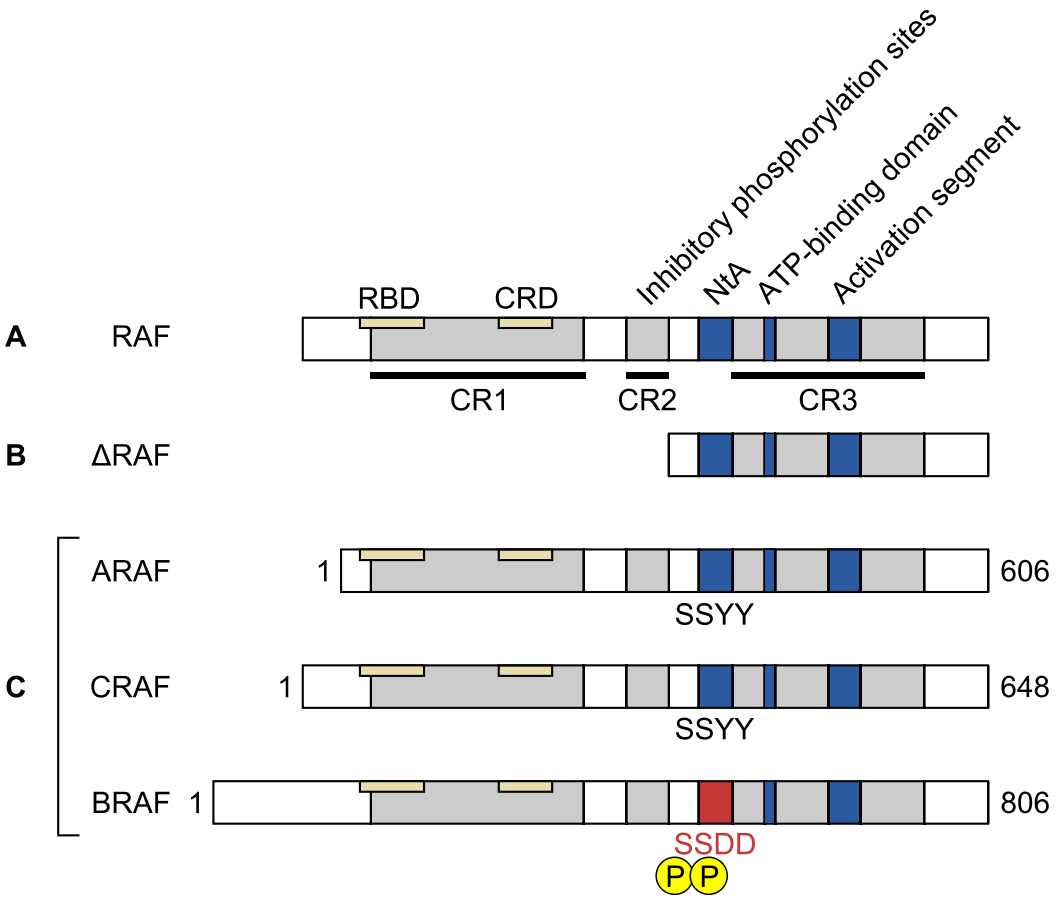

Figure 1.11: Similarities and differences of RAF kinase isoforms. RAF kinases share conserved structural features. All RAF isoforms have three conserved regions (CR1 – 3). CR1 contains a Ras-binding domain (RBD) and cysteine-rich domain (CRD), which are involved in Ras-binding. CR2 contains inhibitory phosphorylation sites that act to restrain the kinase activity. CR3 contains the active site and other features including the N-terminal acidic (NtA) motif and activation segment, which must be phosphorylated to achieve full kinase activity. (B) The regulatory N-domain (CR1 and CR2) of A, B or CRAF inhibits the kinase activity of the catalytic C-domain. Removal of CR1 and CR2 generates truncated and constitutively active ΔRAF kinases. (C) During activation, the NtA of ARAF and CRAF, which is comprised of serine (S) and tyrosine (Y) residues, must be phosphorylated to allow asymmetric RAF dimerisation, allosteric transactivation and cis-autophosphorylation of the activation segment. The presence of aspartic acid (D) residues and constitutive serine phosphorylation confers a constitutive negative charge to the BRAF NtA, “priming” it for single-step activation through phosphorylation of the activation segment. As a result, BRAF exhibits relatively high endogenous kinase activity and is particularly prone to activating mutations that mimic activation segment phosphorylation, for example the oncogenic V600E mutation. Image adapted from Matallanas (2011).

1.7.2 RAF/MEK/ERK signalling in cancer

The RAF/MEK/ERK signalling pathway is frequently activated in cancer through oncogenic mutations to RTKs, Ras, and RAF proteins (Table 1.4). The “priming” negative charge of the N-region not only underlies the high endogenous activity of BRAF, but also results in its frequent mutation in cancer; BRAF can be activated by single point mutations that mimic activation loop phosphorylation, while ARAF and CRAF activation is a multistep process (Emuss et al., 2005). There is a particularly high incidence of BRAF mutations in thyroid, colorectal and biliary tract carcinoma as well as in melanoma (Table 1.4) (Kamata and Pritchard, 2011), with more than 40 different mutations in the *braf* gene identified in human cancer (Cantwell-Dorris et al., 2011). Activating mutations cluster in the glycine-rich loop and activation segments and target residues involved in the stabilisation of interactions between these regions. Mutations frequently disrupt this hydrophobic interaction, destabilising the inactive conformation to render BRAF constitutively active (Cantwell-Dorris et al., 2011).

Over 90% of *braf* mutations are accounted for by a single point mutation at position 1799 (Cantwell-Dorris et al., 2011; Davies et al., 2002). This mutation causes the substitution of valine for glutamic acid at codon 600 (V600E). The negatively charged glutamic acid mimics phosphorylation of the activation segment, and disrupts its self-inactivating interaction with the P-loop (Röring et al., 2012). The V600E mutation increases BRAF activity 500-fold and also renders BRAF insensitive to ERK-mediated negative feedback, leading to increased transcriptional output and ERK-dependent transformation (Pratilas et al., 2009). $BRAF^{V600E}$ activity does not appear to require RAF dimerisation (Röring et al., 2012). and is independent of upstream stimuli, allowing cells to become self-sufficient in growth signals that rely on the RAF/MEK/ERK pathway (Cantwell-Dorris et al., 2011). $BRAF^{V600E}$ mutation alone is insufficient for cell transformation (Tsao et al., 2012) and coincident mutations, for example to p53, may be required for tumourigenesis (Patton et al., 5AD). However, cells exhibit $BRAF^{V600E}$ oncogene addiction, where they depend on sustained ERK signalling to maintain growth factor-independent survival (Wickenden et al., 2008). For these reasons therapeutic targeting of the RAF/MEK/ERK pathway has proved to be relatively successful for certain cancer types (Roberts and Der, 2007).

Tissue	Percentage of cases with point mutations (%)						
	KRAS	NRAS	HRAS	BRAF	CRAF	ARAF	MEK1
Adrenal gland	0.2	2.4	1.2	1	0	0	0
Autonomic ganglia	0.2	1.3	0.3	0.3	0.3	0	0.2
Biliary tract	23.4	2.5	0.5	5.5	0.8	1.6	0
Bone	1.7	1.8	1.3	7.8	0	0	0
Breast	1.6	0.7	0.3	1.2	0.3	0.4	0.4
Central nervous system	0.9	0.7	0.3	7.9	0.1	0	0
Cervix	5.8	0.5	4.5	0.8	0	0	0
Endometrium	14.1	2.1	0.5	1.4	2	2.3	0.9
Eye	1.6	2.3	0	9.5	0	0	0
Genital tract	8.8	2.7	1.1	2	0	0	0
Haematopoietic/lymphoid	4.4	8.7	0.2	10.2	0.1	0.1	1.5
Kidney	0.5	0.3	0.1	2.1	0.3	0.2	0.1
Large intestine	34.4	4.1	0.5	12.5	2.9	2.2	2.6
Liver	2.1	0.4	0.1	1.5	0.8	0.6	0.1
Lung	16.5	0.6	0.5	2.2	0.7	0.8	0.6
Meninges	0	6.6	0	0.7	0	0	0
Oesophagus	1.8	0	0.4	0.4	0.2	0.3	0
Ovary	11.6	0.8	0.1	7.1	0.1	0.4	0.1
Pancreas	57	0.8	0	1.5	0.3	0.1	0.1
Peritoneum	45.2	0	0	0	0	0	0
Pituitary	0	0	3.2	17.8	0	0	0
Pleura	3.4	3.6	0	2.3	0	0	0
Prostate	4.5	0.7	2.6	1.5	0.5	0	0.1
Salivary gland	2.5	0.7	8.7	0.6	0	0	0
Skin	2.3	15.6	11.5	41.3	2.1	1	4.8
Small intestine	22.9	0.8	0	4.4	0	0	0
Soft tissue	3.9	3.4	3.2	1.8	0.3	0	0.2
Stomach	6	1	1.2	1.1	2	2	1.8
Testis	3.8	2.4	3.9	2.6	0	0	0
Thyroid	1.8	6.7	3.8	41.3	0.2	0.2	0
Upper aerodigestive tract	2	1.5	5.9	1	0.5	0	0.2
Urinary tract	4.3	1.2	9.1	2.2	0.4	0.4	0

Table 1.4: A summary of RAS/RAF/MEK/ERK pathway mutations in primary human cancer samples. Mutations that activate the RAS/RAF/MEK/ERK pathway are common in cancer. There is particular high incidence of KRAS mutations in pancreatic, colorectal and biliary tract cancers, although Ras will simultaneously activate other signalling pathways in addition to the RAF/MEK/ERK pathway. Specific activating mutations at the level of RAF are also common, with BRAF more frequently mutated than CRAF or ARAF. BRAF mutations are particularly prevalent in thyroid, colorectal and biliary tract carcinoma, as well as in melanoma. (ND) not determined. Rare point mutations to CRAF and ARAF are indicated by the number of cases in brackets. Data obtained from the Catalogue of Somatic Mutations in Cancer (COSMIC) database (Forbes et al., 2014).

1.7.3 Experimental modulation of RAF/MEK/ERK signalling

Specific activation of the RAF/MEK/ERK pathway has been achieved through the expression of variously modified versions of kinases at each tier of the cascade. MEK can be rendered constitutively active by introducing a double S218/222D mutation, mimicking RAF-dependent regulatory site phosphorylation (Lemieux et al., 2011). Constitutively active ERK constructs have recently been generated by introducing L84P/S162D mutations in the active site and an additional D330N mutation to inhibit the binding of inhibitory phosphatases to the CD site (Rian et al., 2013). Conversely MEK^{K97M} and ERK^{K52R} mutations generate catalytically inactive kinases (Khoo et al., 2003; Mansour et al., 1994). Deletion of the conserved N-terminal CR1 and CR2 regions of all three RAF isoforms yield constitutively active forms (ΔARAF, ΔBRAF ΔCRAF) that can elicit cell transformation (Figure 1.11B) (Stanton et al., 1989).

Although useful in an experimental setting, the expression of *bona fide* oncogenic variants, such as $BRAF^{V600E}$, presents a more pathologically relevant approach. The different transcriptional outputs of cells transformed by RTK or $BRAF^{V600E}$ mutation indicate that although various mutations activate the RAF/MEK/ERK pathway, differences in regulatory and feedback mechanisms can result in distinct biological outcomes (Pratilas et al., 2009). In addition, fusion of the N-terminally truncated ΔRAF proteins to the ligand-binding domain of the estrogen receptor generates inducible-activity constructs – the activity of which is dependent on the presence of an activating ligand hormone (McMahon, 2001). This approach has recently been extended to generate conditionally active versions of $BRAF^{V600E}$, providing a method of rapidly and reversibly activating the RAF/MEK/ERK pathway. These tools offer increased control of signal strength and duration and the ability to study temporal or dynamic effects on cell phenotype and behaviour.

In addition to catalytically inactive MEK and ERK kinase constructs, the RAF/MEK/ERK pathway can be effectively inhibited using small molecule inhibitors of MEK. PD0325901 is a second generation selective and non ATP-competitive inhibitor of MEK1 and 2, with IC_{50} values of approximately 1nM (Thompson and Lyons, 2005). PD0325901 is one of a series of benzhydroxamate MEK inhibitors that bind to an interior hydrophobic pocket adjacent to the ATP binding site. As a result, the MEK catalytic site is partially blocked, preventing entry of the ERK activation loop and its subsequent phosphorylation (Thompson and Lyons, 2005). PD0325901 exhibits greater potency than commonly used MEK inhibitors such as U0126, effectively blocking phosphorylation of ERK1 and 2 at 25nM compared to 10μM U0126 (Bain et al., 2007). Only a small number of other kinases are marginally inhibited by

PD0325901, even at higher concentrations of 10μM (Bain et al., 2007). Therefore, although clinically limited by concerns over neurological toxicity (Pratilas and Solit, 2010), the use of PD0325901 in an experimental setting provides the ability to inhibit RAF/MEK/ERK pathway signalling in a highly specific manner. Specific small molecule inhibitors in combination with oncogenic and inducible activity RAF kinase constructs provide a set of molecular tools for probing the specific contribution of the RAF/MEK/ERK signalling pathway to TJ regulation.

1.8 Tight junction regulation by the RAF/MEK/ERK pathway

1.8.1 ERK activity correlates with renal epithelial permeability

In the kidney, blood is forced into the Bowman's capsule under high pressure, and the resulting filtrate passes along the nephron, through the proximal tubule, loop of Henle, distal tubule and collecting duct, and accumulates in the bladder (Figure 1.12). As the tubule contents pass along the nephron, the selective reabsorption of salts and water through transcellular and paracellular pathways produces an increasingly concentrated filtrate. The epithelial barrier gradually increases, from a "leaky" permeable epithelium in the proximal tubule, to a "tighter" resistant epithelium in the distal tubule and collecting duct (Figure 1.12). This increase in epithelial sealing is required to effectively contain the concentrated filtrate and prevent diffusion into the surrounding tissue via the paracellular pathway (Flores-Benítez et al., 2007). Epithelial tightness correlates with ERK activity *in vivo* (Masaki et al., 2004). Differential claudin expression is observed in different renal nephron segments (Hou et al., 2013). For example, the cation-pore forming claudin-2 is confined to the highly permeable proximal tubule and descending limb of Henle (Figure 1.12) (Hou et al., 2013). Renal epithelial permeability is inversely correlated with the expression of EGF/EGFR (Ikari 2011). Furthermore, in normal human and rat kidney, phosphorylated ERK is largely confined to the cytoplasm of cells in the high resistance collecting duct (Masaki et al., 2004). These observations suggest that EGFR signalling may influence the composition or properties of the TJ, at least partially through the RAF/MEK/ERK pathway (Figure 1.2).

Consistent with *in vivo* observations, ERK activity correlates with the TER of renal cell lines *in vitro* (summarised in Table 1.5). MDCKI cells exhibit high endogenous levels of active ERK and a high TER of ~4000Ω.cm^2, whereas MDCKII cells exhibit low active ERK levels and have much lower TER values of <300Ω.cm^2 (Dukes et al., 2011a). 94D mouse renal collecting duct cells also exhibit high TER values of ~4000Ω.cm^2 and have high baseline levels of phosphorylated ERK (Lipschutz et al., 2005). Crucially, leaky and tight renal cell lines can be interconverted by the activation or inhibiton of RAF/MEK/ERK signalling. The TER of leaky MDCKII cells can be increased through

treatment with EGF or HGF, or the expression of hormone-inducible RAF kinase or constitutively active MEK kinase constructs, in a MEK-dependent manner (Lipschutz 2005, Hansen 2000). This correlates with the specific downregulation of the pore-forming claudin-2, at both the mRNA and protein level (Ikari 2011, Doehn 2009, Lipschutz 2005, Singh and Harris 2004). Furthermore, inhibition of ERK activity in MDCKI or 94D cells decreases their TER to levels comparable with those observed in MDCKII cells (Table 1.5) (Lipschutz et al., 2005). Further evidence for TJ regulation by the RAF/MEK/ERK pathway has come from studies utilising the expression of RAF and MEK kinases, as well as treatment with various growth factors and hormones that regulate epithelial barrier properties in a MEK-dependent manner.

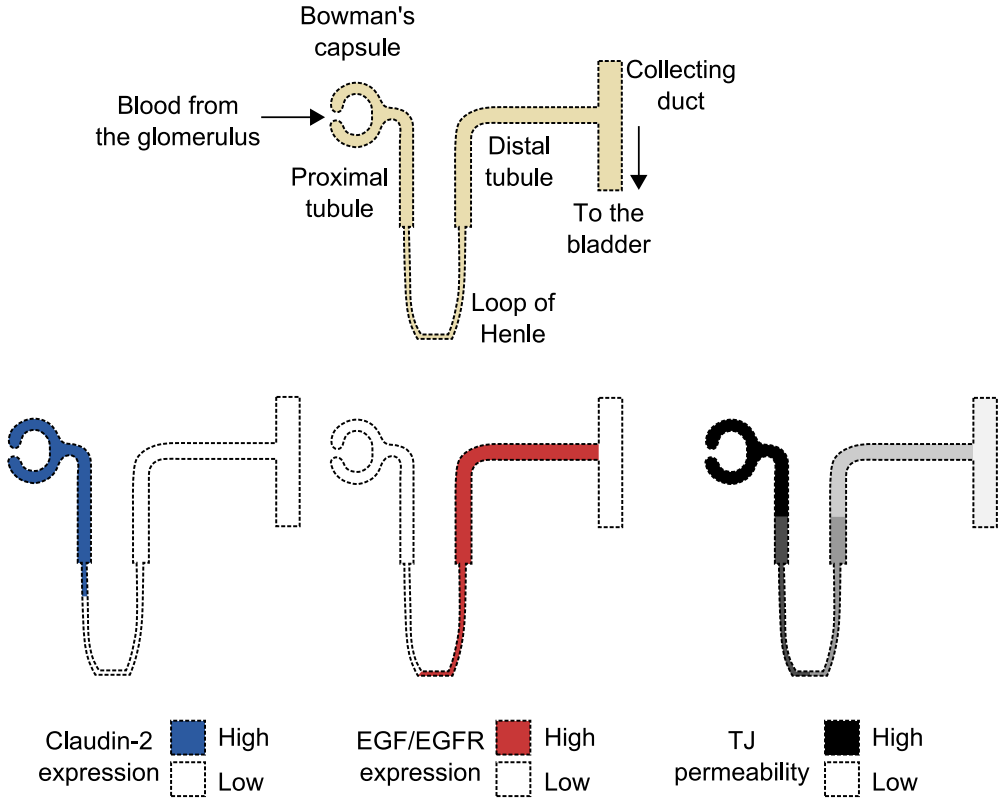

Figure 1.12: TJ permeability correlates positively with claudin-2 expression, and negatively with EGF/EGFR expression along the renal nephron. Epithelial permeability varies in a segment-specific manner in the renal nephron (Hou et al., 2013). Downstream activation of the RAF/MEK/ERK pathway by EGFR activation has been implicated in mediating the transcriptional downregulation, as well as internalisation and degradation of claudin-2 (Ikari et al., 2011c). EGFR may also exert effects on the TJ independently of RAF/MEK/ERK signalling. Representative TER values of different renal segments and the effect of RAF/MEK/ERK activation or inhibition are summarised in Table 1.5.

Cell line	94D	MDCKI	MDCKII
Representative of tissue type	Collecting duct	Distal tubule	Proximal tubule*
TER ($\Omega.cm^2$)	~4000	~4000	<300
Basal ERK activity	High	High	Low
Effect of ERK activation on TER	No change	No change	Transient increase
Effect of MEK inhibitors on TER	Decrease	Decrease	No change

Table 1.5: Correlation between basal ERK activity and transepithelial resistance of renal cell lines derived from different nephron segments. Transepithelial resistance (TER), a measure of TJ permeability, is correlated with basal ERK activity in various renal cell lines. MDCKII cells are representative of the proximal tubule of the kidney nephron, and exhibit low TER, while MDCKI and 94D cell lines represent more distal nephron segments, have high basal ERK activity and low epithelial permeability to effectively contain increasingly concentrated nephron contents. Importantly, high and low resistance cell lines can be interconverted by the activation or inhibiton of the RAF/MEK/ERK pathway, highlighting a key role for this signalling pathway in regulating the TJ and epithelial permeability. (MDCK) Madin-Darby canine kidney cells, strain I and II, (94D) mouse renal collecting duct cells. ***The parental MDCK-NBL2 cell line was derived from the distal tubule, but the MDCKII strain exhibits properties of the proximal tubule, including low TER and abundant claudin-2 expression. Data obtained from Lipschutz et al (2005) and Dukes et al (2011).

1.8.2 Tight junction regulation by RAF kinases

Specific activation of the RAF/MEK/ERK pathway using constitutively active or hormone-dependent RAF or MEK kinase constructs is associated with transcriptional changes that affect a number of TJ proteins in a tissue-specific manner. A recent genome-wide microarray in MDCKII cells utilised an inducible activity ΔCRAF:ER kinase construct to identify 1089 genes whose expression was regulated by increased ERK activity, and a further subset of 228 genes which were also dependent on RSK kinase activity (Doehn et al., 2009). This study identified RSK kinase as a key effector that coordinates multiple transcription-dependent mechanisms to stimulate motility and invasion. Several TJ proteins were identified, with differential dependencies on ERK and RSK kinase activity (summarised in Table 1.6). RAF/MEK/ERK activity is sufficient to drive the complete loss of claudin-2 mRNA expression, with a relative increase in mRNA expression of claudins -4, -6, -7 and -18. Interestingly, increased mRNA expression of these claudins is Rsk-dependent, while the decrease in claudin-2 mRNA is Rsk-independent (Table 1.6). Another study identifying Rnd3/RhoE as key regulator of RAF/MEK/ERK-mediated MDCK transformation observed a transient 3-fold increase in MDCK TER, which peaked at 18 hours following ΔCRAF:ER activation (Hansen et al., 2000). Although limited in number, these studies indicate that activation of the ERK pathway is sufficient to drive changes in TJ protein expression and epithelial permeability properties, but have mainly focussed on transcriptional changes to individual TJ components.

Protein	Fold change(ΔCRAF:ER +4HT)	MEK-dependent?	Rsk-dependent?
Claudin-2	↓ 150x (complete loss)	Yes	No
Claudin-4	↑ 2x	Yes	Yes
Claudin-6	↑ 30x (not normally expressed)	Yes	Yes
Claudin-7	↑ 2x	Yes	Yes
Claudin-18	↑ 3x	Yes	Yes
E-cadherin	↑ 2x	Yes	No
β-catenin	↓ 2x	Yes	No
ZO-2	↑ 5x	Yes	No
ZONAB	↑ 5x	Yes	No
Occludin	Not identified in study		
Claudin-1	Not identified in study		
ZO-1	Not identified in study		

Table 1.6: Transcriptional changes to genes encoding junction proteins associated with ΔCRAF:ER activation. A genome-wide microarray utilised a hormone-dependent RAF kinase fusion protein (ΔCRAF:ER) in combination with small molecule inhibitors of MEK and RSK kinases to determine genes that are transcriptionally regulated by the RAF/MEK/ERK/Rsk pathway. In MDCKII cells, specific activation of the RAF/MEK/ERK pathway caused the downregulation of claudin-2, the upregulation of claudin-4, -6, -7 and -18 and altered expression other TJ/AJ-associated genes. Specificity of the response to RAF/MEK/ERK pathway activation was confirmed with a MEK inhibitor, and individual genes exhibited differential requirements for downstream Rsk activity. Data obtained from Doehn et al (2009).

CRAF activity is associated with the transcriptional downregulation of occludin in rat salivary gland Pa-1 cells, via activation of the transcription factor, Slug (Li and Mrsny, 2000; Wang et al., 2007). However, the majority of studies have failed to report a link between RAF/MEK/ERK activity and the altered transcription of occludin in renal cell lines. Post-translational phosphorylation and membrane recruitment of occludin is observed following inhibition of MEK in Ras-transformed MDCK cells, although no change in mRNA level is observed (Chen et al., 2000). This highlights the tissue- and cell line-specific effects of RAF/MEK/ERK activation on TJ protein regulation. As previously discussed, these complex effects are likely to be, at least in part, due to tissue-variable expression of relevant transcription factors. Although RAF/MEK/ERK activity induces changes in the transcription and expression of individual TJ components, its impact on the trafficking and distribution of the existing protein pools has not been studied in great detail. Studies involving growth factors and small molecule inhibitors implicate the RAF/MEK/ERK pathway in the modulation of TJ protein endocytosis and stability, but may be complicated by the simultaneous activation of additional signalling pathways.

1.8.3 Tight junction regulation by Ras

Early observations in MDCKII cells indicated that KRas-transformation caused cell multilayering and the diminished localisation of apical, but not basolateral plasma membrane proteins (Schoenenberger et al., 1991). Although ZO-1 appeared to localise correctly to the apex of the lateral membrane, Ras-transformed monolayers exhibited increased transepithelial resistance (Schoenenberger et al., 1991). More recent studies show that epithelial permeability is regulated by specific regulation of individual TJ components (Chen et al., 2000; Mullin et al., 2005). Ras-transformed MDCK cells exhibit a fibroblastic phenotype and express low levels of E-cadherin. In contrast, the TJ proteins claudin-1, occludin and ZO-1 are expressed but sequestered in the cytoplasm (Chen et al., 2000). These TJ proteins are rapidly recruited to areas of cell-to-cell contact following the addition of an inhibitor of MEK, but not of PI3K. This membrane recruitment appears to be a post-translational process, as respective mRNA levels are unaffected by MEK inhibition. MEK inhibition causes a concomitant four-fold increase in TER and and increase in TJ strand formation onfirmed by electron microscopy. MEK inhibition increased both the tyrosine phosphorylation and half-lives of ZO-1 and occludin, but not of claudin-1, suggesting that MEK-dependent post-translational modification of TJ proteins may influence TJ barrier formation.

Another study carried out in LLC-PK1 cells, a low-resistance porcine renal epithelial cell line with similar characteristics to MDCKII cells, observed a similar increase in TER

of approximately 40% following oncogenic $KRas^{G12V}$ expression (Mullin et al., 2005). This proceeded with the concurrent loss of claudin-2 protein and increased expression of claudin-1, -4 and -7 (Mullin et al., 2005). Interestingly Ras-transformation also increased the flux of mannitol tracers up to 10Kda, indicating increased leak pathway permeability (Mullin et al., 2005). Rather than reflecting a complete loss of epithelial integrity, the selective nature of the permeability changes suggests that they proceed through the modulation of individual TJ components that determine its specific properties (Mullin et al., 2005). Although these studies implicate the RAF/MEK/ERK pathway in TJ regulation, Ras will simultaneously activate additional signalling pathways. The exact contribution of the RAF/MEK/ERK pathway and the mechanisms through which it exerts its effects on TJ permeability remain unclear.

1.8.4 Tight junction regulation by epidermal growth factor

EGF regulates epithelial barrier properties in various tissues. In MDCKII cells, EGF treatment is associated with the transcriptional downregulation of claudin-2, upregulation of claudin-4 and a concurrent increase in TER. EGFR-mediated increases in TER have variously been reported to be blocked by independent inhibition of MEK (Ikari et al., 2011c; Singh and Harris, 2004), Src (García-Hernández et al., 2015), PKC (protein kinase C) (Singh and Harris, 2004), PI3K (phosphatidylinositol 3-kinase) (Singh et al., 2007), STAT3 (García-Hernández et al., 2015) or blocking antibodies against β1-integrin (Singh et al., 2007) or the accessory protein, CD9 (Singh et al., 2007).

Treatment of MDCKII cells with EGF causes the downregulation of claudin-2, at both the mRNA and protein levels and this is blocked by co-treatment with either U0126 or PD98059, small molecule inhibitors of MEK1/2, but not by inhibitors of PI3K, JNK or p38 MAP kinases (Ikari et al., 2011c). Furthermore, claudin-2 protein levels are decreased by CA-MEK, but not DN-MEK (Ikari et al., 2011c). This suggests that ERK activity alone is sufficient to drive the depletion of claudin-2 protein. Elsewhere, the EGF-mediated downregulation of claudin-2 was shown to be blocked by inhibitors of MEK, Src or the transcription factor STAT3 (García-Hernández et al., 2015). It is unclear from this study alone whether, MEK, Src and STAT3 function in a linear pathway downstream of EGFR activation.

In addition to transcriptionally downregulating claudin-2, EGF was reported to increase its clathrin-dependent endocytosis and lysosomal degradation. This conclusion was drawn as claudin-2 protein depletion could be blocked by clathrin siRNA, or monodansylcadaverine, an inhibitor of endocytosis (Ikari et al., 2011c). Furthermore,

EGF treatment appeared to increase the association between claudin-2 and the clathrin adaptor, adaptin α. Treatment of MDCKII cells with EGF and chloroquine, an inhibitor of lysosomal degradation, resulted in the accumulation of claudin-2 in a late endosomal/lysosomal compartment. Although EGF increased the rate of claudin-2 degradation when protein neosynthesis was blocked by cycloheximide, rates of internalisation and endocytic recycling were not actually measured. EGF also increases claudin-4 mRNA and protein expression in a MEK-dependent manner (Ikari et al., 2009). This is recapitulated by the expression of CA-MEK and is dependent on the transcription factor Sp1. EGF-mediated increases in claudin-4 expression are also sensitive to inhibition of MEK, Src and STAT3, in a similar fashion to the downregulation of claudin-2 (García-Hernández et al., 2015).

EGF treatment is associated with an increase in MDCKII TER, which is consistent with claudin-2 downregulation. However, this process is also associated with increased junctional localisation of the barrier-promoting claudins -1, -3 and -4 (Singh and Harris, 2004). Although total claudin-1 protein levels are increased, translocation into the TJ still occurs in the presence of cycloheximide. In contrast, incorporation of claudin-3/-4 into the TJ is largely dependent on protein neosynthesis (Singh and Harris, 2004). EGF has no effect on the expression level or localisation of ZO-1, occludin, E-cadherin or β-catenin, suggesting that the effects are at least somewhat specific to claudins (Singh and Harris, 2004). The increase in TER is also blocked by inhibitors or EGFR (PD153035), MEK (PD98059) or PKC (staurosporine) (Singh and Harris, 2004). However, this study did not address the specific pathways responsible for the diverse effects on specific claudin species.

Expression of a non-cleavable membrane-bound heparin-binding EGF-like growth factor (HB-EGF) had similar effects to exogenous EGF treatment on claudin-2 expression and claudin-1/-3/-4 localisation (Singh et al., 2007). However, stable expression of a secretable HB-EGF led to MDCK dedifferentiation and transformation, exhibited by loss of cell-cell contact and complete loss of TER. This suggests that either the duration or magnitude of EGFR activation may influence the effects on MDCK barrier function. Alternatively, the mode of EGFR activation, i.e. juxtacrine as opposed to auto- or paracrine, may affect the TJ response (Singh et al., 2007).

In intestinal Caco-2 cells, hydrogen peroxide drives TJ disruption through the tyrosine phosphorylation, threonine-dephosphorylation and cellular redistribution of occludin and ZO-1 from the TJ to the cytoplasm (Basuroy et al., 2006). This disruption can be prevented by the treatment with EGF, and this protection is dependent on MEK/ERK

signalling. Phosphorylated ERK colocalised and coimmunoprecipitated with occludin, demonstrating an interaction between ERK and a TJ component. However, the conservation and potential consequences of this interaction in different tissues are unclear, especially as the permeability of intestinal and renal cells is differentially regulated by the RAF/MEK/ERK pathway

1.8.5 Tight junction regulation by ouabain

Ouabain, or g-strophanthin, is a cardiac glycoside that exhibits high toxicity due to inhibition of the basolateral Na^+/K^+ ATPase transporter. At high concentrations (>300nM), ouabain induces cell detachment through the internalisation of claudin-2, claudin-4, occludin and ZO-1 by an EGFR-Src-ERK1/2 signalling pathway. These proteins are differentially regulated at the protein and mRNA level and are also differentially sensitive to MEK inhibiton. Increased expression of occludin and claudin-4 is MEK-dependent, as is the induced decrease in expression of ZO-1, but not claudin-2 (Rincon-Heredia et al., 2014). These observations suggest that ouabain may engage multiple signalling pathways to modulate TJ protein expression.

Ouabain is also thought to be produced at low concentrations by the human hippocampus and adrenal glands to function as a hormone, which regulates sodium homeostasis in the kidney (Larre et al., 2010). Low concentrations of ouabain (10nM), which do not affect Na^+/K^+ pumping, cell detachment or apoptosis, are sufficient to increase MDCK TER, which occurs concurrently with an increase in claudin-1, -2 and -4 protein levels (Larre et al., 2010). This is at least partially due to increased levels of their respective mRNA transcripts (Larre et al., 2010). This increase in TER is blocked by inhibition of Src, but only partially by inhibition of MEK (Larre et al., 2010). Studies involving both EGF and ouabain implicate an EGFR-Src-ERK1/2 signalling axis in regulating the expression and localisation of individual claudin species. However, these effects appear to be differentially blocked by inhibitors of EGFR, Src and MEK. Furthermore, the duration, magnitude and mode of activation determine the specific changes for TJ protein expression. Therefore, the RAF/MEK/ERK signalling pathway is implicated in mediating the altered expression and distribution of various TJ proteins in a stimulus-dependent manner (Table 1.7) Although informative, these studies reinforce the need for specific tools and methods that allow the exact contribution of individual signalling pathways to be examined.

Treatment	TJ protein	Claudin-1	Claudin-2	Claudin-3	Claudin-4	Claudin-7	Occludin	ZO-1	ZO-2	TER
EGF	mRNA	(-)[d]	(↓)[c]		(↑)[d]		-			Transient (↑)[a,c,e]
	Protein	(-)[d]	(↓)[c]	(-)[a]	(↑)[d], (-)[a]	(-)[a]	(-)[a]	(-)[d]		
	Distribution	Increased level at TJ [e]	Endocytosis and degradation [c]	Increased level at TJ [e]	Increased level at TJ [e]			(-)[d]		
HGF	mRNA	(-)[f]	(↓)[f]	↑f	(↓)[f]	(↓)[f]	(↓)[f]	(-)[f]	(-)[f]	Transient (↑)[a]
	Protein	(↓)[a]	(↓)[a]	(-)[a]	(-)[a]	(-)[a]	(-)[a]	(-)[a]		
	Distribution			Reduced mobility at the TJ [h]			(-)[h]	(-)[h]		
DN-MEK	mRNA		(-)[a,c]							(-)[a]
	Protein	(-)[c,d]	(-)[a,c]		(-)[d]			(-)[d]		
	Distribution							(-)[d]		
CA-MEK	mRNA		(↓)[a,c]							Transient (↑)[a]
	Protein	(-)[c,d]	(↓)[a,c]		(↑)[d]			(-)[d]		
	Distribution							(-)[d]		
RAF	mRNA	(-)[j]	(↓)[j]	(-)[j]	(↑)[j]	(↑)[j]	(-)[j]	(-)[j]	(↑)[j]	Transient (↑)[i]
	Protein									
	Distribution									
Ras	mRNA	(-)[b]	*(↓)[g]	*(-)[g]	*(↑)[g]	*(↑)[g]	(-)[b]	(-)[b]		Sustained (↓)[b]
	Protein	(-)[b]	*(↓)[g]	*(-)[g]	*(↑)[g]	*(↑)[g]	(-)[b]	(-)[b]		
	Distribution	Cytoplasmic retention [b]					Cytoplasmic retention [b]	Cytoplasmic retention [b]		

Table 1.7: Stimuli that activate the RAF/MEK/ERK pathway have differential effects on the expression and distribution of individual tight junction components. The RAF/MEK/ERK pathway is implicated in regulating the expression and distribution of TJ proteins downstream of various growth factor receptors and Ras. However, differential TJ regulation by these different stimuli suggests that there are important contributions from other signalling pathways. Specific activation of the RAF/MEK/ERK pathway using constitutively active RAF or MEK constructs indicate a role in transcriptional regulation of the TJ, but its specific role in post-translationally regulating TJ protein distribution and trafficking rates is not known. (-) not affected, (↑) increased, (↓) decreased. Data obtained from (a) Lipschutz et al (2005), (b) Chen et al (2000), (c) Ikari et al (2011), (d) Ikari et al (2009), (e) Singh and Harris (2004), (f) Balkovetz et al (2004), (g) Mullin et al (2005), (h) Twiss et al (2013), (i) Hansen et al (2000) and (j) Doehn et al (2009). Summary data from MDCKII or (*)LLC-PK1 cells. Table 1.7 is presented on the previous page.

1.9 Introduction summary

- TJs are essential organising features of epithelia, regulating paracellular permeability, apicobasal polarity, intracellular signalling and cell migration.

- Individual TJ proteins are diversely regulated by various stimuli at the transcriptional level, as well as through altered rates of internalisation and post-endocytic trafficking to recycling or degradative pathways.

- The exact contribution of different signalling pathways to TJ protein trafficking and function is poorly understood in both physiological and pathological settings.

- The RAF/MEK/ERK pathway appears to regulate ionic homeostasis in the kidney and has been implicated in mediating TJ disruption in response to diverse stimuli, in inflammatory diseases and during tumourigenesis.

- This is partially achieved through the transcriptional downregulation of claudin-2, but post-transcriptional changes involving altered distribution and/or trafficking of claudins -1, -2, -3 and -4 have been reported in growth factor based studies.

- The exact role that the RAF/MEK/ERK pathway plays in regulating these post-translational changes is unclear.

- The effects of RAF/MEK/ERK activity on the rates of TJ protein internalisation, degradation and recycling have not been determined. This may represent a novel regulatory mechanism that modulates TJ composition and epithelial permeability in health and disease.

1.10 Aims and objectives

The key aims of this thesis are to:

1. Determine how specific activation of the RAF/MEK/ERK pathway influences the TJ and associated barrier properties.

2. Assess RAF/MEK/ERK-mediated changes in TJ protein expression and localisation.

3. Define how rates of TJ protein internalisation, degradation and recycling are specifically regulated by the RAF/MEK/ERK pathway.

These aims will be achieved by completing following objectives:

- Generate recombinant adenoviruses to efficiently express $BRAF^{WT}$ and $BRAF^{V600E}$ transgenes in MDCKII cells.

- Characterise the downstream activation of MEK and ERK by immunoblot and high-content microscopy.

- Evaluate epithelial barrier function by measuring transepithelial resistance in $BRAF^{WT/V600E}$-expressing monolayers.

- Determine the effects of specific RAF/MEK/ERK pathway activation on TJ protein level by immunoblot.

- Assess the role of RAF/MEK/ERK activity on TJ protein localisation using confocal microscopy.

- Measure rates of TJ protein internalisation, degradation and endocytic recycling using inducible-activity RAF:ER fusion proteins and surface-biotinylation based biochemical trafficking assays.

Chapter 2: Materials and Methods

2.1 Materials

All general laboratory chemicals were of analytical grade and purchased from Sigma-Aldrich (Poole, Dorset, UK) or Fisher Scientific (Loughborough, UK) unless otherwise stated. Treated tissue culture grade flasks and plates were purchased from Corning, (Arlington UK), unless otherwise stated.

2.1.1 Buffers

Phosphate-buffered saline (PBS)

154mM NaCl, 12.5mM $Na_2HPO_4.12H_2O$, pH7.2.

PBS/CM

154mM NaCl, 12.5mM $Na_2HPO_4.12H_2O$, 0.9mM $CaCl_2$, 0.33mM $MgCl_2$, pH7.2.

Tris-buffered saline (TBS)

10mM Tris.Cl, pH7.4, 154mM NaCl.

TBS-Tween

10mM Tris.Cl, pH7.4, 154mM NaCl, 0.1% Tween-20.

TBS/C (for dilution of 2-mercaptoethanesulphonate)

50mM Tris.Cl, pH8.6, 100mM NaCl, 2.5mM $CaCl_2$.

Lysogeny broth (LB)

1% (w/v) Bacto-tryptone, 0.5% (w/v) Yeast extract, 1% (w/v) NaCl, pH7.5.

Agar plates (with ampicillin)

1% (w/v) Bacto-tryptone, 0.5% (w/v) Yeast extract, 1% (w/v) NaCl, 1.5% (w/v) Agar, 50µg/ml ampicillin, pH7.5.

5X Tris-Borate-EDTA (TBE) buffer

1.1M Tris.Cl, pH8.3, 900mM Borate, 25mM EDTA.
Diluted 1/10 in ddH_2O to a working 0.5X solution.

2X Hank's buffered salt solution (HBSS)

280mM NaCl, 10mM KCl, 1.5mM $Na_2HPO_4.12H_2O$, 12mM D+glucose, 50mM 4-(2-hydroxyethyl)-1-piperazineethanesulphonic acid (HEPES).

Standard lysis buffer

10mM Tris.Cl, pH7.6, 5mM EDTA, 1mM EGTA, 50mM NaCl, 30mM sodium pyrophosphate, 50mM NaF, 1mM DTT, 100µM sodium orthovanadate, 1% (v/v) Triton X-100, SigmaFAST protease inhibitors (Sigma-Aldrich).

Non-reducing lysis buffer for biotinylation assays and neutravidin pulldowns

50mM Tris.Cl, pH 8.0, 1.25% (v/v) Triton X-100, 0.25% (w/v) SDS, 150mM NaCl, 5mM EDTA, 5mg/ml iodoacetamide, 10ug/ml 4-Amidinophenylmethanesulphonyl Fluoride Hydrochloride (APMSF).

Neutravidin bead wash buffer

50mM Tris.Cl, pH 8.0, 0.5% (v/v) Triton X-100, 0.1% (w/v) SDS, 150mM NaCl, 5mM EDTA.

Reducing sample buffer

30mM Tris.Cl, pH6.8, 1% SDS, 5% glycerol, 100mM DTT, 0.05% bromophenol blue.

Resolving gel buffer

1.5M Tris.Cl, pH8.8.

Stacking gel buffer

0.5M Tris.Cl, pH6.8

SDS-PAGE running buffer

25mM Tris.Cl, pH6.3, 0.2M glycine, 0.1% (w/v) SDS.

Semi-dry transfer buffer

25mM Tris.Cl, 0.2M glycine.

Membrane blocking buffer

5% milk powder (w/v) in TBS-Tween.

Enhanced chemiluminescence reagent

Solution A – 100mM glycine in NaOH, pH10.0, 0.4mM luminol, 8mM 4-iodophenol.

Solution B – 0.12% (w/w) hydrogen peroxide in ddH_2O.

Solutions A and B were mixed in 1:1 ratio immediately prior to use.

2.1.2 Antibodies

Antibody suppliers, product information and dilutions for different applications are summarised in Table 2.1. For immunoblotting, primary and secondary antibodies were diluted in TBS-Tween. For immunostaining, primary and secondary antibodies were diluted in PBS containing 2% (v/v) normal goat serum (NGS) (Invitrogen, Paisley, UK).

Antibody (Clone)	Species	Supplier	Code	Dilution	MW (kDa)
α-claudin-1	Rabbit pAb	Thermo Fisher	59-9000	WB - 1:2000 IF 1:50	~22
α-claudin-2 (12H12)	Mouse mAb	Thermo Fisher	32-5600	WB - 1:2000 IF 1:200	~22 - 23
α-claudin-4 (3E2C1)	Mouse mAb	Thermo Fisher	32-9400	WB - 1:2000 IF 1:50	~22
α-ZO-1 (1A12)	Mouse mAb	Thermo Fisher	33-1900	WB - 1:2000 IF 1:50	195
α-occludin (OC-3F10)	Mouse mAb	Thermo Fisher	33-1500	WB - 1:2000 IF 1:100	65
α-E-cadherin (4AC7)	Mouse mAb	Thermo Fisher	33-4000	WB - 1:2000 IF 1:100	120
α-ppERK1/2 (MAPK-YT)	Mouse mAb	Sigma-Aldrich	M9292	WB - 1:2000 IF 1:200	ERK1 44 ERK2 42
α-ERK1/2 (137F5)	Rabbit mAb	Cell Signaling Technology	4695S	WB - 1:2000 IF 1:200	ERK1 44 ERK 42
α-MEK1/2 (L38C12)	Mouse mAb	Cell Signaling Technology	4694S	WB - 1:2000	45
α-ppMEK1/2 (41G9)	Rabbit mAb	Cell Signaling Technology	9154S	WB - 1:2000	45
α-GFP (4B10)	Mouse mAb	Cell Signaling Technology	2955S	WB - 1:2000	~30 (monomeric)
α-myc-Tag (71D10)	Rabbit mAb	Cell Signaling Technology	2278S	WB - 1:2000 IF - 1:200	0.2 (monomeric)
α-HA-Tag (C29F4)	Rabbit mAb	Cell Signaling Technology	3724S	WB - 1:1000 IF - 1:200	1.1 (monomeric)
α-Transferrin Receptor/CD71 (H68.4)	Mouse mAb	Thermo Fisher	13-6800	WB - 1:1000	95
α-mouse Alexa® Fluor 546	Goat pAb	Thermo Fisher	A-11030	IF - 1:500	-
α-rabbit Alexa® Fluor 647	Goat pAb	Thermo Fisher	A-21245	IF - 1:500	-
α-mouse-HRP	Goat pAb	Sigma-Aldrich	A4416	WB - 1:5000	-
α-rabbit-HRP	Goat pAb	Pierce	31210	WB - 1:5000	-

Table 2.1: Antibodies used for immunostaining and immunoblotting. Antibody clones are provided where available. Dilutions are of original supplied stocks in appropriate buffer. (WB) Western blot, (IF) immunofluorescence, (pAb) polyclonal antibody, (mAb) monoclonal antibody, (HRP) horseradish peroxidase Antibodies were sourced from Cell Signaling Technology (Hitchin, UK), Sigma-Aldrich (Poole, Dorset, UK), Fisher Scientific (Loughborough, UK) or Pierce (Loughborough, UK).

2.2 Methods

2.2.1 Cell culture

MDCKII cells (Madin-Darby canine kidney cells #00062107, European Collection of Cell Cultures, Salisbury, UK) were maintained at 37°C and 5% CO_2 in Dulbecco's modified Eagle's medium (DMEM) without phenol red (Lonza, Slough, UK) supplemented with 10% (v/v) fetal bovine serum (FBS) (Invitrogen) and 2mM L-glutamine (Invitrogen). Cells were passaged twice weekly at a dilution of 1/10 and maintained in culture for a maximum of 15 passages (approximately 2 months). Cells were washed once in PBS and once with trypsin-EDTA (Invitrogen), prior to incubation in fresh trypsin-EDTA for 10 minutes at 37°C, 5% CO_2. Trypsin was neutralised by resuspending cells in DMEM containing serum and pelleting at 200 x g for 2 minutes. The pellet was resuspended in 10ml of complete DMEM and passaged at a 1/10 dilution. For freezing MDCKII cell stocks, one T75 tissue culture flask was trypsinised and pelleted as outlined above. The resulting pellet was resuspended in 2ml of 10% (v/v) DMSO in FBS and split into four 0.5ml aliquots in sterile cryogenic storage vials (Invitrogen). Vials were frozen at a controlled rate by placing in an isopropanol chamber at -80°C overnight before transferring to liquid nitrogen. To thaw cells, a single vial was thawed at 37°C, resuspended in 20ml of complete DMEM in a T75 tissue culture flask and incubated at 37°C overnight. Media was refreshed after 24 hours to remove excess cell debris and DMSO.

Prior to plating cells for experiments, a sample of resuspended cells was counterstained with trypan blue to assess viability. Cells were counted using a haemocytometer and diluted to a plating concentration of $2x10^5$cells/ml. MDCKII cells were grown until fully confluent, as assessed by stable TER readings, for a minimum of 8 days, with media changes every 2 days prior to experimental use. Cells were transduced and maintained in serum- and phenol red-free DMEM to minimise ΔCRAF:ER activation in the absence of hormone. ΔCRAF:ER activity was induced through the addition of 1μM 4-hydroxytamoxifen (4HT) (Sigma-Aldrich) to the culture medium.

HEK293 cells (a kind gift from Professor James Uney, University of Bristol, UK) were maintained between passages 30 and 40 at 37°C, 5% CO_2 in DMEM (Invitrogen) supplemented with 10% (v/v) FBS. Cells were passaged twice weekly by briefly washing in PBS and incubating with trypsin-EDTA for 5 minutes at 37°C, 5% CO_2. Cells were resuspended in 12ml of complete DMEM and passaged at a dilution of 1/12. HEK293 cells were frozen for storage and thawed as outlined above. All cell lines were

routinely tested for mycoplasma using the MycoAlert detection kit (Lonza), according to the manufacturer's instructions.

2.2.2 Calcium phosphate transfection

HEK293 cells were transfected using a calcium phosphate based method for generating recombinant adenovirus. HEK293 cells were plated at a density of $2x10^5$ cells/ml in a T25 tissue culture flask and incubated at 37°C, 5% CO_2 for two days, until 50 – 80% confluent. A total of 6µg of plasmid DNA was diluted to a final volume of 140µl in DNase/RNase-free ddH_2O. 19.8µl of 2M $CaCl_2$ was added dropwise to the DNA solution. 159.8µl of 2x HBSS was added dropwise to form a precipitate. The solution was incubated at room temperature for 20 minutes, mixed thoroughly by pipetting and added dropwise to the cell culture medium. Cells were incubated at 37°C, 5% CO_2 for 4 hours. The media was removed and cells were rinsed with PBS. Cells were then incubated in fresh culture medium at 37°C, 5% CO_2.

2.2.3 Microscopy

Confocal imaging

MDCKII cells were plated at a density of $2x10^5$cells/ml on 8-well µ-slides (Ibidi, Glasgow, UK). 24 hours after adenoviral transduction, cells were treated as described. Cells were fixed and permeabilised in ice-cold methanol at -20°C for 10 minutes and rinsed three times in PBS. Non-specific binding sites were blocked using 10% (v/v) normal goat serum (NGS) in PBS for 30 minutes. Primary antibodies were diluted as previously described in 2% (v/v) NGS/PBS. Appropriate species-specific fluorophore-conjugated secondary antibodies were also diluted in 2% (v/v) NGS/PBS. Primary antibody incubations were performed overnight at 4°C and secondary antibody incubations at room temperature for 2 hours. Cells were washed five times in PBS between antibody incubations. For phalloidin staining of the actin cytoskeleton, 1µg/ml TRITC-phalloidin/PBS (Invitrogen) was added to cells for 40 minutes at room temperature. Cells were washed three times with PBS prior to nuclear counterstaining. Nuclei were counterstained with 300nM DAPI in PBS and stored at 4°C until required. Slides were imaged using a Zeiss LSM510META laser-scanning confocal microscope (Plan-ApoChromat 63x/1.4 Oil Phase objective). Confocal images are presented as overhead composite projections of multiple 1µM Z-slices through the MDCKII monolayer, accompanied by an orthogonal cross-section view. All images were processed using ImageJ software (National Institutes of Health). Images from different experimental conditions were processed in an identical fashion. Presented images are representative of three independent experiments.

High-content microscopy and analysis

MDCKII cells were plated at $2x10^5$ cells/ml in 96-well plates. Cells were fixed and permeabilised with methanol and stained as outlined above. Plates were imaged using an INCell Analyzer 2000 (GE Healthcare, Buckinghamshire, UK). Images were analysed using INCell Developer Toolbox software. For claudin expression analysis, the average immunofluorescence intensity was measured across each image and therefore provides population averages, rather than single cell data. Data are normalised to the average intensity at t=0 and presented as mean values ±s.e.m. from three biological repeats, each consisting of 8 fields of view from wells treated in duplicate.

For single cell measurements of ERK1/2 and ppERK1/2 immunostaining intensity, images were segmented based on the nuclear DAPI stain. The imaged was then "declumped" to ensure that each nuclear object referred to a single cell. This nuclear mask was dilated to generate a mask encompassing the cytoplasm and nucleus. A cytoplasmic mask was generated by subtracting the initial nuclear mask from the whole cell mask. Individual nuclear, cell and cytoplasmic targets were linked based on overlap. Integrated (Intensity x Area) immunostaining intensity was then measured in each compartment. Nuclear:cytoplasmic ratios were calculated by dividing the integrated immunostaining intensity in the nuclear objects by those measured in the cytoplasmic objects. For data presentation, cell values were divided into subpopulations based on their level of transgene expression, which was determined by cytoplasmic GFP fluorescence intensity, unless otherwise stated. A schematic of the segmentation strategy is provided in Section 3.3.1 (Figure 3.2).

2.2.4 Protein biochemistry

Endocytosis, recycling and degradation biotin assays

Biotinylation assays to assess endocytosis, recycling and degradation of integral cell-surface proteins were performed as previously described (Dukes et al., 2011b; Nishimura and Sasaki, 2008). A schematic of the biotinylation assay is provided in Section 1.5.3 (Figure 1.8).

Confluent MDCKII cells were rinsed in ice-cold PBS/CM to block membrane trafficking. Cells were surface-labelled on ice for 30 minutes with 1ml of 0.25mg/ml EZ-link sulpho-NHS-SS-biotin (Pierce, Loughborough, UK), a membrane-impermeable and cleavable biotin moiety that forms peptide bonds with accessible lysine side chains. EZ-link sulpho-NHS-SS-biotin was diluted in ice-cold PBS/CM. Free biotin was quenched using 50mM NH_4Cl in PBS/CM for 15 minutes, followed by three PBS/CM washes to remove

residual NH_4Cl. For endocytosis assays, prewarmed DMEM was added and cells were returned to 37°C for 1 hour. Cells were transferred to ice and rinsed with ice-cold PBS/CM to halt membrane trafficking. Remaining surface biotin was removed by four 10 minute washes in 2-mercaptoethanesulphonate (MESNA) (Sigma-Aldrich) in TBS/CM. Internalised biotinylated proteins were protected from the MESNA strip by the intact plasma membrane. Free –SH groups were quenched by three 5 minute incubations in ice-cold 0.5mg/ml iodoacetamide in PBS/CM.

For the recycling assay, MESNA-stripped cells were returned to 37°C for 20 minutes. Biotinylated proteins that had been recycled to the cell surface were again prone to surface-stripping. Cells were lysed both before a second MESNA strip, to control for degradation of protein during this incubation, and after to assess the relative amount of biotinylated cargo that had been returned to the cell surface. The amount of recycled cargo is indicated by the decrease in pulldown signal between the “degradation” and “recycling” stages of the assay. Cells were lysed in 800µl of non-reducing lysis buffer, incubated for 20 minutes on ice with regular vortexing, briefly sonicated and centrifuged at 16,000 x g to remove large cell debris. 100µl of the lysate was kept to assess total protein levels, while the remaining lysate was used for neutravidin pulldown of biotinylated protein. 30µl of neutravidin beads (Pierce) were added to the remaining lysate and incubated overnight with constant rotation at 4°C.

Neutravidin beads were collected by centrifugation at 1000 x g for 3 minutes. Bead pellets were washed 3 times in neutravidin bead wash buffer (see Section 2.2.1) and neutravidin-bound protein was eluted by heating to 95°C for 10 minutes in 150µl reducing sample buffer (see Section 2.2.1). Neutravidin beads were separated by centrifugation at 1000 x g for 3 minutes. The eluted protein and whole cell lysate samples were subjected to SDS-PAGE and immunoblotting for the protein(s) of interest. For biotinylation assay experiments, immunoblots are presented for both neutravidin pulldowns and whole cell lysate inputs. Quantified band intensity data are presented for either pulldown or lysate alone, or pulldown/lysate, where pulldown values were normalised to lysate values, as indicated in the text. All immunoblots are representative of three biological repeats unless otherwise stated.

A “no biotin” control ensured that the neutravidin pulldown was specific for biotinylated protein. The “surface label” control represents a sample that has been lysed immediately after surface-labelling, without surface-stripping. This indicates the maximum amount of surface protein initially biotinylated at the cell surface. A “surface strip” control involved the surface-stripping of biotin immediately after the initial label.

This revealed the strip efficiency, which was consistent for each protein studied but varied between 80 – 95%, depending on the protein of interest.

Cumulative degradation and internalisation assays

For biotinylation-based degradation assays, the endocytosis stage of the biotinylation assay was performed, but the duration of the 37°C incubation was varied as described. A similar protocol was used to measure cumulative degradation of surface-biotinylated claudins. In this case, cells were not surface-stripped following incubation, so any decrease in the level of biotinylated protein can be attributed to protein degradation. For cycloheximide chase assays, cells were treated with 30µM cycloheximide (Sigma-Aldrich) in the presence or absence of 1µM 4HT. Cell lysates were subjected to SDS-PAGE and claudin levels were determined by immunoblot. Band intensities were quantified using ImageJ and are normalised to either t=0 or the surface label control as described. Data are presented as mean values ±s.e.m. from three biological repeats. Data were analysed using a two-way ANOVA with Bonferroni post-test to compare relative levels in control and 4HT-treated conditions at each time point.

Protein assays

The bicinchoninic acid (BCA) protein assay (Pierce) was used to determine lysate protein concentrations prior to neutravidin pulldown and/or SDS-PAGE. A standard curve was generated using 0 – 5mg/ml bovine serum albumin (BSA) diluted in the appropriate lysis buffer. A BCA working solution was prepared by mixing Reagent A and B together in a ratio of 50:1. 200µl of working solution was added to 10µl of each lysate or standard in each well of clear-bottomed 96-well plates (Corning). The plate was incubated at 37°C for 30 minutes and absorbance readings at 565nm were taken using a Spectra Rainbow microplate spectrophotometer (Thermo Fisher). Protein concentrations were determined from the BSA standard curve in Microsoft Excel. Proteins values were normalised between samples by adjustment with additional lysis buffer.

SDS-PAGE

Proteins were separated according to molecular weight by sodium dodecyl sulphate – polyacrylamide gel electrophoresis (SDS-PAGE) using the Laemmli discontinuous buffer system (Laemmli, 1970) and the Mini-PROTEAN® Tetra Cell Electrophoresis Chamber (BioRad, Hemel Hempstead, UK). 1mm thick mini-gels were prepared with resolving and stacking gels of different compositions, depending on the molecular weight of the markers being assessed (Table 2.2). Low molecular weight claudin proteins (~20kDa) were effectively separated on 15% gels, while others markers were

generally resolved on 10 – 12.5% gels. Resolving gels were topped with a lower percentage stacking gel (pH6.8). Gel recipes are presented in Tables 2.2 and 2.3. Cell lysates were solubilised by heating to 95°C in reducing sample buffer for 10 minutes. 10µl of each sample was loaded onto gels alongside 5µl of Novex Sharp Pre-stained Protein Standards (3.5 – 160kDa) (Invitrogen). Electrophoresis was carried out at a constant voltage of 120V for approximately 90 minutes, or until the gel front had run off the gel.

Reagent	Volume required for 2X 1mm gels		
	10%	**12.5%**	**15%**
1.5M Tris.Cl, pH8.8	2.5ml	2.5ml	2.5ml
30% (w/v) 37:1 acrylamide:bisacrylamide	3.3ml	4.2ml	5.0ml
ddH_2O	4.0ml	3.1ml	2.3ml
10% SDS	200µl	200µl	200µl
10% APS	67µl	67µl	67µl
TEMED	4µl	4µl	4µl

Table 2.2 Recipes for SDS-PAGE resolving gels. Different percentage gels were used depending on the molecular weight of the marker in question. Volumes provided for two mini-gels.

Reagent	Volume required for 2X 1mm gels
0.5M Tris.Cl, pH6.8	1.26ml
30% (w/v) 37:1 acrylamide:bisacrylamide	0.8ml
ddH_2O	2.9ml
10% SDS	100µl
10% ammonium persulphate	33µl
N,N,N',N-tetramethylethylenediamine (TEMED)	5µl

Table 2.3: Recipe for SDS-PAGE stacking gels. Volumes provided are sufficient for two mini-gels.

Semi-dry protein transfer

PVDF membranes (Millipore) were cut to the size of each SDS-PAGE gel, pre-soaked in methanol for 1 minute and equilibrated in semi-dry transfer buffer for 10 minutes. The PVDF membrane and SDS-PAGE gel were sandwiched between 3 layers of transfer buffer-saturated filter paper in the Trans-Blot SD Semi-Dry Transfer Cell (Biorad). Air bubbles were removed by rolling each layer with 10ml pipette. Semi-dry transfer was carried out at a constant voltage of 15V for 30 minutes.

Immunoblotting

PVDF membranes were blocked in membrane blocking buffer for 1 hour at room temperature. Excess membrane blocking buffer was removed by rinsing in TBS-

Tween. Primary antibodies were diluted in TBS-Tween as described in Table 2.1. Membranes were incubated in primary antibody overnight at 4°C. Membranes were subjected to three 5 minute washes in TBS-Tween and incubated in the appropriate species-specific horseradish-peroxidase (HRP)-conjugated secondary antibody, diluted in TBS-Tween, for 2 hours at room temperature. Membranes were washed in TBS-Tween as before and twice quickly with ddH_2O to remove residual Tween. Membranes were incubated for 1 minute in ECL reagent. Images were developed using the Fusion-SL Chemiluminescence System (Vilber Lourmat, Marne-la-Vallée, France). Band intensities were quantified using ImageJ. The bands detected by each antibody, and their approximate molecular weight in comparison to molecular weight markers, are described in results chapters 1 – 3 upon their first use. All immunoblots are representative of three biological repeats unless otherwise stated.

2.2.5 Transepithelial resistance (TER) measurements

MDCKII cells were grown on transwell polyethylene terephthalate (PET) filters with a pore size of 0.4µm (Millipore, Nottingham, UK). Filters were placed in a 24-well plate, with 1ml of media in the basolateral compartment, and 200µl of a $2x10^5$ MDCKII cell suspension added to the apical compartment. Cells were grown past confluence for 8 days, with media changes every 2 days, until resistance measurements had plateaued. Resistance measurements were taken using an EVOMX epithelial voltohmmeter and Endohm-6 chamber (World Precision Instruments, Hitchin, UK). Resistance values were normalised by subtracting the raw resistance value of a blank filter from those of each experimental sample. TER was calculated by multiplying the blank-corrected resistance reading by the filter surface area ($0.33cm^2$). TER readings were then normalised to the average TER reading at t=0 across all repeats. Relative TER readings are presented as mean values ±s.e.m. from three independent experiments. Data were analysed using a repeated measures two-way ANOVA with Bonferroni post-test, comparing replicate means against the control treatment at each time point.

2.2.6 Molecular biology

Restriction digests

Restriction enzymes were used to digest DNA plasmids, both for subcloning and analytical DNA gels. Restriction enzymes used are presented in Table 2.4. Digests were performed according to the manufacturers' instructions. Analytical digests were performed for 1 hour at 37°C, while digests performed for the purpose of subcloning were performed overnight at 37°C to achieve more complete digestion.

Restriction enzyme	Supplier	Product Code	Restriction Site
AvrII	Fermentas	FD1564	C^CTAGG
BamHI	Fermentas	FD0054	G^GATCC
Kpn2I (BspEI)	Fermentas	FD0534	T^CCGGA
KpnI	Fermentas	FD0524	GGTAC^C
NotI	New England Biolabs	RO547	TTAAT^TAA
PacI	Fermentas	FD1253	A^CTAGT
SpeI	Fermentas	FD0694	C^TCGAG
XhoI	Fermentas	FD0593	GC^GGCCGC

Table 2.4: Restriction enzymes used for DNA digestion. The relevant restriction sites and supplier information for restriction enzymes used in construct generation and cloning. Restriction enzymes were sourced from New England Biolabs (Hitchin, UK) or Fermentas Thermo Scientific (Loughborough, UK).

DNA agarose gel electrophoresis

PCR products or digested DNA samples were combined with bromophenol blue loading buffer and loaded onto 0.6 – 1 % (w/v) agarose TBE gels containing SYBR® Safe DNA Gel Stain (Thermo Fisher) alongside 5µl of 1kB DNA Ladder (Promega, Southampton, UK). DNA gels were run at approximately 10V/cm of gel until the gel front approached the end of the gel. DNA was visualised using a non-UV Dark Reader Transilluminator (Clare Chemical Research, CO, US). Where necessary, gel extraction was performed using the Wizard SV Gel and PCR Clean-Up System (Promega) according to the manufacturer's instructions.

Transformation of competent E.coli

5-alpha competent *E. coli* (High Efficiency) cells (New England Biolabs) were thawed on ice and dispensed into 25µl aliquots. 2.5µl of plasmid solution was added to each aliquot and incubated on ice for 30 minutes. Negative "no DNA" and positive pUC19 vector control transformations were included according to the manufacturer's instructions. Samples were heat-shocked at 42°C for 30s and placed on ice for 2 minutes. 250µl of prewarmed SOC medium (New England Biolabs) was added and samples were incubated at 37°C for 1 hour with vigorous shaking. Bacteria were pelleted by brief centrifugation at 10,000 x g and resuspended in 100µl SOC medium. The bacterial solution was then spread onto LB agar plates containing 50µg/ml ampicillin. Spread plates were incubated at 37°C overnight to allow colony formation.

Bacterial culture

Successful transformation was indicated by successful colony formation of pUC19 positive control, vector-transformed samples. Colonies corresponding to the desired plasmid product were expanded by picking a single colony with a pipette tip and adding

to prewarmed LB containing 50µg/ml ampicillin (5ml for miniprep, and 250ml for maxiprep cultures). Cultures were grown overnight at 37°C with vigorous shaking.

Plasmid purification

Plasmids were purified from overnight cultures using either the Wizard *Plus* SV Minipreps DNA Purification System (Promega) or the GenElute™ HP Maxiprep Kit (Sigma-Aldrich) according to the manufacturers' instructions. Prior to adenoviral generation, pacAd5 9.2 – 110 sub360 backbone and pAd5CMV K-NpA shuttle vectors were purified by ethanol precipitation. 0.1 volumes of 3M sodium acetate solution and 0.7 volumes of isopropanol were added to each plasmid preparation. Samples were mixed by inversion and centrifuged at 16,000 x g for 30 minutes. The supernatant was decanted with a fine glass pipette and the DNA pellet was rinsed with 70% ethanol and centrifuged as before for >10 minutes. The supernatant was decanted as before and the pellet was air-dried to remove residual ethanol. The DNA pellet was resuspended in 100µl of DNase/RNase-free ddH_2O and stored at -20°C.

Adenoviral shuttle vector production

In order to generate recombinant adenoviruses, desired transgenes were initially subcloned into the pAd5CMV K-NpA adenoviral shuttle vector (a kind gift from Beverly Davidson, University of Iowa, IA). Plasmid maps and analytical digests are presented in the Appendix (Figures A1 – A8). Successful subcloning was confirmed by sequencing provided by Source Biosciences (Nottingham, UK).

pAd5CMV GFP-myc-BRAF^{WT} and pAd5CMV GFP-myc-BRAF^{V600E}

pJET1.2 GFP-myc-BRAF^{WT} and pJET1.2 GFP-myc-BRAF^{V600E} (kind gifts from Professor Catrin Pritchard, University of Leicester, UK) were digested with SpeI and NotI and cloned into the multiple cloning site of pAd5CMV K-NpA. The SpeI/NotI-digested pAd5CMV K-NpA vector was treated with Antarctic Phosphatase (New England Biolabs) according to the manufacturer's instructions to remove 5' phosphates and minimise recircularisation by self-ligation. Antarctic Phosphatase was heat inactivated at 70°C for 5 minutes. Digested vectors and inserts were ligated using T4 DNA ligase (Promega) according to the manufacturer's instructions. A "no insert" reaction was included to control for the efficiency of target vector digestion and self-ligation. A vector:insert molar ratio of 1:3 was used to optimise ligation efficiency, and was calculated using the following equation:

$$Insert\ mass\ (ng) = 3\ \times \left[\frac{Insert\ length\ (bp)}{Vector\ length\ (bp)}\right] \times Vector\ mass\ (ng)$$

Ligation reactions were used to transform competent *E. coli* and prepare spread plates as previously described. Successful ligation was indicated by colony growth on the LB plates containing ampicillin – circularisation due to successful ligation permitted expression of the AmpR cassette, allowing colony growth under ampicillin-restricted conditions.

pAd5CMV GFP-myc-BRAF^{WT}:ER^{T2} and pAd5CMV GFP-mycBRAF^{V600E}:ER^{T2}

pJET1.2 BRAF^{WT}:ER^{T2} and pJET1.2 BRAF^{V600E}:ER^{T2} (kind gifts from Dr. Martin McMahon, UCSC, CA, USA) were subcloned into the existing pAd5CMV GFP-myc-BRAF constructs using a BspEI/NotI digest. These constructs retained the GFP and myc epitope tags and 5' end of the existing BRAF constructs. The C-terminal was replaced with BRAF-ER^{T2}, maintaining the in-frame fusion of BRAF and ER^{T2} sequences.

pAd5CMVeGFPΔCRAF:ER

pCMVNeoMyc1ΔRaf-1ER* (a kind gift from Dr. Simon Cook, Babraham Institute, UK) was digested with BamHI and subcloned into BamHI-digested pAd5CMVeGFP (provided by Dr. Jim Caunt and Dr. Paul Whitley).

pAd5CMVmycΔCRAF:ER and pAd5CMVHAΔCRAF:ER

Myc- and HA-tagged versions of ΔCRAF:ER were generated from the parent pCMVNeoMyc1ΔRaf-1ER* vector using the polymerase chain reaction (PCR) with primers designed to incorporate the epitope tags, as well as terminal SpeI and NotI restriction sites (Table 2.5). PCR was carried out using Phusion® High-Fidelity DNA Polymerase (New England Biolabs) and Techne Genius PCR Thermal Cycler. PCR conditions are presented in Tables 2.6 and 2.7. Resulting PCR products were digested with SpeI and NotI and ligated into SpeI/NotI-digested pAd5CMV GFP-myc-BRAF^{WT}.

Primer	Forward/ Reverse	Sequence
mycCRAF 2014 SpeI	Forward	AGTAGA**A^CTAGTG**CCACCATGGAACAAAAGTTGATTTCTGAAGAAGATTTAATGGGCTGGTCACAGCC
HACRAF 2014 SpeI	Forward	AGTAGA**A^CTAGT**GCCACCATGTACCCATACGATGTTCCAGATTACGCTATGGGCTGGTCACAGCC
ER NotI Rev	Reverse	TTGTA**CG^CGGCCGC**TCAGTTATCTATGTGGCAGGG

Table 2.5: Primers used for cloning. Primer sequences used in the generation of pAd5CMVmycΔCRAF:ER and pAd5CMVHAΔCRAF:ER. Restriction sites are highlighted in bold. Myc and HA epitope tag sequences are underlined. Primers were sourced from Invitrogen.

Reagent	Stock Concentration	Final concentration	Volume (µl)
5x HiFi buffer	5X	1X	5
Forward primer	10µM	0.3µM	0.75
Reverse primer	10µM	0.3µM	0.75
dNTPs	10mM	0.3mM each	0.75
Template DNA (pCMVNeoMyc1ΔRaf-1:ER*)	10ng/µl	10 - 100ng	1 - 10
ddH_2O	N/A	N/A	16.25
HiFi DNA polymerase	1U/µl	1U	0.5
Total	N/A	N/A	25

Table 2.6: PCR reaction setup. PCR reactions used in the generation of mycΔCRAF:ER and HAΔCRAF:ER. Reaction conditions are summarised in Table 2.7.

Cycles	Stages	Temperature (°C)	Time
1	Initial denaturation	95	3 minutes
30	Denaturation	98	20 seconds
	Annealing	67	15 seconds
	Extension	72	2 minutes (15 - 60seconds/kb)
1	Final extension	72	5 minutes
∞	Hold	10	Hold

Table 2.7: PCR reaction conditions. PCR cycles used in the generation of mycΔCRAF:ER and HAΔCRAF:ER. An elongation time of 2 minutes was used for the predicted PCR product of ~2kb.

Generation of recombinant adenovirus

Recombinant adenoviruses were generated and purified to a high titre using a RapAd system developed by the University of Iowa Gene Transfer Vector Core (Anderson et al., 2000). The desired transgene is initially subcloned into the pAd5 K-NpA shuttle vector, which is cotransfected with the pacAd5 9.2 – 100 sub360 backbone vector into a HEK293 helper cell line. Homologous recombination of PacI-digested vectors generates a continuous sequence for viral particle production. However, the pacAd5 9.2 – 100 sub360 backbone vector is devoid of packaging signals and the E1 gene, which encodes an ATP-dependent helicase that is required for DNA unwinding and polymerase recruitment. The generated recombinant adenovirus is therefore replication-deficient and requires endogenous E1 expression in the host cell line to replicate itself. E1-expressing HEK293 cells are therefore a suitable helper cell line for adenovirus production. The adenoviral-mediated delivery of genetic information to HEK293 cells initiates an infectious cycle. Genetic material is therefore delivered by adenoviral "infection". In contrast, the generated adenoviruses cannot replicate in E1-deficient MDCKII cells. Therefore, transgenes are transiently expressed in MDCKII cells following adenoviral "transduction".

Individual shuttle vectors and the pacAd5 9.2 – 100 sub360 backbone vector were digested with PacI (New England Biolabs, Hitchin, UK), mixed and cotransfected into HEK293 cells by calcium phosphate transfection (4.5µg of pacAd5 9.2 – 100 sub360 backbone vector combined with 1.5µg of pAd5 shuttle vector). Transfected cells were incubated at 37°C to allow recombination and for a visible cytopathic effect to become evident. Cytopathic plaques were evident by localised areas of cell death with rounded cells at the periphery (Figure 2.A and B). In the case of GFP-tagged transgenes, high fluorescence levels were visible at the plaque periphery (Figure 2A and B). Lysates were collected and used for further virus bulking. 10x T175 tissue culture flasks of HEK293 cells were infected and incubated at 37°C, 5% CO_2 for 1 – 3 days until cells easily detached from the flask surface. Cells were carefully collected and pelleted at 200g for 10 minutes. The cell pellet was resuspended in 3ml of 100mM Tris.Cl, pH7.5, snap-frozen in liquid nitrogen and stored at -80°C. Cells were lysed by three freeze-thaw cycles. Cell debris was removed by centrifugation at 1500 x g for 10 minutes. The viral supernatant was combined with 0.6 volumes of CsCl-saturated 100mM Tris.Cl, pH7.5 and transferred to an ultracentrifuge tube (Beckman Coulter, High Wycombe, UK). The supernatant was topped up with a solution of 1 volume 100mM Tris.Cl:0.6 volumes CsCl-saturated 100mM Tris.Cl. The tubes were heat-sealed and subjected to ultracentrifugation at 65000rpm in a VTi65 rotor (Beckman Coulter) for 6 – 8 hours. The tubes were depressurised by inserting 3 needles into the neck of each tube. The white

band of adenovirus particles (Figure 2.1C) was removed using a 21G needle and syringe and added to a fresh ultracentrifuge tube, which was filled with a solution of 1 volume 100mM Tris.Cl:0.6 volumes CsCl-saturated 100mM Tris.Cl. Samples were ultracentrifuged as before for 12 hours. The adenoviral band was removed and inserted into a 10kDa cut-off Slide-A-Lyzer™ dialysis cassette (Pierce). To remove residual CsCl, the purified adenovirus was dialysed in 1L of 3% (w/v) sucrose in PBS for 3 hours, with hourly changes of dialysis solution. The virus was removed from the dialysis cassette, snap-frozen in single-use 20µl aliquots and stored at -80°C. All adenoviral waste was sterilised in Virkon (Fisher Scientific).

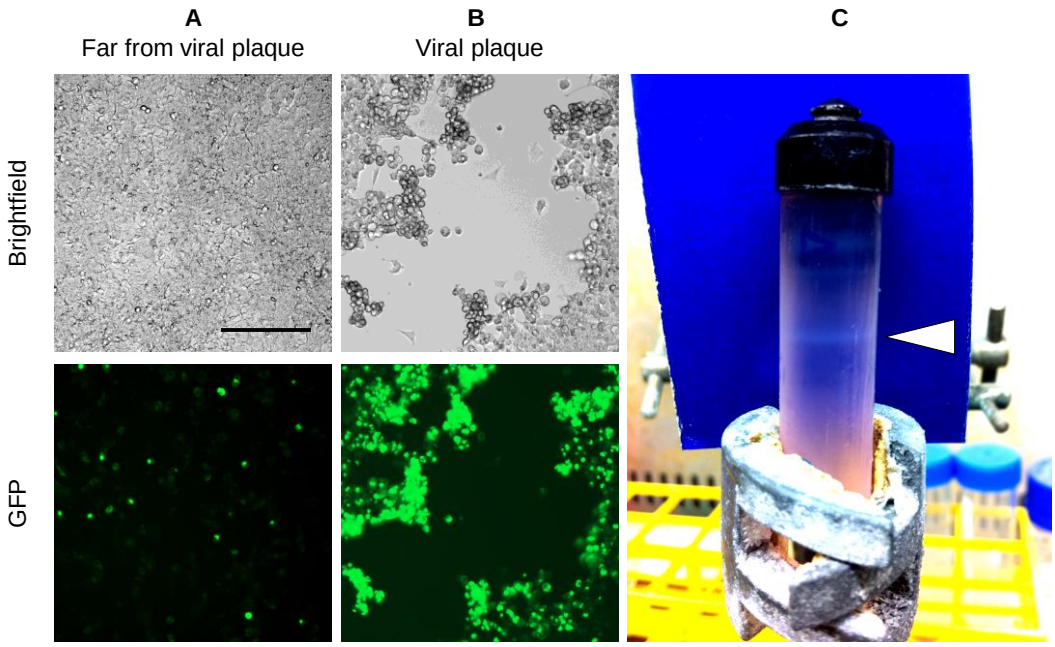

Figure 2.1: Generation and purification of recombinant adenovirus. (A) HEK293 cells 10 days after cotransfection with PacI-digested pacAd5 9.2 – 100 sub360 backbone and pAd5CMVeGFPΔCRAF:ER shuttle vectors. Cells maintain low levels of fluorescence due to expression of eGFPΔCRAF:ER from the shuttle vector. (B) Following homologous recombination between the backbone and shuttle vector, cell lysis causes the formation of viral plaques, which appear as areas of localised cell death with rounded cells expressing high levels of transgene at the periphery. Scale bar = 200µm. (C) CsCl-gradient ultracentrifugation generates a distinct adenoviral band at the interface between two CsCl solutions (white arrowhead). Images acquired with the EVOS® FL Cell Imaging System (Life Technologies).

2.2.7 Real time quantitative PCR (RT-qPCR)

RNA was isolated from confluent MDCKII cells using the Reliaprep RNA Cell Miniprep System (Promega) according to the manufacturer's instructions. RNA samples were treated with Turbo DNaseI (Ambion, Warrington, UK) at 37°C for 30 minutes. DNaseI was heat-inactivated at 75°C for 10 minutes. Reverse transcription was performed with the Cloned AMV First Strand Synthesis Kit (Invitrogen) using 1.2µg of extracted RNA and random hexamer primers according to the manufacturer's instructions.

90ng of single-strand cDNA was amplified using SYBR Green PCR Mastermix (Applied Biosystems, Paisley, UK) according to the manufacturer's instructions. Primers used in PCR were previously described by Ikari et al (2011b) are presented in Table 2.8. PCR reactions were carried out using the StepOnePlus RealTime PCR System (Applied Biosystems) and threshold cycles (C_T) were calculated using the instrument software. Primers were validated by PCR reactions with serial dilutions of template cDNA, which generated linear standard curves of C_T plotted against log[cDNA] (see Appendix, Figure A9). Control reactions without reverse transcriptase confirmed the absence of contaminating genomic DNA. Amplification efficiency (E) was calculated from the standard curve of each primer pair using the formula: $E = 10^{-1/slope}$ (Table 2.8) using the Pfaffl method (Pfaffl, 2001). C_T values for each gene were normalised to those obtained for GAPDH. These ΔC_T values were used to calculate the relative change in mRNA expression as the ratio (R) of mRNA expression in treated cells/mRNA expression of control cells using the equation, $R = E^{-\Delta C_T(treatment)-\Delta C_T(control)}$. Data are presented as mean ratio values ±s.e.m. from three biological repeats. Treatments were compared using a one-way ANOVA with Dunnett's post-test.

Target	Forward primer	Reverse primer	Primer efficiency
CLDN1	5'-ATCTACTCGTACGCCGGCGACAAC-3'	5'-AGCAGCGAGTCGAAGACCTTGCAC-3'	1.96
CLDN2	5'-GCACAGGCATAACCCAGTGT-3'	5'-GACAATGCAGGCCAACGAAG-3'	2.07
CLDN4	5'-TGCACCAACTGCGTGGAGGATGAG-3'	5'-ACCACCAGCGGGTTGTAGAAGTCC-3'	2.15
GAPDH	5'-ACGGCACAGTCAAGGCTGAG-3'	5'-CAGCATCACCCCATTTGATGTTGG-3'	2.03

Table 2.8: Primers used for RT-qPCR. Forward and reverse primer sequences used in RT-qPCR to determine mRNA levels of *CLDN1, CLDN2, CLDN4* and *GAPDH.* Primer sequences were previously reported by Ikari et al (2009 and 2011). Primers were sourced from Invitrogen.

2.2.8 Statistical Analysis

Mean and standard error values were calculated using GraphPad software (Prism, La Jolla, CA, USA). All statistical analyses were performed using GraphPad for experiments with at least three independent experiments. Statistical analysis was carried out using either a one-way ANOVA with Dunnett's post-test when comparing a series of treatments to a single control condition, or two-way ANOVA with Bonferroni post-test when comparing mean differences between groups divided on two independent variables (for example, adenovirus type and adenoviral titre). Transepithelial electrical resistance values were compared using a two-way ANOVA with Bonferroni post-test and were corrected for repeated measures, as multiple readings were consecutively taken of the same treated filters. Relevant p-values are indicated where relevant, * $p < 0.05$, ** $p < 0.01$ and *** $p < 0.001$.

Chapter 3: Tight junction regulation by $BRAF^{WT}$ and $BRAF^{V600E}$

3.1 Rationale

The RAF/MEK/ERK pathway has been implicated in mediating alterations in TJ protein expression and localisation downstream of diverse stimuli. However, the simultaneous activation of multiple downstream pathways, by EGFR for example, makes it difficult to determine the unique contribution of individual pathways. Phosphorylation of MEK by RAF, and subsequently of ERK by MEK, is highly specific (Matallanas et al., 2011; Roskoski, 2012). The pathologically relevant activation at the level of RAF allows the specific activation of the RAF/MEK/ERK pathway, independently of upstream input or parallel signalling pathways.

Activating mutations in RAF are frequently observed in cancer, with particularly high incidence in melanoma and ovarian, thyroid and colorectal carcinomas (Davies et al., 2002; Dhomen and Marais, 2007). While the activity of ARAF and CRAF isoforms is tightly regulated by phosphorylation of the N-region, the presence of negatively charged aspartic acid residues and constitutive phosphorylation within this region of BRAF essentially primes it for activation (Brummer et al., 2006; Emuss et al., 2005). Consequently, single point mutations can generate constitutively active oncogenic versions of BRAF, with the V600E mutation being the most frequent BRAF mutation found in human cancer (Roberts and Der, 2007). $BRAF^{V600E}$ is independent of upstream signalling from Ras and insensitive to ERK-mediated negative feedback (Pratilas et al., 2009). Furthermore, overexpression of wild-type BRAF, possibly as a result of gene amplification, can drive constitutive activation of the RAF/MEK/ERK pathway in malignant melanoma (Tanami et al., 2004). Therefore, expression of $BRAF^{WT}$ or $BRAF^{V600E}$ is a powerful experimental technique to achieve specific activation of RAF/MEK/ERK pathway, and is highly relevant for understanding how TJ structure and epithelial barrier properties are regulated in BRAF-driven cancers.

Madin-Darby Canine Kidney (MDCK) II cells are a widely used and well-characterised model cell line for studying polarised epithelia in culture. In contrast to the vast majority of immortalised and cancer cell lines, they readily form functional TJs when grown in simple 2D culture, either on plastic or semi-permeable membrane supports. This has permitted their wide use as a model system for studying TJs and membrane trafficking as well as additional roles in modelling viral infection (Dukes et al., 2011a). MDCKII cells do not harbour any known mutations that affect the RAF/MEK/ERK pathway, permitting their use for studying the impact of growth factors and oncogenes in an unperturbed background. This makes MDCKII cells an ideal model for studying RAF/MEK/ERK signalling *in vitro* and a logical choice for studying downstream effects on TJ trafficking in this thesis.

Several MDCK strains have been developed from a single parental MDCK-NBL-2 strain that was isolated from the distal tubule of the kidney of a healthy female cocker spaniel in the 1950s (Dukes et al., 2011a; Ikari et al., 2011c). MDCK cells lack endogenous $p16^{INK4a}$ expression and are therefore immortalised due to the lack of a functional senescence program (Plath et al., 2000). Two clonal strains are frequently used, MDCKI and MDCKII, which differ in the repertoire of TJ proteins expressed and their paracellular permeability. While MDCKI cells are a high-resistance cell line that does not endogenously express claudin-2 and exhibits typical TER values of ~4000Ω.cm^2, MDCKII cells display characteristics of the more "leaky" proximal tubule (Dukes et al., 2011a; Ikari et al., 2011c). This phenotype is manifested by low TER values of <300Ω.cm^2 (Dukes et al., 2011a) and the abundant expression of claudin-2, which confers junctional permeability to small cations and water (Amasheh et al., 2002). MDCKII cells also endogenously express claudin-1, -2, -3, -4 and -7, the TAMP family member occludin and the peripheral proteins zonula occludens (ZO)-1/-2 (Dukes et al., 2011a; Hou et al., 2006).

One potential difficulty with working with MDCKII cells is that they are typically difficult to transfect with traditional lipid- or calcium phosphate-based approaches. Transfection efficiency is typically too low for transient expression experiments. Stable transfection of MDCKII cells can be achieved using retroviral or lentiviral vectors. However, these approaches require a selection procedure, typically using antibiotics. In addition to being time-consuming, clonal selection has been reported to generate MDCK subclones with varying properties (Milatz et al., 2010). Furthermore, various MDCK strains exhibit significant genetic drift when maintained in culture, which may generate unpredictable clonal artefacts (Cassio, 2013). It is therefore important to maintain working MDCKII cultures at a low passage to minimise the divergence of cell lines used within and between different laboratories (Cassio, 2013).

The use of adenoviral vectors overcomes these issues and provides a more flexible experimental setup. Recombinant adenoviruses can be rapidly generated to deliver transgenes of up to approximately 7kb (Anderson et al., 2000). Viral uptake is extremely efficient in any cell line that expresses the coxsackie adenovirus receptor (CAR), which is itself an integral TJ protein (Coyne and Bergelson, 2005). For this reason, control adenoviruses will be used to control for the effect of transduction on TJ integrity and composition. Following transduction, transgene expression is typically detectable within 24 hours. Furthermore, the relative level of transgene expression can be regulated by titrating the concentration of adenoviral particles used for transduction. This easily permits the study of transgene "dose" responses and also allows the

expression of different mutants to be closely matched, revealing the intrinsic properties that point mutations, for example $BRAF^{V600E}$, have on protein function and downstream signalling.

Importantly, adenoviruses have successfully been used as transgene vectors in MDCKII cells, with no reported effects of using control AdGFP viruses (Dukes et al., 2011b). Therefore, adenoviral vectors provide the ability to express desired transgenes in a highly efficient, reproducible and controllable manner, while avoiding the necessity for time-consuming and potentially problematic selection procedures.

3.2 Aims and objectives

The aims of this chapter are to establish how specific activation of the RAF/MEK/ERK pathway affects the expression levels and subcellular distribution of individual TJ components and the impact that this has on epithelial permeability. This will be achieved by completing the following objectives:

1. Generate recombinant adenoviruses to express $BRAF^{WT}$ and oncogenic $BRAF^{V600E}$ in MDCKII cells.

2. Characterise $BRAF^{WT}$ and $BRAF^{V600E}$-mediated downstream activation of MEK and ERK by immunoblot and high-content microscopy.

3. Evaluate changes in epithelial barrier function through transepithelial electrical resistance measurements.

4. Determine changes in TJ protein expression by immunoblot.

5. Assess changes in the subcellular distribution of TJ proteins using confocal microscopy.

3.3 Results

3.3.1 Characterisation of BRAF^{WT} and BRAF^{V600E} fusion proteins

Adenoviruses were generated to express N-terminally GFP- and myc-tagged full-length BRAF^{WT} and oncogenic BRAF^{V600E} in MDCKII cells (AdBRAF^{WT} and AdBRAF^{V600E}, respectively). To assess their ability to activate the RAF/MEK/ERK pathway, transduced cell lysates were subjected to SDS-PAGE and immunoblot to determine levels of phosphorylated MEK1/2 (ppMEK1/2) and ERK1/2 (ppERK1/2). Antibodies for ERK1/2 and ppERK1/2 each detected a specific pair of bands, migrating marginally below a 50kDa molecular weight marker. This is consistent with the predicted molecular weights of 44 and 42kDa for ERK1 and ERK2, respectively. Antibodies for MEK1/2 and ppMEK1/2 each detected a single band that migrated marginally below the 50kDa molecular weight marker, consistent with their predicted molecular weight of 45kDa. Nontransduced lysates exhibited low levels of ppERK1/2 and ppMEK1/2, which were barely detectable by immunoblot (Figure 3.1A).

Transgene expression level can be regulated by varying the adenoviral titre used for transduction. Approximate viral titres of 3, 10 and 30 pfu/nl achieved a range of transgene expression levels, which were detected using an antibody raised against GFP (Figure 3.1A). Both BRAF^{WT} and BRAF^{V600E} transgenes have a predicted molecular weight of approximately 122kDa (BRAF ~95kDa, GFP ~27kDa and myc epitope ~0.2kDa) and were detectable as single bands migrating close to a 110kDa molecular weight marker (Figure 3.1A). Expression levels were closely matched between BRAF^{WT} and BRAF^{V600E} (Figure 3.1B). Increasing BRAF^{WT} expression positively correlated with downstream ppMEK1/2 and ppERK1/2 (Figure 3.1C,D), which is consistent with the relatively high basal kinase activity of wild-type BRAF (Pritchard et al., 1995). Oncogenic BRAF^{V600E} exhibited greater specific activity, strongly inducing downstream phosphorylation of MEK1/2 and ERK1/2 even at low expression levels (Figure 3.1C and D). Total MEK1/2 and ERK1/2 levels controls and were not affected by expression of BRAF^{WT} or BRAF^{V600E}, indicating that they are regulated by phosphorylation and not at the total protein level (Figure 3.1E and F).

Downstream activation of MEK and ERK by the generated BRAF constructs was further characterised using high-content microscopy. This permits the high-throughput quantification of RAF/MEK/ERK pathway activation at the single cell level, allowing the relationship between transgene expression levels and pathway activation to be established. Stimulation of the RAF/MEK/ERK pathway results in phosphorylation and translocation of ERK into the nucleus, where it is rapidly dephosphorylated by nuclear phosphatases (Caunt and Keyse, 2013; Lenormand et al., 1993). As a result, ERK

accumulates in the nucleus in a dephosphorylated state (Cagnol and Rivard, 2012; Pouysségur et al., 2002; Rushworth et al., 2014). In contrast, cytoplasmic ppERK is a more durable and sustained signal (Cagnol and Rivard, 2012). Transduced cells were fixed and immunostained to determine downstream ERK pathway activation by quantifying relative cytoplasmic ppERK1/2 levels, as well as the nuclear to cytoplasmic ratio of total ERK1/2. Each image was segmented to identify individual cells based on a nuclear DAPI stain (Figure 3.2A). This nuclear mask was dilated to generate an approximate whole cell mask. A cytoplasmic mask was generated by subtracting the nuclear mask from the whole cell mask. RAF/MEK/ERK pathway activation was determined by measuring the integrated intensity of ERK1/2 and ppERK1/2 in each compartment (Figure 3.2B). As both $BRAF^{WT}$ and $BRAF^{V600E}$ are cytoplasmic kinases, relative transgene expression was determined by measuring cytoplasmic GFP intensity.

Confluent MDCKII cells were transduced with GFP, $BRAF^{WT}$ or $BRAF^{V600E}$ and RAF/MEK/ERK pathway activation was assessed by immunostaining for total and phosphorylated ERK1/2 (Figure 3.3A). Expression of GFP did not increase nuclear ERK1/2 or cytoplasmic ppERK1/2 above the basal levels observed in nontransduced cells (Figure 3.3B and C), indicating that adenoviral transduction alone does not activate the ERK pathway (Figure 3.3B). Increasing $BRAF^{WT}$ expression caused an increase in levels of total ERK1/2 in the nucleus (Figure 3.3B) and phosphorylated ppERK1/2 in the cytoplasm (Figure 3.3C). $BRAF^{V600E}$ expression resulted in near maximal levels of nuclear ERK1/2 and cytoplasmic ppERK1/2, even at the lowest detectable expression levels (Figure 3.3A, B and C). Rare nontransduced cells within the $BRAF^{V600E}$-expressing population exhibited low levels of cytoplasmic ppERK1/2 and excluded total ERK1/2 from the nucleus (Figure 3.3A), indicating that $BRAF^{V600E}$ activates the ERK pathway in a cell-autonomous manner. Although the cell population exhibits heterogeneous transgene expression levels, the vast majority of cells exhibit elevated ERK pathway activity due to high adenoviral transduction efficiency in combination with the constitutive and feedback-insensitive activity of $BRAF^{V600E}$, which leads to unrestrained signal amplification.

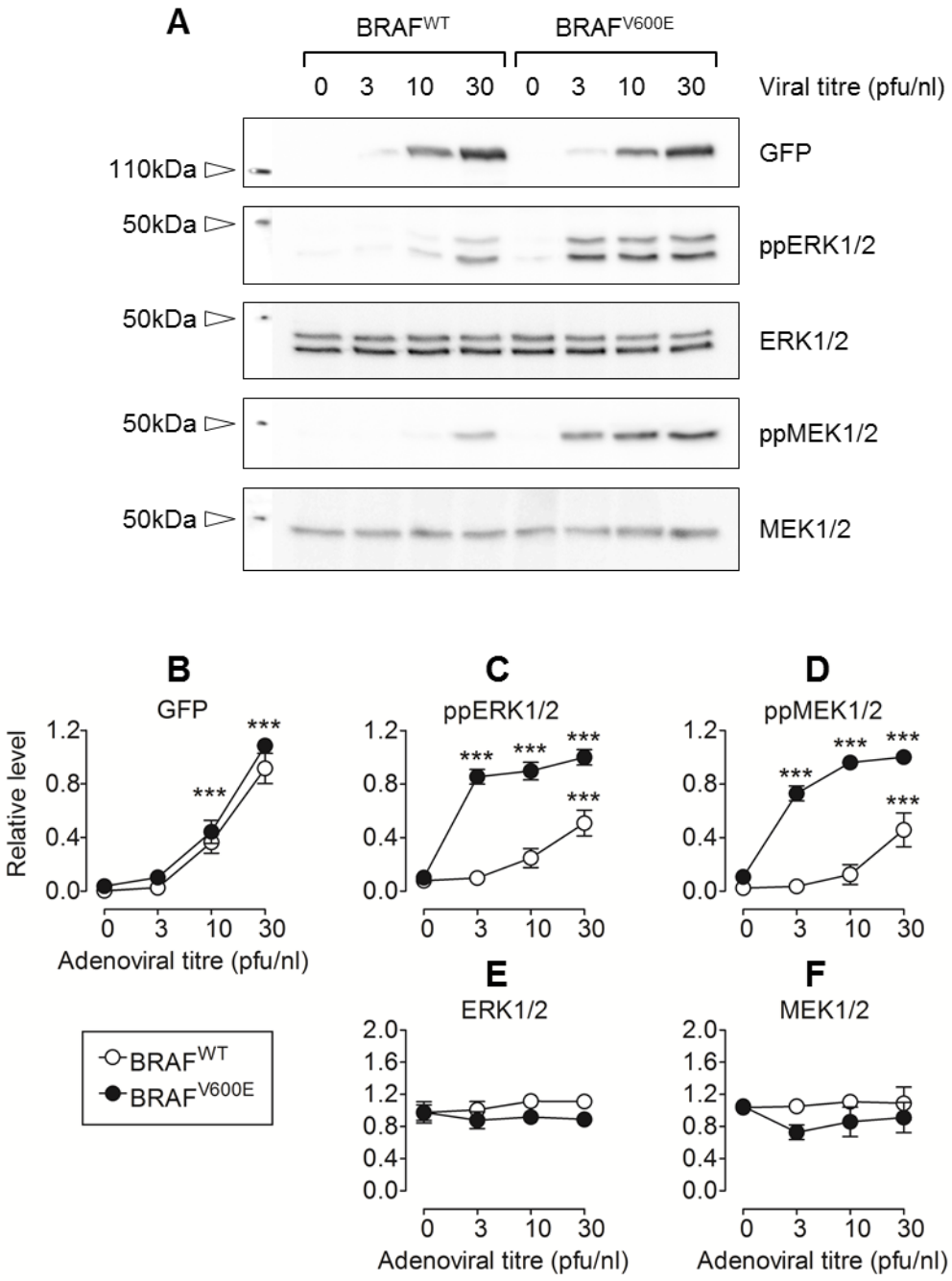

Figure 3.1: Modulation of RAF/MEK/ERK pathway signalling by BRAF^{WT} and BRAF^{V600E} expression. Confluent MDCKII cells were transduced with recombinant adenoviruses to express GFP-/myc-tagged BRAF^{WT} or BRAF^{V600E} or 24 hours. (A) Cell lysates were subjected to SDS-PAGE and immunoblot to determine downstream phosphorylation of MEK1/2 and ERK1/2. Transgene expression was regulated by varying the viral titre used for transduction and quantified by immunoblotting for GFP. Immunoblots are representative of three biological repeats. (B) Quantification of immunoblots revealed that transgene expression levels were closely matched, and highlight the functional consequence of V600E mutation. BRAF^{V600E} expression dramatically increased downstream phosphorylation of ERK1/2 (C) and MEK1/2 (D), while higher levels of BRAF^{WT} expression were required to elicit the same response. Total levels of ERK1/2 (E) and MEK1/2(F) were not affected under the same conditions. Molecular weight markers are superimposed on the left-hand side of each immunoblot. Each antibody generated bands consistent with the predicted molecular weight provided by the manufacturer. The same lysates were used to asses TJ protein levels in figure 3.4. Data are presented as mean values ±s.e.m from 3 biological repeats. BRAF^{V600E} and BRAF^{WT} treatments were compared to controls using a two-way ANOVA with Bonferroni post-test, *** $p<0.001$.

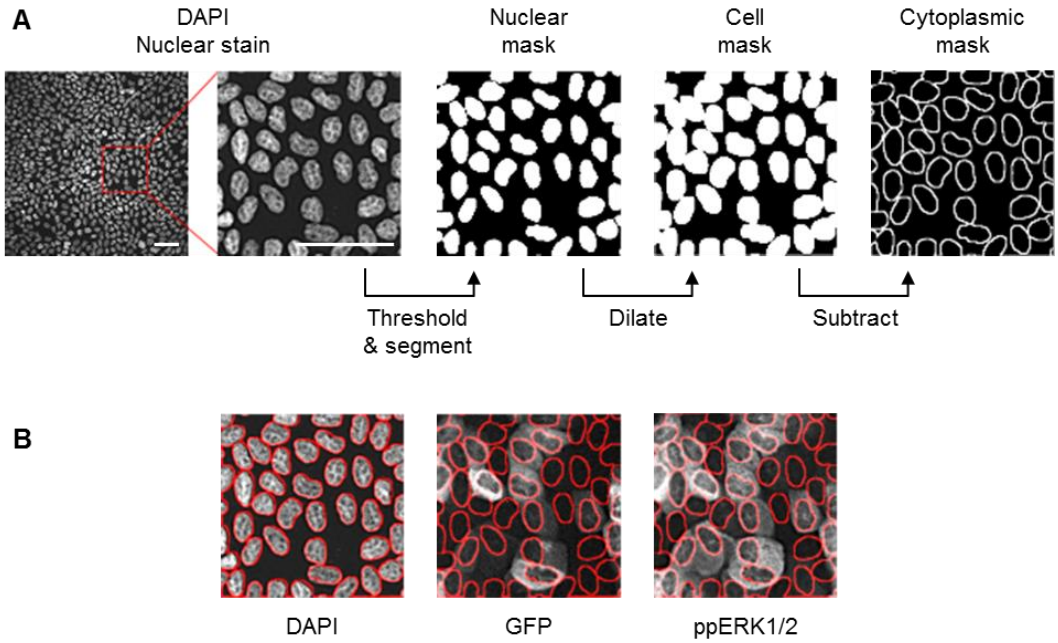

Figure 3.2: The segmentation strategy for quantifying immunostaining intensity in nuclear and cytoplasmic compartments. (A) A nuclear mask was generated by setting a threshold intensity value across each DAPI-stained image. Nuclei were "declumped", ensuring each nucleus corresponded to a single object. This nuclear mask was dilated to obtain a cell mask. A cytoplasmic mask was subsequently generated by subtracting the nuclear mask from the cell mask. Each image represents 1/16th of one field of view. Each experimental condition is quantified from 12 fields of view over 3 separate wells and therefore involves the measurement of thousands of cells. (B) The generated masks are then applied to each fluorescence channel, allowing the quantification of immunostaining intensity for different markers in each subcellular compartment. Nuclear, cell and cytoplasmic targets are linked together based on their overlap. Images were processed using INCell Developer Toolbox software (GE Healthcare Life Sciences). Example images are of MDCKII cells transduced with AdBRAF^{WT}. Scale bar = 50µm.

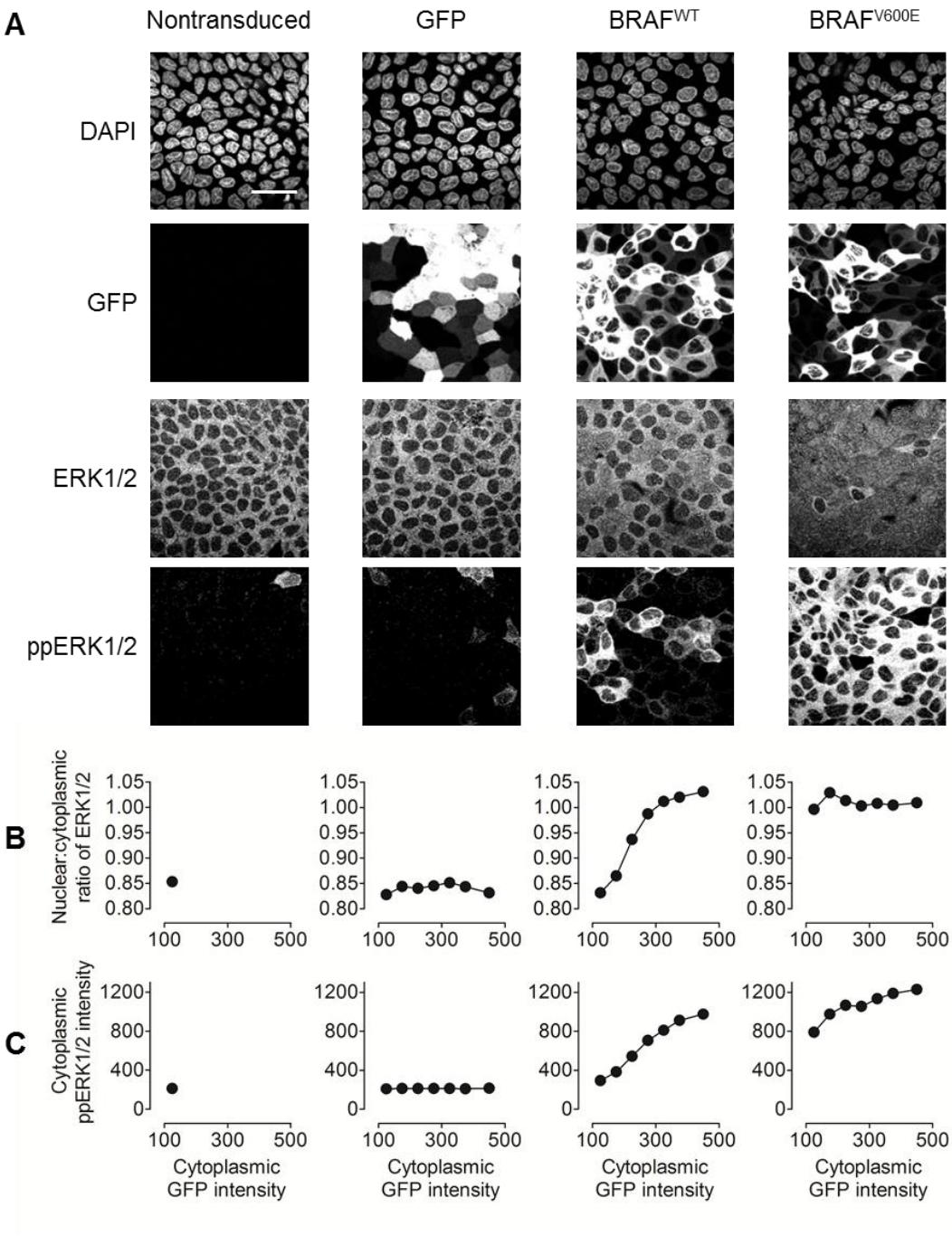

Figure 3.3: Regulation of RAF/MEK/ERK pathway output by BRAF^{WT} and BRAF^{V600E}. Confluent MDCKII cells were adenovirally transduced to express GFP or GFP-/myc-tagged BRAF^{WT} or BRAF^{V600E} for 24 hours. Cells were fixed and immunostained to determine downstream phosphorylation of ERK1/2 using high-content microscopy. (A) Representative images of MDCKII cells expressing the indicated transgene that have been fixed and immunostained for total and phosphorylated ERK1/2. Scale bar = 40µm. (B) Cytoplasmic and nuclear ERK1/2 intensities were quantified using the segmentation strategy outlined in figure 3.2. Nuclear translocation of ERK1/2 was exhibited by an increase in the ratio of nuclear:cytoplasmic ERK1/2. (C) Downstream phosphorylation of ERK1/2 was assessed by quantifying the intensity of ppERK1/2 immunostaining in the cytoplasm. Accumulation of total ERK1/2 in the nucleus and phosphorylated ERK1/2 in the cytoplasm indicate that BRAF^{V600E} expression potently activates the RAF/MEK/ERK pathway, whereas high levels of BRAF^{WT} expression are required to stimulate a similar response. Data are representative of three biological repeats.

3.3.2 BRAF^{V600E} activity differentially regulates junction protein levels

To determine if specific activation of the RAF/MEK/ERK pathway induced changes in junction protein levels after 24 hours, transduced cell lysates were subjected to SDS-PAGE and immunoblot for a variety of TJ- and AJ-associated proteins. Occludin and E-cadherin each migrated as single bands corresponding to their predicted molecular weights of 65 and 120kDa, respectively (Figure 3.4A). Levels of occludin and E-cadherin were unaffected by the expression of BRAF^{WT} or BRAF^{V600E} in this time frame (Figure 3.4A – C). Claudin-1, -2 and -4 each migrated as single bands of approximately 20kDa, consistent with their respective predicted molecular weights of ~22kDa, ~22 – 23kDa and ~22kDa. Levels of claudin-1, and to a greater extent, claudin-2, were decreased following expression of BRAF^{V600E}, but not BRAF^{WT} (Figure 3.4D and E). Under the same experimental conditions, total levels of claudin-4 were not affected (Figure 3.4E), indicating that individual claudin protein levels are differentially regulated by RAF/MEK/ERK pathway activation.

To confirm that the observed downregulation of claudin-1 and -2 was not an indirect effect of adenoviral transduction, confluent MDCKII cells were transduced with AdBRAF^{WT} or AdBRAF^{V600E}, alongside a control AdGFP adenovirus, and lysed after 24 hours (Figure3.5A). Transduction with AdGFP did not increase ppERK1/2 levels (Figure 3.5C) or affect the levels of claudin-1 or -2 (Figure 3.5E and F), confirming that the observed RAF/MEK/ERK pathway activation and claudin-1/-2 downregulation are specific to BRAF-mediated signalling and not a more general effect of adenoviral transduction. Although BRAF^{WT} expression marginally increased ppERK1/2 levels (Figure 3.5C), claudin-1 and -2 levels were not significantly affected (Figure 3.5E and F). Expression of BRAF^{V600E} induced a significant decrease in claudin-2 (Figure 3.5F), and to a lesser extent, claudin-1 levels, which were not statistically significant in this particular series of experiments (Figure 3.5E).

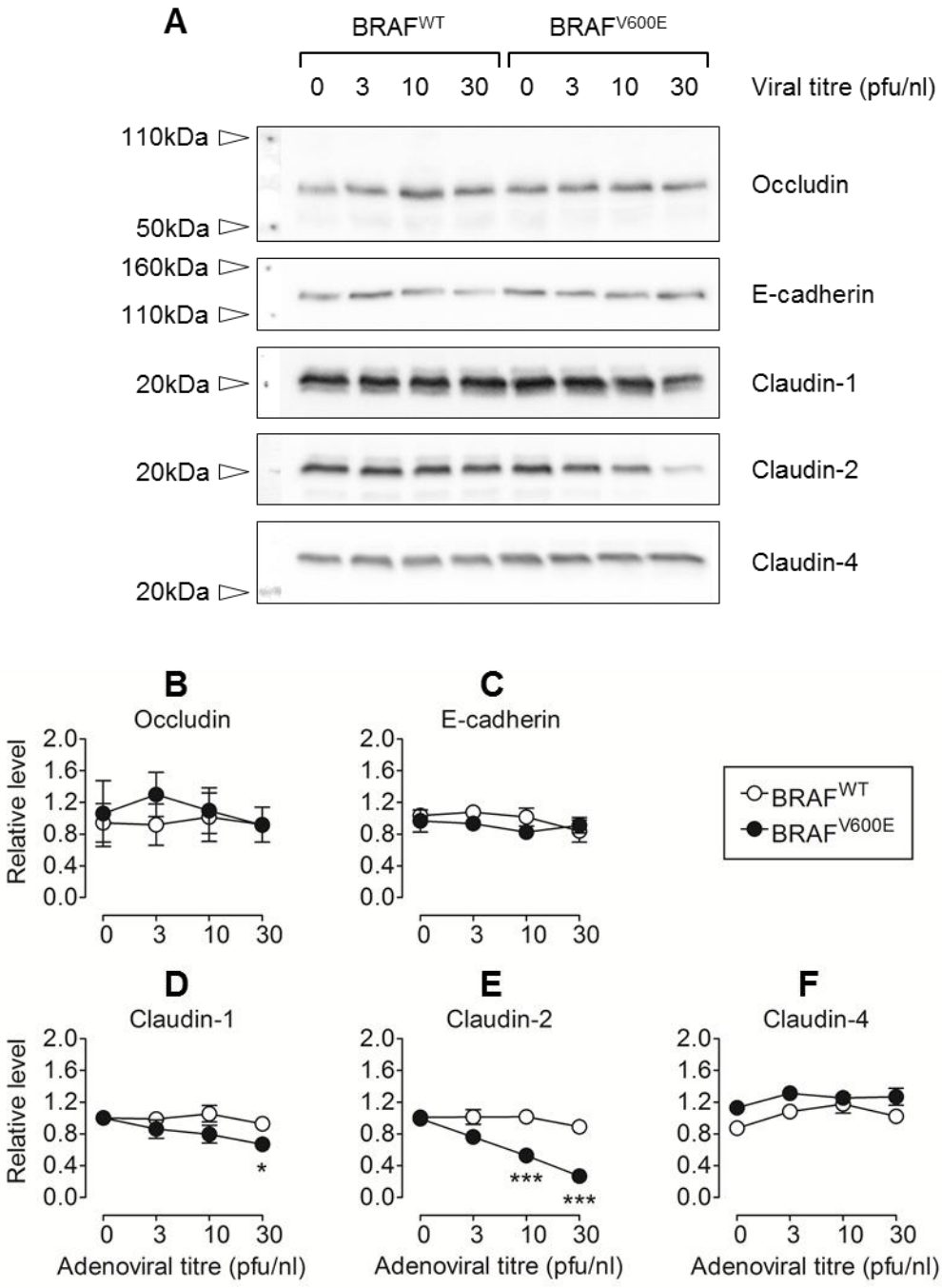

Figure 3.4: BRAF^{V600E} differentially regulates junction protein levels. Confluent MDCKII cells were adenovirally transduced to express GFP-/myc-tagged BRAF^{WT} or BRAF^{V600E} for 24 hours. (A) Cell lysates were subjected to SDS-PAGE and immunoblot to determine levels of occludin, E-cadherin, claudin-1, -2 and -4. Immunoblots are representative of three biological repeats. BRAF^{V600E} expression did not alter total levels of occludin (B) or E-cadherin (C), but differentially regulated claudin protein levels. Claudin-1 (D), and to a greater extent, claudin-2 (E) levels were decreased following the expression of BRAF^{V600E}, but not BRAF^{WT}. By contrast, total levels of claudin-4 were not affected (F). Molecular weight markers are superimposed on the left-hand side of each immunoblot. Each antibody generated bands consistent with the predicted molecular weight provided by the manufacturer. Immunoblots from figure 3.1 were obtained using the same cell lysates. The following pairs of immunoblots were obtained from the same gel: ERK1/2 and claudin-1, ppERK1/2 and claudin-2, E-cadherin and occludin. Data are presented as mean values ±s.e.m from 3 biological repeats. BRAF^{V600E} and BRAF^{WT} treatments were compared to control treatments using a two-way ANOVA with Bonferroni post-test, * $p<0.05$ *** $p<0.001$.

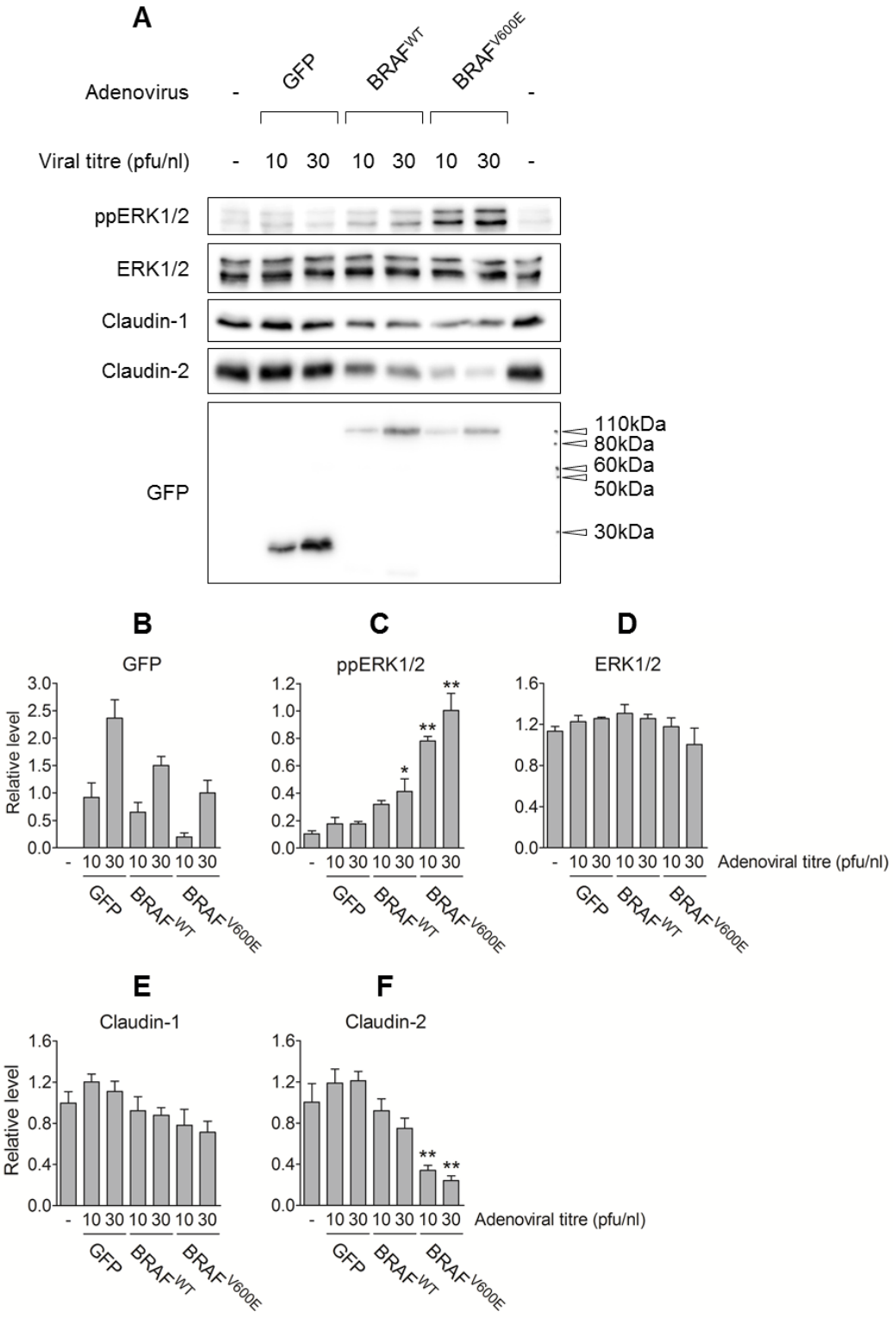

Figure 3.5: Claudin-1 and -2 levels are not influenced by transduction with a control GFP adenovirus. Confluent MDCKII cells were adenovirally transduced to express GFP or GFP-/myc-tagged BRAF^{WT} or BRAF^{V600E} for 24 hours. (A) Cell lysates were subjected to SDS-PAGE and immunoblot to determine levels of claudin-1 and -2, as well as downstream ERK phosphorylation. (B) Transgene expression was confirmed by immunoblotting for GFP, which generated bands of ~30kDa and ~120kDa, corresponding to monomeric GFP and BRAF fusion proteins, respectively. Expression of GFP did not affect levels of ppERK1/2 (C), ERK1/2 (D), claudin-1 (E) or claudin-2 (F). Expression of BRAF^{V600E}, but not BRAF^{WT} caused a significant decrease in claudin-2, and a marginal, yet statistically insignificant decrease in claudin-1 levels (E and F). Data are presented as mean values ±s.e.m from 3 biological repeats. BRAF^{V600E} and BRAF^{WT} were compared at each viral titre using a two-way ANOVA with Bonferroni post-test, * $p<0.05$, ** $p<0.01$.

3.3.3 BRAF^{V600E} transiently increases MDCKII transepithelial resistance

As claudins are major determinants of paracellular ionic permeability (Balkovetz, 2009; Günzel and Fromm, 2012), transepithelial resistance (TER) was determined in MDCKII cells expressing GFP, BRAF^{WT} or BRAF^{V600E}. MDCKII cells were grown until confluent on semi-permeable transwell filters. TER readings of approximately 150Ω.cm^2 were stable in nontransduced control monolayers over 48 hours of measurement (Figure 3.6A). Following transduction, TER readings were normalised to the nontransduced control readings at each time point (Figure 3.6, bottom row). Expression of GFP or BRAF^{WT} did not significantly affect TER at any time point (Figure 3.6B and C). In contrast, 24 – 32 hours after transduction, BRAF^{V600E} expression caused a transient increase in TER of approximately 1.8-fold. At later time points, TER readings had decreased to approximately baseline levels (Figure 3.6D), indicating epithelial barrier function is regulated by the RAF/MEK/ERK pathway in a manner dependent on signal duration.

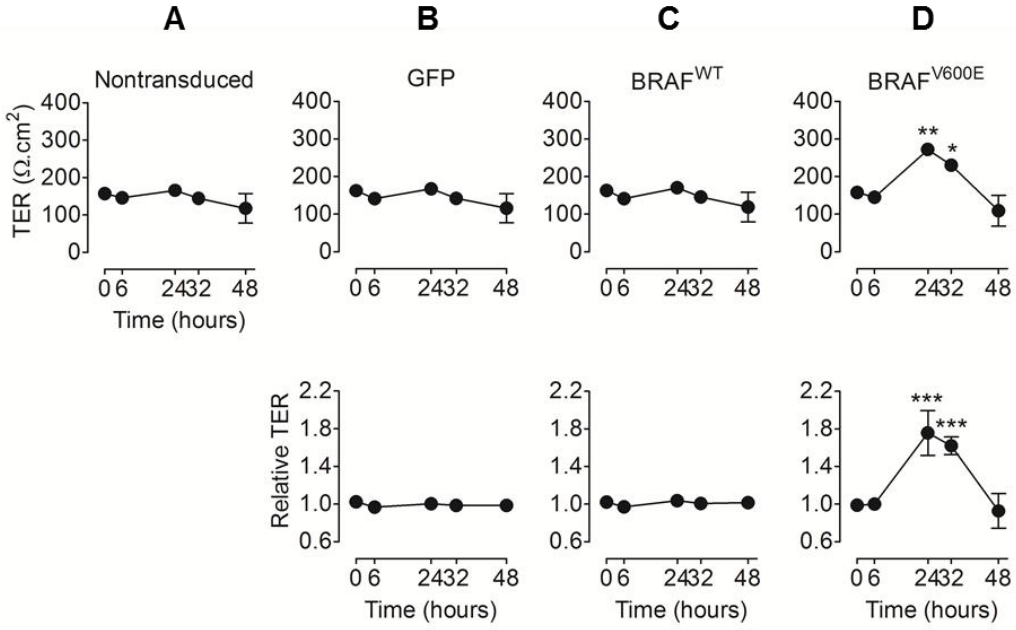

Figure 3.6: BRAF^{V600E} expression transiently increases MDCKII transepithelial resistance. Confluent MDCKII cells were adenovirally transduced to express GFP or GFP-/myc-tagged BRAF^{WT} or BRAF^{V600E}. TER readings were taken 6, 24, 32 and 48 hours after transduction. (A) Nontransduced control monolayers exhibited stable TER readings of approximately 150Ω.cm^2 over the course of the experiment. Expression of GFP (B) or BRAF^{WT} (C) did not affect MDCKII transepithelial resistance (TER). (D) BRAF^{V600E} expression caused a transient increase of approximately 1.8-fold in TER at 24 – 32 hours post-transduction. Actual TER values (top row) and those normalised to the nontransduced control treatment at each time point (bottom row) are presented as mean values ±s.e.m from 3 biological repeats. Data were compared to the nontransduced control are each time point using a repeated measures two-way ANOVA with Bonferroni post-test, * $p<0.05$, ** $p<0.01$, *** $p<0.005$.

3.3.4 BRAF activity differentially regulates junction protein distribution

To determine if RAF/MEK/ERK activity affected the subcellular distribution of TJ markers, MDCKII monolayers were immunostained and examined using confocal microscopy. Confluent MDCKII cells expressing $BRAF^{WT}$ or $BRAF^{V600E}$ were fixed and costained for claudin-1 and -2. Figure 3.7 shows overhead projections of MDCKII monolayers accompanied by an orthogonal cross-section taken through the monolayer.

Under nontransduced control conditions, claudin-2 localises to the most apical-tip of the lateral membrane, with claudin-1 predominantly associated with the lateral membrane (Figure 3.7A). Junctional claudin-2 staining was dramatically decreased in cells expressing $BRAF^{WT}$ (Figure 3.7B and C) and almost completely lost in those expressing $BRAF^{V600E}$ (Figure 3.7D and E). In contrast, claudin-1 staining appears throughout the cytoplasm following $BRAF^{WT}$ or $BRAF^{V600E}$ expression (Figure 3.7C – E). Although junctional staining initially appears to be lost, the orthogonal views reveal that claudin-1 persists at the apical side of the plasma membrane even as cells begin to overlap and form multi-layered structures (Figure 3.7E). Cells transduced with the control AdGFP virus maintained claudin-1 at the lateral membrane (Figure 3.8A and B) and claudin-2 at the apical junction (Figure 3.8C and D), indicating the observed effects are not a consequence of adenoviral transduction. Control cells and those expressing either GFP or $BRAF^{WT}$ exhibited perinuclear and lateral membrane-associated claudin-4 (Figure 3.9A – C). Cells expressing $BRAF^{V600E}$ exhibit higher overall levels of claudin-4, which localises to areas of cell-cell contact and throughout the cytoplasm (Figure 3.9D).

Under control conditions, E-cadherin extensively localises along the lateral membrane (Figure 3.10A). Lateral membrane staining was consistently observed in cells expressing GFP (Figure 3.10B), $BRAF^{WT}$ (Figure 3.10C) or $BRAF^{V600E}$ (Figure 3.10D), with minimal cytoplasmic staining detectable under any experimental condition. Occludin is predominantly concentrated at the apical junction (Figure 3.11A). Although high levels of $BRAF^{V600E}$ expression generates a diffuse cytoplasmic occludin signal (Figure 3.11D), strong junctional occludin staining is maintained in cells expressing GFP, $BRAF^{WT}$ or $BRAF^{V600E}$ (Figure 3.11B – D). The peripheral TJ protein ZO-1 is also precisely targeted to the apical junction in nontransduced cells (Figure 3.12A), and is unaffected in cells expressing either GFP (Figure 3.12B) or $BRAF^{WT}$ (Figure 3.12C). $BRAF^{V600E}$-expressing cells maintained strong junctional staining of ZO-1, but also exhibited a diffuse signal across the cytoplasm, in manner similar to that of occludin. Cells expressing $BRAF^{V600E}$ also exhibited nuclear ZO-1 staining, with 1 – 2 discrete structures per nuclei (Figure 3.12D). Data are summarised in Table 3.1

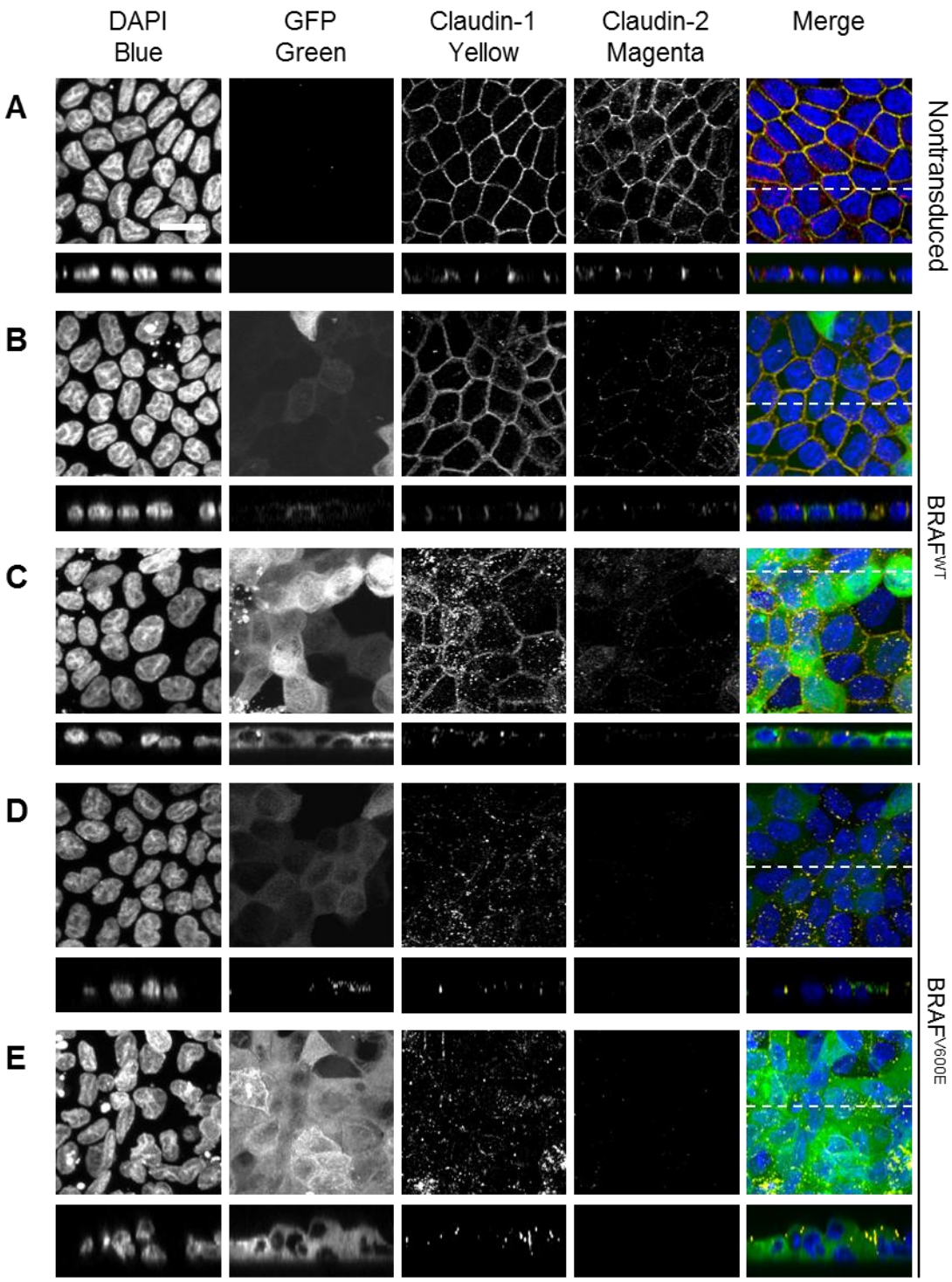

Figure 3.7: Expression of BRAF^{WT} or BRAF^{V600E} activity causes the downregulation of claudin-2 and the altered distribution of claudin-1. Confluent MDCKII cells were transduced to express either BRAF^{WT} or BRAF^{V600E}for 24 hours prior to fixation and immunostaining for claudin-1 or -2. (A) Claudin-2 normally localises to the apical junction. Junctional claudin-2 was dramatically decreased in cells expressing BRAF^{WT} (B and C) and almost completely lost in those expressing BRAF^{V600E} (D and E). Claudin-1 normally localises more laterally than claudin-2 (A). Expression of BRAF^{WT} or BRAF^{V600E} leads to diffuse cytoplasmic staining of claudin-1, but orthogonal views taken in the indicated plane (white dashed line) show that claudin-1 is maintained at cell-cell contacts towards the apical side of the monolayer in each condition (C – E) . Images are representative of three biological repeats. Orthogonal views were taken in the indicated plane (dashed line). Scale bar = 20µm.

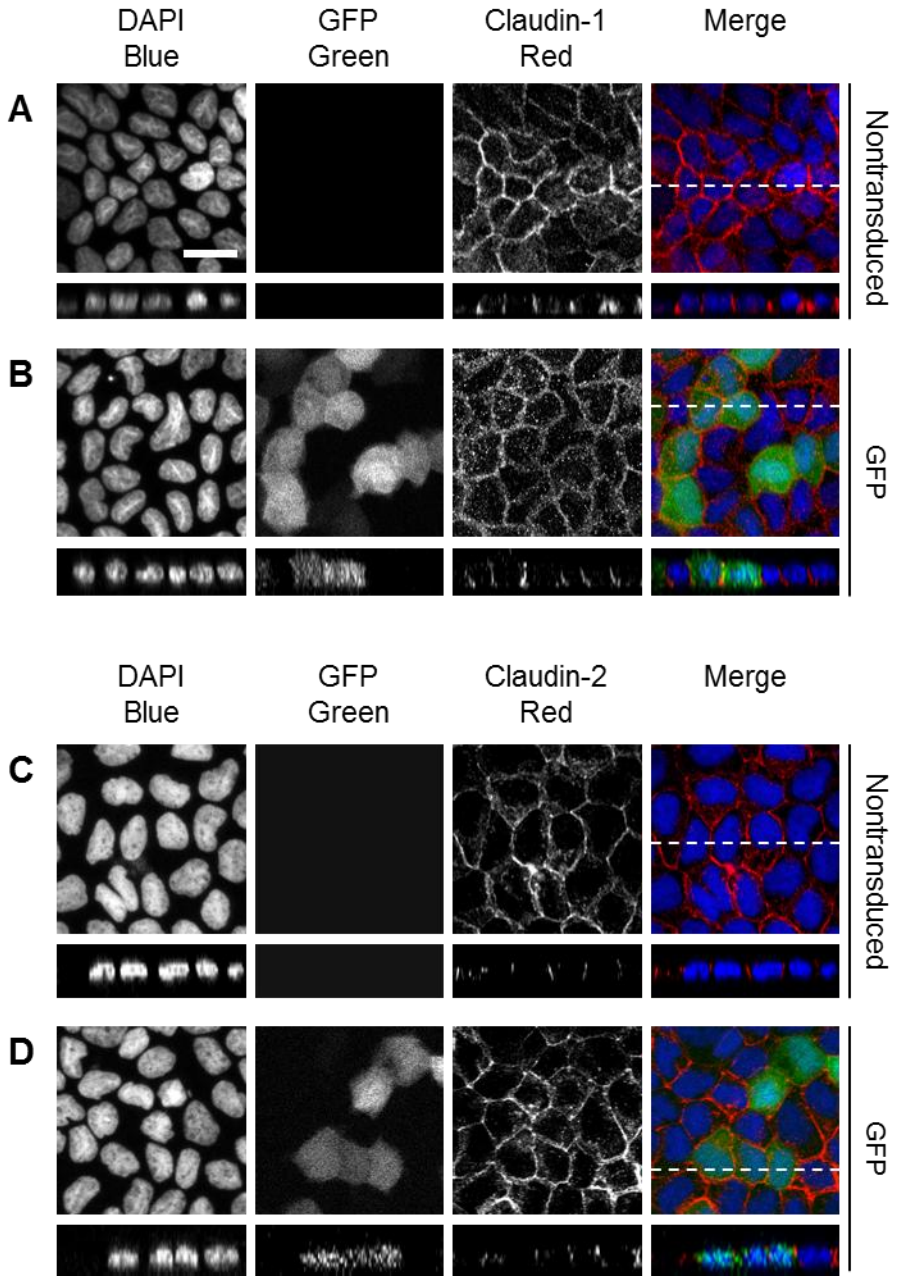

Figure 3.8: The distribution and levels of claudin-1 and –2 are not affected by transduction with a control GFP adenovirus. To control for the effects of adenoviral transduction on the distribution of claudin-1 and -2, confluent MDCKII cells were transduced with a control adenovirus to express GFP. Claudin-1 is maintained at the lateral membrane (A and B), and claudin-2 at the apical junction (C and D), in control AdGFP-transduced cells**.** Images are representative of three biological repeats. Orthogonal views were taken in the indicated plane (dashed line). Scale bar = 20µm.

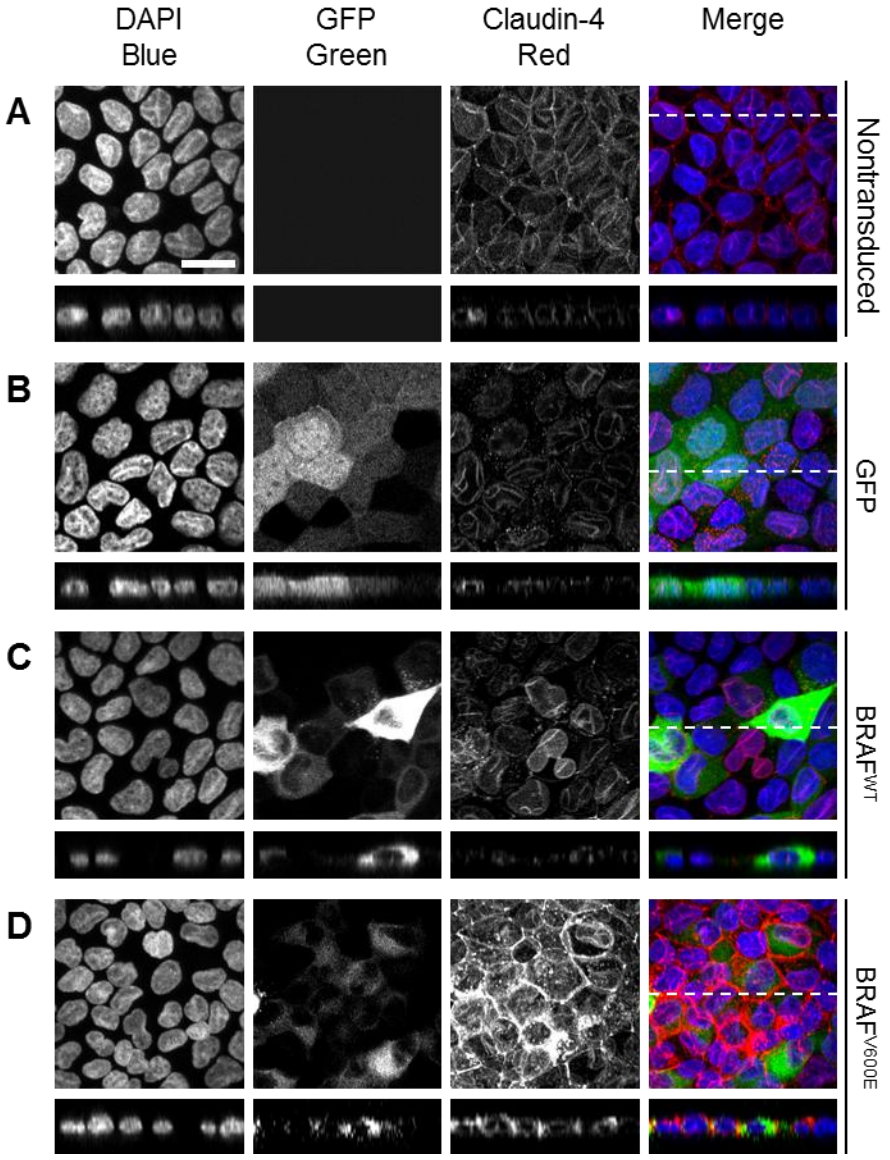

Figure 3.9: BRAF^{V600E} expression increases junctional levels of claudin-4. Confluent MDCKII cells were transduced to express GFP, BRAF^{WT} or BRAF^{V600E}for 24 hours prior to fixation and immunostaining for claudin-4. (A) Nontransduced control cells stain relatively weakly for claudin-4, which exhibits perinuclear and partial plasma membrane localisation. This is largely maintained in cells expressing either GFP (B) or BRAF^{WT}(C). (D) BRAF^{V600E}-expressing cells exhibit higher overall levels of claudin-4, with strong staining evident at areas of cell-cell contact as well as throughout the cytoplasm. Images are representative of three biological repeats. Orthogonal views were taken in the indicated plane (dashed line). Scale bar = 20µm.

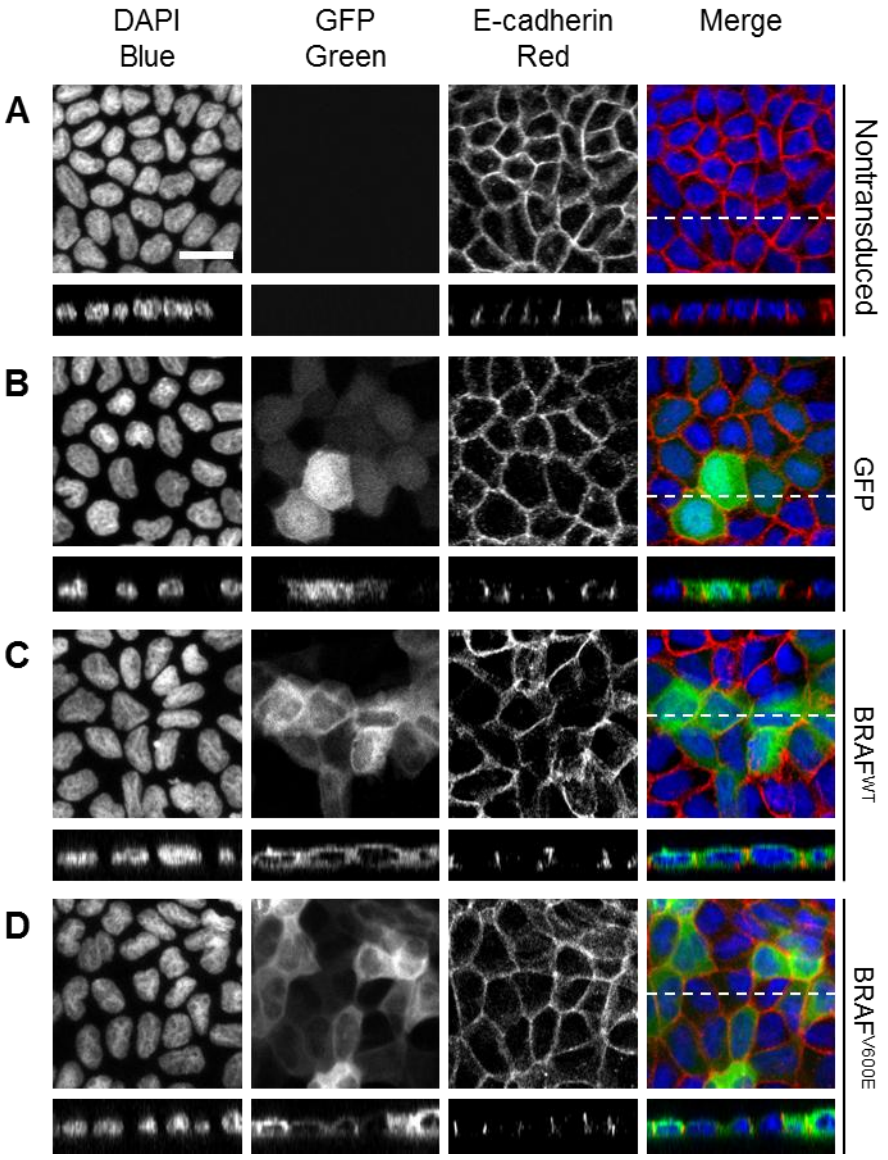

Figure 3.10: BRAF^{V600E} expression does not influence the distribution of E-cadherin. Confluent MDCKII cells were transduced to express GFP, BRAF^{WT} or BRAF^{V600E} for 24 hours prior to fixation and immunostaining for E-cadherin. (A) E-cadherin normally localises to the lateral membrane and this expression pattern is preserved in cells expressing GFP (B), BRAF^{WT} (C) and BRAF^{V600E} (D). Images are representative of three biological repeats. Orthogonal views were taken in the indicated plane (dashed line). Scale bar = 20µm.

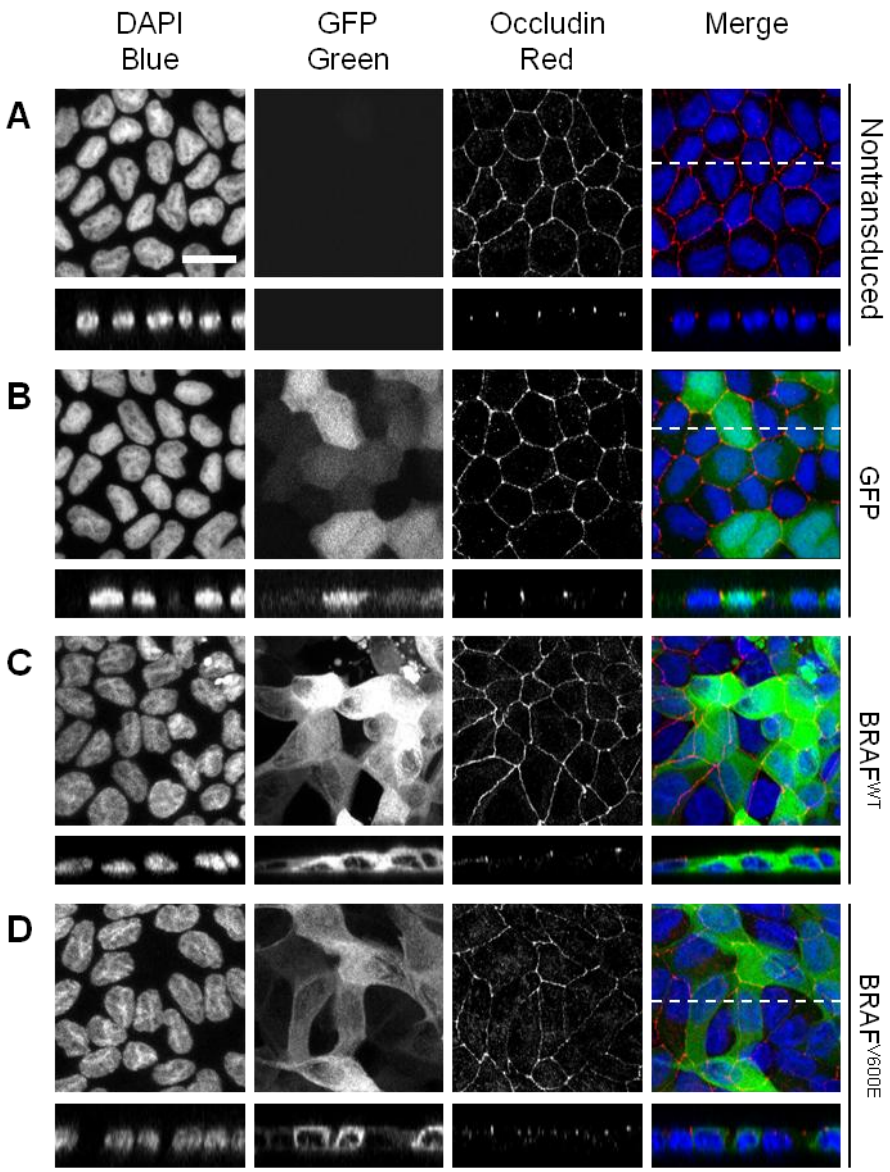

Figure 3.11: Junctional occludin is maintained following BRAF^{V600E} expression. Confluent MDCKII cells were transduced to express GFP, BRAF^{WT} or BRAF^{V600E}for 24 hours prior to fixation and immunostaining for occludin. (A) Occludin normally localises to the apical junction and this expression pattern is largely preserved in cells expressing GFP (B), BRAF^{WT} (C) and expressing BRAF^{V600E} (D). (D) BRAF^{V600E} expression also causes a slight increase in diffuse occludin staining throughout the cytoplasm. Images are representative of two biological repeats. Orthogonal views were taken in the indicated plane (dashed line). Scale bar = 20µm.

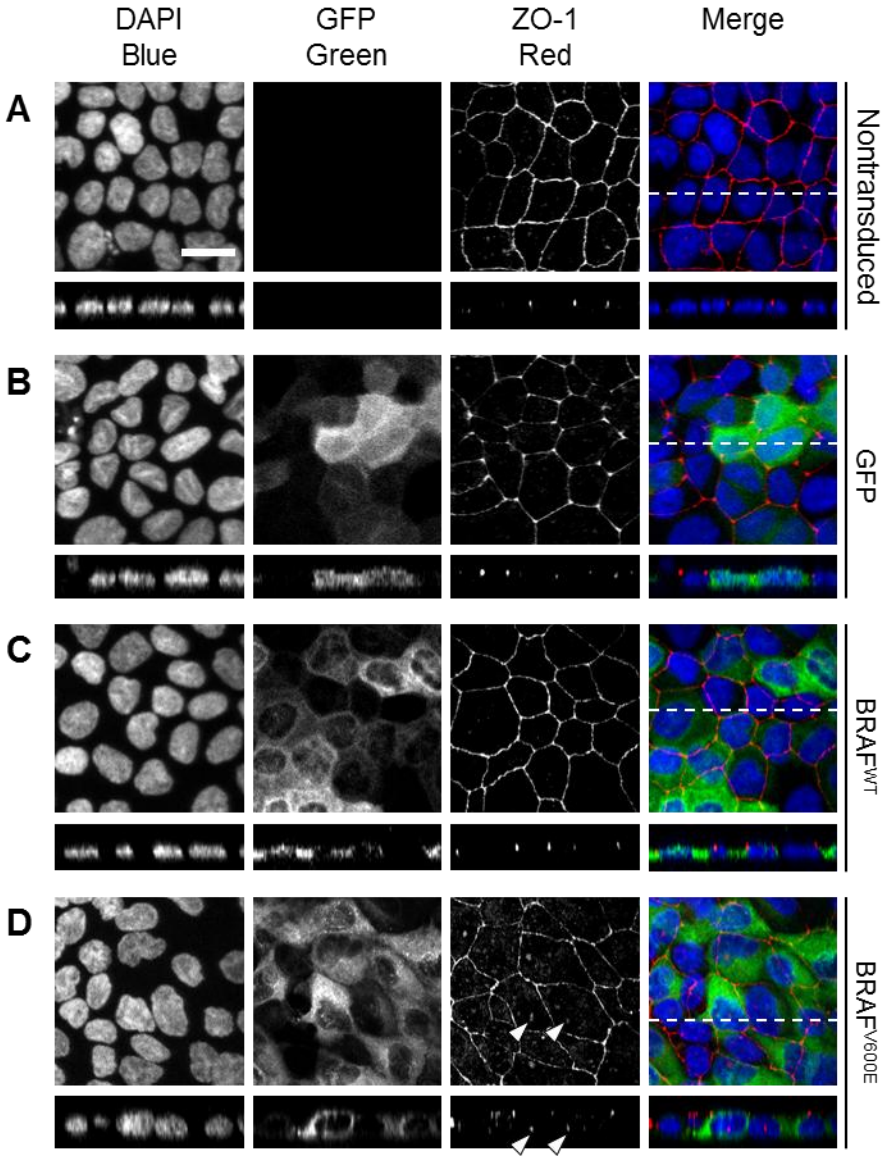

Figure 3.12: BRAF^{V600E} expression has diverse effects on the subcellular distribution of ZO-1. Confluent MDCKII cells were transduced to express GFP, BRAF^{WT} or BRAF^{V600E} for 24 hours. (A) Immunostaining of fixed cells revealed that ZO-1 precisely localises to the apical junction under control conditions, and in cells expressing either GFP (B) or BRAF^{WT} (C). BRAF^{V600E}-expressing cells maintain continuous junctional staining, with ZO-1 also diffusely distributed across the cytoplasm and is present in discrete structures within the nucleus (white arrowheads) (D). Images are representative of three biological repeats. Orthogonal views were taken in the indicated plane (dashed line). Scale bar = 20μm.

3.3.5 BRAF^{WT} and BRAF^{V600E} expression is lost following MEK inhibition

To confirm that the diverse effects on TJ remodelling were mediated by RAF/MEK/ERK pathway activation, MDCKII cells were transduced in media containing DMSO or the MEK inhibitor PD0325901. Treatment with PD0325901 alone did not affect total claudin-2 levels, indicating that inhibiton of RAF/MEK/ERK signalling does not further increase claudin-2 expression. BRAF^{WT} and BRAF^{V600E}-mediated increases in ppERK1/2 levels were successfully blocked by PD0325901 treatment (Figure 3.13A and B). As expected, BRAF^{V600E} expression dramatically decreased claudin-2 levels, and this was completely blocked by PD0325901 treatment (Figure 3.13D). Surprisingly, BRAF^{WT} and BRAF^{V600E} expression, as assessed by immunoblotting for the associated myc tag, was completely lost in PD0325901-treated conditions (Figure 3.13E).

To determine if the presence of PD0325901 in the transduction media affected adenovirus integrity or uptake, cells were transduced in the absence of PD0325901. 24 hours after transduction, DMSO or PD0325901 was added to the culture medium for a further 24 hours prior to cell lysis (Figure 3.14A). PD0325901 successfully inhibited BRAF-mediated ERK phosphorylation (Figure 3.14B and C). The BRAF^{V600E}-driven decrease in claudin-2 levels were also restored by PD0325901 treatment, indicating that the loss of claudin-2 is a reversible process when elevated ERK signalling is subsequently blocked (Figure 3.14D). However, BRAF transgene expression was still suppressed following the delayed addition of PD0325901 to the culture medium, indicating that PD0325901 did not suppress BRAF transgene expression by inhibiting adenoviral transduction. Decreased levels of BRAF^{WT} and BRAF^{V600E} were evident in immunoblots using antibodies against either myc (Figure 3.14E) or GFP tags (Figure 3.14F). Of note, PD0325901 did not affect the expression level of GFP alone (Figure 3.14F), suggesting some degree of specificity of PD0325901 to the suppression of BRAF construct levels. Taken together, these data suggest that PD0325901 may specifically affect either the synthesis or stability of the generated BRAF^{WT} and BRAF^{V600E} constructs. Therefore, it could not definitively be stated that claudin-2 protein depletion was dependent on ERK signalling, as the apparent “rescue” of claudin-2 levels by PD0325901 may have been mediated through the unexpected loss of transgene expression.

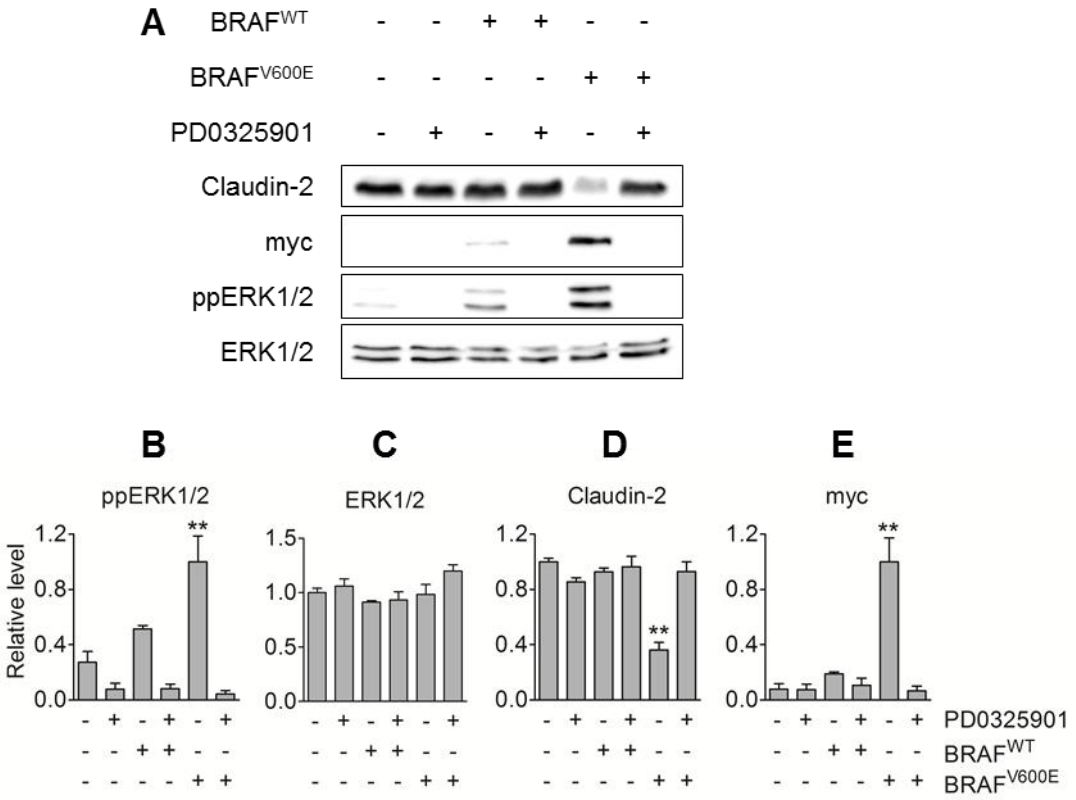

Figure 3.13: The MEK inhibitor PD0325901 impairs BRAF^{WT} and BRAF^{V600E} transgene expression. MDCKII cells were transduced in media containing DMSO or the MEK inhibitor, PD0325901. (A) Cell lysates were subjected to SDS-PAGE and immunoblot. MEK inhibition successfully blocked BRAF-mediated increases in ERK phosphorylation (B and C) and decreases in claudin-2 (D). However, BRAF transgene expression was completely lost in PD0325901-treated conditions (E), making it impossible to determine if the apparent claudin-2 rescue is due to the blockade of downstream signalling or the loss of BRAF expression. Immunoblots are representative of three biological repeats. The following pairs of immunoblots were obtained from the same gel: myc and ERK1/2, ppERK1/2 and claudin-2. Data are presented as mean values ±s.e.m from three biological repeats. Data were compared to the nontransduced and vehicle-treated control using a one-way ANOVA with Dunnett's post-test, ** $p<0.01$.

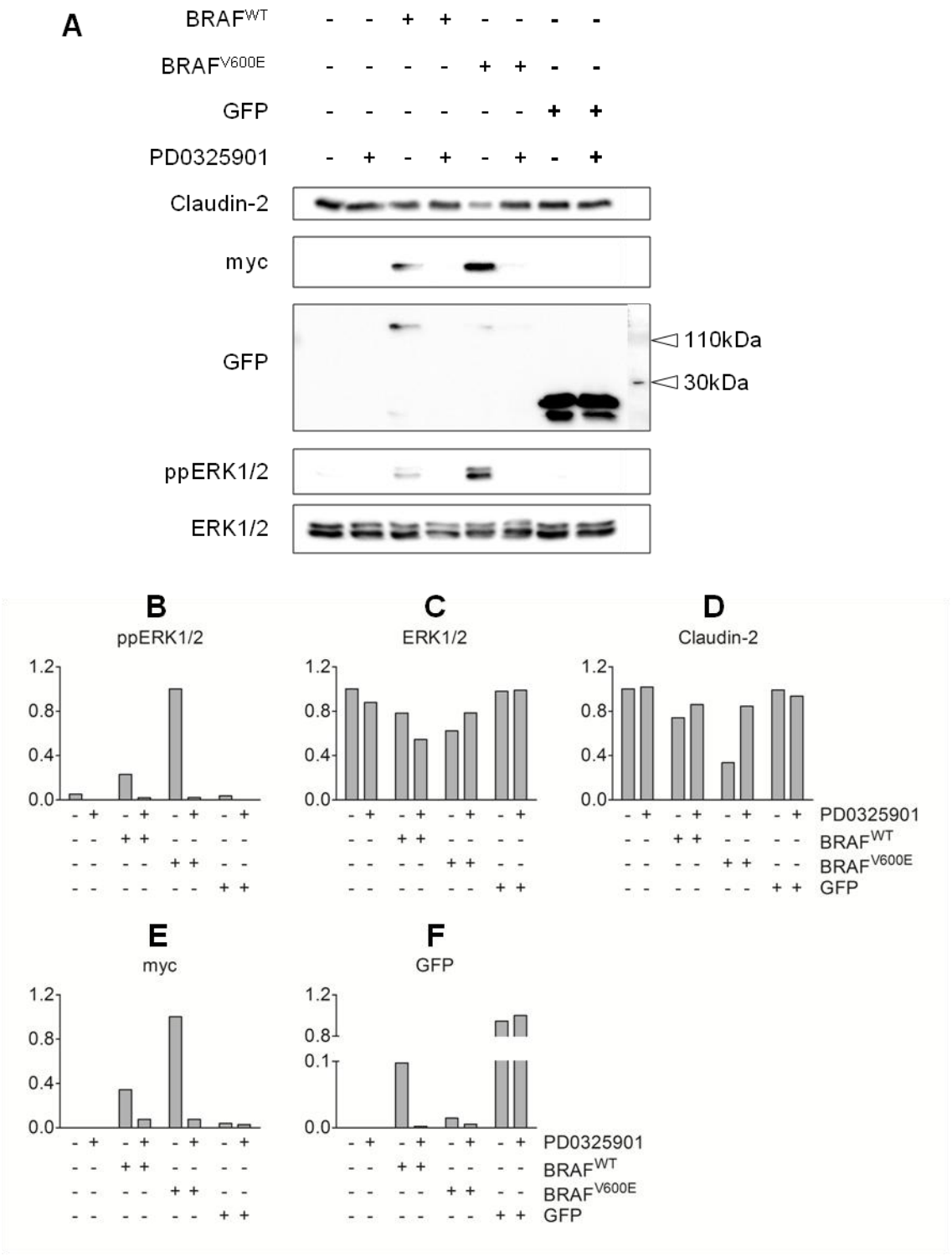

Figure 3.14: Delayed addition of the MEK inhibitor PD0325901 decreases BRAF^{WT} and BRAF^{V600E} transgene expression. MDCKII cells were transduced in media lacking PD0325901. After 24 hours, 5µM PD0325901 was added to the culture medium for a further 24 hours prior to cells lysis and immunoblot (A). MEK inhibition successfully blocked BRAF-mediated increases in ERK phosphorylation (B and C) and reversed the downregulation of claudin-2 (D). BRAF transgene expression was completely lost in PD0325901-treated conditions, as assessed by immunoblotting for myc (E) or GFP tags (F). Immunoblots for ppERK1/2 and claudin-2 were obtained from the same gel. Data is presented from a single biological repeat.

3.3.6 BRAF^{V600E} induces a transformation-associated phenotype

In addition to distinct regulation of TJ protein expression levels and localisation, expression of BRAF^{WT} and BRAF^{V600E} had wider ranging effects on MDCKII cell morphology and proliferation associated with cell transformation. Confluent MDCKII cells are characterised by an extensive network of actin stress fibres that line the basal membrane and cortical actin fibres that are associated with the lateral and apical membrane domains (Figure 3.15A). Expression of BRAF^{WT} or BRAF^{V600E} leads to loss of basal stress fibres and increased levels of cortical actin at the apical surface (Figure 3.15C and D). This remodelling of the actin cytoskeleton is accompanied by dramatic changes in the morphology of individual MDCKII cells and the organisation of the monolayer. MDCKII cells typically adopt a compact polygonal shape as cells tightly pack into a multicellular monolayer. Expression of BRAF^{V600E} leads to cells adopting an elongated morphology, with protrusions that overlap with one another (Figure 3.16D). In some instances, cells stack on top of each other to form disorganised multi-layered structures (Figure 3.16E).

To determine if expression of BRAF^{WT} or BRAF^{V600E} increased the rate of cell proliferation, transduced cells were fixed and costained for the proliferation marker, Ki67, and the mitotic marker, phospho-histone H3 (pHH3) (Figure 3.17). Expression of BRAF^{V600E}, and BRAF^{WT} at high levels, increased the mean Ki67 immunostaining intensity (Figure 3.17E), suggesting that their expression increases MDCKII cell proliferation. The mitotic index was calculated in each condition by calculating the percentage of total cells that stained positively for both markers. Control samples exhibited a mean mitotic index of approximately 0.5% (Figure 3.17A and F), indicating that at any one time, 1 out of 200 cells is undergoing mitosis. This was not affected by the expression of GFP (Figure 3.17B and F), but high levels of BRAF^{WT} expression doubled the mitotic index to approximately 1.0% (Figure 3.17C and F). At the same viral titre, expression of BRAF^{V600E} increased the mitotic index to approximately 2.0%, with partial increases observed at lower levels of expression (Figure 3.17D and F). Taken together, these data indicate that expression of BRAF^{WT} or BRAF^{V600E} has wide-ranging effects on MDCKII cells inducing cytoskeleton remodelling and changes in cell shape, the loss of cellular organisation and increased proliferation rates, which are all consistent with a transformed phenotype (Huang et al., 2012)

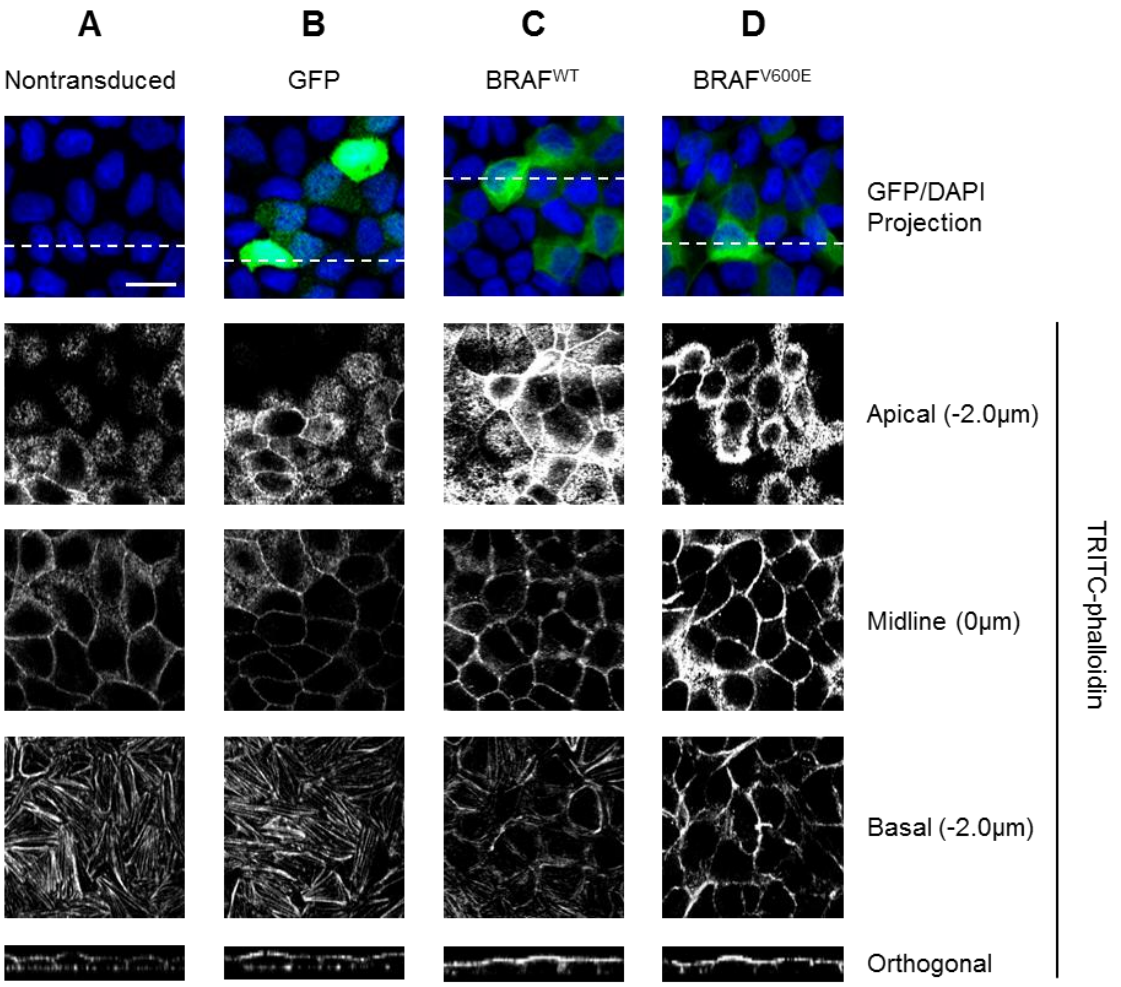

Figure 3.15: Expression of BRAF^{WT} and BRAF^{V600E} causes remodelling of the actin cytoskeleton. Confluent MDCKII cells were transduced to express GFP, BRAF^{WT} or BRAF^{V600E} for 24 hours prior to fixation. The actin cytoskeleton was stained with TRITC-phalloidin. (A) Successive optical slices proceeding from the apical to basal surfaces revealed that control cells exhibit cortical plasma membrane associated staining at the apical surface and midline, as well as an extensive meshwork of basal stress fibres. This pattern is maintained in GFP-expressing cells (B). In contrast, cells expressing BRAF^{WT} and BRAF^{V600E} lose basal stress fibres and exhibit increased levels of cortical actin (D and C, respectively). Images are representative of three biological repeats. Orthogonal views were taken in the indicated plane (dashed line). Scale bar = 20µm.

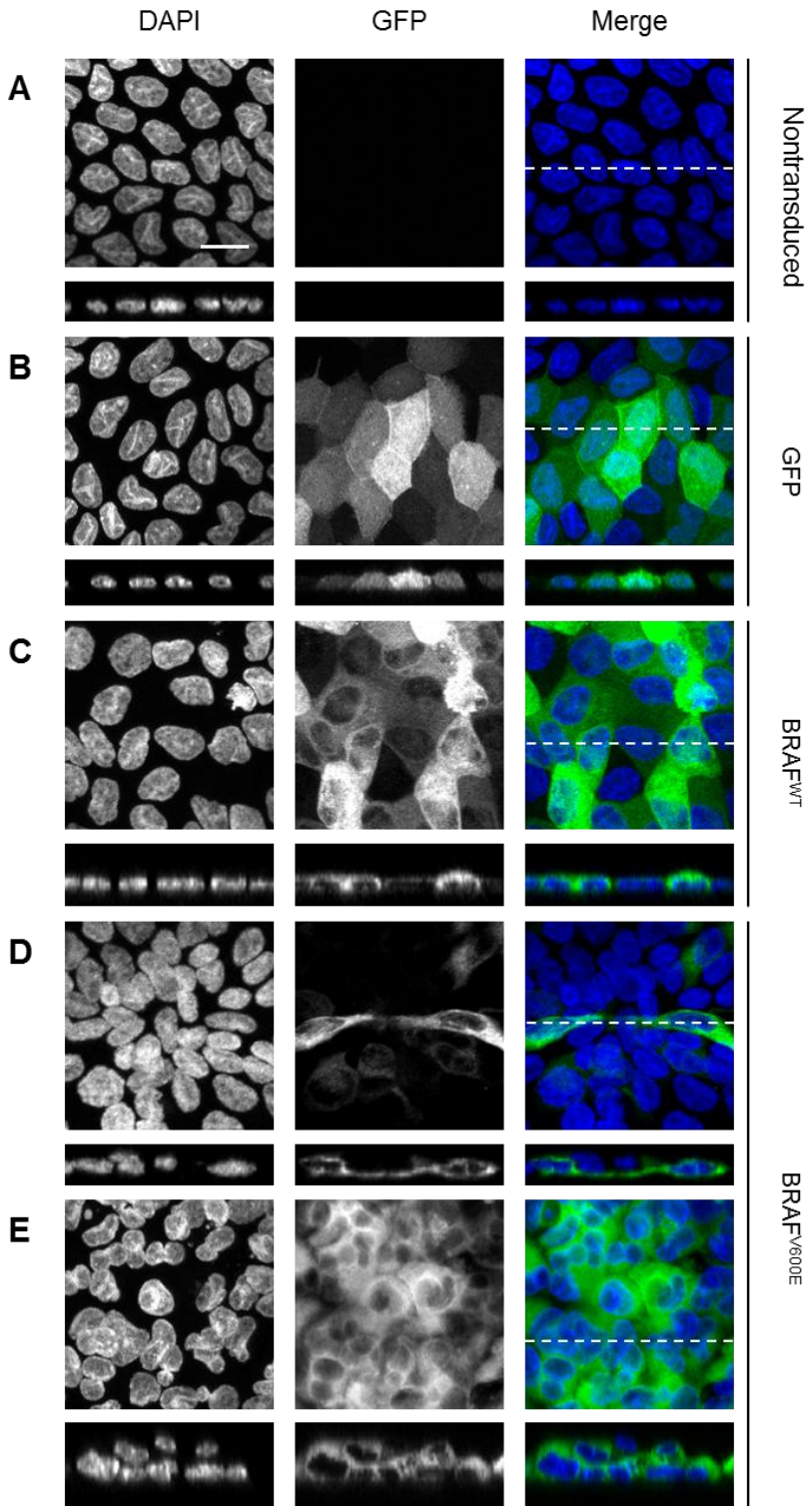

Figure 3.16: BRAF^{V600E} expression disrupts MDCKII monolayer organisation. Confluent MDCKII cells were transduced with 30pfu/nl adenovirus to express GFP, BRAF^{WT} or BRAF^{V600E}. Fixed cells were examined by confocal microscopy. Control cells (A), and those expressing GFP (B) or BRAF^{WT} (C), adopt a highly organised structure where cells are tightly packed together to form a monolayer. Expression of BRAF^{V600E} leads to cells adopting an elongated mesenchymal-like shape, with protrusions that reach below neighbouring cells (D). Groups of cells expressing high levels of BRAF^{V600E} overlap with one another, forming a highly disorganised multi-layered structure (E). Images are representative of three biological repeats. Orthogonal views were taken in the indicated plane (dashed line). Scale bar = 20µm.

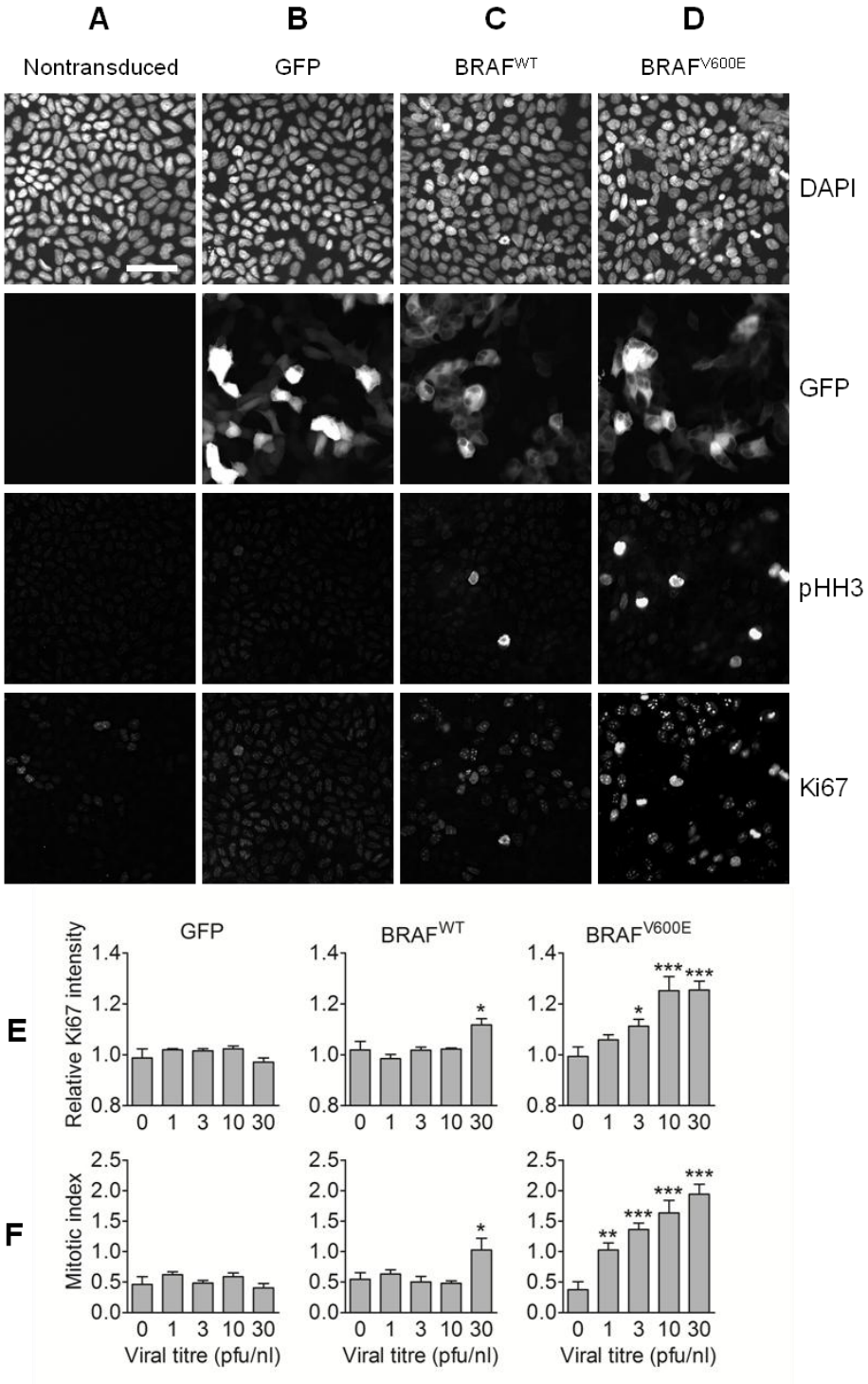

Figure 3.17: Expression of BRAF^{WT} and BRAF^{V600E} increases measures of MDCKII cell proliferation. Confluent MDCKII cells were transduced to express GFP, BRAF^{WT} or BRAF^{V600E} for 24 hours. Fixed cells were immunostained for the mitotic marker phospho-histone H3 (pHH3) and the proliferation marker Ki67. (A – D) Images of MDCKII cells expressing the indicated transgenes are representative of three biological repeats. Scale bar = 50µm. (E) Expression of BRAF^{V600E}, and high levels of BRAF^{WT}, increased the mean immunostaining intensity of the proliferation marker Ki67 (E). Mitotic cells were identified as those exhibiting pHH3 and Ki67 intensities above set threshold values. The mitotic index was calculated by dividing the number of mitotic cells by the total number of cells identified. (F) Expression of BRAF^{V600E}, and high levels of BRAF^{WT}, increased the mitotic index of MDCKII cells. Data are presented as mean values ±s.e.m from three independent experiments. Data were compared to the nontransduced control treatments using a two-way ANOVA with Bonferroni post-test, * p<0.05, ** p<0.01, *** p<0.005.

3.4 Discussion

Specific activation of the RAF/MEK/ERK pathway through the expression of $BRAF^{WT}$ and $BRAF^{V600E}$ alters the composition of the TJ through surprisingly diverse mechanisms, where individual TJ proteins are differentially regulated in terms of their total levels and distribution (summarised in Table 3.1).

Marker	Protein level		Localisation
	Immunoblot	Immunofluorescence	
Claudin-1	↓	-	Punctate cytoplasmic staining Retained at the apical junction
Claudin-2	↓↓↓	↓↓↓	Staining is lost
Claudin-4	-	↑	Increased levels at areas of cell-cell contact
Occludin	-	-	Diffuse cytoplasmic staining Retained at the apical junction
ZO-1	ND	ND	Diffuse cytoplasmic staining Retained at the apical junction Discrete nuclear staining
E-cadherin	-	-	Retained at the lateral membrane
Actin	ND	Total levels largely unaffected	Loss of basal stress fibres Increased apical membrane levels

Table 3.1: A summary of junction protein regulation following $BRAF^{WT/V600E}$ expression. Reported effects of RAF/MEK/ERK activity on junction protein level and subcellular distribution induced through the expression of $BRAF^{WT}$ or $BRAF^{V600E}$. (↓) marginally downregulated, (↓↓↓) strongly downregulated, (↑) marginally upregulated, (-) unaffected, (ND) not determined.

Protein levels of claudin-2, and to a lesser extent claudin-1, were decreased, as assessed by immunoblot and confocal microscopy. However, claudin-1 was maintained at the apical junction in $BRAF^{V600E}$-expressing cells, as well as being present in cytoplasmic compartments. In contrast, following $BRAF^{V600E}$ expression, claudin-4 immunostaining levels were increased. However, this may be a localised effect on claudin-4 distribution as this was not detectable by immunoblot. Although increased claudin-4 levels appeared throughout the cytoplasm, they were largely concentrated at areas of cell-cell contact following RAF/MEK/ERK activation. Overall levels of occludin and E-cadherin were not affected by expression of $BRAF^{WT}$ or $BRAF^{V600E}$ and although they exhibited increased diffuse cytoplasmic staining, both markers were largely conserved at areas of cell-cell contact. Similarly, ZO-1 was maintained at the apical junction, but also localised diffusely throughout the cytoplasm and was present as discrete punctae within the nucleus. This was accompanied by a concomitant transient increase in TER, which peaked at 24 hours after transduction with $AdBRAF^{V600E}$, before

falling again at later time points, indicating that epithelial barrier function was regulated by RAF/MEK/ERK activity in a manner dependent on signal duration.

Claudin-1 is downregulated, but retained at cell-cell contacts, following RAF/MEK/ERK activation.

By immunoblot, claudin-1 protein levels were marginally downregulated in response to BRAF^{V600E}-expression. Immunostaining revealed that in BRAF^{V600E}-expressing cells, claudin-1 was redistributed from the lateral membrane, with punctate staining visible throughout the cytoplasm. However, claudin-1 was retained at areas of cell-cell contact towards the apical side of the lateral membrane. Claudin-1 mRNA levels are not affected by EGF (Ikari et al., 2011c) HGF (Balkovetz 2004) or by the expression of a conditionally active ΔCRAF:ER fusion protein (Doehn et al., 2009). However, levels of claudin-1 protein, but not mRNA, are decreased in MDCKII cells after 24 hours of HGF treatment. Therefore, the downregulation of claudin-1 protein levels may proceed by post-transcriptional mechanisms. Alternatively, the redistribution of claudin-1 may influence its detergent-solubility and retrieval following cell lysis. Further experiments involving quantitative microscopy and lysis buffers containing stronger detergents are presented in chapter 5.

The distribution of claudin-1 was also affected by ERK pathway activation. The normal lateral membrane-associated pool was largely lost, with punctate staining visible throughout the cytoplasm. Furthermore, claudin-1 was retained towards the apical side of the lateral membrane. Ras-transformed MDCKII cells exhibit the loss of adhesive cell junctions (Chen et al., 2000). Although some junction proteins like E-cadherin are transcriptionally repressed, claudin-1 is sequestered in the cytoplasm (Chen et al., 2000). Furthermore, claudin-1 is rapidly restored to areas of cell contact following the addition of a MEK inhibitor, suggesting that RAF/MEK/ERK activity may influence the endocytic trafficking and subcellular distribution of claudin-1.

In contrast, EGF treatment has been shown to increase the proportion of claudin-1 at the lateral membrane of MDCKII cells (Singh and Harris, 2004). This is not fully blocked by co-treatment with cycloheximide, suggesting that the translocation of existing claudin-1 protein contributes to this junctional accumulation (Singh and Harris, 2004) . However, the mechanisms or changes in trafficking that are associated with this redistribution are currently unknown. Furthermore, EGF treatment and the expression of oncogenic Ras will activate multiple signalling pathways, and this highlights the requirement for using more specific tools that activate individual signalling pathways. This is desirable to study the unique contribution of each pathway to TJ regulation, in

comparison to inhibitor-based studies that do not exclude combinatorial regulatory mechanisms.

RAF/MEK/ERK activity leads to the downregulation of claudin-2 protein levels

Expression of BRAF^{V600E} led to a dramatic decrease in claudin-2 levels, as assessed by immunoblot and confocal microscopy, echoing studies showing that activation of the ERK pathway negatively correlates with renal claudin-2 mRNA and protein expression, both *in vitro* and *in vivo* (Lipschutz et al., 2005; Masaki et al., 2004). Treatment of MDCKII cells with EGF or HGF, or the expression of CA-MEK or ΔCRAF:ER, leads to the downregulation of claudin-2 at both the mRNA and protein level, in a MEK-dependent manner (Doehn et al., 2009; Ikari et al., 2011c; Lipschutz et al., 2005). A genome-wide microarray utilising an inducible activity ΔCRAF:ER fusion protein further showed that claudin-2 is transcriptionally downregulated by specific activation of the RAF/MEK/ERK pathway (Doehn et al., 2009). Therefore, the observed decrease in claudin-2 levels is likely to be at least partially due to decreased mRNA levels and protein synthesis. In addition, recent studies implicate ERK signalling in the post-translational regulation of claudin-2 protein levels; EGF is reported to accelerate its clathrin-mediated endocytosis and lysosomal degradation in a MEK-dependent manner (Ikari et al., 2011c). However, the actual rates of these processes have not been measured. From the current microscopy data, it is unclear whether claudin-2 accumulates intracellularly prior to its degradation, as immunofluorescence staining is almost completely lost by the time transgene levels become detectable. This makes it difficult to ascertain if specific activation of the ERK pathway regulates claudin-2 internalisation or degradation rates. These aspects of claudin-2 regulation necessitate the use of inducible-activity constructs and are studied later in chapter 5.

RAF/MEK/ERK activity increases junctional claudin-4 levels

While immunoblots suggest that claudin-4 levels are not influenced by BRAF^{WT} or BRAF^{V600E} expression, the immunostaining data indicates that total claudin-4 levels are increased by BRAF^{V600E}, and that the majority of this claudin-4 appears to be TJ-associated. This junctional incorporation may underlie the apparent discrepancy between the immunoblot and immunostaining data; the incorporation of proteins into the TJ is associated with decreased detergent solubility (Nusrat et al., 2000). Therefore, following BRAF^{V600E} expression, the majority of claudin-4 may exist in a relatively detergent-insoluble fraction that is inefficiently retrieved using lysis buffers containing mild detergents such as Triton X100, wich were used in the immunoblotting experiments. In addition to immunostaining, the relative distribution of claudin-4 could

be further assessed by extracting detergent-soluble and insoluble fractions using stronger detergents, such as NP40 or SDS.

RAF/MEK/ERK activity positively correlates with claudin-4 expression in MDCKII cells. EGF treatment increases claudin-4 levels in a Src- and MEK-dependent manner (García-Hernández et al., 2015; Ikari et al., 2009) and specific activation of the RAF/MEK/ERK pathway with ΔCRAF:ER also increases claudin-4 mRNA levels (Doehn et al., 2009). These reports suggest that ERK activity may increase *CLDN4* mRNA levels to increase claudin-4 protein synthesis. EGF treatment is also associated with promoting the incorporation of claudin-4 into cell-cell junctions (García-Hernández et al., 2015; Singh and Harris, 2004). This consistent with the presented confocal microscopy data, suggesting that claudin-4 was enriched at areas of cell-cell contact following BRAF^{V600E} expression. The EGF-mediated increase in junctional claudin-4 is blocked by the co-treatment with cycloheximide, suggesting that its junctional accumulation is predominantly due to the synthesis of new protein (Singh and Harris, 2004). Importantly, the specific roles of the ERK pathway, and its contribution to claudin-4 trafficking rates, have not been studied in detail.

Occludin is maintained at the apical junction in following RAF/MEK/ERK activation

Total occludin levels were unaffected by the expression of BRAF^{WT} or BRAF^{V600E}, either by immunoblot or confocal microscopy. Although increased diffuse cytoplasmic staining was observed following BRAF^{V600E} expression, occludin remained mostly localised at the apical junction. Previous studies in rat salivary gland Pa-4 cells established that activation of the ERK pathway with ΔCRAF:ER results in the transcriptional downregulation of occludin and subsequent loss of protein expression (Li and Mrsny, 2000), and a similar downregulation was reported in mouse hepatocytes (Lan et al., 2004). However, studies in tissues of different origins may not be directly relevant as it is widely recognised that RAF/MEK/ERK activity exhibits tissue-specific regulation of individual TJ proteins (Inai et al., 2013). Occludin was not identified as an ERK-regulated transcript in the ΔCRAF:ER genome-wide microarray in MDCKII cells (Doehn et al., 2009). Furthermore, the expression level and distribution of occludin is not affected by treatment with HGF, or the MEK inhibitor U0126 (Lipschutz et al., 2005). Taken together with the current data, these studies suggest that although occludin is transcriptionally regulated by the ERK pathway in some tissues, this is not conserved in MDCKII cells. This may be due to the tissue-specific expression of relevant transcription factors, or as a result of trafficking differences between cell types. In MDCKII cells, occludin is recycled to a far lesser extent than claudin-1 or -2, whereas

significant and rapid recycling of occludin has been observed in other cell types including mouse mammary MTD-1A epithelial cells and basic hamster kidney (BHK) fibroblasts (Morimoto et al., 2005).

In a manner similar to that of claudin-1, Ras-transformed MDCK cells maintain occludin in the cytoplasm, which is rapidly targeted to areas of cell contact upon MEK inhibition (Chen et al., 2000). This suggests that long-term activation of the ERK pathway may lead to the internalisation of occludin and its cytoplasmic sequestration. Cytoplasmic occludin staining following $BRAF^{V600E}$ expression is diffuse, compared to the distinct punctate staining of claudin-1. It is currently unclear if occludin and claudin-1 are redistributed in a complimentary manner.

ZO-1 exhibits increased cytoplasmic and nuclear staining, but is largely conserved at the apical junction following RAF/MEK/ERK activation

Although total levels of ZO-1 were not determined by immunoblot, the total levels were not significantly affected by immunofluorescence. $BRAF^{V600E}$ expression generated a similar response to that of occludin, where continuous junctional ZO-1 was maintained, despite an apparent increase in diffuse cytoplasmic staining. ZO-1 expression is maintained but confined to the cytoplasm of Ras-transformed MDCK cells. In a similar fashion to occludin and claudin-1, ZO-1 is rapidly translocated to areas of cell-cell contact upon MEK inhibition (Chen et al., 2000). Furthermore, MEK inhibition increases the half-life of ZO-1 by approximately 50%, suggesting that RAF/MEK/ERK activity may influence ZO-1 distribution and stability (Chen et al., 2000). As ZO-1 is a peripheral, rather than integral, membrane protein, its subcellular localisation is not necessarily governed by endocytic trafficking. However, as ZO-1 binds occludin and claudins via GUK and PDZ domain-mediated interactions, respectively (Fanning et al., 1998; Itoh et al., 1999), it could potentially be trafficked in complex with these, or other, TJ proteins. Alternatively, activation of the ERK pathway may lead to post-translational modification or altered protein-protein interactions at the TJ, which could potentially displace ZO-1 from the junctional complex and result in its diffuse distribution through the cell.

Interestingly, $BRAF^{V600E}$ expression also caused apparent accumulation of ZO-1 in the nucleus. ZO-1 may interact with nucleolar proteins under proliferative or promigratory conditions (Gottardi et al., 1996). This is associated with the G1/S transition and implicates ZO-1 as an important protein that can communicate signals between areas cell-cell contacts and nucleus (Benezra et al., 2007; Gottardi et al., 1996; Lopez-Bayghen et al., 2006).

RAF/MEK/ERK activity did not influence E-cadherin expression or distribution

The total protein levels and subcellular distribution of E-cadherin were not affected by the expression of $BRAF^{WT}$ or $BRAF^{V600E}$. Similar observations were made in MDCK cells stably expressing an inducible activity ΔCRAF:ER construct, where lateral E-cadherin staining is preserved, even when cells undergo extensive morphological rearrangements (Hansen et al., 2000).The transcriptional downregulation of E-cadherin and disassembly of Adherens junctions is associated with cell transformation and the epithelial-mesenchymal transition (Huang et al., 2012). The current data therefore suggests that modulation of TJ protein expression and localisation is a relatively early event following the induction of RAF/MEK/ERK signalling. While ERK activity is sufficient to increase E-cadherin phosphorylation, co-treatment with TGFβ is required to induce its subsequent ubiquitination, endocytosis and degradation (Janda et al., 2006). Even after this combined treatment, total E-cadherin levels are only significantly decreased after 2-3 days of treatment. This delayed post-translational regulation still precedes transcriptional downregulation, which only occurs after 5 days of cell treatment. Therefore, the simultaneous and sustained activation of multiple signalling pathways may be required to drive the redistribution and ultimate depletion of E-cadherin associated with EMT.

MDCKII barrier function is regulated by RAF/MEK/ERK signalling in a manner dependent on signal duration

$BRAF^{V600E}$ expression generated a transient increase in TER, which was lost at later time points. The paracellular pathway, which is regulated by the TJ, is the major determinant of TER in low resistance monolayers, including those comprised of MDCKII cells (Kahle et al., 2004). Epithelial permeability can be regulated by the overexpression or RNAi-mediated depletion of individual claudins (Hou et al., 2006). Claudin-2 confers cation-selective permeability, and its depletion increases MDCKII TER from ~75Ω.cm^2 to ~250Ω.cm^2 (Hou et al., 2006). Conversely, claudin-4 depletion decreases TER to ~50Ω.cm^2 and increases cation permeability (Hou et al., 2006). Therefore, the reciprocal downregulation of claudin-2 and upregulation of claudin-4 protein levels is consistent with the observed increase in TER after 24 – 32 hours, although other claudins or TJ proteins may also contribute to the regulation of epithelial permeability.

After 48 hours, TER levels began to decrease towards baseline levels, despite BRAF construct expression, ERK pathway activation and claudin-2 depletion being maintained at in this time frame. Therefore, this later decrease in TER is unlikely to be due to a reversal in cell phenotype. Long-term RAF/MEK/ERK pathway activation is

associated with cell dedifferentiation and transformation (Chen et al., 2000; Hansen et al., 2000; Lemieux et al., 2009), which occurs through the disassembly of epithelial junctions and loss of epithelial barrier function (Huang et al., 2012). Therefore, the later decrease in TER is more likely to be due to the physical disruption of the monolayer as cell movement breaks contacts required for TJ formation between adjacent cells.

This is consistent with studies involving the expression of a conditionally active ΔCRAF:ER fusion protein in MDCKII cells (Hansen et al., 2000), and reports concerning the differential effects of transient and sustained EGFR activation. While acute, transient EGFR activation results in increased TER (Singh and Harris, 2004), chronic activation through the stable expression of secreted heparin-binding EGF-like growth factor (hbEGF) resulted in cell transformation, increased cell proliferation, migration and loss of TER (Singh et al., 2004). Taken together with the current study, these data suggest that stimulus duration may affect the cellular response in terms of cell adhesion and barrier properties.

RAF/MEK/ERK activity mediates actin cytoskeleton remodelling and cell morphology changes

$BRAF^{V600E}$ expression led to the loss of epithelial organisation and dramatic changes in cell shape, which are associated with cell transformation. MDCKII cells normally form an organised monolayer, where individual cells adopt a compact polygonal shape. Expression of $BRAF^{V600E}$ caused cells to adopt a more elongated mesenchymal-like phenotype, and the formation of multi-layered structures. Although RAF/MEK/ERK activity is frequently insufficient for the transformation of melanocytes (Tsao et al., 2012) and epithelial cells (Du et al., 2004), this phenotype is consistent with studies demonstrating that the expression of active RAF (Hansen et al., 2000) or MEK (Montesano et al., 1999) is sufficient to transform MDCK cells.

These changes in cell morphology and organisation were accompanied by severe remodelling of the actin cytoskeleton. Unstimulated MDCK cells are characterised by stress fibres localised close to the basal membrane, which provide tension across the monolayer to promote the formation of focal adhesions (Guasch et al., 1998). Basal and lateral actin filaments also act to maintain a cylindrical cell shape (Nusrat et al., 1995). The apical domain is comprised of a perijunctional actomyosin ring, which is thought to regulate TJ permeability, and an ordered array of bundles that stabilise the structure of the apical plasma membrane domain (Nusrat et al., 1995). Expression of $BRAF^{V600E}$, and to some extent $BRAF^{WT}$, led to the loss of basal stress fibres and increased cortical actin associated with the apical plasma membrane domain. The

BRAF-induced stress fibre loss is likely to be mediated by modulation of Rho GTPase activity (Hansen et al., 2000) and be associated with decreased substrate adhesion and increased migratory capacity (Guasch et al., 1998). The increase in cortical actin may have a role in regulating the observed changes in epithelial permeability at these time points (Nusrat et al., 1995).

Expression of $BRAF^{V600E}$, and higher levels of $BRAF^{WT}$, also increased MDCKII cell proliferation. This is consistent with studies where HGF treatment increased MDCKII cell proliferation in a MEK-dependent manner (Li et al., 2004). ERK activity, cell proliferation and cell density are inextricably linked; as MDCK cell density increases, ERK phosphorylation and growth rates decrease due to a process termed contact inhibition of proliferation (Li et al., 2004). Although high cell density and junction formation appear to downregulate ERK activity and restrain growth rates (Laprise et al., 2004), expression of $BRAF^{V600E}$, or high levels of $BRAF^{WT}$, was sufficient to overcome contact inhibition of proliferation in MDCKII cells. From the current data, it is not possible to determine if increased proliferation rates are causative, or a consequence, of junction disassembly. Alternatively, TJ proteins and cell proliferation may be independently regulated when ERK activity is induced in confluent MDCKII monolayers.

PD0325901 suppresses the expression of $BRAF^{WT}$ and $BRAF^{V600E}$

Attempts to inhibit or reverse the BRAF-mediated effects on claudin expression and distribution were confounded by the unexpected loss of transgene expression following the addition of the MEK inhibitor PD0325901. This appeared to be specific to the expressed BRAF transgenes as PD0325901 treatment did not affect the level of endogenously expressed GFP. As the expression of both the BRAF transgenes and GFP were driven by the same CMV promoter, this suggests repression may have been at the post-transcriptional level. Alternatively, expression from the CMV promoter may be sensitive to MEK inhibition, with differences in stability influencing the degradation rates of monomeric GFP and BRAF transgenes. However, there is a lack of data regarding the effects of small molecule inhibitors on the activity of commonly used promoters. This highlights the importance of confirming sustained transgene expression when assigning functional relevance to downstream signalling pathways based on the use of small molecule inhibitors. Although ERK phosphorylates RAF kinases in both positive and negative feedback loops, this is generally associated with altered RAF dimerisation and activity, rather than protein stability (Ritt et al., 2010; Sturm et al., 2010). Further work studying the effects of distinct MEK inhibitors on the

half-lives of endogenous RAF kinases would be required to establish if RAF kinase stability is physiologically regulated in a MEK/ERK-dependent manner.

3.5 Limitations and future work

Expression of $BRAF^{WT}$ and $BRAF^{V600E}$ clearly indicates that specific activation of the RAF/MEK/ERK pathway induces TJ remodelling by differentially regulating the total level and subcellular distribution of individual TJ components. However, with the current experimental setup, it is hard to manipulate the duration of ERK signalling in a coordinated manner across the whole cell population. As a result, it is difficult to determine the relevant mechanisms of downregulation and redistribution. There are also wider ranging effects of RAF/MEK/ERK activation on MDCK cells, including changes in cell morphology, organisation and proliferation that are associated with cell transformation. It is therefore hard to distinguish mechanisms that may specifically regulate TJ remodelling in response to RAF/MEK/ERK pathway activation from consequences of gross changes in cell arrangement and interaction. Furthermore, mechanistic insights are limited by the surprising inhibition of BRAF construct expression levels through the treatment with the MEK inhibitor, PD0325901.

TJ protein levels assessed by immunoblot may be influenced by their subcellular distribution and resulting detergent-solubility. It will be important to further investigate changes in TJ protein level using lysis buffers containing stronger detergents that will more fully solubilise TJ-associated proteins, or alternative microscopy and imaging based approaches.

By the time that BRAF transgene becomes detectable, extensive changes in TJ protein expression and subcellular distribution have already occurred, making it impossible to determine the rates of degradation or endocytic trafficking that may underlie some of these changes. In order to achieve coordinated ERK activation with increased temporal control, inducible-activity RAF:ER fusion proteins will be generated in the next chapter, with the aim of studying the downstream effects on rates of TJ protein internalisation, degradation and recycling. This approach will potentially allow the study of ERK signalling on TJ remodelling, prior to broader changes associated with transformation and in a manner more amenable to pharmacological intervention than the current $BRAF^{WT}$ and $BRAF^{V600E}$ constructs.

3.6 Summary

- Adenoviral vectors allow the efficient transduction of MDCKII cells and the expression of $BRAF^{WT}$ and $BRAF^{V600E}$ constructs that specifically activate the RAF/MEK/ERK pathway.

- Specific activation of the RAF/MEK/ERK pathway is sufficient to cause a transient increase in TER, which occurs concurrently with the differential regulation of TJ protein levels and localisation.

- Consistent with this increase in TER, claudin-2 protein levels are dramatically decreased, while junctional claudin-4 levels are increased.

- Claudin-1, occludin, and ZO-1 are retained at the apical junction, but also exhibit varying degrees of intracellular staining.

- TJ remodelling occurs prior to any changes in E-cadherin protein level or subcellular distribution.

- RAF/MEK/ERK activity is also associated with a transformed phenotype consisting of cytoskeletal remodelling, changes in cell morphology and organisation and increased rates of proliferation, which may potentially contribute to TJ remodelling and epithelial barrier regulation.

Chapter 4: Generation of inducible-activity RAF:ER fusion proteins

4.1 Rationale

By studying the effects of $BRAF^{WT}$ and $BRAF^{V600E}$ expression, as described in chapter 3, it is clear that RAF/MEK/ERK pathway activation has dramatic effects on TJ composition, as well as more widespread effects on cell proliferation and morphology associated with cell transformation. However, observations using these constructs are limited by the time required for transgene expression to become detectable. Studying ERK-mediated effects at earlier time points is complicated as it is difficult to establish when sufficient transgene expression levels are reached to elicit downstream activation of MEK and ERK. The ability to conditionally activate a protein of interest is desirable for studying temporal aspects of downstream signalling. In terms of this study, a conditionally active RAF kinase construct would allow the coordinated activation of the RAF/MEK/ERK pathway across a cell population, permitting the study of ERK-dependent effects on rates of TJ protein trafficking, expression and degradation over shorter and tightly controlled time frames.

Fusion of a protein of interest, typically a kinase or transcription factor, to the hormone-binding domain (HBD) of a steroid receptor frequently yields a product which is regulated by the presence of the cognate steroid hormone in the culture medium (McMahon, 2001). The benefits of using HBD fusion proteins include: i) rapid and reversible activation of the protein of interest through posttranscriptional modes of activation, ii) the ability to titrate the activity of the protein of interest by varying the concentration of the cognate steroid hormone, and iii) the relative ease of construct generation and use. Inducible-activity RAF kinase constructs will allow specific activation of the RAF/MEK/ERK pathway independently of other signalling pathways. In contrast to the constitutively active constructs, these fusion proteins will allow the coordinated activation of the ERK pathway through the addition of 4-hydroxytamoxifen (4HT) to the culture medium, allowing tighter control of the point of activation and the duration of signalling across the whole cell population.

A series of molecular tools have been generated by fusing RAF proteins to the HBD (residues 282-595) of the human estrogen receptor (hbER) (Pritchard et al., 1995; Samuels et al., 1993). RAF kinase activity can be regulated by 17β-estradiol, the physiological agonist of the estrogen receptor, 4-hydroxytamoxifen or 4HT, a selective estrogen receptor modulator (SERM) that can be agonistic or antagonistic in different contexts, or the ICI series of estrogen receptor “pure” antagonists (Feil et al., 1997). Various mutations have been introduced to improve selective fusion protein activation and alleviate “leaky” or undesirable activation by estrogen-like compounds, such as phenol red, which are common in cell culture media (Figure 4.1) (Feil et al., 1997). A

G400V mutation (ER^{VG}) reduces estradiol-sensitivity by approximately 10-fold, resulting in ER^{VG}, which exhibits low baseline activity, but is strongly activated by estradiols, 4HT or ICI (Feil et al., 1997). Although useful *in vitro*, where sources of estradiols can be removed, the requirement to use these types of constructs *in vivo* drove the development of estradiol-insensitive ER mutants (Feil et al., 1997). ER^{GR}/ER^{T} was generated by a G525R mutation, which reduced estradiol sensitivity by approximately 1000-fold but maintained the ability to be activated by 4HT or ICI (Feil et al., 1997). Two further estradiol-resistant ER mutants, L539A/L540A (ER^{T1}) and M543A/L544A (ER^{T2}) have been characterised and exhibit distinct sensitivities to 4HT and ICI, with ER^{T1} preferentially activated by ICI, and ER^{T2} by 4HT (Feil et al., 1997).

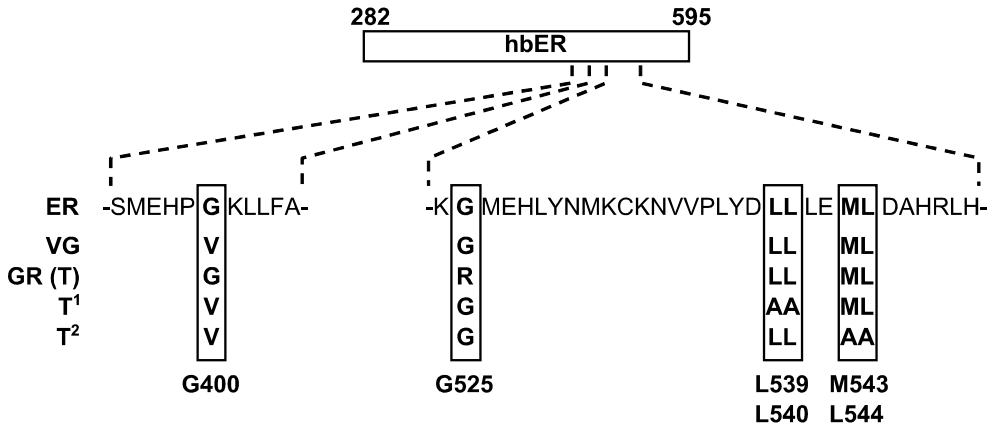

ER	Sensitivity		
	17β-estradiol	4-hydroxytamoxifen	ICI-182780
VG	Y	Y	Y*
GR (T)	N	Y	Y*
T^1	N	Y	Y
T^2	N	Y	Y*

Figure 4.1: ER domain mutants exhibit distinct sensitivities to activating ligands. Proteins fused to the hormone-binding domain of the estrogen receptor (hbER, residues 282-595 of the human estrogen receptor) were initially sensitive to estradiol-mediated activation. Various mutations (ER^{VG} and ER^{T}) have been introduced to reduce baseline activity and inappropriate activation by endogenous sources of estradiols *in vitro* and *in vivo*. More recent ER^{T1} and ER^{T2} iterations exhibit greater estradiol-resistance and can be potently and selectively activated by 4HT or ICI compounds. (Y) Potently activated (EC_{50} ≤ 20nM), (Y*) activated, but activity did not plateau in presence of up to 250nM ligand (i.e. weakly activated), (N) not activated in presence of up to 250nM ligand. Figure and table adapted from Feil (1997). Sensitivity to different ligands is based on the *in vitro* activity of various Cre:ER recombinase mutants.

ER domain optimisation has resulted in the generation of fusion proteins that exhibit lower baseline activity and has alleviated concerns regarding inappropriate activation by endogenous ligands, either *in vitro* or *in vivo.* Furthermore, activating ligands can be used at lower concentrations, reducing the potential for off-target effects while achieving more complete fusion protein activation.

Cell lines have been generated that stably express these RAF:ER fusion proteins. However, the generation of stable cell lines is time-consuming and requires antibiotic selection, which can influence cell phenotype. Although the generation of stably transfected MDCKII lines has been reported, clonal selection can often result in altered epithelial permeability properties and claudin expression levels (Milatz et al., 2010). To allow a more flexible experimental setup, we aimed to generate adenoviruses to express RAF:ER fusion proteins in MDCKII cells, providing the benefits of high efficiency transduction and regulation of construct expression level, while avoiding the requirement for selection protocols.

Initial RAF:ER fusion proteins consisted solely of the constitutively active truncated C-terminal kinase domain fused to the ER domain (ΔRAF:ER) (Pritchard et al., 1995; Samuels et al., 1993). Subsequent studies indicated that full-length CRAF could be rendered hormone-dependent in a similar manner, although these full-length CRAF fusion proteins exhibit lower kinase activity than ΔCRAF:ER constructs (McMahon, 2001). Mutation of the CRAF NtA from SSYY to SSDD increased the activity of CRAF:ER (Bosch et al., 1997), suggesting that full-length BRAF fusion proteins, which already harbour this sequence, may prove to be useful experimental tools. More recently, highly potent and pathophysiologically relevant full length $BRAF^{V600E}$:ER fusions have successfully been used to study temporal aspects of RAF/MEK/ERK signalling (Cagnol and Rivard, 2012; Liu et al., 2007). To further the initial studies involving hormone-independent $BRAF^{WT}$ and $BRAF^{V600E}$, we initially attempted to generate recombinant adenoviruses to efficiently express myc- and GFP-tagged $BRAF^{WT}$:ER and $BRAF^{V600E}$:ER fusion proteins in MDCKII cells. Characterisation of fusion protein activity and inducibility will primarily be achieved using high-content microscopy. The high-throughput nature of this approach will allow the efficient characterisation of a number of variables, including adenoviral titre, hormone concentration and time frame of downstream pathway activation. Furthermore, this approach will permit the study of RAF:ER activity on the single cell level, which will be important when studying the distribution of TJ proteins by confocal microscopy.

4.2 Aims and objectives

The aim of this chapter is to generate and characterise inducible-activity RAF:ER fusion proteins to permit the study of tight junction protein trafficking at earlier time points. This will be achieved by completing the following objectives:

1. Generate recombinant adenoviruses to express hormone-dependent $BRAF^{WT}$:ER and $BRAF^{V600E}$:ER fusion proteins in MDCKII cells.

2. Characterise basal construct activity and inducibility using immunostaining and high-content microscopy to assess downstream ERK phosphorylation.

3. Optimise the experimental setup with respect to viral titres, hormone concentrations and timescales of fusion protein activation.

4.3 Results

4.3.1 Generation of full-length BRAF:ER fusion proteins

Two inducible-activity BRAF:ER fusion constructs consisting of $BRAF^{WT}$ or $BRAF^{V600E}$ N-terminally tagged with GFP and myc, and fused to the T2 version of the ligand binding domain of the human estrogen receptor (ER^{T2}) were expressed under the control of the cytomegalovirus (CMV) promoter. These fusion proteins are hence referred to as $BRAF^{WT}$:ER and $BRAF^{V600E}$:ER (Figure 4.2). Recombinant adenoviruses were generated and purified to a high titre to efficiently express each fusion protein in MDCKII cells.

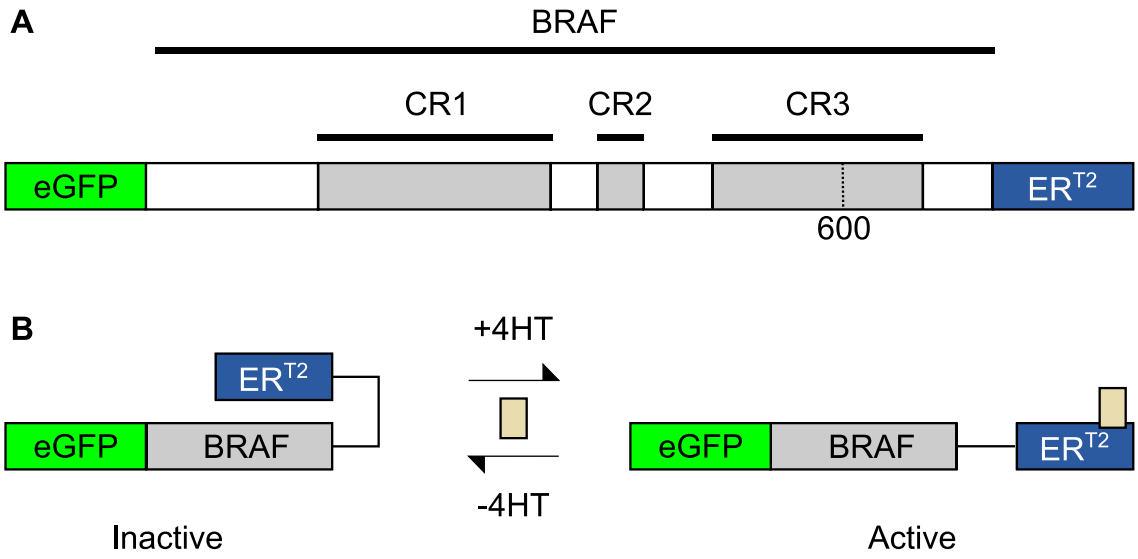

Figure 4.2: A schematic representation of inducible activity BRAF:ER fusion proteins. (A) A schematic of BRAF:ER fusion protein design. $BRAF^{WT}$ or $BRAF^{V600E}$ are fused to the ER^{T2} domain and N-terminally labelled with both eGFP and myc epitope tags. Constitutive expression is driven by the cytomegalovirus (CMV) promoter. (B) A proposed model for BRAF:ER activation. In the absence of activating ligand, the ER^{T2} domain is proposed to impair the catalytic activity of the kinase domain through steric inhibition. Rapid activation is achieved upon the addition of activating hormone ligands, such as 4-hydroxytamoxifen (4HT). While some ER fusion proteins are activated solely through increased protein stability, conformational changes underlie the rapid and protein synthesis-independent activation of RAF:ER proteins (McMahon, 2001).

To establish the relative activity and inducibility of the generated BRAF:ER fusion proteins, transduced and treated cells were fixed and immunostained to determine relative levels of fully active, dual phosphorylated ERK1/2 (ppERK1/2). Relative ppERK1/2 levels were quantified based on the immunostaining intensity using INCell Developer Toolbox software, using the segmentation and analysis strategy outlined in Chapter 3 (Figure 3.2).

MDCKII cells were transduced to express either GFP alone, $BRAF^{WT}$:ER or $BRAF^{V600E}$:ER and treated with a range of 4HT concentrations for 2 hours. Both the localisation and expression level of each construct was determined based on GFP intensity (Figure 4.3). GFP alone localised uniformly throughout the cell, while $BRAF^{WT}$:ER was unexpectedly concentrated at the plasma membrane at areas of cell-to-cell contact (Figure 4.3A). $BRAF^{V600E}$:ER was expressed throughout the cytoplasm, but was excluded from the nucleus and, in contrast to $BRAF^{WT}$:ER, did not accumulate at the cell periphery (Figure 4.3A).

4.3.2 RAF/MEK/ERK pathway activation by $BRAF^{WT}$:ER and $BRAF^{V600E}$:ER

Surprisingly, high-content microscopy revealed that ppERK1/2 levels were not stimulated above basal nontransduced levels following the expression of $BRAF^{WT}$:ER, in either the absence or presence of 4HT (Figure 4.3A). In contrast, ppERK1/2 levels were unexpectedly elevated following the expression of $BRAF^{V600E}$:ER, in both control and 4HT-treated conditions (Figure 4.3A). Based on population mean values, quantification of ppERK1/2 immunostaining intensity revealed $BRAF^{V600E}$:ER expression alone led to an approximate 4-fold increase in ppERK1/2 intensity, while $BRAF^{WT}$:ER expression did not increase ppERK1/2 intensity beyond basal levels (Figure 4.3B). While $BRAF^{WT}$:ER did not induce ERK phosphorylation at any concentration of 4HT tested, high basal $BRAF^{V600E}$:ER activity could be further increased following the addition of 4HT at 0.1, 1 or 10µM 4HT for 2 hours (Figure 4.3B). Therefore, neither $BRAF^{WT}$:ER or $BRAF^{V600E}$:ER exhibited desirable hormone-dependent activity; $BRAF^{WT}$:ER is an inactive kinase and $BRAF^{V600E}$:ER exhibits unacceptable levels of basal or “leaky” activity in the absence of activating hormone.

To determine whether high fusion protein expression levels were responsible for the inappropriate basal activity of $BRAF^{V600E}$:ER in the absence of 4HT, individual cells were grouped into subpopulations, or “binned”, according to their GFP intensity as a measure of construct expression level (Figure 4.3C). Plotting $BRAF^{V600E}$:ER expression level against ppERK1/2 output generated a sigmoidal response curve where increasing expression levels correlated with increased ppERK1/2 intensity (Figure 4.3C). The

relationship between $BRAF^{V600E}$:ER expression level and ERK phosphorylation was identical between control and 4HT-treated conditions, with $logEC_{50}$ values of 2.50, 2.48, 2.47 and 2.46 at 0, 0.1, 1 and 10µM 4HT, respectively (Figure 4.3C). This indicates that $BRAF^{V600E}$:ER exhibits equally potent activity in control and 4HT-treated conditions and that the high basal activity of $BRAF^{V600E}$:ER observed was not a result of excessively high expression levels. $BRAF^{WT}$:ER was unable to induce downstream ERK phosphorylation at any expression level or 4HT concentration (Figure 4.3C).

4.3.3 $BRAF^{WT}$:ER and $BRAF^{V600E}$:ER activity is not influenced by phenol red

The ER^{T2} domain used to generate these proteins is reportedly insensitive to estradiol-mediated activation (Feil et al., 1997). Phenol red is a pH indicator commonly used in cell culture media, but is also a weak estrogen agonist (Samuels et al., 1993). The utilisation of ER^{T2} should eliminate the necessity to exclude phenol red from the culture medium and, as expected, both $BRAF^{WT}$:ER and $BRAF^{V600E}$:ER displayed similar properties when cells were cultured in phenol red-free media (Figure 4.4A). $BRAF^{V600E}$:ER expression caused constitutive downstream phosphorylation of ERK1/2 in the absence of 4HT (Figure 4.4B) and this was evident at all measured expression levels (Figure 4.4C). As all experiments were carried out in serum-free conditions to minimise the activation of other signalling pathways and simplify experimental analysis, the high basal activity of $BRAF^{V600E}$:ER, could not be attributed to undue activation by phenol red or serum-associated estradiols (Figure 4.4). $BRAF^{WT}$:ER was inactive under all experimental conditions (Figure 4.4B and C). As these full-length BRAF:ER fusions did not provide the desirable qualities of an inducible-activity system, alternative ΔCRAF:ER constructs were generated and characterised.

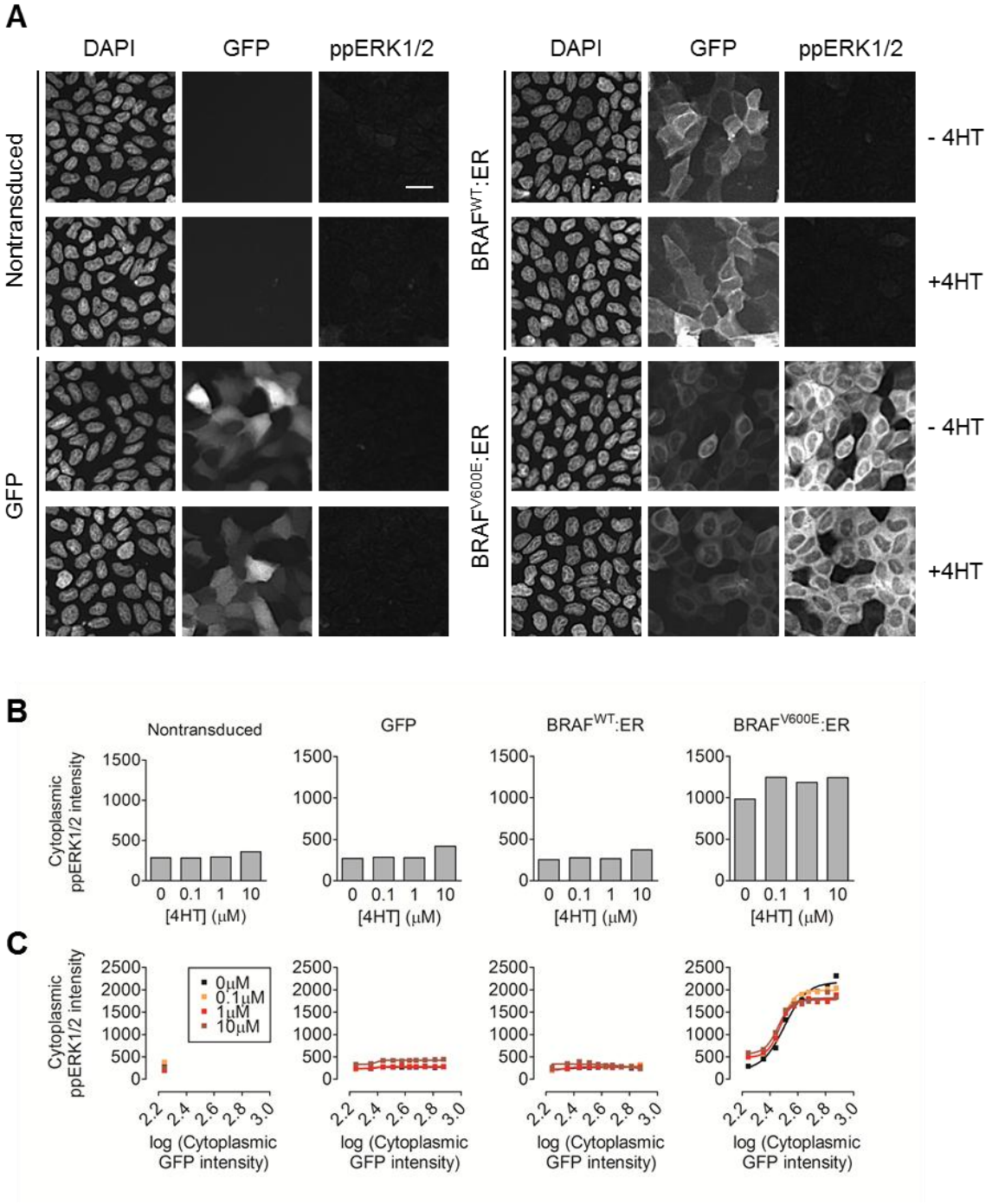

Figure 4.3: Characterisation of BRAF^{WT}:ER and BRAF^{V600E}:ER fusion protein activity. Confluent MDCKII cells were adenovirally transduced to express GFP, BRAF^{WT}:ER or BRAF^{V600E}:ER and treated with the indicated concentrations of 4HT for 2 hours. (A) Representative images of MDCKII cells immunostained for ppERK1/2, Construct expression level and localisation were assessed by GFP intensity. Downstream RAF/MEK/ERK pathway activation was assessed by the intensity of ppERK1/2 in the cytoplasm. (B) Mean cytoplasmic ppERK1/2 intensity measurements revealed that while GFP alone and BRAF^{WT}:ER do not increase ERK phosphorylation, BRAF^{V600E}:ER is highly active, in both the absence and presence of 4HT. (C) Cells were grouped into subpopulations based on transgene expression level. While BRAF^{V600E}:ER expression positively correlates with ERK1/2 phosphorylation, it is equally potent in the control and 4HT-treated conditions. Images and data are representative of two biological repeats. Scale bar = 20μm.

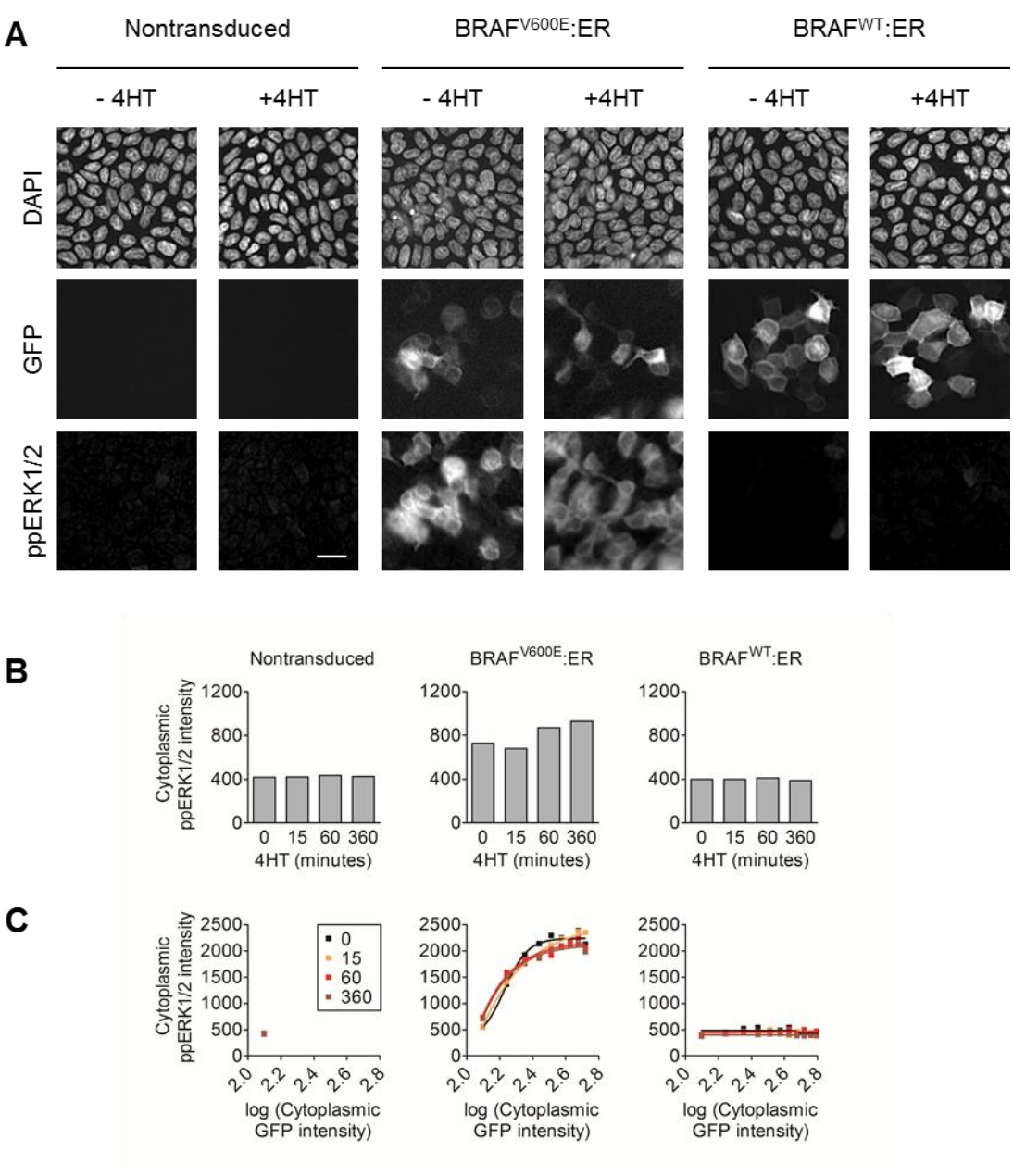

Figure 4.4: Characterisation of BRAF^{WT}:ER and BRAF^{V600E}:ER activity in media lacking phenol red. Confluent MDCKII cells were adenovirally transduced to express GFP, BRAF^{WT}:ER or BRAF^{V600E}:ER and treated with 1µM 4HT for the indicated time periods. (A) Representative images of MDCKII cells fixed and immunostained for ppERK1/2. Construct expression level and localisation were assessed by GFP intensity. Downstream RAF/MEK/ERK pathway activation was assessed by the intensity of ppERK1/2 in the cytoplasm. (B) Mean cytoplasmic ppERK1/2 intensity measurements of MDCKII cells expressing GFP, BRAF^{WT}:ER or BRAF^{V600E}:ER. BRAF^{WT}:ER remains inactive and BRAF^{V600E}:ER retains high basal activity even when phenol red is excluded from the culture medium. (C) MDCKII cells were grouped into subpopulations based on transgene expression level. The specific activity of BRAF^{WT}:ER and BRAF^{V600E}:ER is not affected by the presence of 4HT over a time period of 6 hours. Images and data are representative of two biological repeats. Scale bar = 20µm.

4.3.4 Generation of ΔCRAF:ER fusion proteins

As the previously described BRAF:ER fusion proteins were unsuitable for subsequent studies, alternative ΔCRAF:ER fusion proteins were generated. These earlier iterations have been widely used and are more fully characterised than full-length BRAF:ER fusion constructs (Pritchard et al., 1995; Samuels et al., 1993). ER^T is fused to the C-terminal of the human CRAF kinase domain (residues 305 – 648), which is N-terminally tagged with either eGFP, HA or myc epitope tags (Figure 4.5). The fusion proteins expressed are referred to as eGFPΔCRAF:ER, mycΔCRAF:ER and HAΔCRAF:ER, respectively.

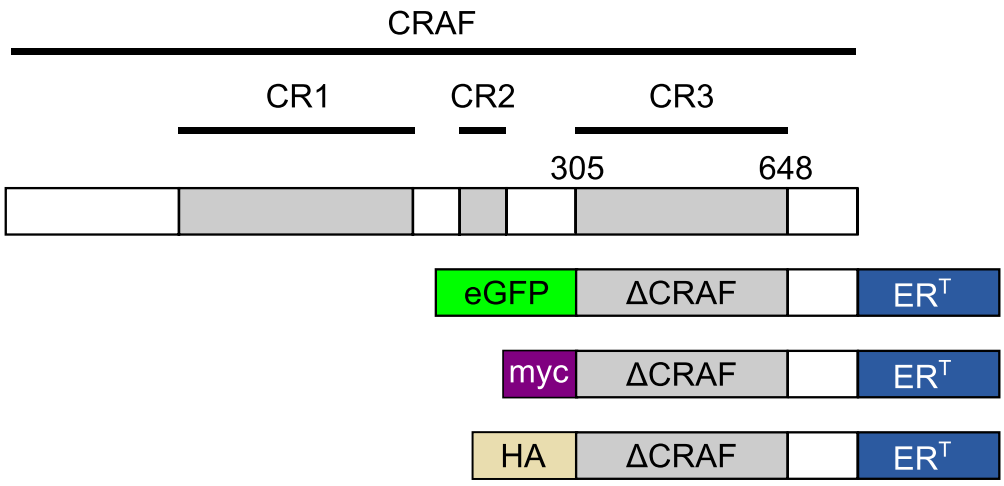

Figure 4.5: A schematic representation of eGFP-, HA- and myc-tagged inducible activity ΔCRAF:ER fusion proteins. The kinase domain (residues 305-648) of the human CRAF protein is fused to ER^T and N-terminally labelled with eGFP, HA or myc tags. Hormone-dependent activation of ΔCRAF:ER fusion proteins is thought to proceed through rapid post-translational conformational changes as outlined in Figure 4.2.

4.3.5 eGFPΔCRAF:ER provides improved control of RAF/MEK/ERK activity

Initial characterisation of eGFPΔCRAF:ER demonstrated that it exhibited improved properties, with lower basal activity that could be enhanced by 4HT treatment (Figure 4.6A). MDCKII cells expressing eGFPΔCRAF:ER were treated with a range of 4HT concentrations for 1 hour prior to fixation. Quantification of immunostaining revealed a concentration-dependent increase in downstream ERK phosphorylation, with increasing cytoplasmic ppERK1/2 levels evident at 0.1μM 4HT, which then plateaued at a concentration of 1μM (Figure 4.6B). Increasing the 4HT concentration to 10μM did not further increase downstream ERK phosphorylation (Figure 4.6B). This concentration-dependent response was evident based on cell population means (Figure 4.6B) and when cells were "binned" according expression level (Figure 4.6C), indicating that maximal eGFPΔCRAF:ER activity was achieved using 1μM 4HT. Although increasing ΔCRAF:ER expression levels correlated with downstream ERK1/2 phosphorylation (Figure 4.6C), mean cytoplasmic GFP intensity measurements revealed that cells generally express relatively low levels of eGFPΔCRAF:ER (Figure 4.6D), and will exhibit the desired combination of low basal activity with rapid activation upon 4HT treatment.

4HT treatment increased the amount of eGFPΔCRAF:ER protein that was detectable, both by high-content microscopy (Figure 4.6D) or by immunoblot (Figure 4.6E). As samples were either fixed or lysed simultaneously, this increase in expression level is due to 4HT treatment and not increased incubation times. Increased ERK phosphorylation preceded the observed increase in eGFPΔCRAF:ER expression (Figure 4.6E) and 4HT treatment clearly increased the specific activity of eGFPΔCRAF:ER (Figure 4.6C). Immunoblotting revealed that on a population level, eGFPΔCRAF:ER expression alone did not increase ppERK1/2 levels (Figure 4.6E). However, ppERK1/2 levels were dramatically increased by a 1 hour treatment with 1μM 4HT (Figure 4.6E), which was sustained for at least 48 hours while 4HT was present in the culture medium (Figure 4.6E). Therefore, eGFPΔCRAF:ER has the required characteristics for the subsequent use in TJ trafficking studies.

4.3.6 RAF/MEK/ERK pathway activation by HA- or myc-tagged ΔCRAF:ER

Two additional versions of ΔCRAF:ER, with either an N-terminal HA or myc epitope tag (Figure 4.5), exhibited similar properties, where both mean ppERK1/2 levels and specific activity were increased following the addition of 4HT to the culture medium (Figure 4.7A). Each ΔCRAF:ER fusion protein had similar properties to eGFPΔCRAF:ER and exhibited low levels of intrinsic basal activity, which were rapidly increased upon the addition of 4HT to the culture medium (Figure 4.7B and C).

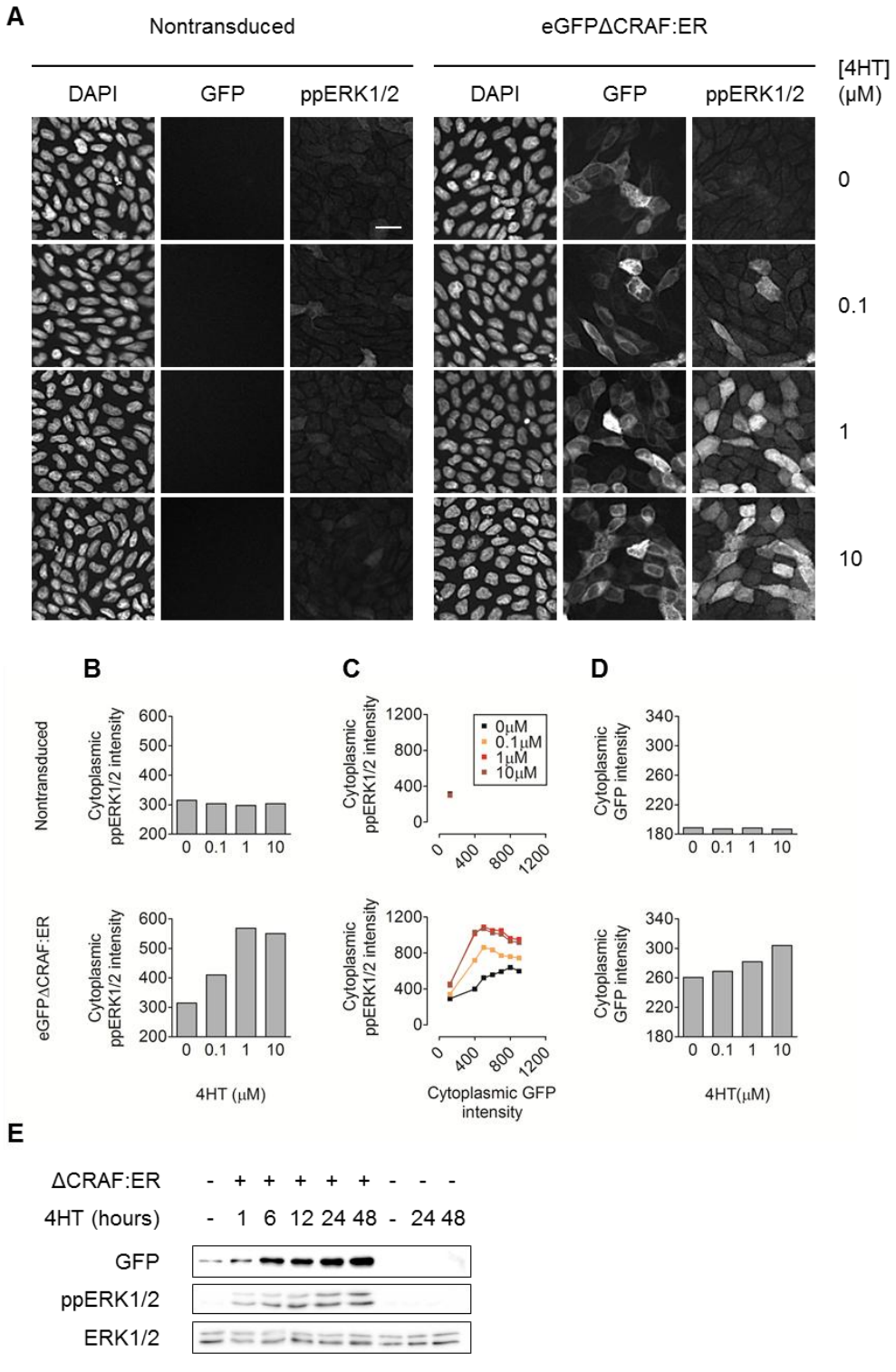

Figure 4.6: Characterisation of eGFPΔCRAF:ER fusion protein activity. Confluent MDCKII cells were transduced to express eGFPΔCRAF:ER and treated with the indicated concentrations of 4HT for 1 hour. (A) Representative images of MDCKII cells fixed and stained for ppERK1/2. (B) Mean cytoplasmic ppERK1/2 intensity measurements reveal that eGFPΔCRAF:ER exhibits low basal activity, as values are not increased compared to nontransduced control cells in the absence of 4HT. ppERK1/2 levels are increased by 4HT in a concentration-dependent manner. (C) The specific activity of eGFPΔCRAF:ER is increased by 4HT in a concentration-dependent manner, plateauing at 1μM. Although eGFPΔCRAF:ER expression correlates with cytoplasmic ppERK1/2 intensity, this aberrant activity is largely confined to those cells expressing higher levels of the fusion protein. (D) Mean GFP intensity measurements reveal that transgene expression levels are relatively low; as a result, basal activity is minimal, but also 4HT-responsive. Images and data are representative of two biological repeats. Scale bar = 20μm.

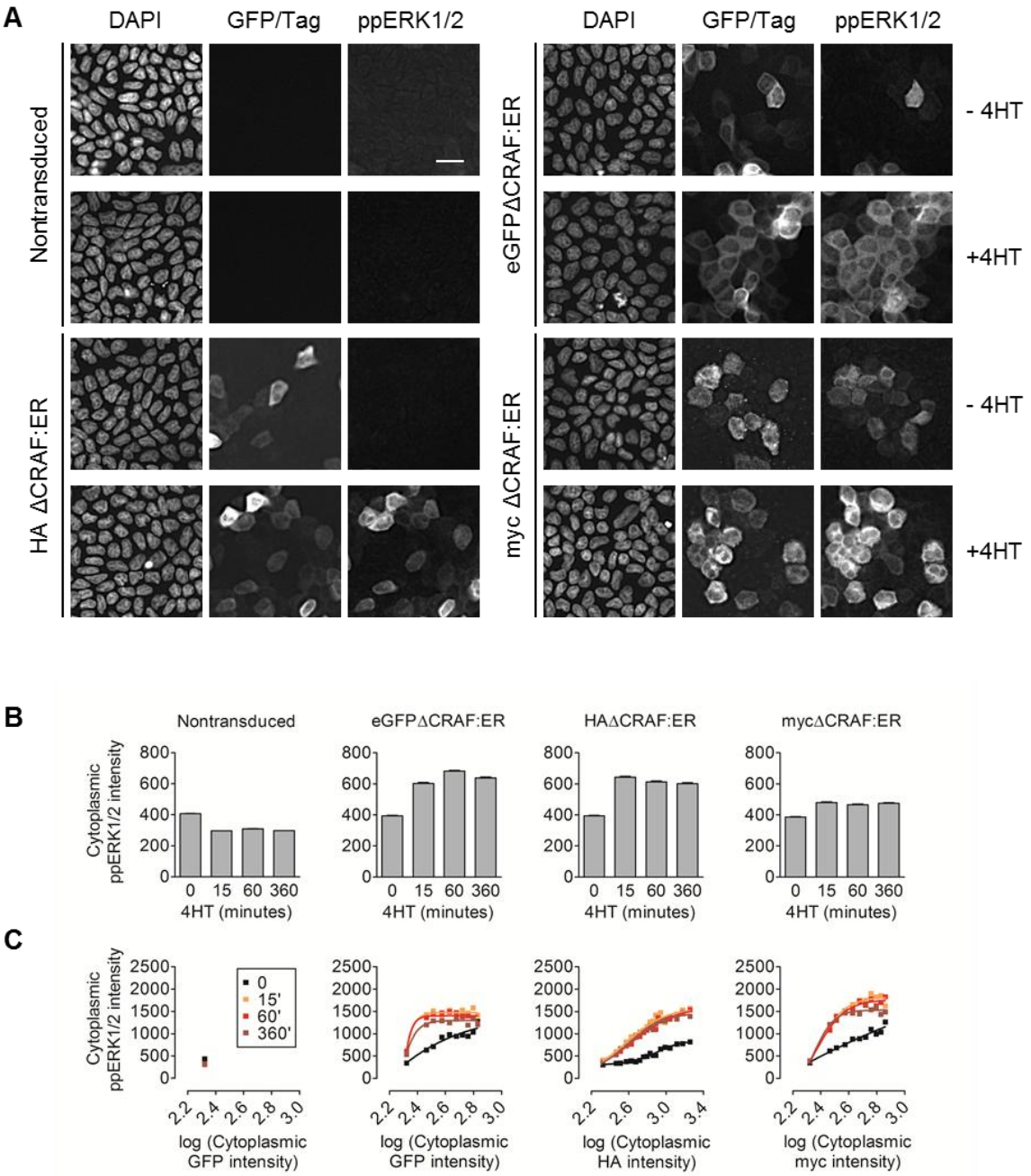

Figure 4.7: Characterisation of HA- and myc-tagged ΔCRAF:ER fusion protein activity. ΔCRAF:ER was subcloned into pAd5CMV K-NpA using alternative forward primers to incorporate either an HA or myc epitope tag in place of eGFP. (A) Representative images of MDCKII cells expressing eGFP-, HA- or myc-tagged ΔCRAF:ER that have been fixed and immunostained for ppERK1/2. (B) Mean cytoplasmic ppERK1/2 measurements reveal that HA- and mycΔCRAF:ER exhibit similar properties to eGFPΔCRAF:ER, with low basal activity in the absence of 4HT, which is rapidly increased upon the addition of 4HT. (C) MDCKII cells were grouped into subpopulation based on transgene expression level, revealing that 4HT treatment increases the specific activity of each ΔCRAF:ER construct. Images and data are representative of two biological repeats. Scale bar = 20µm.

4.3.7 4HT-dependent eGFPΔCRAF:ER-mediated changes in morphology

As eGFPΔCRAF:ER displayed the required biochemical characteristics, its ability to recapitulate the biological effects of $BRAF^{V600E}$ expression was evaluated using confocal microscopy. Confocal microscopy revealed that eGFPΔCRAF:ER could phenocopy $BRAF^{V600E}$-mediated changes in MDCKII morphology in a 4HT-dependent manner (Figure 4.8). The characteristic monolayer organisation and compact cell shape (Figure 4.8A) was maintained following the treatment of nontransduced cells with 4HT (Figure 4.8B), or following the expression of eGFPΔCRAF:ER in the absence of 4HT (Figure 4.8C). Cell elongation was clearly evident after 24 hours of 4HT treatment (Figure 4.8D) with multi-layered structures observed in some areas (Figure 4.8E). Therefore, eGFPΔCRAF:ER provides a conditionally active tool that can be used to model RAF/MEK/ERK pathway activation, providing the regulation of signal initiation and duration required for subsequent studies into TJ protein trafficking rates.

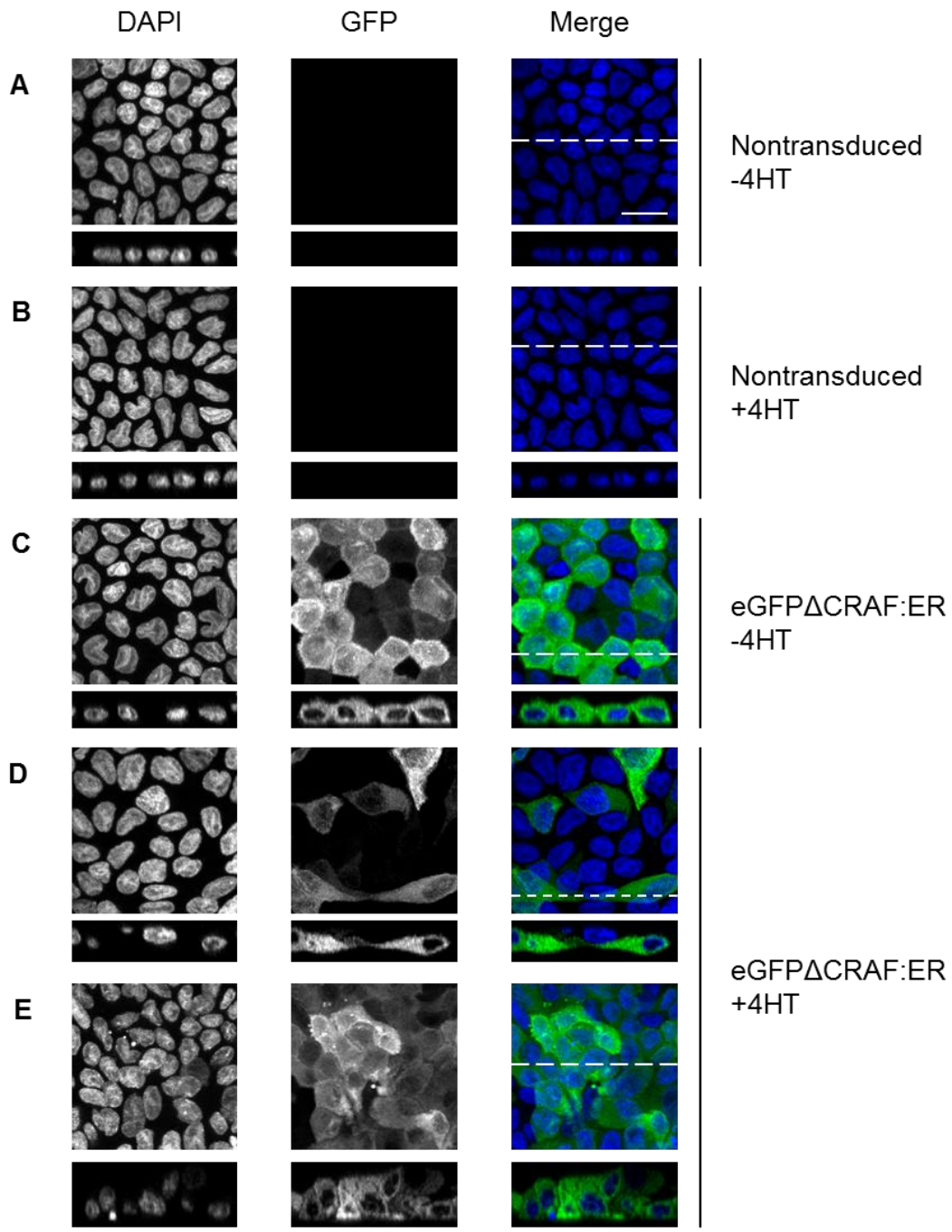

Figure 4.8: eGFPΔCRAF:ER disrupts MDCKII monolayer organisation in a 4HT-dependent manner. Representative images are presented of MDCKII cells expressing eGFPΔCRAF:ER treated with or without 1μM 4HT for 24 hours. (A) Nontransduced MDCKII cells adopt a compact cell shape and form an organised monolayer. This is maintained in nontransduced cells treated with 4HT (B), or eGFPΔCRAF:ER–expressing cells cultured in the absence of 4HT (C). After 24 hours of stimulation, eGFPΔCRAF:ER–expressing cells form extended protrusions (D) and form multi-layered structures (E), phenocopying the effects of $BRAF^{V600E}$ expression reported in chapter 3. Images are representative of three biological repeats. Scale bar = 20μm.

4.4 Discussion

This chapter has outlined the successful design and characterisation of a series of ΔCRAF:ER fusion proteins that exhibit hormone-regulated activity, providing the ability to specifically activate the RAF/MEK/ERK pathway in an inducible manner. Neither of the initially proposed BRAF:ER fusion proteins displayed the required properties of an inducible-activity system. $BRAF^{WT}$:ER was unable to induce downstream ERK phosphorylation, while $BRAF^{V600E}$:ER exhibited unacceptably high basal activity, indicating that the intrinsic kinase activity was not suitably restrained through fusion to the ER^{T2} domain. In contrast, eGFP-, HA- and myc-tagged ΔCRAF:ER^{T} fusions each exhibited low activity in the absence of 4HT, but could be activated in a rapid and sustained manner following the addition of 4HT. Furthermore, eGFPΔCRAF:ER was capable of inducing cell transformation in a similar fashion to $BRAF^{V600E}$, in a 4HT-dependent manner. Therefore, eGFPΔCRAF:ER provides coordinated and tight control over signal duration required for the proposed TJ protein trafficking assays in chapter 5.

$BRAF^{V600E}$:ER induces 4HT-independent activation of the RAF/MEK/ERK pathway

The use of full length $BRAF^{V600E}$:ER fusion proteins has been reported elsewhere (Cagnol and Rivard, 2012; Liu et al., 2007) and is desirable to study the impact of the pathologically relevant oncogenic $BRAF^{V600E}$ mutation in a temporally regulated manner. These studies involved the generation of stably transfected cell lines, where uniform expression levels are likely to be observed between cells. One advantage of using adenoviruses is the ability to modulate transgene expression by varying the viral titre used. However, heterogeneous expression levels are observed between cells in a commonly transduced population, and a subpopulation of cells will express more transgene than the population average. Therefore, low levels of basal activity could potentially have been magnified through $BRAF^{V600E}$:ER overexpression. Although downstream ERK phosphorylation positively correlated with level of transgene expressed, this expression level-response relationship was not affected by the addition of 4HT. This indicates that the specific activity of $BRAF^{V600E}$:ER was not increased by hormone stimulation and that the desired inducible properties were not evident even at low expression levels.

It therefore remains unclear why $BRAF^{V600E}$:ER is constitutively active. $BRAF^{V600E}$:ER^{T1} and $BRAF^{V600E}$:ER^{T2} have been used in IEC-6 intestinal epithelial cells and Melan-A melanocytes, respectively, to study spatiotemporal aspects of RAF/MEK/ERK signalling (Bergeron et al., 2010; Cagnol and Rivard, 2012; Liu et al., 2007), validating the initial proposed use of $BRAF^{V600E}$:ER fusion proteins in these studies. Although

BRAF:ER fusion proteins have not been used in MDCKII cells, this cell line has repeatedly been used in conjunction with ΔCRAF:ER constructs to study RAF/MEK/ERK-mediated epithelial transformation (Doehn et al., 2009; Hansen et al., 2000; Lehmann et al., 2000). This suggests that MDCKII cells are amenable to the use of similar RAF:ER fusion proteins.

The length and specific nature of linker sequence between $BRAF^{V600E}$ and the N-terminal of ER^{T2} may differ between the generated construct and those reported elsewhere. Unfortunately, the full sequences of the fusion proteins used in these studies are unavailable. Alternatively, the transgene selection process involved in generating stable cell lines may have resulted in adaptation to downregulate basal ERK activity. The results of this chapter indicate the need to carefully characterise such systems prior to use.

$BRAF^{WT}$:ER is incapable of inducing downstream activation of the RAF/MEK/ERK pathway

$BRAF^{WT}$:ER was unable to induce downstream ERK phosphorylation at any expression level, indicating that low expression levels were not responsible for this apparent lack of activity. Furthermore, the activity of $BRAF^{WT}$:ER was not influenced by the exclusion of serum and phenol red from the cell culture medium. Of note, $BRAF^{WT}$:ER accumulated at the plasma membrane. Following activation of cell surface receptors, endogenous BRAF is recruited to the plasma membrane by Ras, where it is activated by phosphorylation at a number of sites by various kinases. Therefore, $BRAF^{WT}$:ER may associate with some of these proteins at the plasma membrane, while retaining an inactive conformation, potentially acting in a dominant negative manner to prevent activation of endogenous RAF proteins. In a similar vein, $BRAF^{WT}$:ER may potentially dimerise with endogenous RAF protomers, but lack transactivation ability. However, the ability to activate the RAF/MEK/ERK pathway through alternative means in $BRAF^{WT}$:ER-expressing cells was not investigated, and therefore the designation of $BRAF^{WT}$:ER as a dominant negative construct would require additional work.

$BRAF^{D594A}$, $BRAF^{D594V}$ and the catalytic lysine mutant $BRAF^{K483A}$ lack kinase activity but retain the ability to transactivate CRAF and constitutively phosphorylate MEK in the presence of active Ras (Heidorn et al., 2010). Furthermore, RAF/MEK/ERK signalling can be impaired through the expression of catalytically inactive MEK^{K97R} or ERK^{K52R} or by the treatment with a growing number of inhibitors that act at each level of the kinase cascade (Poulikakos and Solit, 2011; Roberts and Der, 2007). Therefore, it would be difficult to justify using $BRAF^{WT}$:ER to impair RAF/MEK/ERK signalling in an

experimental setting, when so many established and well-characterised alternative approaches are available.

ΔCRAF:ER fusion activate the RAF/MEK/ERK pathway in a 4HT-dependent manner

In contrast to the full-length BRAF:ER fusion proteins, a series of alternatively tagged ΔCRAF:ER constructs exhibited low levels of basal activity, but could be induced by 4HT treatment in a rapid and sustained manner. HA-, myc- and eGFP-tagged ΔCRAF:ER behaved in a similar fashion, providing a diverse range of molecular tools that have the potential to be used in conjunction with a variety of other tagged constructs, lending flexibility to experimental design. Further characterisation of eGFPΔCRAF:ER has revealed the kinetics of activation, highlighting important considerations for future TJ trafficking experiments.

ΔCRAF:ER fusion proteins exhibit low basal activity

Downstream phosphorylation of ERK positively correlated with eGFPΔCRAF:ER expression, even in the absence of 4HT, indicating a degree of “leaky” basal activity. However, there is a clear increase in the specific activity of eGFPΔCRAF:ER at all expression levels. Furthermore, on a population level, basal activity is extremely low, as assessed either by immunoblot or by mean values from immunostaining data. This indicates that the viral titre of approximately 10pfu/nl achieves suitable levels of transgene expression. Measurement of the average GFP intensity, a measure of construct expression, revealed that the majority of cells express relatively low levels of transgene, where basal activity is low, but is dramatically increased upon 4HT addition. As the majority of assays to be performed depend on population averages, this basal activity is unlikely to influence future results. However, it is worth considering, especially when studying individual cells by microscopy. Furthermore, control treatments involving transduced but unstimulated cells will be included wherever possible.

Kinetics and mechanisms of ΔCRAF:ER activation

Upon the addition of 4HT, downstream ERK phosphorylation is rapidly induced, with a clear increase evident within 15 minutes of 4HT addition. ERK phosphorylation is sustained for up to 48 hours while 4HT is present in the media. ΔCRAF:ER activation is reported to be reversible upon the removal of 4HT from the culture medium. This has the potential to allow the study of the junction reformation when normal levels of ERK signalling are reinstated.

High-content microscopy and immunoblotting revealed that eGFPΔCRAF:ER expression levels increased over time when stimulated with 4HT. As cells were fixed or lysed at the same time, this was not a result of increased time in culture. Similar hormone-mediated increases in transgene level have been observed with ΔCRAF:ER, ΔBRAF:ER, ΔARAF:ER and MEK1:ER (Greulich and Erikson, 1998; McMahon, 2001; Pritchard et al., 1995; Samuels et al., 1993). This increase in expression level is at least in part, a consequence of increased stability of RAF:ER fusion proteins upon hormone binding, with initial reports indicating a 4 – 5-fold increase in ΔCRAF:ER half-life following estradiol treatment (McMahon, 2001). While the inducible activity of MEK1:ER is largely regulated by this increase in expression level over 6 – 12 hours (Greulich and Erikson, 1998), expression-activity plots reveal a clear increase in the specific activity of each ΔCRAF:ER fusion protein within 15 minutes of 4HT addition. Furthermore, ΔCRAF:ER activation is reported to be insensitive to cycloheximide (Samuels et al., 1993), and hormone removal leads to rapid inactivation of ΔCRAF:ER, without the concurrent loss of transgene expression. These observations indicate that the activation is independent of protein neosynthesis and that a more rapid conformational change is the most relevant mechanism of hormone-mediated RAF:ER activation. This may involve the removal of the heat shock protein 90 (hsp90) chaperone from the hbER portion of the fusion protein, possibly permitting ΔCRAF:ER dimerisation and downstream pathway activation. Interestingly, although $BRAF^{V600E}$ can form dimers, it is active in a monomeric state. Therefore, dimerisation alone is probably inadequate to explain the hormone-dependent activity of $BRAF^{V600E}$:ER constructs described elsewhere (Bergeron et al., 2010; Cagnol and Rivard, 2012; Liu et al., 2007). Alternatively, 4HT binding may relieve steric hindrance of the CRAF active site to increase MEK substrate access (McMahon, 2001).

Although the three identified RAF isoforms ARAF, BRAF and CRAF have conserved structural similarities, they exhibit distinct biochemical properties, with BRAF exhibiting greater endogenous kinase activity than CRAF, and in turn ARAF. This is partially explained by a pair of tyrosine residues in CRAF and ARAF, which are phosphorylated when these kinases are activated. The analogous residues in BRAF are both replaced with aspartic acid, conferring a constitutive negative charge to this region. An additional serine residue within the N-region is constitutively phosphorylated in BRAF, but not ARAF or CRAF. The constitutive negative charge in the N-region primes BRAF for activation and consequently the basal activity of BRAF is considerably higher than that of ARAF and CRAF (Mason et al., 1999). This hierarchy of RAF kinase activity is maintained when ER fusion proteins are generated using their respective kinase domains. ΔBRAF:ER is 10-fold more potent than ΔCRAF:ER, which is in turn 50-fold

more potent than ΔARAF:ER (Pritchard et al., 1995). Unpublished observations suggest that ΔBRAF:ER may exhibit increased nuclear localisation and therefore behave differently to both $BRAF^{WT}$ and $BRAF^{V600E}$, which are primarily cytoplasmic. Cytoplasmic ΔCRAF:ER still exhibits high specificity for MEK, leads to downstream phosphorylation of ERK, and is capable of phenocopying $BRAF^{V600E}$ by inducing MDCKII transformation. This suggests that their modes of action and potency are relatively consistent. The discrepancy between the specific activity of BRAF and CRAF, and their respective ER fusion proteins, is unlikely to be relevant in this study; pathway output is determined by ΔCRAF:ER expression level, which can be regulated by varying the adenoviral titre.

Potential off-target effects of 4HT

4HT increased the activity of eGFPΔCRAF:ER in a concentration-dependent manner. Maximal activation was achieved at a concentration of 1μM 4HT, with partial activation achieved at lower concentrations. Increasing the concentration to 10μM 4HT failed to increase either mean or specific activity. Tamoxifen has been reported to reduce MDCK cell viability by increasing intracellular calcium concentrations, $[Ca^{2+}]_i$. This is achieved by triggering the release of Ca^{2+} from multiple intracellular stores and through Ca^{2+} influx from the extracellular space (Jan et al., 2000). 4HT has been reported to mediate a similar ATP-dependent increase in $[Ca^{2+}]_i$ through the upregulation of protein phosphatase 1 alpha (PP1alpha) and the inositol 1,4,5-triphosphate receptor (IP3R) (Bollig et al., 2007). Therefore, at high concentrations, ER antagonists can exhibit non-estrogen receptor mediated toxicity. Effects on calcium handling are of particular importance as cell adhesion is calcium-dependent (Hirano et al., 1987). Furthermore, cadherin-cadherin interactions induce transient fluxes of $[Ca^{2+}]_{i,}$ which are associated with actin remodelling and the reinforcement of cell contact through catenin and cadherin recruitment (Ko et al., 2001). However, in MDCKII cells, $[Ca^{2+}]_i$ was not increased by 1μM tamoxifen, although a minor decrease in viability was evident (Jan et al., 2000). Of note, 1μM tamoxifen, but not 1μM 4HT, induces apoptosis in mammary epithelial cells (Dietze et al., 2001). This suggests that tamoxifen and 4HT are not entirely equivalent in terms of function or undesirable side effects. Importantly, the use of 1μM 4HT to activate RAF:ER fusion proteins in MDCK cells in this work is consistent with previous studies, where no off-target effects have been reported (Doehn et al., 2009; Hansen et al., 2000). However, for subsequent experiments, it will be important to include 4HT control treatments of nontransduced cells wherever possible to account for potential effects of calcium handling or decreased cell viability.

Specificity of RAF:ER fusion proteins

The only *bona fide* substrates of RAF proteins are MEK kinases (Matallanas et al., 2011), which selectively phosphorylate ERK (Roskoski, 2012). Previous characterisation of RAF:ER fusion proteins using a variety of estrogen receptor agonists and antagonists have indicated that the reported biological effects are not due to activation of endogenous estrogen receptors (Pritchard et al., 1995). Activation of the ERK pathway is rapid, but additional phosphorylation and activation of the JNK pathway has been reported 24-48 hours after RAF:ER activation (Pritchard et al., 1995). This is thought to occur as a result of ERK-mediated secretion of heparin-binding EGF (hbEGF), which activates the JNK pathway in an autocrine fashion (Pritchard et al., 1995). Of note, JNK signalling is required for TER development in airway epithelia and can promote TJ formation downstream of CDC42 (Tanos et al., 2015). This is still a biologically relevant effect of long-term RAF/MEK/ERK pathway activation, and JNK signalling represents just one of many potential mediators that may execute ERK-mediated changes in TJ structure and function. As RAF:ER activation is independent of protein neosynthesis, immediate-early and delayed transcriptional responses can be distinguished through the use of cycloheximide. In contrast to the full-length BRAF constructs described in chapter 3, subsequent experiments presented in chapter 5 indicate that PD0325901 effectively blocks ERK phosphorylation downstream of eGFPΔCRAF:ER activation, without causing a complete loss of transgene expression. This may be due to the counteracting increase in eGFPΔCRAF:ER stability following hormone addition (McMahon, 2001). Therefore, there is also scope to use small molecule inhibitors to probe the requirement for different downstream signalling pathways on specific TJ-associated effects of ΔCRAF:ER activation.

Broad utility of generated vectors

As well as providing the ability to activate the RAF/MEK/ERK pathway in a specific and rapid fashion, ΔCRAF:ER proteins provide a potential tool for studying the role of RAF regulation and feedback. ΔCRAF:ER consists solely of the kinase domain and lacks the N-terminal regulatory region. ΔCRAF:ER therefore lacks five out of six ERK phosphorylation sites, making it resistant to ERK-mediated feedback regulation (Samuels et al., 1993; Sturm et al., 2010). The ability to break these feedback loops can help to determine their biological significance. $BRAF^{V600E}$ is immune to ERK-mediated negative feedback, so recognising the underlying biology has important implications for understanding the pathogenesis of $BRAF^{V600E}$-driven tumours. This is also the first instance of developing inducible-activity RAF:ER fusion proteins in adenoviral vectors. These vectors have broad utility as the constructs can easily and

efficiently be expressed in a wide array of cell types that express the coxsackie adenovirus receptor (CAR), without requiring stable transfection. This has the potential for achieving specific ERK pathway modulation in cell lines that are typically hard to transfect, such as neurones or primary human cells.

4.5 Limitations and future work

Adenoviral vectors have the potential to allow ΔCRAF:ER expression in a variety of cells types. This will allow the study of RAF/MEK/ERK signalling with increased control of signal strength and duration in a broad variety of conditions. eGFPΔCRAF:ER does exhibit a relative degree of leaky activity in the absence of hormone, and although this appears to be largely limited to a small proportion of cells expressing high levels of transgene, this must be considered when analysing images of individual transduced cells. It will be important to include eGFPΔCRAF:ER-expressing cells that have not been stimulated with 4HT as a control wherever possible. This leaky activity should prove less of an issue on the population level, as increased ppERK1/2 levels are not detectable in the absence of hormone by immunoblot. Going forward, ΔCRAF:ER fusion proteins will therefore allow coordinated activation of the RAF/MEK/ERK pathway to study temporal aspects of TJ protein regulation, in terms of expression and rates of degradation and trafficking.

4.6 Summary

- $BRAF^{V600E}$:ER exhibits unacceptably high levels of basal activity, while $BRAF^{WT}$:ER is unable to induce ERK phosphorylation.

- HA-, myc- or eGFPΔCRAF:ER exhibit relatively low levels of basal activity but are activated upon the addition of 4HT.

- Maximal ΔCRAF:ER activation is achieved using 1μM 4HT, a concentration that is unlikely to have significant off-target effects.

- ΔCRAF:ER activation is rapid and sustained while 4HT is present in the culture medium.

Chapter 5: Tight junction regulation by ΔCRAF:ER

5.1 Rationale

RAF/MEK/ERK activity negatively correlates with claudin-2 expression, both at the mRNA and protein level (Doehn et al., 2009; García-Hernández et al., 2015; Ikari et al., 2011c; Singh and Harris, 2004). Activation of ΔCRAF:ER leads to the downregulation of *CLDN2* mRNA, indicating that its downregulation is at least partially due to decreased transcription. Additionally, recent studies involving EGF and small molecule MEK inhibitors implicate the RAF/MEK/ERK pathway in increasing claudin-2 protein turnover (Ikari et al., 2011c). The loss of claudin-2 protein downstream of EGFR activation is effectively complemented by inhibition of clathrin-mediated endocytosis or lysosomal function (Ikari et al., 2011c). These observations alone indicate that the existing membranous claudin-2 protein pool must be turned over by trafficking from the cell surface and along the degradative pathway (Ikari et al., 2011c). In the same study, EGF induced a MEK-dependent decrease in claudin-2 stability in the presence of cycloheximide, while earlier reports concluded that cycloheximide did not influence the EGF-mediated decrease in claudin-2 protein levels, in detergent-soluble or -insoluble fractions (Singh and Harris, 2004). Therefore, the consequences of EGF treatment, and specifically the downstream role of the RAF/MEK/ERK pathway, on claudin-2 degradation rates need to be addressed. Furthermore, the actual rates of claudin-2 internalisation and recycling have not been determined. It is therefore unclear to what extent RAF/MEK/ERK activity regulates claudin-2 protein synthesis, trafficking and turnover.

While sustained activation of the RAF/MEK/ERK pathway by long-term expression of oncogenic Ras or soluble HB-EGF results in the loss of barrier function and the cytoplasmic sequestration of various TJ proteins, transient activation with EGF leads to the junctional accumulation of claudin-1, -3 and -4. The EGF-mediated junctional accumulation of claudin-3 and -4 is largely blocked by cycloheximide, suggesting that increased junctional levels are mainly due to increased protein synthesis. In contrast, junctional fraction levels of claudin-1 still increased in the presence of cycloheximide, suggesting that post-translational mechanisms may underlie the translocation of existing claudin-1 protein. Although altered endocytic trafficking is proposed as a potential mechanism for claudin redistribution, this has not been studied in any detail. Furthermore, these effects were not attributed to any specific downstream signalling pathway and it is unclear if specific activation of the RAF/MEK/ERK pathway is sufficient to drive similar changes in the distribution of claudin-1, -3 and -4. Increased junctional levels of claudin-1, -3 and -4 could potentially be mediated by reduced rates of endocytosis or increased recycling, rather than degradation, of internalised protein.

The generation of adenoviruses to express hormone-dependent ΔCRAF:ER constructs provides the ability to conditionally activate the RAF/MEK/ERK pathway in a coordinated manner across a whole cell population. Therefore, these constructs permit the immediate effects of RAF/MEK/ERK pathway activation to be studied, prior to gross changes in epithelial morphology elicited by longer-term expression of oncogenic $BRAF^{V600E}$ observed in chapter 3. Most importantly, the initiation and duration of signalling can be tightly regulated through the addition and removal of 4HT to culture medium, allowing the biochemical analysis of claudin protein degradation, internalisation and recycling rates.

5.2 Aims and objectives

The aims of this chapter are to establish how specific activation of the RAF/MEK/ERK pathway affects the rates of claudin internalisation, degradation and endocytic trafficking. This will be achieved by completing the following objectives:

1. Characterise the time course of claudin regulation by ΔCRAF:ER activation using a combination of immunoblotting, confocal microscopy and high-content imaging.

2. Evaluate the time scale of changes in epithelial barrier function through transepithelial electrical resistance measurements.

3. Determine the specific effect of RAF/MEK/ERK activity on relevant *CLDN* mRNA levels using real-time quantitative PCR.

4. Assess the impact of RAF/MEK/ERK activity on the subcellular distribution and rates of internalisation, degradation and recycling using a surface-biotinylation based biochemical trafficking assay.

5.3 Results

5.3.1 ΔCRAF:ER activation differentially regulates claudin expression

To characterise ΔCRAF:ER-mediated changes in TJ protein levels, confluent MDCKII cells were transduced with AdCMVeGFPΔCRAF:ER and treated with 1μM 4HT for 1 – 48 hours (Figure 5.1A). ΔCRAF:ER expression was confirmed by GFP immunoblot (Figure 5.1A). As demonstrated in the previous chapter, ΔCRAF:ER expression levels increased between 6 and 48 hours (Figure 5.1B). ppERK1/2 levels were more rapidly increased within 1 hour of 4HT addition, and maintained for at least 48 hours while 4HT was present in the culture medium (Figure 5.1C). Levels of ppERK1/2 were not affected in nontransduced cells treated with 1μM 4HT for up to 48 hours (Figure 5.1C), indicating that RAF/MEK/ERK pathway activation was due to targeted activation of ΔCRAF:ER. Total levels of ERK1/2 were unaffected, indicating regulation by phosphorylation rather than at the total protein level (Figure 5.1D).

Claudin protein levels were determined by immunoblot under the same conditions. Protein levels of claudin-1 and -2 gradually decreased between 6 and 48 hours of ERK activation (Fig. 5.1E and F), whereas claudin-4 levels were largely unaffected (Figure 5.1G).

Claudin levels were also determined by high-content microscopy. 4HT-treated cells were fixed and immunostained for claudin-1, -2 and -4 (Figure 5.2). The average immunofluorescence intensity across each image was quantified and used to compare relative claudin protein levels between different experimental conditions (Figure 5.3). In ΔCRAF:ER-expressing cells, claudin-2 intensity decreased after 6 – 24 hours of 4HT treatment. Claudin-2 intensity had decreased by approximately 60% after 24 hours (Figure 5.3B). Claudin-1 intensity was not affected under the same conditions (Figure 5.3A), but a minor yet significant increase of approximately 20% in claudin-4 intensity was observed (Figure 5.3C). Claudin-1, -2 and -4 intensity levels were not affected by either ΔCRAF:ER expression or 4HT treatment alone (Figure 5.3, top row).

Altered claudin protein levels occurred with a concomitant 1.5 – 2-fold increase in TER, before beginning to decrease towards baseline levels at later time points (Figure 5.4D). The TER of nontransduced cells was stable over this 24 hour period (Figure 5.4A) and was not affected by 4HT treatment (Figure 5.4B). ΔCRAF:ER expression alone led to a minor yet gradual increase in TER over 48 hours, but this did not reach statistical significance when compared to untreated MDCKII monolayers (Figure 5.4C).

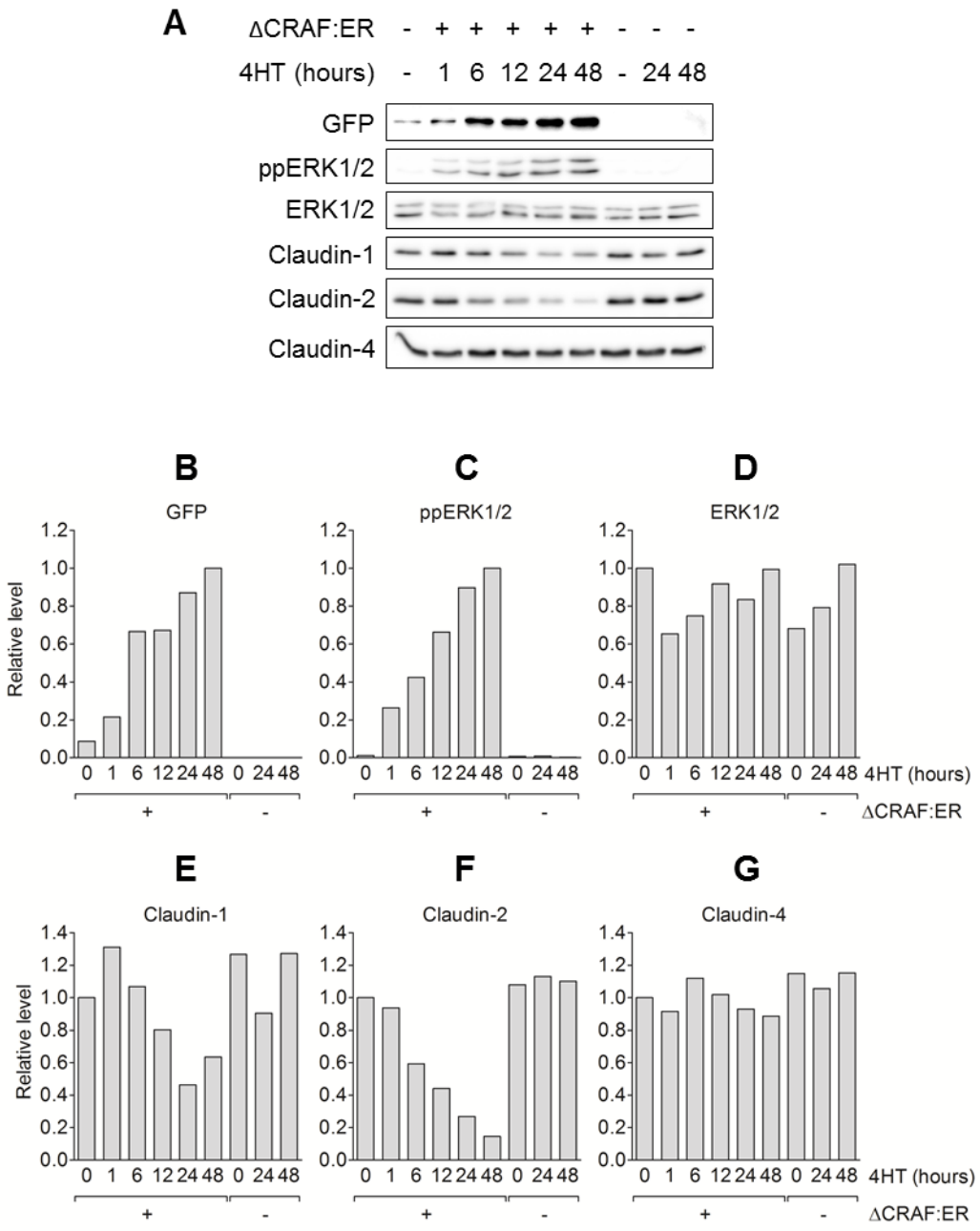

Figure 5.1: ΔCRAF:ER activation differentially regulates protein levels of claudin-1, -2 and -4. Confluent MDCKII cells were transduced to express ΔCRAF:ER and treated with 1μM 4HT for the indicated times, prior to cell lysis. (A) Cell lysates were subjected to SDS-PAGE and immunoblot to determine downstream ERK1/2 phosphorylation and effects on claudin protein levels. ΔCRAF:ER expression was confirmed by immunoblotting for GFP (B). Increased ppERK1/2 levels were detected within 1 hour of 4HT addition (C), while total ERK1/2 levels were not affected (D). Increased ERK1/2 phosphorylation correlated with decreased total levels of claudin-1 (E) and claudin-2 (F), while claudin-4 levels were unaffected (G). The following pairs of immunoblots were obtained from the same gel: ERK1/2 and claudin-1, ppERK1/2 and claudin-2. Data is presented from a single biological repeat. Similar results are reported in Figure 5.5.

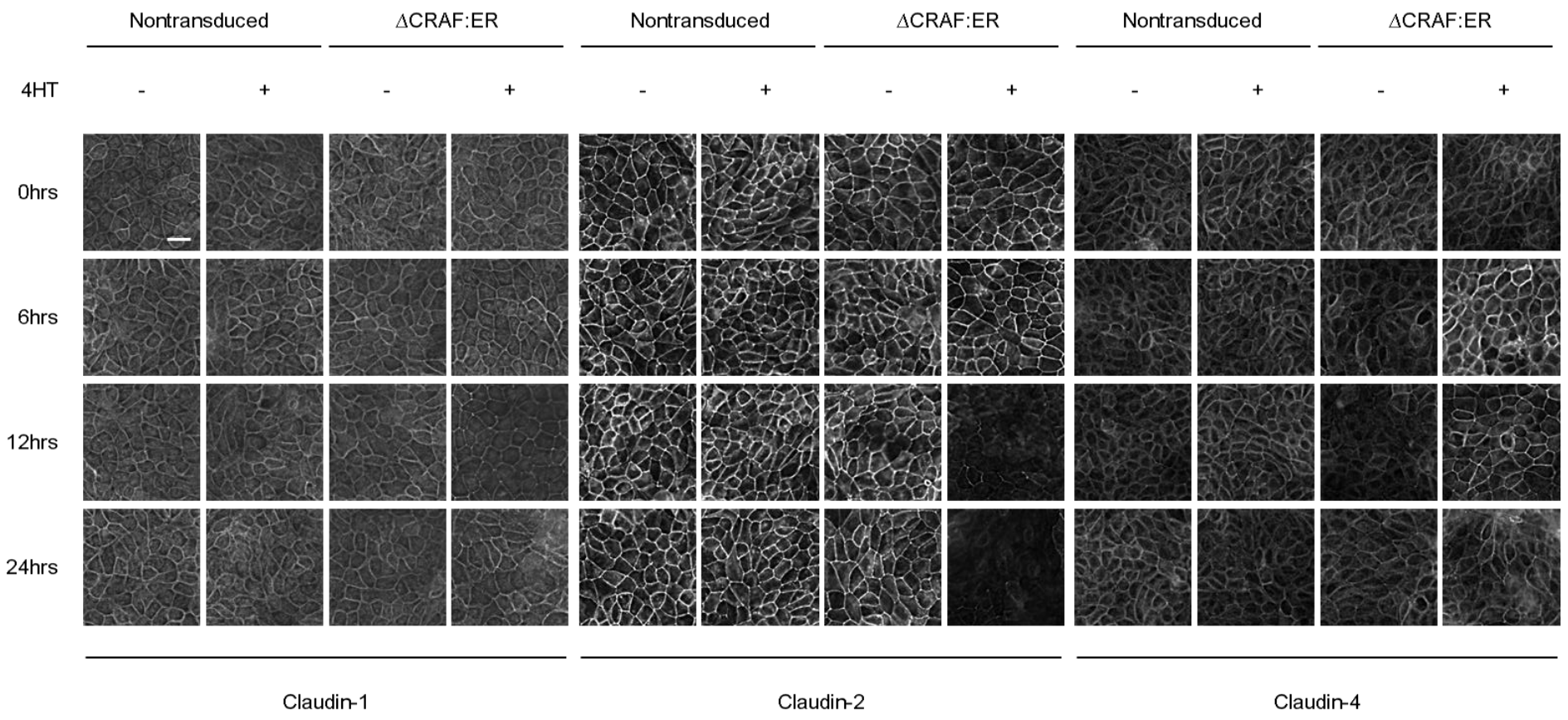

Figure 5.2: Differential regulation of claudin protein levels following ΔCRAF:ER activation. Confluent ΔCRAF:ER MDCKII cells were treated with 1µM 4HT prior to fixation and immunostaining. ΔCRAF:ER activation decreased claudin-2 intensity, and increased claudin-4 intensity. Claudin-1 intensity was not significantly affected by ΔCRAF:ER activation. Average claudin intensity across the entirety of each image was measured using INCell Developer Toolbox software. Quantification of data is presented in Figure 5.3. Images are representative of three independent experiments. Scale bar = 20µm.

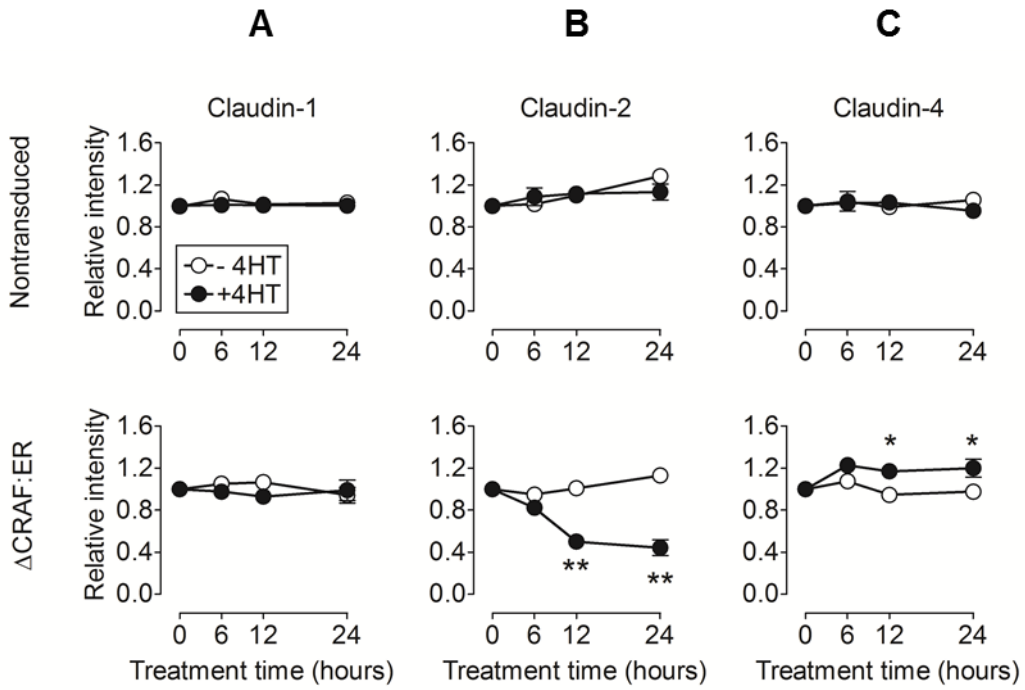

Figure 5.3: ΔCRAF:ER activation differentially affects claudin immunostaining intensity. Nontransduced or ΔCRAF:ER-expressing MDCKII cells were fixed and immunostained for claudin-1 (A), -2 (B) or -4 (C). The average immunostaining intensity for each marker was quantified using INCell Developer Toolbox software and used to compare claudin levels between experimental conditions. 4HT treatment did not affect claudin intensity in nontransduced cells (top row). ERK activation did not affect claudin-1 intensity, but led to a gradual decrease in claudin-2 intensity after 6 – 24 hours of 4HT treatment. In contrast, claudin-4 intensity was increased by approximately 20% under the same conditions. Data are presented as mean values ±s.e.m. from three biological repeats. Data were compared to nontransduced -4HT conditions at each time point using a two-way ANOVA with Bonferroni post-test, * p<0.05, ** p<0.01. Representative images are presented in Figure 5.2.

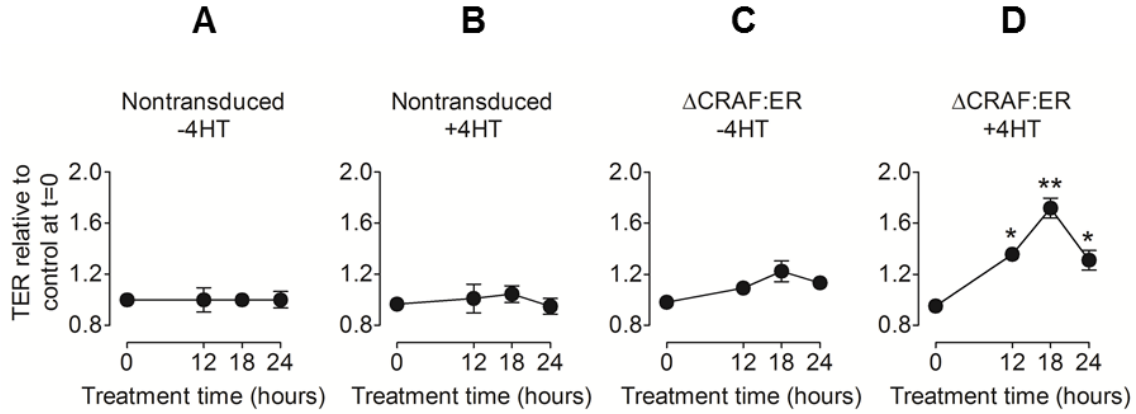

Figure 5.4: ΔCRAF:ER activation increases MDCKII transepithelial resistance. The epithelial permeability of MDCKII monolayers were determined by measuring transepithelial resistance (TER). TER was stable over the course of the experiment in nontransduced cells, in either the absence (A) or presence (B) of 1μM 4HT. Expression of ΔCRAF:ER caused a minor yet insignificant increase in TER (C). ΔCRAF:ER activation with 1μM 4HT caused a significant increase in TER between 12 and 24 hours after treatment commenced (D). TER began to decrease at later time points, but remained elevated compared to basal conditions. Data are presented as mean values ±s.e.m. from three biological repeats. Data were compared at each time point using a repeated measures two-way ANOVA with Bonferroni post-test, * p<0.05, ** p<0.01.

To confirm that the observed decrease in claudin-2 protein levels was due to activation of the ERK pathway, transduced cells were treated with 4HT in combination with the MEK inhibitor, PD0325901 (Figure 5.5A). 24 hour 4HT treatment led to a consistent yet statistically insignificant decrease in claudin-1 levels (Figure 5.5B). This apparent decrease was not evident when cells were treated with 4HT in combination with either PD0325901 or chloroquine (Figure 5.5B). This suggests that any minor decrease in claudin-1 levels driven by ΔCRAF:ER is dependent on elevated MEK activity and proceeds via lysosomal degradation. 24 hour 4HT treatment significantly decreased claudin-2 protein levels by approximately 80%, and this was completely blocked by co-treatment with PD0325901 (Figure 5.5C). Claudin-2 protein depletion was also effectively blocked by co-treatment with chloroquine, an inhibitor of lysosomal degradation (Figure 5.5C). Interestingly, treatment with chloroquine alone led to an increase in levels of claudin-1 and -2, which was not evident when cells were also treated with 4HT (Figure 5.5C). This suggests that ΔCRAF:ER activation may inhibit the synthesis of claudin-1 and -2.

In contrast, claudin-4 levels were not affected by ΔCRAF:ER activation (Figure 5.5D). However, claudin-4 levels did increase following treatment with chloroquine. Which was marginally potentiated by the addition of 4HT (Figure 5.5D). Taken together with the immunostaining data (Figure 5.3C), this suggests that a minor increase in total claudin-4 levels may be as a result of increased claudin-4 synthesis.

Altered mRNA levels could potentially account for changes in claudin protein level. The effect of RAF/MEK/ERK activity on *CLDN* transcript levels was therefore determined by RT-qPCR. *CLDN1* and *CLDN4* mRNA levels were not significantly affected following the treatment of ΔCRAF:ER-expressing cells with 1μM 4HT for 24 hours (Figure 5.6A and C). Under the same conditions, *CLDN2* mRNA levels were decreased by over 8-fold in comparison to control (Figure 5.6B). ΔCRAF:ER expression or 4HT treatment alone failed to affect any *CLDN* mRNA transcript level (Figure 5.6). To conclude, activation of the RAF/MEK/ERK pathway alone is sufficient to drive an increase in MDCKII TER, which occurs concurrently with the differential regulation of claudin-1, -2 and -4. Claudin-2 is depleted at both the mRNA and protein level, claudin-4 protein, but not mRNA, levels are marginally increased and claudin-1 protein levels are marginally downregulated without a concomitant change in mRNA level.

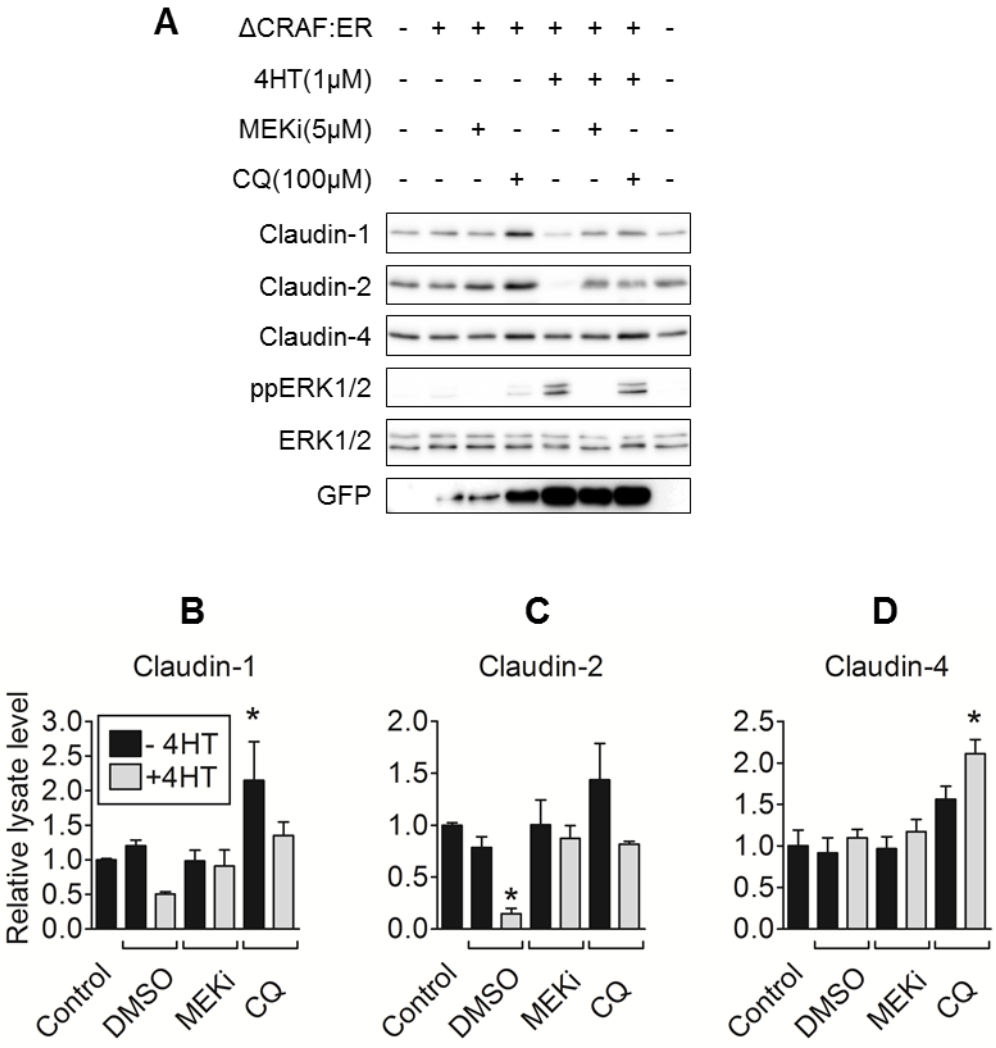

Figure 5.5: Combined effects of ΔCRAF:ER activation, MEK inhibition and chloroquine treatment on claudin protein levels. ΔCRAF:ER-expressing MDCKII cells were treated with 1μM 4HT, 5μM PD0325901 (MEKi) or 100μM chloroquine (CQ) (a lysosomal inhibitor) for 24 hours as indicated. (A) Cells were lysed and relative claudin levels were determined by immunoblot. Claudin-2 depletion was effectively blocked by treatment with either PD0325901 or chloroquine (C). MEK inhibition did not significantly alter levels of claudin-1, -2 or -4. Claudin-1 and -2 accumulate in the presence of chloroquine alone, but not when co-treated with 4HT. Conversely, chloroquine-mediated claudin-4 accumulation is potentiated by 4HT. Immunoblots are representative of three biological repeats. Data is presented as mean values ±s.e.m. from three independent experiments. The following pairs of blots were obtained from the same gel: ERK1/2 and claudin-1, ppERK1/2 and claudin-2. Data were compared to control conditions using a one-way ANOVA with Dunnett's post-test, * $p<0.05$.

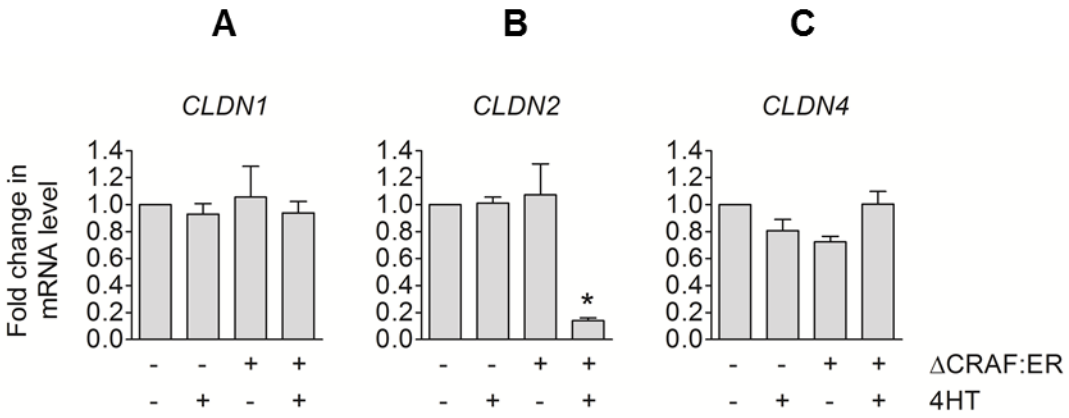

Figure 5.6: Levels of *CLDN1*, *CLDN2* and *CLDN4* mRNA are differentially regulated by ΔCRAF:ER activation. Nontransduced or ΔCRAF:ER-expressing MDCKII cells were treated with or without 1µM for 24 hours prior to total RNA isolation.. Relative *CLDN* mRNA levels were determined by RT-qPCR RAF/MEK/ERK activity decreased mRNA levels of *CLDN2* (B) without affecting those of *CLDN1* (A) or *CLDN4* (C). Data are presented as mean fold changes ±s.e.m. from three independent experiments. Data were compared to control treatments using a one-way ANOVA with Dunnett's post-test, * $p<0.05$.

5.3.2 RAF/MEK/ERK activity causes claudin-2 protein depletion without inducing its prior accumulation in the cytoplasm

To establish if RAF/MEK/ERK activity influences claudin-2 protein localisation in addition to expression levels, its subcellular distribution was determined by confocal microscopy. Claudin-2 normally localised to the apical-most tip of the lateral membrane (Figure 5.7A), consistent with its localisation at the TJ. This distribution was maintained in nontransduced cells treated with 4HT (Figure 5.7B) or those expressing ΔCRAF:ER (Figure 5.7C). 24 hours after 4HT addition, claudin-2 intensity was almost completely lost in cells expressing ΔCRAF:ER, while apical junction staining was maintained in neighbouring nontransduced cells (Figure 5.7D), indicating that activation of the RAF/MEK/ERK pathway alone caused claudin-2 protein depletion in a cell-autonomous manner. Moreover, the reduction in TJ-localised claudin-2 did not coincide with a concomitant increase in cytoplasmic claudin-2 (Figure 5.8), indicating that junctional claudin-2 was not endocytosed *en masse* prior to its degradation.

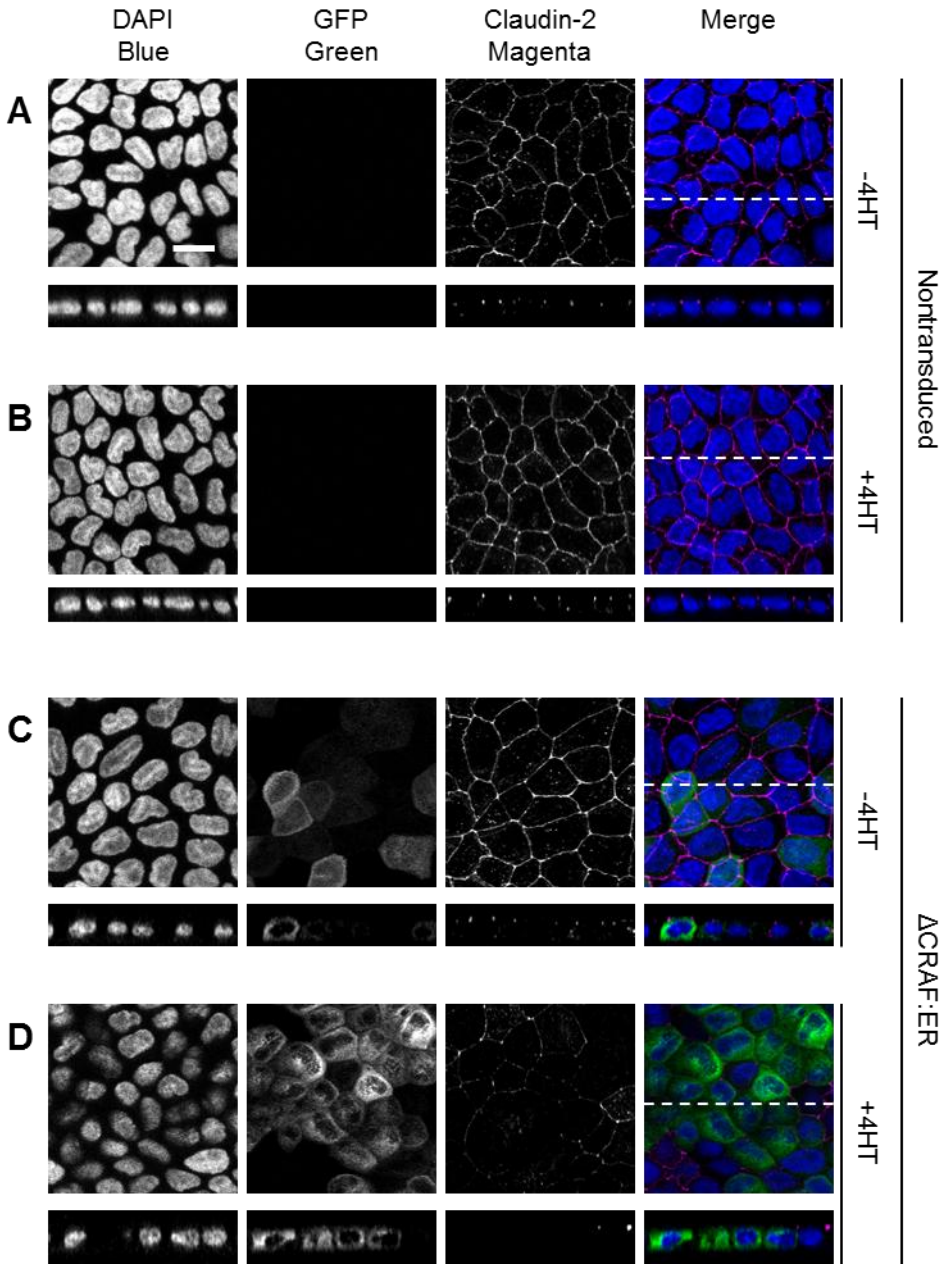

Figure 5.7: ΔCRAF:ER activation causes the cell-autonomous depletion of claudin-2 protein. Nontransduced or ΔCRAF:ER-expressing MDCKII cells were treated with 1μM 4HT for 24 hours prior to fixation. Claudin-2 distribution was assessed by immunostaining and confocal microscopy. Each condition shows an overhead projection of multiple Z-slices, with an orthogonal cross section taken through indicated plane (dashed line). (A) In control conditions, claudin-2 localises to the apical-most tip of the lateral membrane, and this is maintained in nontransduced cells treated with 4HT (B) or in those expressing ΔCRAF:ER (C). Following ΔCRAF:ER activation with 4HT, claudin-2 is almost completely lost in ΔCRAF:ER-expressing cells, while it is maintained in adjacent nontransduced cells. Images are representative of three independent experiments. Scale bar = 20μm.

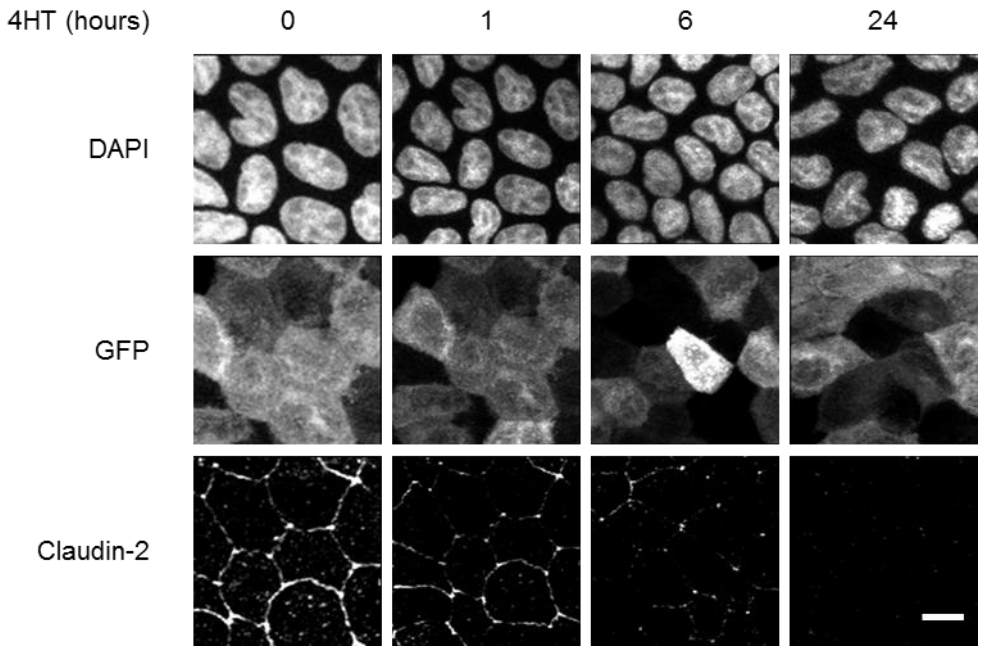

Figure 5.8: Claudin-2 does not accumulate internally prior to degradation. Confluent MDCKII cells expressing ΔCRAF:ER were treated with 1μM 4HT for the indicated times. Cells were fixed and stained for claudin-2. Junctional claudin-2 intensity gradually decreases over 24 hours, without a concomitant increase in cytoplasmic claudin-2 staining. This suggests claudin-2 is not internalised *en masse* prior to degradation. Images are representative of three biological repeats. Scale bar = 10μm.

5.3.3 RAF/MEK/ERK activity causes claudin-1 and -4 to accumulate at the tight junction

By immunoblot, total claudin-1 levels were marginally downregulated (Figure 5.1), although not to a statistically significant level (Figure 5.5). Claudin-1 distribution was determined using confocal microscopy to establish if RAF/MEK/ERK signalling had more pronounced effects on its subcellular localisation. In contrast to claudin-2, which localised to the apical junction, claudin-1 was predominantly localised along the lateral membrane (Figure 5.9A). Claudin-1 staining was continuous, but overlapped minimally, with that of ZO-1, a peripheral protein commonly used as a TJ marker (Figure 5.9A). This localisation pattern was maintained in nontransduced cells treated with 4HT (Figure 5.9B) or cells expressing ΔCRAF:ER (Figure 5.9C). However, there was a clear change in distribution following ΔCRAF:ER activation; claudin-1 was depleted from the lateral membrane and accumulated at the apical junction, where it colocalised with ZO-1 (Figure 5.9D). Strong junctional ZO-1 staining was maintained under these conditions, although increased diffuse cytoplasmic staining was also evident (Figure 5.9D). Confocal microscopy revealed a redistribution of claudin-4 similar to that of claudin-1 (Figure 5.10). Under each control condition, cells maintained weak lateral membrane claudin-4 staining (Figure 5.10A – C) but there was a striking accumulation of claudin-4 at the apical junction following ΔCRAF:ER activation (Figure 5.10D).

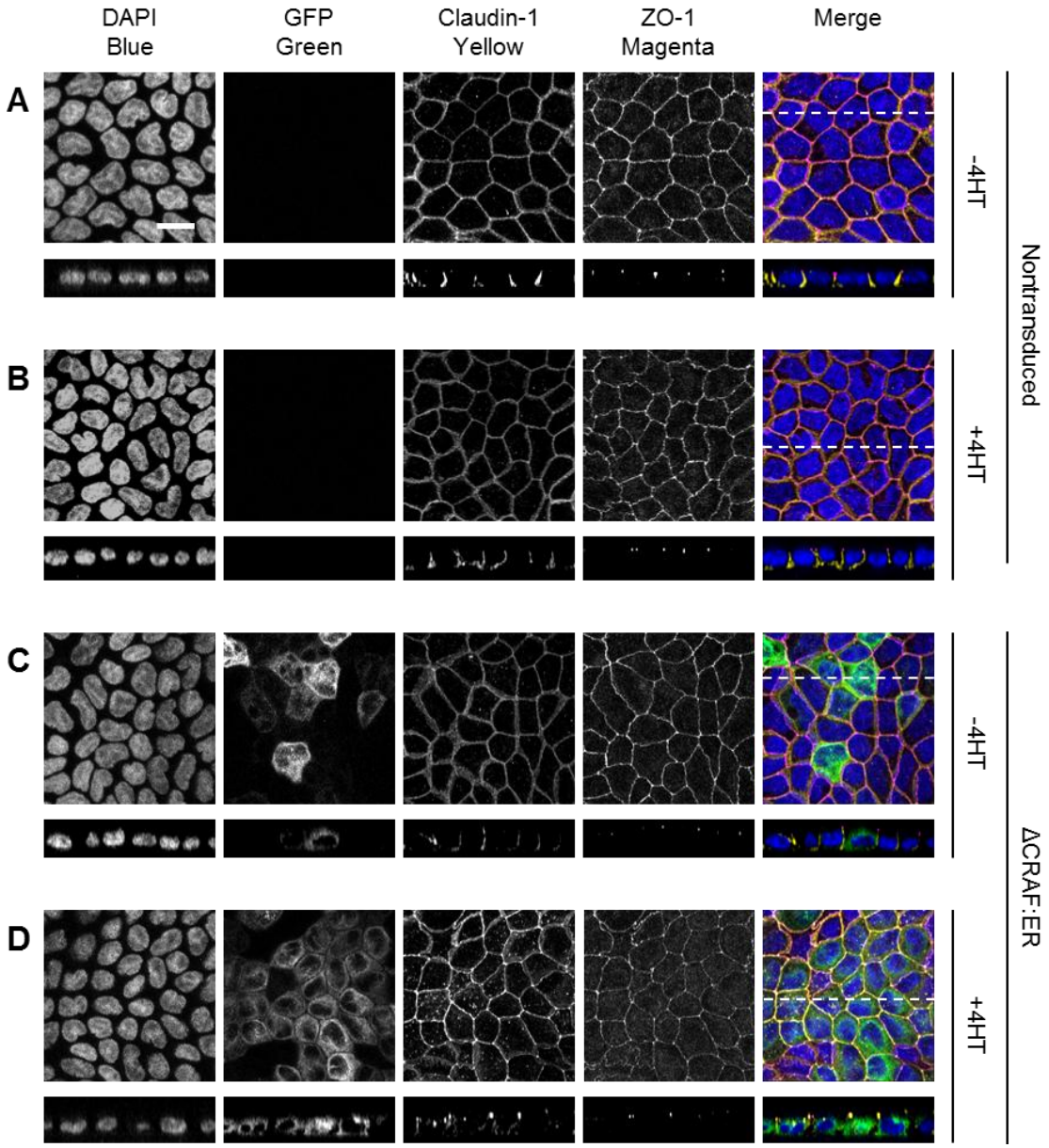

Figure 5.9: ΔCRAF:ER activation causes claudin-1 to accumulate at the apical junction and throughout the cytoplasm. Confluent ΔCRAF:ER-expressing MDCKII cells were treated with 1μM 4HT for 24 hours prior to fixation and immunostaining for claudin-1 and ZO-1. Images are overhead projections of multiple Z-slices. Orthogonal views were taken in the indicated plane (dashed line). Confluent MDCKII cells expressing ΔCRAF:ER were treated with or without 1μM 4HT for 24 hours prior to fixation. (A) Claudin-1 is normally associated with the lateral plasma membrane, where it localises basally to the apical junction marker, ZO-1. This immunostaining pattern is maintained in nontransduced cells treated with 4HT (B), or in ΔCRAF:ER-expressing cells cultured in the absence of 4HT (C). (D) Following ΔCRAF:ER activation, claudin-1 accumulates at the apical junction, colocalising with ZO-1. Punctate claudin-1 staining is also visible throughout the cytoplasm. Continuous junctional ZO-1 staining is conserved following ΔCRAF:ER activation, although diffuse cytoplasmic staining is also visible. Images are representative of three independent experiments. Scale bar = 20μm.

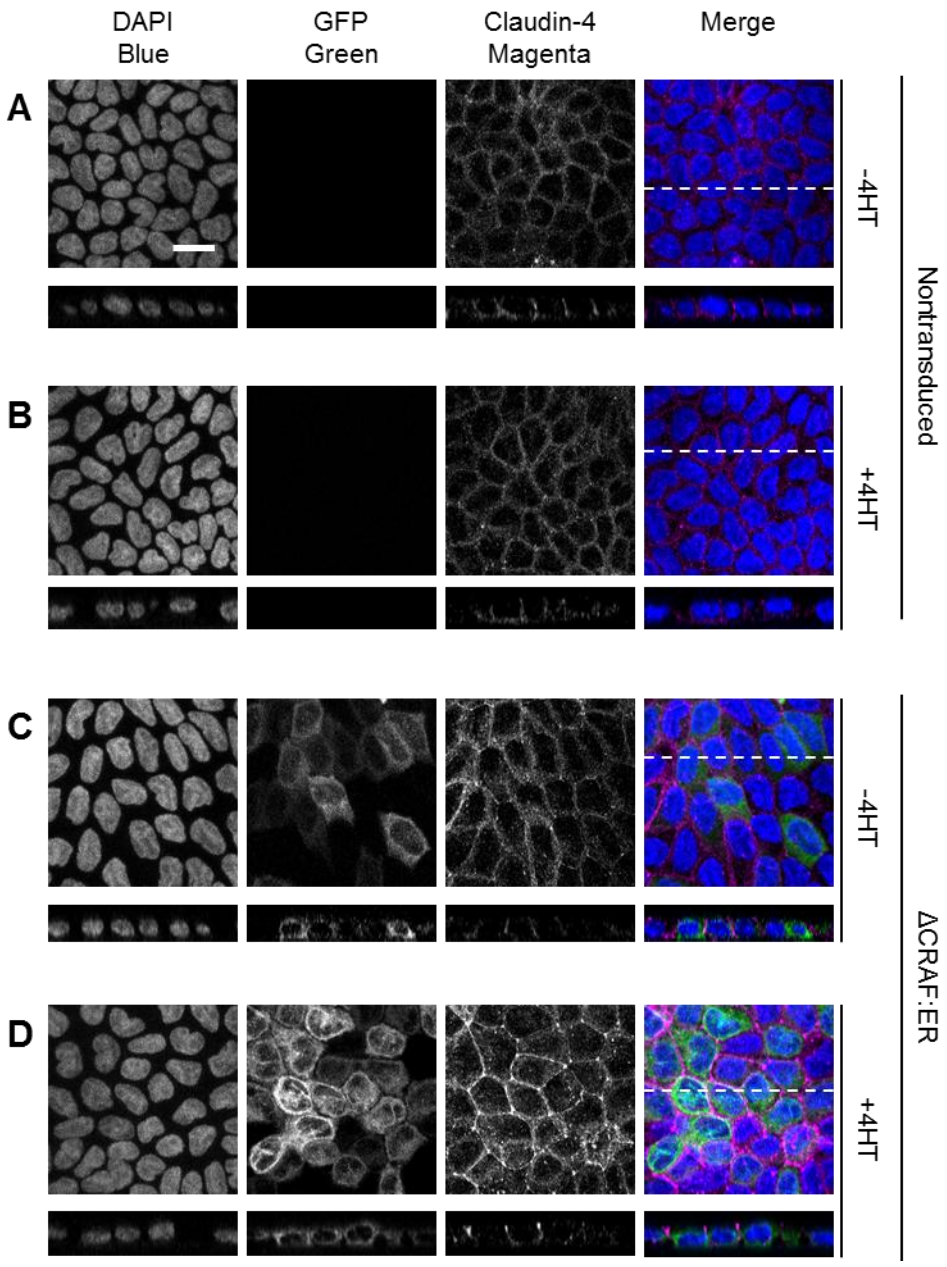

Figure 5.10: ΔCRAF:ER activation causes claudin-4 to accumulate at the apical junction and throughout the cytoplasm. Confluent ΔCRAF:ER-expressing MDCKII cells were treated with 1μM 4HT for 24 hours prior to fixation and immunostaining for claudin-4. Images are overhead projections of multiple Z-slices. Orthogonal views were taken in the indicated plane (dashed line). Confluent MDCKII cells expressing ΔCRAF:ER were treated with or without 1μM 4HT for 24 hours prior to fixation. (A) Claudin-4 is normally associated with the lateral plasma membrane, and this is maintained in nontransduced cells treated with 4HT (B), or in ΔCRAF:ER-expressing cells cultured in the absence of 4HT (C). (D) Following ΔCRAF:ER activation, claudin-4 accumulates at the apical junction. Increased claudin-4 staining is also visible throughout the cytoplasm. Images are representative of three independent experiments. Scale bar = 20μm.

5.3.4 Claudin-1 and -4 colocalise at the apical junction and in common cytoplasmic compartments

In addition to increased junctional staining, ΔCRAF:ER activation induced the accumulation of claudin-1 and -4 in discrete cytoplasmic punctae (Figures 5.9D and 5.10D). MDCKII cells were costained for claudin-1 and -4 to determine if they colocalised following treatment. In control-treated cells, claudin-1 and -4 extensively colocalised along the lateral membrane (Figure 5.11A – C). Following ΔCRAF:ER activation, claudin-1 and -4 also colocalised at the apical junction and in common cytoplasmic compartments (Figure 5.11D).

To determine if this internal accumulation represented universal or bulk internalisation of all TJ components, MDCKII cells were costained for claudin-1 and occludin under the same experimental conditions (Figure 5.12). Occludin was predominantly concentrated at the apical junction, with weaker lateral plasma membrane staining that partially colocalised with that of claudin-1 (Figure 5.12A). This staining pattern was maintained in nontransduced cells treated with 4HT (Figure 5.12B), or in ΔCRAF:ER-expressing cells cultured in the absence of 4HT (Figure 5.12C). Following 24 hours of ΔCRAF:ER activation, claudin-1 exhibited increased junctional staining and was present in discrete cytoplasmic structures (Figure 5.12D). However, the subcellular distribution of occludin was largely unaffected; apical junction and lateral membrane staining were conserved, and although there was a slight diffuse cytoplasmic signal, occludin did not colocalise with claudin-1 in the cytoplasm (Figure 5.12D). Therefore, in a similar manner to $BRAF^{V600E}$ expression, ΔCRAF:ER activation has distinct effects on the subcellular distribution of individual TJ components. RAF/MEK/ERK activation appears to drive the loss of claudin-2 expression and specifically increase the junctional levels of claudin-1 and -4, but not occludin or ZO-1.

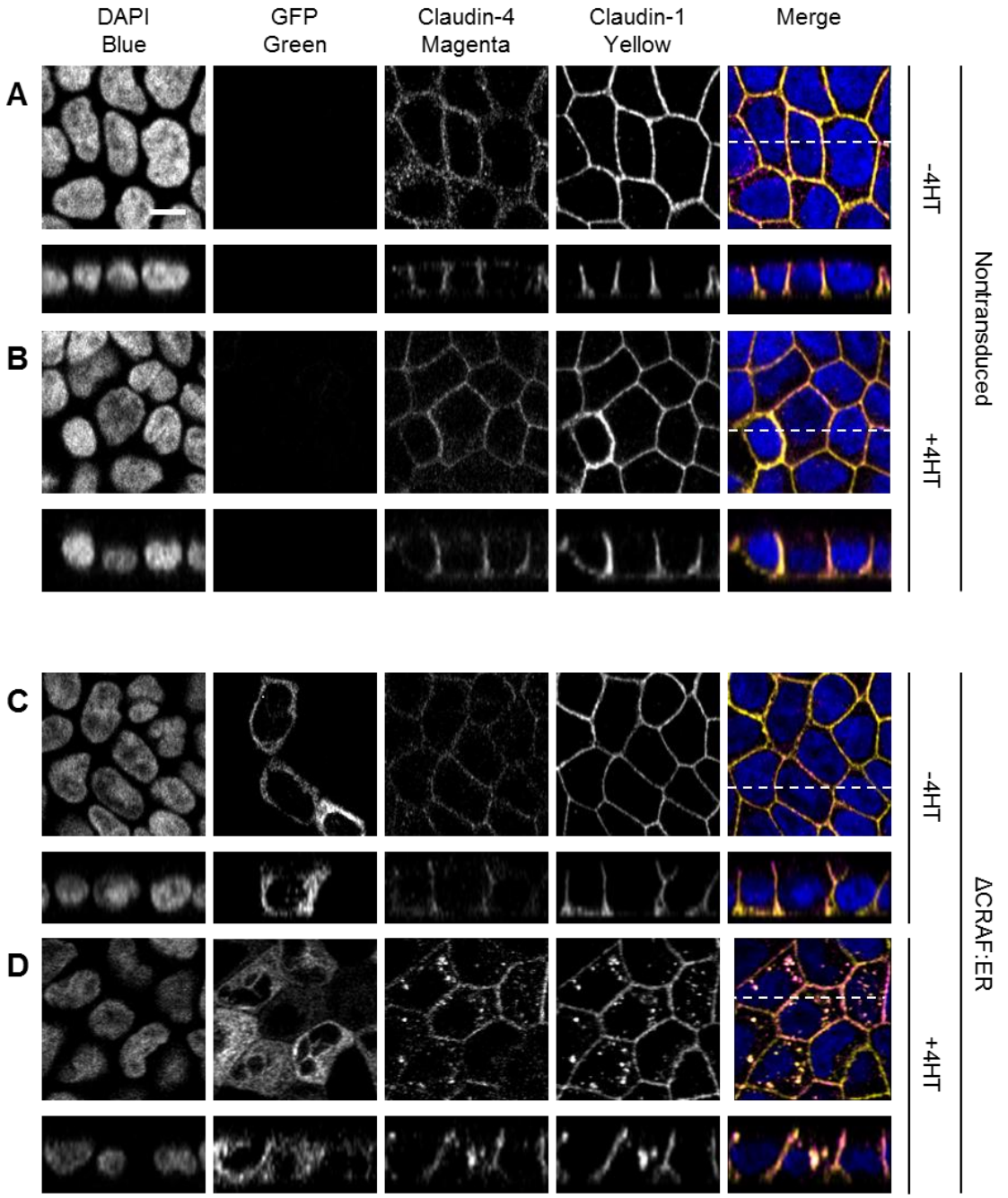

Figure 5.11: Claudin-1 and -4 extensively colocalise in both control and 4HT-treated conditions. Confluent ΔCRAF:ER-expressing MDCKII cells were treated with 1μM 4HT for 24 hours prior to fixation. Images are representative of cells costained for claudin-4 and claudin-1. Overhead projections are shown with orthogonal views taken in the indicated plane (dashed line). (A) Claudin-1 and -4 normally colocalise along the lateral plasma membrane, and this staining pattern is maintained in nontransduced cells treated with 4HT (B), or in unstimulated ΔCRAF:ER-expressing cells (C). (D) Following activation of ΔCRAF:ER with 4HT, claudin-1 and -4 colocalise at the apical junction, along the lateral membrane and in common cytoplasmic compartments. Images are representative of two independent biological repeats. Scale bar = 10μm.

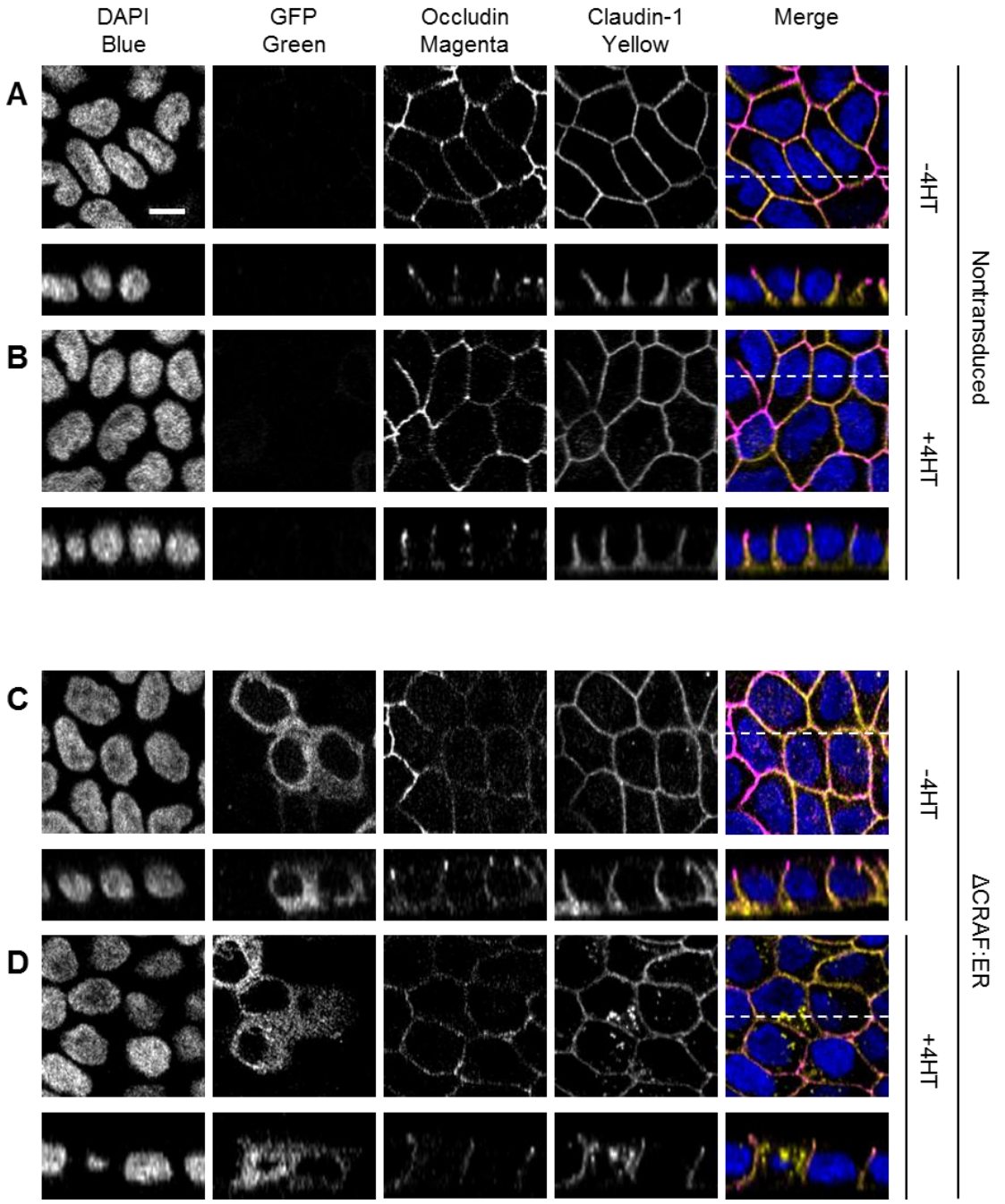

Figure 5.12: Occludin does not accumulate with claudin-1 at the apical junction or in cytoplasmic punctae. Confluent ΔCRAF:ER-expressing MDCKII cells were treated with 1μM 4HT for 24 hours prior to fixation. Images are representative of cells costained for occludin and claudin-1. Overhead projections are shown with orthogonal views taken in the indicated plane (dashed line). (A) Occludin normally accumulates at the apical junction, with weaker lateral membrane staining that partially colocalised with claudin-1. This staining pattern is maintained in nontransduced cells treated with 4HT (B), or in unstimulated ΔCRAF:ER-expressing cells (C). After 24 hours of ΔCRAF:ER activation, claudin-1 exhibited increased localisation at the apical junction and in discrete cytoplasmic punctae (D). However, occludin was maintained at the lateral membrane and apical junction and did not colocalise with claudin-1 in the cytoplasm (D). Images are representative of two independent biological repeats. Scale bar = 10μm.

5.3.5 Characterisation of a surface-biotinylation biochemical trafficking assay

A surface-biotinylation-based biochemical trafficking assay was utilised to determine the effects of ΔCRAF:ER activation on the rates of claudin internalisation, degradation and endocytic recycling. The assay was initially validated by assessing the trafficking rates of the transferrin receptor (TfR), a cell surface protein commonly used as a marker that undergoes rapid and constitutive endocytic recycling (Fuller and Simons, 1986). Surface TfR was labelled with a membrane-impermeant biotin moiety, which could be retrieved by neutravidin pulldown (Figure 5.13A). Immunoblots revealed that the α-TfR antibody detected a single major band of approximately 100kDa, consistent with its predicted molecular weight ~90kDa (Figure 5.13A) (Fuller and Simons, 1986). A band of the same molecular weight was retrieved following neutravidin pulldown of surface-biotinylated, but not mock-labelled cells, indicating the specificity of the pulldown for biotinylated proteins (Figure 5.13A). Furthermore, cytoplasmic ERK1/2 was not detectable in pulldown samples, indicating the specificity of the biotinylation label for cell surface proteins (Figure 5.13B). Biotin was efficiently removed from labelled TfR with 2-mercaptane ethane sulphonate (MESNA), a membrane-impermeant reducing agent. To assess endocytosis, surface proteins were biotinylated on ice and incubated at 37°C to allow trafficking to resume. Biotin was stripped from remaining surface proteins, while internalised proteins were protected by the intact plasma membrane. After 1 hour, approximately 40% of surface-biotinylated TfR was resistant to surface-stripping, compared to less than 10% in strip control conditions, indicating the relative degree of TfR internalisation (Figure 5.13A).

The fate of internalised TfR was investigated by surface-labelling and subjecting cells to the endocytosis assay before a second 20-minute incubation at 37°C to allow recycling back to the plasma membrane. Cells were then lysed, either before or after surface-stripping, to assess the relative extent of TfR degradation and recycling over the course of the second incubation. This revealed that the vast majority of internalised TfR was recycled rather degraded (Figure 5.13A). Interestingly, significantly more TfR and E-cadherin were initially labelled after 24 hours of ΔCRAF:ER activation (Figure 5.13A and C). In MDCKII cells, TfR and E-cadherin are largely confined to the basolateral membrane (Fuller and Simons, 1986; Miranda et al., 2001), and the ability to label more of these proteins with apically applied biotin suggests that ΔCRAF:ER activation increases leak pathway biotin permeability. However, the proportion of labelled TfR that is endocytosed, degraded and recycled was similar in both control and 4HT-treated conditions. Furthermore, E-cadherin underwent negligible endocytosis under any experimental condition (Figure 5.13C), indicating the ability of the surface-

biotinylation assay to distinguish between the trafficking rates of different cell surface proteins.

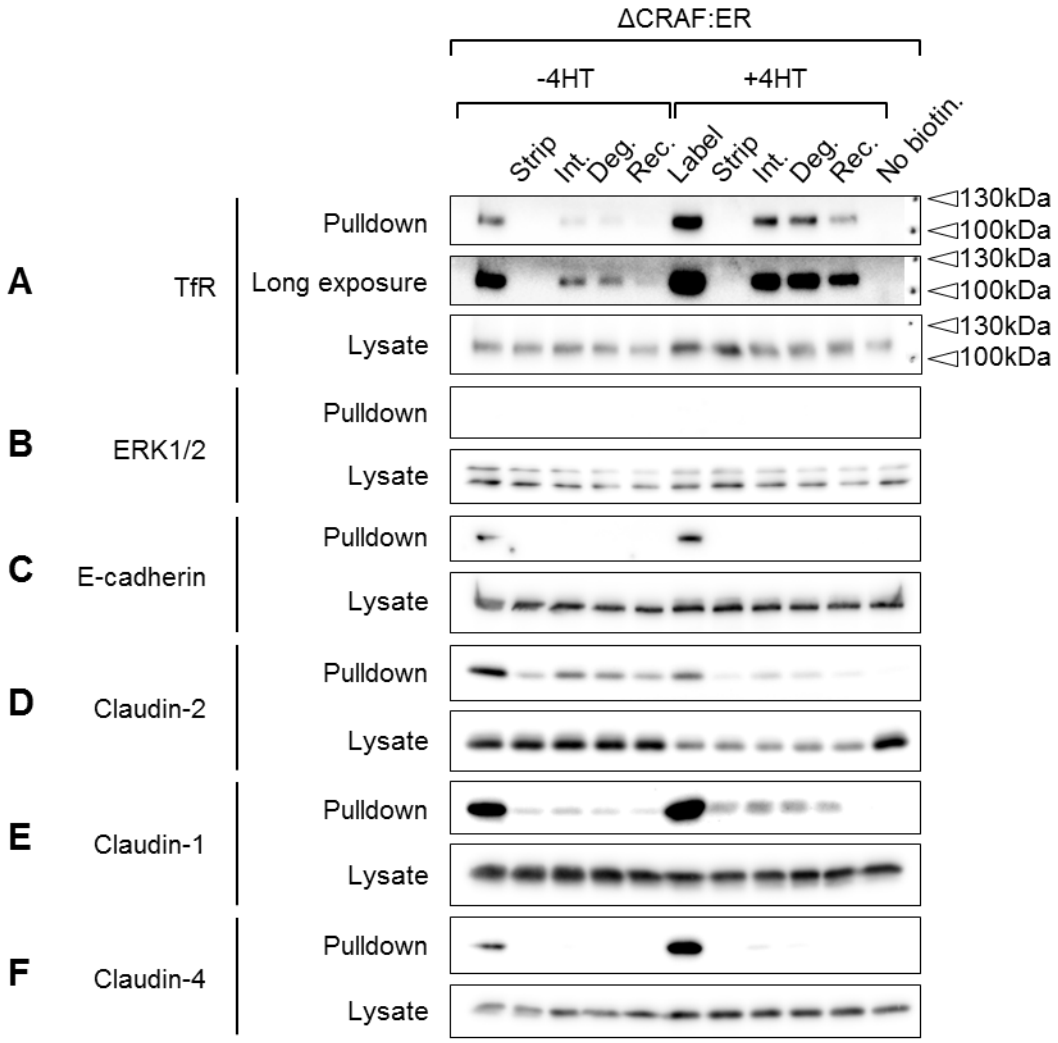

Figure 5.13: ΔCRAF:ER activation does not influence the endocytic trafficking of claudin-1, -2 or -4. Confluent MDCKII cells expressing ΔCRAF:ER were treated with or without 1μM 4HT for 24 hours. Cells were surface-biotinylated and subjected to the biochemical trafficking assay. The "label" lane indicates the amount of protein initially biotinylated at the cell surface. Internalised protein is resistant to surface-stripping. Relative degradation is shown by a minor reduction in signal between internalisation and degradation lanes. (A) The assay was validated by measuring endocytic trafficking of the transferrin receptor (TfR), a cell-surface protein that undergoes rapid and constitutive recycling. Approximately 40% of surface-labelled TfR is endocytosed after 1 hour. The majority of this internalised TfR is subsequently recycled back to the plasma membrane within 20 minutes allowing its removal by a second surface-strip. Increased amounts of basolateral TfR were labelled following ΔCRAF:ER activation, despite TfR lysate input levels remaining constant. (B) Surface-biotinylation was specific to cell-surface proteins as cytoplasmic ERK1/2 was only detectable in whole cell lysates, and not neutravidin pulldowns. (C) The increase ability to apically biotinylate the basolateral proteins E-cadherin and TfR suggest that ΔCRAF:ER activation increases paracellular leak pathway permeability to biotin. (D) The amount of claudin-2 retrieved by neutravidin pulldown was decreased by approximately 50% following ΔCRAF:ER activation at each stage of the assay. Whole cell lysate levels were decreased by a similar extent and quantification presented in Figure 5.14 indicates that claudin-2 trafficking was unaffected by ΔCRAF:ER activation. Similar conclusions were drawn for claudin-1 (E) and -4 (F); despite increased initial surface-labelling, the proportion of this labelled protein that was internalised, degraded and recycled was not affected by ΔCRAF:ER activation (see Figure 5.15 and 5.16, respectively). Immunoblots are representative of three independent biological repeats. Claudin-1 and ERK1/2 lysate immunoblots were obtained from the same gel.

5.3.6 RAF/MEK/ERK activity does not influence claudin-2 trafficking

Although claudin-2 did not appear to accumulate in the cytoplasm prior to its loss (Figure 5.8), internalised claudin-2 could potentially have been degraded at a rate sufficient to prevent its internal accumulation. To address the possibility that accelerated protein turnover acts in concert with reduced mRNA synthesis to downregulate claudin-2 levels, the surface-biotinylation based trafficking assay was utilised to track the rates of claudin-2 trafficking and degradation. In unstimulated ΔCRAF:ER-expressing cells, claudin-2 was successfully retrieved by neutravidin pulldown following biotinylation, but not in the "no biotin" control sample, and was efficiently removed by surface-stripping with MESNA (Figure 5.13D). After 1 hour, approximately 40% of surface-biotinylated claudin-2 was resistant to surface-stripping, compared to approximately 20% in strip control conditions, indicating the relative degree of claudin-2 internalisation (Figure 5.13D). Following the second incubation, the majority of internalised claudin-2 was recycled, while a small amount was degraded (Figure 5.13D).

The biotinylation assay was performed in parallel with ΔCRAF:ER-expressing cells that had been pre-treated with 1μM 4HT for 24 hours (Figure 5.13D and 5.14). The amount of surface-biotinylated claudin-2 retrieved by neutravidin pulldown was decreased by approximately 50% at each step of the biotinylation assay (Figure 5.14A). However, the amount of claudin-2 in the whole cell lysates was decreased by a similar amount (Figure 5.14B). When the pulldown levels were normalised to those in the whole cell lysate, there was no significant difference in the amount of claudin-2 that was initially surface-labelled (Figure 5.14C). Furthermore, the proportion of surface-biotinylated claudin-2 that was internalised, degraded and recycled was identical in both control and 4HT-treated conditions (Figure 5.14D). This indicates that although ΔCRAF:ER activation decreased total claudin-2 levels, the proportion of the remaining claudin-2 pool existing at the cell surface was not affected. Moreover, this surface-biotinylated claudin-2 underwent similar rates of internalisation, degradation and recycling compared to claudin-2 in control-treated cells.

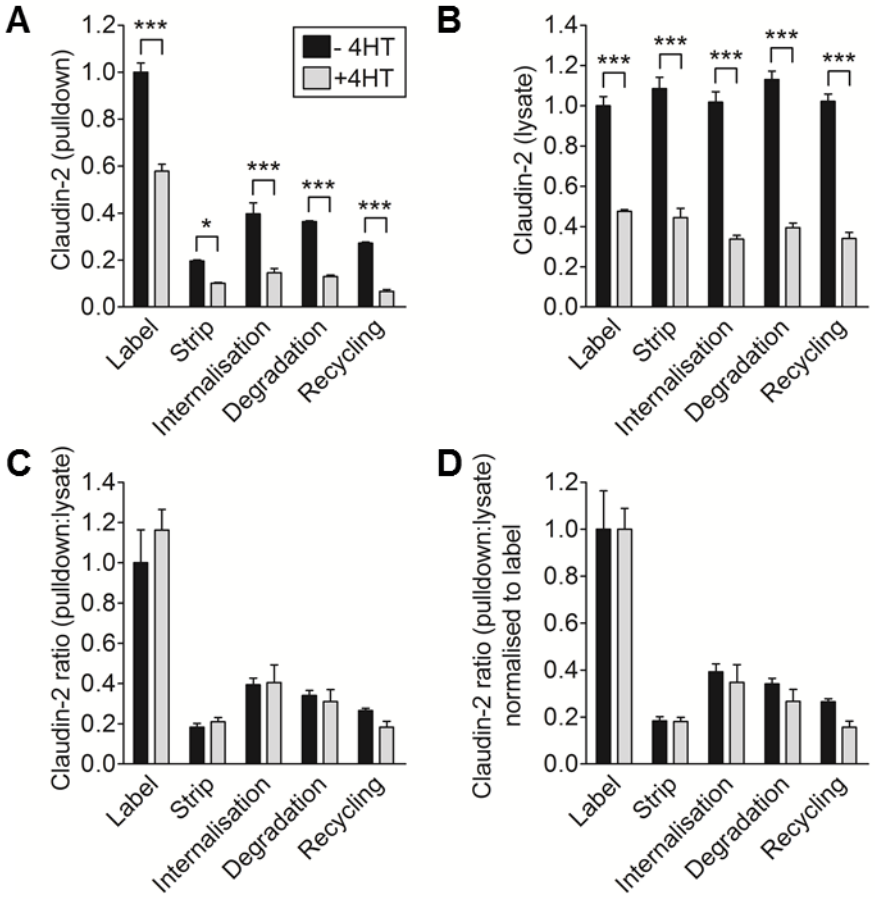

Figure 5.14: ΔCRAF:ER activation causes claudin-2 depletion without affecting its subcellular distribution or endocytic trafficking. The data presented are quantified values of the biotinylation assay immunoblots presented in Figure 5.13. Confluent MDCKII cells expressing ΔCRAF:ER were treated with or without 1μM 4HT for 24 hours. Cells were surface-biotinylated and subjected to the trafficking assay. The "label" lane indicates the amount of claudin-2 initially biotinylated at the cell surface. Internalised protein is resistant to surface-stripping. Relative degradation is shown by a minor reduction in signal between internalisation and degradation lanes. Recycling is indicated by the reduction of signal in the recycling lane relative to the degradation lane. ΔCRAF:ER activation reduces claudin-2 pulldown (A) and lysate levels (B) by approximately 50%. (C) Normalisation of claudin-2 pulldown and lysate levels reveals the proportion of remaining claudin-2 that is surface-biotinylated is identical between control and 4HT-treated conditions. (D) Normalisation of each stage of the biotinylation assay to the relevant surface-label control reveals that claudin-2 was internalised, degraded and recycled to similar extents in control and 4HT-treated conditions. Data are presented as mean values ±s.e.m. from three independent experiments. 4HT and control treatments were compared at each stage of the assay using a two-way ANOVA with Bonferroni post-test, * $p<0.05$, *** $p<0.001$.

5.3.7 RAF/MEK/ERK activity does not influence the endocytic trafficking of claudin-1 or -4

The confocal microscopy data raised the possibility that ERK activation caused a shift of claudin-1 and -4 from lateral membrane domains into the apical junction. To determine if altered rates of endocytic trafficking contributed to this altered distribution pattern, the rates of claudin-1/-4 internalisation, degradation and recycling were investigated using the surface-biotinylation assay. Approximately twice as much claudin-1 was labelled by apically applied biotin following 4HT treatment (Figures 5.13 and 5.15A). Under the same conditions, there was no significant change to claudin-1 levels in the whole cell lysate (Figures 5.13 and 5.15B). Therefore, when pulldown levels were normalised to those in the whole cell lysates, the amount of claudin-1 that was labelled at the apical cell surface was still increased by approximately 60% following 4HT treatment (Figure 5.15C). Although this could potentially reflect the increased amount of claudin-1 in an apically accessible pool, the increased labelling of basolateral TfR and E-cadherin under the same conditions suggests it is at least partially due to increased access to the basolateral plasma membrane domain (Figure 5.13).

A relatively small amount of the surface-biotinylated claudin-1 was endocytosed after 1 hour compared to the strip control lane (Figure 5.15A). However, a reduction in signal in the recycling lane suggests that this claudin-1 was rapidly recycled. Importantly, ΔCRAF:ER activation did not affect the relative amount of claudin-1 retrieved by neutravidin pulldown or in the whole cell lysates at the internalisation, degradation or recycling stages of the biotinylation assay (Figure 5.15A and B). When each stage of the trafficking assay was normalised to the relevant surface-label, rates of endocytic trafficking and degradation were identical under control and 4HT-treated conditions (Figure 5.15D).

Similar results were obtained for claudin-4. After 24 hours of ΔCRAF:ER, more claudin-4 was initially labelled at the cell surface (Figures 5.13 and 5.16A), probably due to increased access of apically applied biotin to basolateral pools. In contrast to claudin-1 and -2, the biotinylation trafficking assay revealed that claudin-4 did not undergo detectable endocytosis over the course of this experiment in either control or 4HT-treated conditions (Figures 5.13 and 5.16A). Although ΔCRAF:ER activation increased the total amount of claudin-4 in the whole cell lysates (Figures 5.13 and 5.16B), the nature of the assay distinguishes between the trafficking of existing protein and the effects of newly synthesised protein. Importantly, after normalising each step of the trafficking assay to the relevant surface-label control, ΔCRAF:ER activation had no

detectable effect on the degree of claudin-4 internalisation. This prevented the subsequent assessment of degradation and recycling rates. Taken together with the confocal imaging, these data indicate that RAF/MEK/ERK activity is sufficient to drive the accumulation of claudin-1 and -4 at the apical junction, but that this proceeds without any concomitant changes in the rates of their endocytic trafficking to and from the plasma membrane.

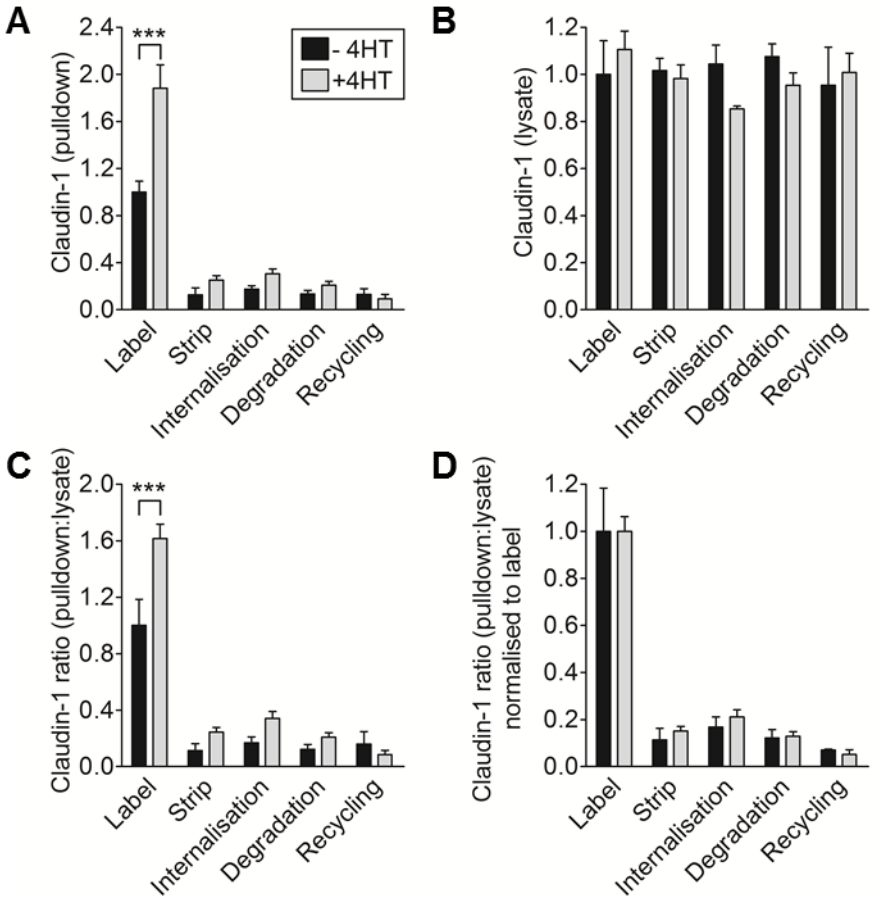

Figure 5.15: ΔCRAF:ER activation does not affect the endocytic trafficking rates of claudin-1. The data presented are quantified values of the biotinylation assay immunoblots presented in Figure 5.13. Confluent ΔCRAF:ER-expressing MDCKII cells were treated with or without 1μM 4HT for 24 hours. Surface-biotinylation and trafficking assays were performed as previously described. (A) ΔCRAF:ER activation increases the amount of claudin-1 initially labelled at the cell surface, and at each stage of the trafficking assay. (B) ΔCRAF:ER activation did not affect the whole cell lysate claudin-1 levels. (C) Normalisation of claudin-1 pulldown and lysate levels revealed that an increased proportion of whole cell claudin-1 pool is surface-biotinylated at the cell surface following ΔCRAF:ER activation. (D) However, normalisation of each stage of the trafficking assay to the relevant surface-label control reveals that claudin-1 underwent similar rates of internalisation, degradation and endocytic recycling in control and 4HT-treated conditions. Data are presented as mean values ±s.e.m. from three independent experiments. 4HT and control treatments were compared at each stage of the assay using a two-way ANOVA with Bonferroni post-test, * $p<0.05$, *** $p<0.001$.

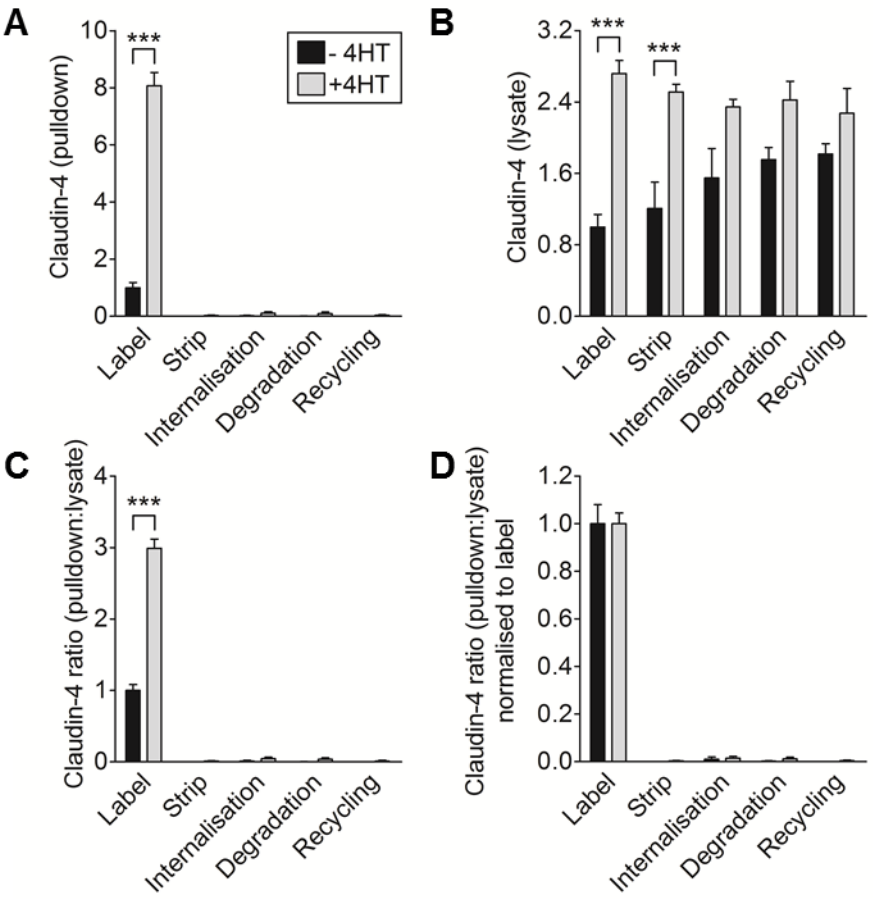

Figure 5.16: ΔCRAF:ER activation does not affect the endocytic trafficking rates of claudin-4. The data presented are quantified values of the biotinylation assay immunoblots presented in Figure 5.13. Confluent ΔCRAF:ER-expressing MDCKII cells were treated with or without 1μM 4HT for 24 hours. Surface-biotinylation and trafficking assays were performed as previously described. (A) ΔCRAF:ER activation increased the amount of claudin-4 initially labelled at the cell surface. (B) ΔCRAF:ER activation consistently increased whole cell lysate claudin-4 levels. (C) Normalisation of claudin-4 pulldown and lysate levels revealed that an increased proportion of whole cell claudin-4 pool is biotinylated at the cell surface under these conditions. (D) Normalisation of each stage of the assay to the relevant surface-label condition revealed that claudin-4 underwent negligible internalisation or trafficking under control or 4HT-treated conditions. Data are presented as mean values ±s.e.m. from three independent experiments. 4HT and control treatments were compared at each stage of the assay using a two-way ANOVA with Bonferroni post-test, * $p<0.05$, *** $p<0.001$.

After 24 hours of ERK activation, the remaining claudin-2 protein pool could have been confined to nontransduced cells, exhibiting normal claudin-2 distribution and trafficking. However, claudin-2 trafficking was unaffected in a similar surface-biotinylation assay where transduced cells were surface-biotinylated prior to the initial addition of 4HT (Figure 5.17A). The relative amounts of claudin-2 retrieved by neutravidin pulldown (Figure 5.18A) and present in the whole cell lysates (Figure 5.18B) were identical in control and 4HT-treated conditions. The rates of claudin-2 internalisation, degradation and recycling were identical between control and 4HT-treated samples when pulldown levels were normalised to whole cell lysate levels (Figure 5.18C). Therefore, RAF/MEK/ERK activity caused the depletion of claudin-2 protein without increasing its rate of internalisation or degradation, or by blocking its recycling back to the plasma membrane.

Similar results were observed for claudin-1 and -4 (Figure 5.17B and C). Surface-biotinylated claudin-1 underwent minimal endocytosis, but again appeared to be recycled (Figures 5.17B and 5.18D). ΔCRAF:ER activation did not influence the total levels of claudin-1 (Figures 5.17 and 5.18E) or the rate of claudin-1 trafficking (Figure 5.18F). Claudin-4 underwent negligible endocytosis (Figures 5.17 and 5.18G) and total levels of claudin-4 were not affected at this earlier time point (Figures 5.17 and 5.18H). ΔCRAF:ER activation did not influence the extent of claudin-4 internalisation (Figure 5.18I), and as a result, the rates of degradation and recycling could not be established. In summary, ΔCRAF:ER activation did not influence the trafficking rates of claudin-1 or -4, prior to, or following observed changes in subcellular distribution.

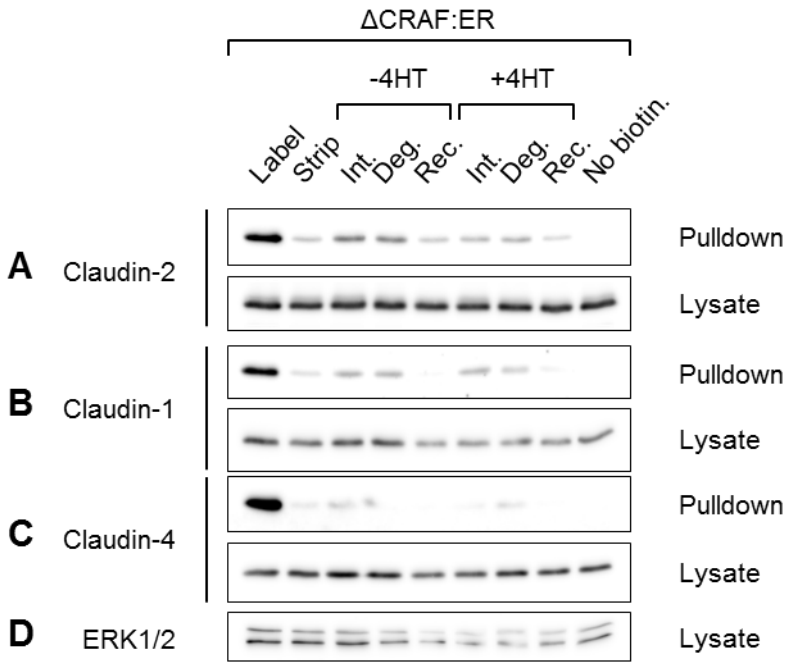

Figure 5.17: Altered claudin trafficking rates do not precede ΔCRAF:ER-mediated changes in tight junction composition. Claudin trafficking rates were determined at earlier time points by surface-biotinylating confluent ΔCRAF:ER-expressing MDCKII cells prior to the initial addition of 4HT. The trafficking assay was performed as previously described. (A) 4HT treatment did not influence the basal rates of internalisation, degradation or recycling of claudin-2 (A), -1 (B) or -4 (C). Whole cells lysate levels of each claudin and ERK1/2 were not influenced by ΔCRAF:ER activation over this time frame. The following pairs of immunoblots were obtained from the same gel: Immunoblots are representative of three independent biological repeats. Immunoblot quantification is presented in Figure 5.18. Claudin-1 and ERK1/2 lysate immunoblots were obtained from the same gel.

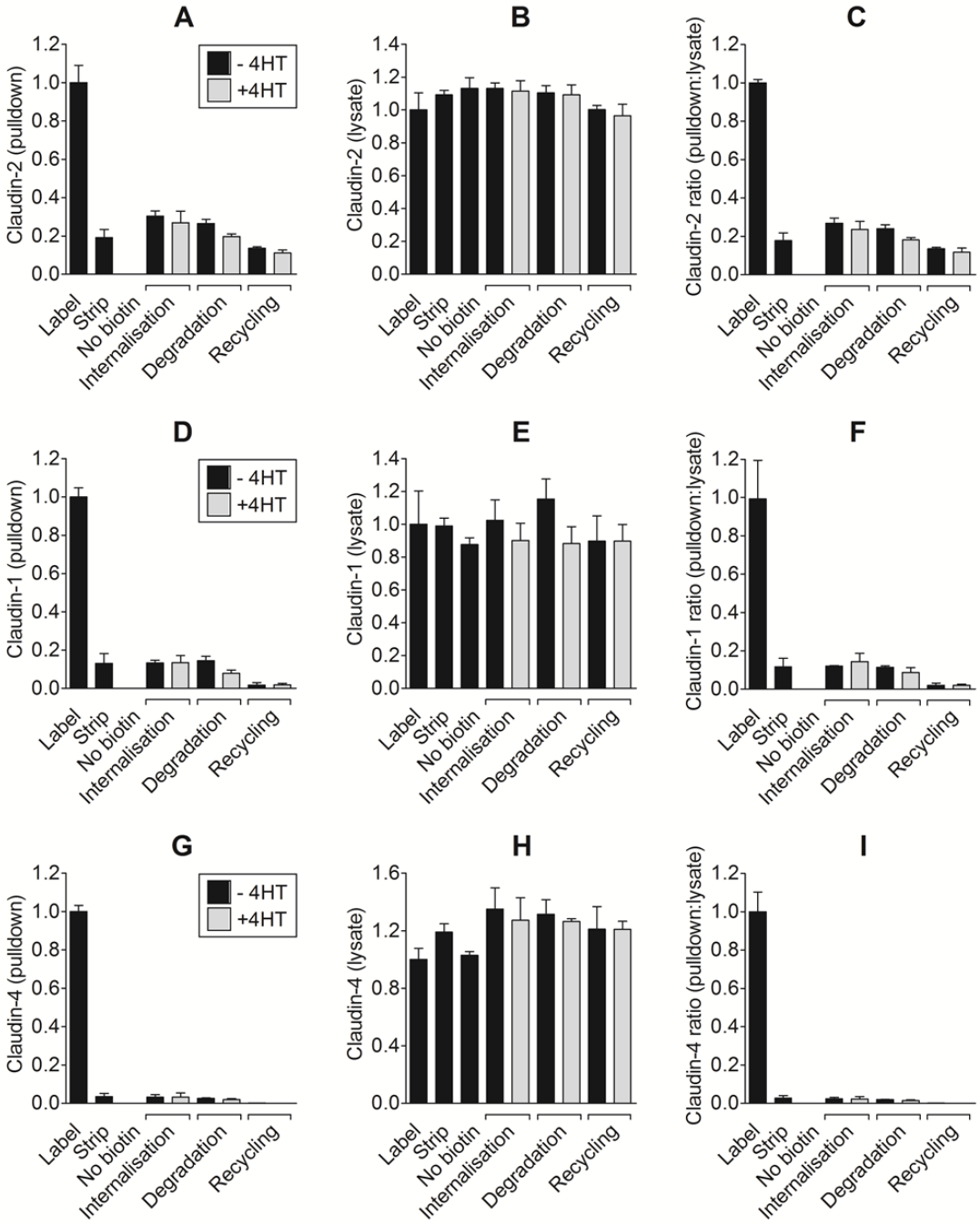

Figure 5.18: **ΔCRAF:ER activity does alter claudin trafficking rates prior to changes in tight junction.** The trafficking assay was carried out in ΔCRAF:ER-expressing cells that were surface-biotinylated prior to the initial addition of 4HT. 4HT was then added for the duration of each incubation. Under these conditions, ΔCRAF:ER activation did not affect claudin-2 pulldown (F) or whole cell lysate levels (G). (H) Normalisation of pulldown to lysate levels indicates that claudin-2 undergoes similar rates of internalisation, degradation and endocytic recycling in control and 4HT-treated conditions. Data are presented as mean values ±s.e.m. from three independent experiments. Immunoblots are representative of these three biological repeats. 4HT and control treatments were compared at each stage of the assay using a two-way ANOVA with Bonferroni post-test, * $p<0.05$, *** $p<0.001$.

.

5.3.8 RAF/MEK/ ERK activity does not influence claudin turnover rate

To address whether ERK activity influenced claudin turnover rates over longer time frames, the endocytosis assay was modified to assess claudin internalisation and degradation rates over a 6 hour period. To assess cumulative internalisation, surface-biotinylated cells were incubated at 37°C for either 1 or 6 hours, in the presence or absence of 4HT. Surface biotin was then stripped, so remaining levels of biotinylated proteins reflected the relative amount of protein internalised during incubation. Surface-biotinylated claudin-2 was internalised after 1 and 6 hours, but this was not increased by the addition of 4HT (Figure 5.19A and C), although total claudin-2 levels decreased by approximately 50% (Figure 5.19C). Therefore, RAF/MEK/ERK activity can drive claudin-2 protein depletion without increasing its rate of internalisation.

The internalisation rates of claudin-1/-4 were assessed to determine if decreased rates of internalisation could explain their junctional accumulation. Surface-biotinylated claudin-1/-4 underwent minimal internalisation compared to the strip control after both 1 and 6 hours, and this was not affected by activation of ΔCRAF:ER with 4HT (Figure 5.19A,B and D). Although whole cell lysate claudin-4 levels increased following 4HT treatment (Figure 5.19D), the nature of the assay allows the discrimination between previously existing and newly synthesised protein. As changes in internalisation rates of claudin-1/-4 were not detectable, their accumulation at the TJ cannot be attributed to decreased rates of internalisation of these proteins from the cell surface.

Increased ERK activity could potentially modulate the degradation rate of internalised claudins. In order to assess claudin degradation rates over longer time periods, the endocytosis assay was modified such that surface-biotinylated cells were lysed immediately after incubation at 37°C, without surface-stripping of remaining biotin. Thus, any decrease in pulldown level could be attributed to protein degradation rather than altered localisation. Claudin-2 pulldown levels were gradually depleted over a 6-hour period, but the rate of decline was not accelerated by ΔCRAF:ER activation (Figure 5.20A and C). However, after 6 hours, total claudin-2 levels were reduced by approximately 50% (Figure 5.20C), indicating that ERK activity drives claudin-2 protein depletion by decreasing its synthesis (Figure 5.6), without increasing its degradation rate. Claudin-1/-4 degradation rates were assessed to determine if an increase in protein stability could explain their increased presence at the TJ. Claudin-1 and -4 pulldown levels decreased over 6 hours, but the rate of decline was not influenced by ΔCRAF:ER activation (Figure 5.20A, B and D). To summarise, RAF/MEK/ERK activity did not alter the overall stability of surface-biotinylated claudin-1 or -4.

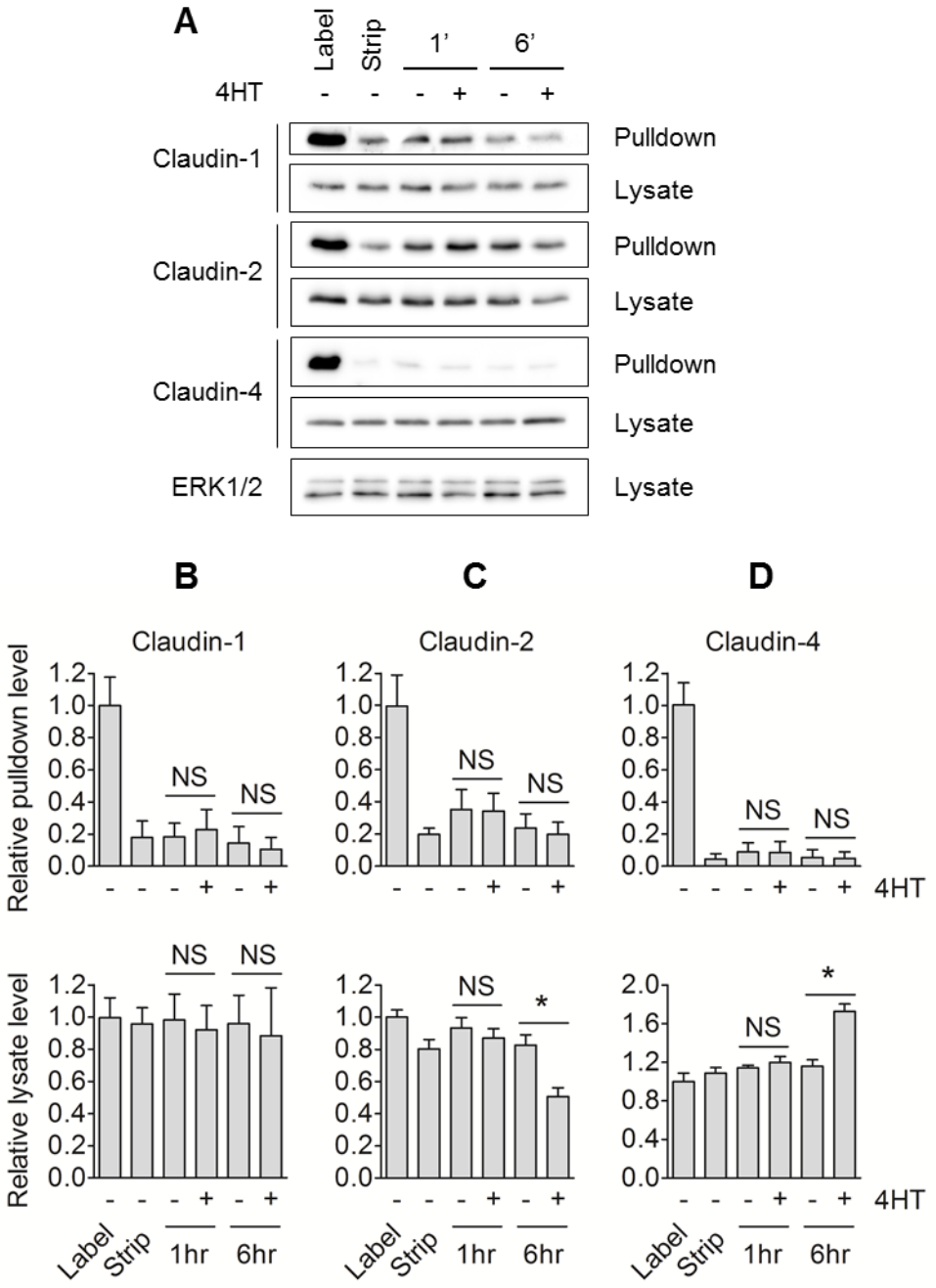

Figure 5.19: Internalisation rates of claudin-1, -2 and -4 are not influenced by ΔCRAF:ER activation. Confluent ΔCRAF:ER-expressing MDCKII cells were surface-biotinylated and incubated with or without 1µM 4HT for the indicated times. Remaining surface biotin was stripped, whereas internalised biotinylated protein was resistant to the surface strip. (A) Biotinylated and total claudin-1, -2 and -4 levels were determined by immunoblot. Immunoblots are representative of three biological repeats. (B) Quantification of claudin-1 immunoblots revealed that ΔCRAF:ER activation did not alter claudin-1 internalisation (top panel) or total levels (bottom panel). (C) ΔCRAF:ER activity does not affect claudin-2 internalisation (top panel), but does cause depletion of total claudin-2 levels after 6 hours (bottom panel). (D) ΔCRAF:ER activation does not alter claudin-4 internalisation (top panel), but does increase total claudin-4 levels after 6 hours (bottom panel). Claudin-1 and ERK1/2 lysate immunoblots were obtained from the same gel. Data is presented as mean values ±s.e.m. from three independent experiments. Relative internalisation at 1 and 6 hours was compared using a two-way ANOVA with Bonferroni post-test, * $p<0.05$.

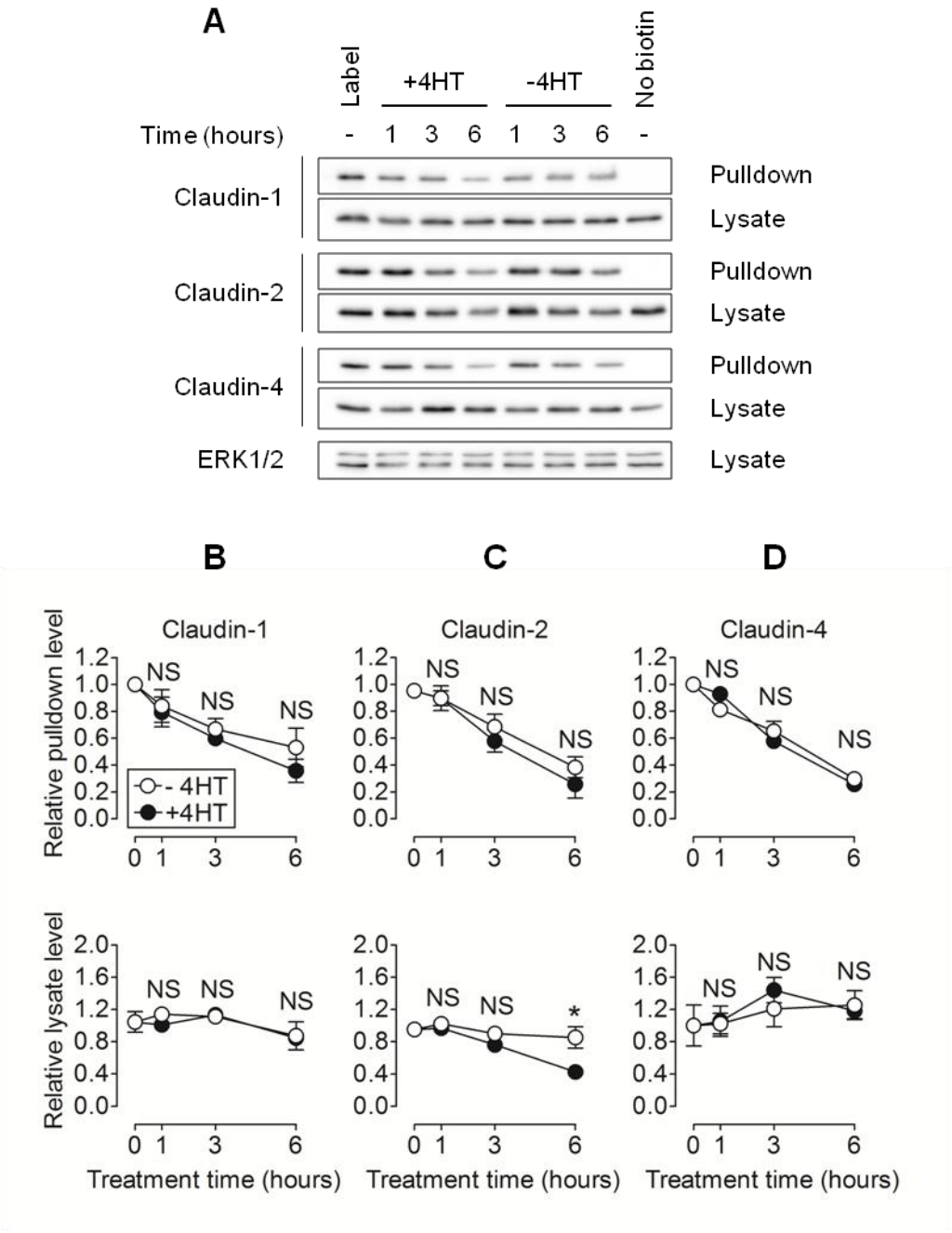

Figure 5.20: ΔCRAF:ER activation does not influence the degradation rate of surface-biotinylated claudin-1, -2 or -4. Confluent ΔCRAF:ER-expressing MDCKII cells were surface-biotinylated and incubated with or without 1μM 4HT for the indicated times. Cells were lysed without surface-stripping, so any decrease in biotinylated protein is attributed to protein degradation. (A) Biotinylated and total claudin-1, -2 and -4 levels were determined by immunoblot. Immunoblots are representative of three independent biological repeats. Quantification of immunoblots revealed ΔCRAF:ER activation did not alter the degradation rate of surface-biotinylated claudin-1 (B, top panel), claudin-2 (C, top panel) or claudin-4 (D, top panel). Total claudin-2 levels were decreased after 6 hours of 4HT treatment (C, bottom panel). Claudin-1 and ERK1/2 lysate immunoblots were obtained from the same gel. Data are presented as mean values ±s.e.m. from three biological repeats. Relative claudin levels are at each time point were compared using a two-way ANOVA with Bonferroni post-test, *p<0.05.

Covalent modification of claudins with biotin could potentially influence the rate at which they are degraded. Therefore, claudin degradation rates were also determined in a biotinylation-free assay by blocking protein neosynthesis with cycloheximide. Claudin degradation rates were initially determined using high-content microscopy (Figures 5.21 and 5.22). Total levels of claudin-1, -2 and -4 were gradually depleted over a 24 hour period when cells were treated with cycloheximide (Figures 5.21 and 5.22).The depletion rates of claudin-1, -2 and -4 were not influenced by co-treatment with 4HT (Figure 5.22A, B and C, respectively). However, high-content imaging revealed that prolonged treatment of MDCKII cells with cycloheximide caused clear changes in cell area and shape (Figure 5.21). MDCKII cells normally adopt a compact cylindrical shape as cells pack tightly into a monolayer. After 12 – 24 hours of cycloheximide treatment, cell area had increased, and cell contacts were straighter and more angular than in control conditions (Figure 5.21). As these morphological changes could have an unpredictable influence on the quantification of immunostaining images, claudin degradation rates were also assessed by immunoblot (Figure 5.23A).

In ΔCRAF:ER-expressing MDCKII cells, 4HT treatment successfully induced downstream phosphorylation of ERK1/2 over a 12 hour period (Figure 5.23B) without affecting total ERK1/2 levels (Figure 5.23C). Claudin-1 levels were gradually depleted over this 12-hour period in cells treated with 30μM cycloheximide (Figure 5.23D). After 12 hours, total claudin-1 levels were significantly lower in samples co-treated with cycloheximide and 4HT compared to cycloheximide treatment alone (Figure 5.23D). This suggests that ΔCRAF:ER activation increases the degradation rate of claudin-1. Total levels of claudin-2 (Figure 5.23E) and claudin-4 (Figure 5.23F) also decreased over a 12 hour period when treated with cycloheximide, but in contrast to claudin-1, the rate of their depletion was not influenced by co-treatment with 4HT, suggesting that ΔCRAF:ER activation does not influence their rate of degradation. The small increase in claudin-1 degradation rate assessed by immunoblot may underlie the observed minor and statistically insignificant decrease in total claudin-1 levels (Figures 5.1 and 5.5). However, both the small decrease in claudin-1 level and increase in degradation rate were only observed when cells were lysed in triton-based lysis buffers. Claudin level and degradation rate were not affected when studied by high-content microscopy or in assays where cells were lysed in SDS-based biotinylation assay lysis buffer. This suggests that both the minor decrease in claudin-1 levels and increase in claudin-1 degradation rate are likely due to decreased detergent-solubility and inefficient retrieval in the triton-based lysis buffer.

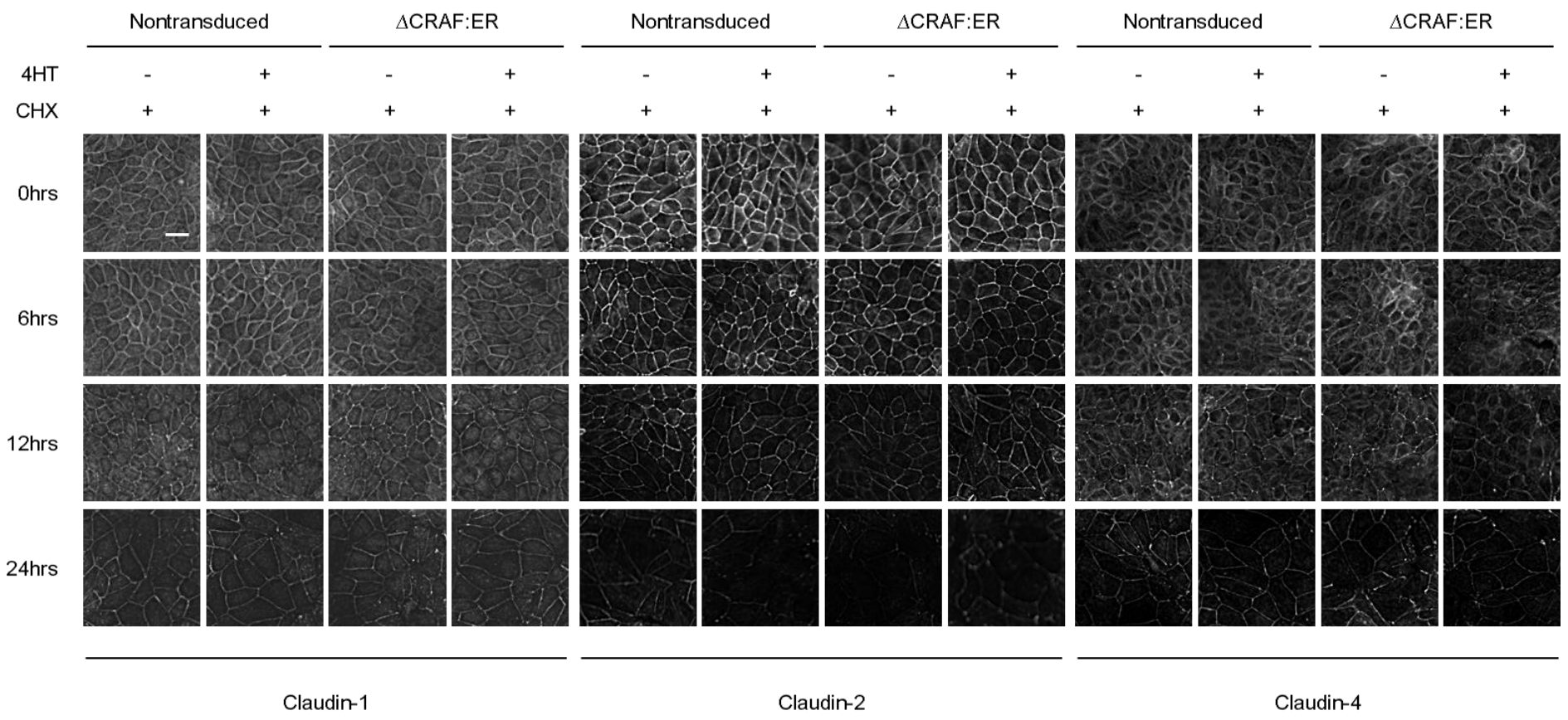

Figure 5.21: ΔCRAF:ER activation does not affect the rate of loss of claudin immunostaining intensity in the presence of cycloheximide. Representative images of cells immunostained for claudin-1, -2 and -4 from three independent experiments Confluent MDCKII cells expressing ΔCRAF:ER were treated with 1μM 4HT and 30μM cycloheximide (CHX) as indicated, prior to fixation and immunostaining. Average claudin intensity was measured using INCell Developer Toolbox software. Quantification of data is presented in Figure 5.22. The average intensity of claudin-1, -2 and -4 each decreased at similar rates in each experimental condition. Prolonged cycloheximide treatment increases cell area and generate increasingly linear and angular cell-cell contacts. Scale bar = 20μm.

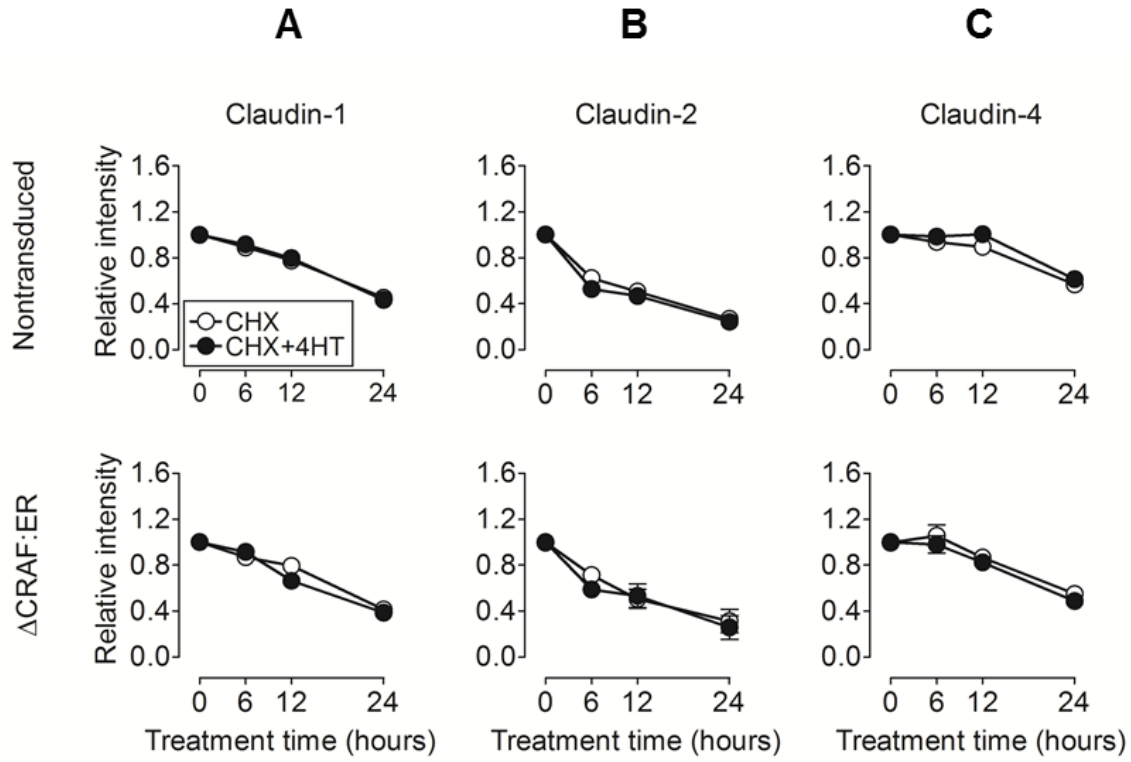

Figure 5.22: ΔCRAF:ER activity does not affect the rate of loss of claudin immunostaining intensity in the presence of cycloheximide. Confluent ΔCRAF:ER-expressing MDCKII cells were treated with 1μM 4HT and 30μM cycloheximide (CHX) as indicated, prior to fixation and immunostaining. Average claudin intensity was measured using INCell Developer Toolbox software. The average intensity of claudin-1 (A), claudin-2 (B) and claudin-4 (C) each decreased at similar rates when treated with cycloheximide, either alone or in combination with 4HT. Representative images are presented in Figure 5.21. Data are presented as mean values ±s.e.m. from three independent experiments. Treatments were compared at each time point using a two-way ANOVA with Bonferroni post-test. Representative images are presented in Figure 5.21.

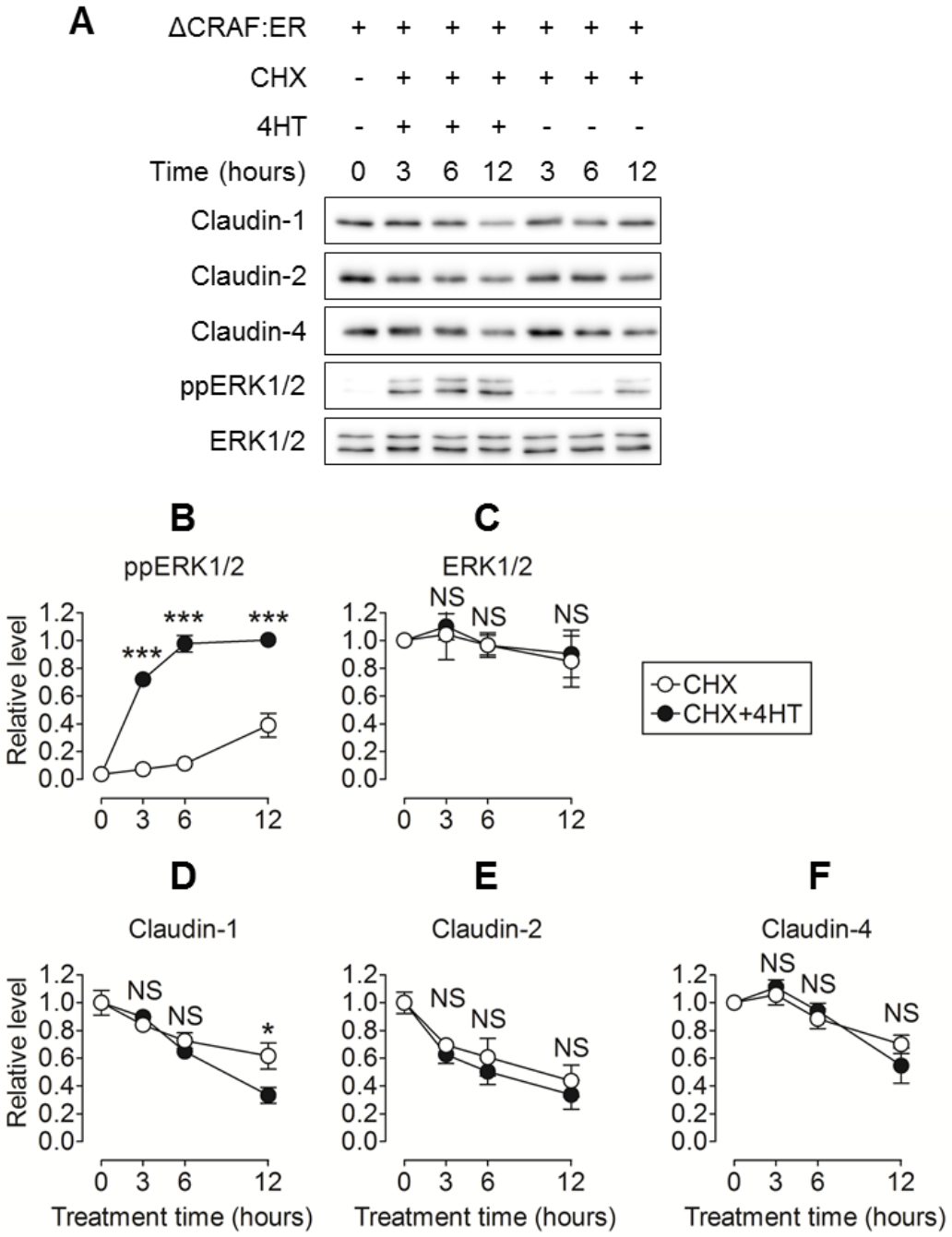

Figure 5.23: ΔCRAF:ER activation increases the degradation rate of whole cell claudin-1, but not claudin-2 or -4. Confluent MDCKII cells expressing ΔCRAF:ER were incubated with 30μM cycloheximide (CHX), either alone or in combination with 1μM 4HT for the indicated times. (A) Cells were lysed and relative claudin levels were determined by immunoblot. Immunoblots are representative of three independent experiments. (B) 4HT treatment successfully induced downstream phosphorylation of ERK1/2 without affecting total ERK1/2 levels (C). Quantification of immunoblots revealed that ΔCRAF:ER activation with 4HT increased the rate of claudin-1 depletion in the presence of cycloheximide (D) without affecting the rate of claudin-2 (E) or claudin-4 (F) loss. The following pairs of immunoblots were obtained from the same gel: ERK1/2 and claudin-1, ppERK1/2 and claudin-2. Data are presented as mean values ±s.e.m. from three independent experiments. Treatments were compared at each time point using a two-way ANOVA with Bonferroni post-test, * $p<0.05$, *** $p<0.001$.

5.4 Discussion

The results in this chapter indicate that RAF/MEK/ERK activity is sufficient to increase MDCKII transepithelial resistance, which occurs with the concurrent modulation of TJ claudin composition through surprisingly diverse mechanisms (summarised in Table 5.1). Claudin-1, -2 and -4 are each controlled by a distinct mode of regulation. Claudin-2 is downregulated at the mRNA and protein level, but turned over by normal rates of internalisation and degradation. By contrast, claudin-4 is redistributed from the lateral membrane to the apical junction and throughout the cytoplasm, which occurs with a concomitant increase in protein, but not mRNA levels. Claudin-1 also accumulates at the apical junctional and in the cytoplasm, although its degradation rate is actually increased. This novel redistribution of the barrier-promoting claudins -1 and -4 from the lateral membrane to the apical junction proceeds in a manner independent of changes in protein level or endocytic trafficking rates.

TJ protein	mRNA level	Protein level	Distribution	Degradation rates
Claudin-1	-	-	Junctional accumulation Cytoplasmic punctae	-
Claudin-2	↓↓↓	↓↓↓	Lost from the apical junction without prior internal accumulation	-
Claudin-4	-	↑	Junctional accumulation Cytoplasmic punctae	-
Occludin	ND	-	Retained at the apical junction and lateral membrane	ND
ZO-1	ND	-	Retained at the apical junction Diffuse cytoplasmic staining	ND

Table 5.1: A summary of ΔCRAF:ER-mediated regulation of individual tight junction proteins. RAF/MEK/ERK activity regulates claudin-1, -2 and -4 through distinct and unique modes of regulation. Claudin-1 accumulates at the TJ, but total levels and degradation rate are unaffected. In contrast, claudin-2 is downregulated at both the mRNA and protein level, with the existing claudin-2 protein pool turned over by normal rates of internalisation and degradation. Claudin-4 levels are marginally upregulated, without a concomitant increase mRNA level. However, junctional claudin-4 accumulation cannot be fully accounted for by this increase in protein level. The total levels and intramembrane distribution of occludin and ZO-1 are not affected by. ΔCRAF:ER activation does induce a diffuse cytoplasmic staining pattern for occludin and ZO-1, but they do not appear in the same discrete cytoplasmic compartments as claudin-1 and -4. RAF/MEK/ERK activity therefore has distinct claudin-specific effects on protein synthesis, degradation and subcellular distribution. (-) no change, (↓) marginally decreased, (↑) marginally increased, (↓↓↓) dramatically decreased (ND) not determined.

ΔCRAF:ER activity negatively regulates claudin-2 synthesis, but the existing protein pool is turned over by normal rates of endocytosis and degradation

RAF/MEK/ERK activity caused a decrease in *CLDN2* mRNA levels, which is likely due to downregulated transcription, and this was mirrored by a significant depletion of claudin-2 protein. Claudin-2 protein depletion was sensitive to chloroquine, suggesting a requirement for lysosomal degradation. Immunofluorescence imaging revealed a progressive decrease in junctional claudin-2 intensity, but this did not occur with a concurrent increase in cytoplasmic claudin-2 staining. Furthermore, ΔCRAF:ER activation had no effect on the cumulative internalisation or degradation of claudin-2 protein using either surface-biotinylation- or cycloheximide-based assays. To conclude, ERK activity decreases claudin-2 protein synthesis, but the existing claudin-2 pool is turned over by normal rates of internalisation from the cell surface and degradation in the lysosome.

This was unexpected as EGF has been reported to decrease claudin-2 protein stability in the presence of cycloheximide in a MEK-dependent manner (Ikari et al., 2011c). The EGF-mediated decrease in claudin-2 mRNA and protein is at least partially prevented by treatment with either the Src inhibitor, PP2, or the MEK inhibitor, U0126 (García-Hernández et al., 2015). As well as being involved in EGFR-mediated activation of the RAF/MEK/ERK pathway, Src is an established effector of endocytic trafficking (Mellman and Yarden, 2013) and may therefore drive EGF-mediated changes in claudin-2 internalisation and/or trafficking in a manner that cannot be recapitulated by activation of the RAF/MEK/ERK pathway alone. Although RAF/MEK/ERK activity may be required to alter claudin-2 protein turnover downstream of EGFR activation, alone it is not sufficient to elicit the same response.

ΔCRAF:ER activation leads to the accumulation of claudin-4 at the apical junction, without affecting rates of endocytic trafficking

Activation of ΔCRAF:ER led to a consistent increase in claudin-4 protein levels of approximately 1.5 to 2-fold, as assessed by immunoblot, which is supported by a significant increase in claudin-4 intensity using high-content microscopy. The lysis buffer used in the biotinylation asays contains SDS, a strong detergent, which will solublise TJ-associated proteins (Singh and Harris, 2005). Under these conditions, ΔCRAF:ER activation increased total claudin-4 levels after 24 hours, which is consistent with the increase observed both by high-content and confocal microscopy. Increased claudin-4 mRNA and protein levels have been reported following stimulation of the RAF/MEK/ERK pathway, both in response to EGF (García-Hernández et al., 2015; Ikari et al., 2009) and ΔCRAF:ER activation (Doehn et al., 2009). After 24 hours

of ΔCRAF:ER activation, claudin-4 mRNA levels were not affected by RT-qPCR. However, an earlier transient increase in claudin-4 synthesis may underlie the observed increase in claudin-4 protein levels (Ikari et al., 2009). Interestingly, confocal microscopy revealed a striking increase in junctional claudin-4 intensity, which cannot be accounted for by increased claudin-4 levels alone. Therefore, the accumulation of claudin-4 at the TJ appears to proceed via additional post-translational mechanisms.

ΔCRAF:ER activation leads to the accumulation of claudin-1 at the apical junction

ΔCRAF:ER activation caused a marginal decrease in total claudin-1 protein levels by immunoblot, though this never reached statistical significance. By contrast, total claudin-1 levels were not influenced by ΔCRAF:ER activation when cells were lysed in the SDS-based biotinylation assay lysis buffer, which is consistent with the high-content microscopy data, suggesting that ΔCRAF:ER activation influences claudin-1 distribution but not total level. Taken together with the confocal microscopy, the data suggests that ΔCRAF:ER activation drives the redistribution of claudin-1 and -4 from the lateral membrane into the TJ. While total claudin-4 levels are marginally increased, its rate of internalisation and degradation and not affected. Claudin-1 degradation rates were not affected as assessed by surface-biotinylation assays, using SDS-based lysis buffers, or in cycloheximide chase experiments using high-content microscopy. This suggests that both the minor decrease in claudin-1 levels and increase in claudin-1 degradation rate are likely due to decreased detergent-solubility and inefficient retrieval in the triton-based lysis buffer. To concldude, the altered distribution of claudin-1 is not accompanied by a change to total claudin-1 levels or turnover rates.

Claudin-1 mRNA levels were not affected by RAF/MEK/ERK pathway activation. This echoes studies in immortalised mouse hepatic cells, where the stable expression of CRAF causes a significant depletion of claudin-1 protein, while mRNA levels are unaffected (Lan et al., 2004). Other studies have failed to detect any change in claudin-1 levels following growth factor treatments (Ikari et al., 2009) or in response to ΔCRAF:ER activation (Doehn et al., 2009). However, sustained ERK signalling, associated with epithelial-mesenchymal transition, may result in transcriptional downregulation of claudin-1 via E-box transcription factors (Martínez-Estrada et al., 2006).

Ras-transformed MDCK cells exhibit cytoplasmic inclusions of occludin, claudin-1 and ZO-1, which are rapidly recruited to the cell membrane following treatment with the MEK inhibitor, PD98059 (Chen et al., 2000). This suggests that long-term activation of

the RAF/MEK/ERK pathway may cause the cytoplasmic sequestration of claudin-1. Claudin-1 did accumulate in cytoplasmic compartments, but it is unclear how this tallies with its apparent accumulation at the TJ. Acute EGFR activation causes TJ remodelling, while chronic activation drives TJ disassembly associated with dedifferentiation (Singh et al., 2007), suggesting that variation in ERK signal duration may influence the TJ response. Cytoplasmic claudin-1 may represent partial TJ disassembly, coinciding with a decrease in TER at later time points, following an earlier redistribution into the TJ. To conclude, RAF/MEK/ERK activity causes the redistribution of claudin-1 from the lateral membrane into the apical junction, but this occurs independently of changes in claudin-1 synthesis or trafficking rates.

The accumulation of claudin-1 and -4 at the TJ is consistent with the reported effect of EGF on their relative triton solubility (Singh and Harris, 2004). Treatment with EGF increased the amount of claudin-1, -3 and -4 in the triton-insoluble fraction, suggesting increased junctional incorporation, even in the absence of protein neosynthesis (Singh and Harris, 2004). The presented data shows that RAF/MEK/ERK activity alone can specifically regulate the distribution of TJ proteins in different plasma membrane domains to increase the junctional pool of claudin-1/-4. Interestingly, recent studies involving the TALEN-mediated knockdown of claudin-2 in MDCKII cells suggest that co-expressed claudin species may be incorporated into the TJ following claudin-2 depletion. This suggests that RAF/MEK/ERK-mediated depletion of claudin-2 may have complex effects on TJ composition, potentially through altering the interactions of existing proteins within the junctional domain. This is further discussed in Chapter 6.

Surface-biotinylation-based assays can be used to assess rates of endocytic trafficking and degradation

Rates of claudin internalisation and recycling were not affected by ΔCRAF:ER activation. However, the surface-biotinylation assay accurately reported the trafficking of the established recycling cargo, TfR. Furthermore, the basal rates of claudin-1, -2 and -4 trafficking are largely consistent with those previously reported; claudin-1 and -2 are constitutively recycled, while claudin-4 does not accumulate internally over the same time frame (Dukes et al., 2011b; Dukes et al., 2012). Large changes in trafficking rates are not necessarily required to mediate profound effects in cell surface protein distribution. For example, depletion of Rab14 causes a 50% reduction in claudin-1 levels at areas of cell-cell contact, due to a relatively modest 10% increase in internalisation detected using a similar surface-biotinylation assay (Lu et al., 2014). In the same study, a 10% increase in occludin recycling increased junctional occludin levels by approximately 20% (Lu et al., 2014). Furthermore, altered rates of recycling

and degradation are frequently reflected in the extent of initial internal accumulation. For example, treatment of MDCKII cells with the PIKfyve inhibitor, YM201636, doubles the amount of claudin-2 that is initially internalised, by blocking recycling of the internalised protein back to the cell surface (Dukes et al., 2012). These observations indicate that the net distribution of cell surface proteins is highly sensitive to small changes in trafficking rates. However, the presented data indicate that ΔCRAF:ER activation consistently failed to induce even minor changes in claudin recycling, either prior to, or after dramatic changes in TJ composition, suggesting that alternative mechanisms are involved.

Potential mechanisms for claudin-1/-4 redistribution

Following RAF/MEK/ERK pathway activation, claudin-2 expression is lost, while claudin-1 and -4 accumulate at the apical junction (Figure 5.24A). Of note, the TALEN-mediated knockout of claudin-2 caused the subsequent accumulation of claudin-1, -3, -4 and -7 at the apical junction (Tokuda and Furuse, 2015). This suggests that competitive interactions between individual claudin species at the apical junction may underlie their initial spatial segregation. The subsequent depletion of claudin-2 may then permit the incorporation of claudin-1 and -4 (and other claudin species) into the apical junction. However, the increased labelling of basolateral proteins by apically applied biotin suggests that leak pathway permeability is also increased, which cannot be explained based on the observations of claudin-2 knockdown and knockout studies (Hou et al., 2006; Tokuda and Furuse, 2015; Van Itallie et al., 2008).

There are at least three potential mechanisms that could account for the accumulation of claudin-1 and -4 at the TJ (Figure 5.24). Following ΔCRAF:ER activation, newly synthesised claudin-1/-4 may be delivered preferentially to the TJ rather than lateral membrane, while existing claudin-1/-4 are turned over at normal rates (Figure 5.24B). This model would result in increased junctional localisation of claudin-1/-4 without the redistribution of existing protein. Alternatively, activation of the RAF/MEK/ERK pathway could stabilise claudins in the TJ or increase the mobility of claudins within the lateral membrane to affect the net claudin distribution (Figure 5.24C). Finally, RAF/MEK/ERK signalling may cause claudin-1 and -4 to be specifically internalised from the basolateral membrane and undergo transcytosis to the apical junction via an as yet unidentified endosomal compartment, reflecting a change in trafficking routes rather than rates (Figure 5.24D).

Activation of the RAF/MEK/ERK pathway with ΔCRAF:ER did not influence the rates of internalisation or recycling of claudin-1, -2 or -4. However, this does not necessarily

rule out a role for endocytic trafficking in mediating the redistribution of claudin-1 and -4 to the apical junction. Access to basolateral proteins will be severely restricted by the presence of an intact TJ, which will block the paracellular passage of apically applied biotin based on its molecular weight and negative charge in solution. Therefore, RAF/MEK/ERK activity could potentially mediate altered trafficking of a specific apically inaccessible claudin-1/-4 pool. However, after 24 hours of ΔCRAF:ER activation, increased amounts of claudin-1/-4, as well as the basolateral proteins TfR and E-cadherin, were initially surface-labelled with apically applied biotin. Despite the increased labelling of these basolateral pools, the rates of claudin-1/-4 internalisation, degradation and recycling were unaffected by ΔCRAF:ER activation. However, transcytosis would involve the rerouting of internalised claudin-1/-4 from the basolateral domain to the apical domain via an as yet unidentified endosomal compartment, and would not necessarily be reflected in increased *rates* of internalisation or recycling.

This hypothesis would be potentially difficult to test using the biochemical techniques employed in these studies. However, increased biotinylation of the basolateral pool could be achieved by growing MDCKII cells on transwell permeable filters. This would allow basolateral application of biotin, providing increased access to the major pools of claudin-1 and -4. Differential trafficking of junctional and lateral membrane pools could then be determined by comparing trafficking rates of apically and basolaterally labelled claudins. Basolateral labelling could be combined with surface-stripping, exclusively of the apical domain, so only proteins that had undergone transcytosis to the apical membrane would become amenable to the surface-strip. However, this approach is likely to be complicated by the apparent effect of RAF/MEK/ERK activity on the MDCKII leak pathway, as ΔCRAF:ER activation increased access of apically applied biotin to basolateral protein pools. Alternatively, approaches using live cell imaging and fluorescently-tagged claudins may be useful in distinguishing modes of dynamic claudin regulation.

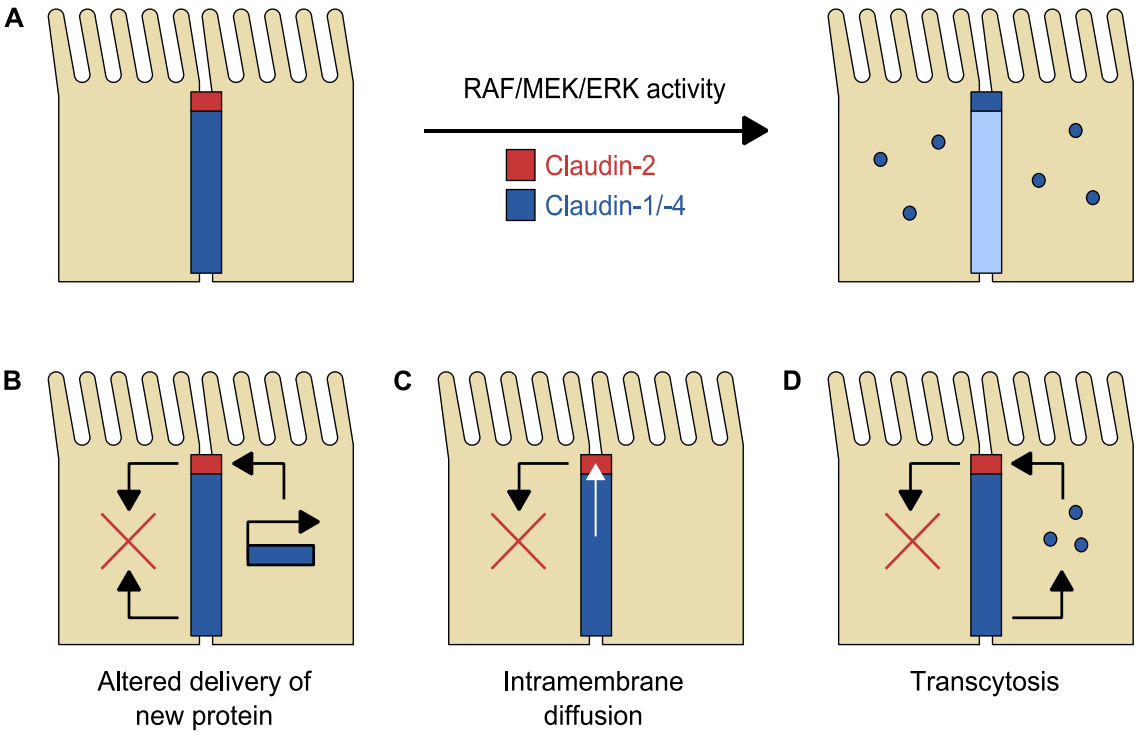

Figure 5.24: Potential mechanisms of ΔCRAF:ER-mediated tight junction remodelling. (A) MDCKII cells are characterised by the expression of claudin-2 specifically at the apical junction (red) and claudin-1 and -4 along the lateral membrane (dark blue). Specific activation of the RAF/MEK/ERK pathway leads to downregulation of claudin-2 synthesis and turnover of the existing protein pool by normal rates of endocytosis and degradation. Claudin-1 and -4 accumulate at the apical junction, as well as in discrete compartments throughout the cytoplasm. Junctional accumulation of claudin-1 and -4 cannot be fully attributed to changes in protein expression level or altered rates of endocytic trafficking. (B) Lateral claudin-1 and -4 may be endocytosed and degraded by normal turnover rates, while newly synthesised claudin-1 and -4 are specifically targeted to the apical junction. (C) Lateral claudin-1 and -4 may diffuse within the plasma membrane to occupy the apical junction region. (D) Claudin-1 and -4 may be endocytosed from the lateral membrane, undergo transcytosis, and be delivered specifically into the apical junction.

ΔCRAF:ER activation increases the amount of claudin-1/-4, TfR and E-cadherin labelled with apically applied biotin

The initial biotinylation assays revealed that ΔCRAF:ER activation increased the amount of claudin-1 and -4 that were initially labelled when biotin was added to apical side of MDCKII monolayers, without affecting the relative extent of internalisation, degradation or recycling. This appeared to be consistent with the redistribution of claudin-1 and -4 from the basolateral membrane to the apical junction, which would increase their presence in the apically accessible pool. However, a similar increase in apical labelling was observed with TfR and E-cadherin, two well-established basolateral protein markers (Fuller and Simons, 1986; Miranda et al., 2001). This suggests that the increased protein labelling may be at least partially accounted for by increased access of apically applied biotin to the basolateral plasma membrane domain and does not necessarily reflect the change in claudin-1/-4 distribution that is so apparent in confocal microscopy images.

Biotin moieties have been extensively used as tracer molecules to probe the TJ leak pathway permeability in various *in vitro* and *in vivo* systems (Ding et al., 2011). Therefore, the ability to label increased amounts of basolateral proteins suggests that RAF/MEK/ERK pathway activation increases the permeability of the paracellular leak pathway, which regulates the passage of larger molecular weight solutes, as well as the pore pathway that determines ionic conductance and can be assessed by TER measurement. Increased epithelial permeability to large non-electrolytes could also be explained by more general disruption of the monolayer due to the detachment of cells (Mullin et al., 2005). A similar increase in MDCK leak pathway permeability was reported following Ras expression (Mullin et al., 2005). In this case, permeability was specifically attributed to leak pathway modulation as increased permeability was limited to tracers of up 10kDa, indicating the presence of a limiting pore size (Mullin et al., 2005). Further characterisation of MDCKII permeability to different sized molecular tracers will be required to further characterise leak pathway modulation by ΔCRAF:ER activation.

Interestingly, leak pathway permeability is be regulated by ZO-1 and occludin (Shen et al., 2011). Although these proteins were largely retained at the apical junction following ΔCRAF:ER activation, both markers also appeared to be distributed diffusely across the cytoplasm. Unfortunately, surface-biotinylated occludin was undetectable following neutravidin pulldown, preventing the assessment of its endocytic trafficking rates. The reasons for this are unclear as occludin has successfully been studied using similar approaches elsewhere (Dukes et al., 2011b; Morimoto et al., 2005; Nishimura and

Sasaki, 2008). As ZO-1 is a peripheral cytoplasmic protein, it cannot be surface-biotinylated, excluding it from these surface-biotinylation-based approaches. Altered stability of these proteins at the TJ may underlie the minor changes in their subcellular distribution and altered leak pathway permeability.

Even when taking the increase in initial labelling into account, the proportion of initially labelled claudin-1 and -4 that is internalised, and subsequently degraded and recycled, is identical in control and 4HT-treated conditions. Furthermore, endocytic trafficking of these claudins was not affected by ΔCRAF:ER activation when cells were labelled under common conditions, prior to the initial addition of 4HT and the associated changes in TJ composition and paracellular permeability. Therefore, claudin-1 and -4 appear to accumulate at the apical junction, as assessed by confocal microscopy, but this cannot be accounted for by altered rates of endocytic trafficking over the time frames studied.

5.5 Limitations and future work

Inducible-activity ΔCRAF:ER constructs have permitted the study of RAF/MEK/ERK signalling on rates of TJ protein internalisation, degradation and recycling, with clear changes in TJ composition and the distribution of individual TJ components. However, the unique contribution of each TJ protein is unclear, as the overall epithelial barrier properties are governed by the specific repertoire of proteins that are expressed and incorporated into the junction. This could potentially be addressed by re-expressing or depleting individual claudins to determine which ΔCRAF:ER-associated phenotypes are modified. Although this study implicates transcriptional downregulation of claudin-2 as the major mechanism driving its depletion, the molecular basis for the increased junctional incorporation of claudin-1 and -4 is unclear. ΔCRAF:ER activation did not induce any changes in their internalisation or recycling rates, and the increased degradation of claudin-1 appears unlikely to contribute directly to its altered subcellular distribution. Future studies, potentially involving fluorescently-tagged TJ proteins, will be required to determine if RAF/MEK/ERK-mediated changes in the dynamics and molecular interactions of TJ proteins underlie the observed changes in TJ composition and barrier function.

5.6 Summary

- RAF/MEK/ERK activity alters MDCKII epithelial barrier properties; ΔCRAF:ER activation causes a transient increase in TER, followed by decreased readings at later time points. Paracellular leak pathway permeability is also increased. This coincides with complex changes in TJ composition.

- RAF/MEK/ERK activity drives the depletion of claudin-2 protein in a cell-autonomous manner.

- *CLDN2* mRNA levels are downregulated, but the existing claudin-2 protein pool is turned over by normal rates of internalisation from the cell surface and degradation in the lysosome.

- Claudin-1 and -4 are redistributed from the lateral membrane to the apical junction, which may be a direct result of claudin-2 depletion.

- Claudin-1 and -4 also accumulate in cytoplasmic compartments, independently of occludin and ZO-1.

- The junctional accumulation of claudin-1 and -4 cannot be fully accounted for by changes in their total levels, increased protein stability or apparent changes in endocytic trafficking rates.

- MDCKII TJs are regulated by a surprisingly diverse array of claudin-specific regulatory mechanisms that act in a coordinated manner to determine epithelial permeability properties.

Chapter 6: Discussion

How are RAF/MEK/ERK-mediated changes in barrier function regulated on different timescales?

MDCKII paracellular permeability appears to be regulated by RAF/MEK/ERK signalling in a manner dependent on signal duration. Activation of the RAF/MEK/ERK pathway, either through $BRAF^{V600E}$ expression or ΔCRAF:ER activation, caused a transient increase in TER after approximately 24 hours of signalling, followed by a subsequent decrease at later time points. This is despite the sustained repression of claudin-2 expression, and maintained expression of other TJ components after peak TER levels were reached. These observations are consistent with previous studies involving the activation of ΔCRAF:ER in MDCKII cells (Hansen et al., 2000). Therefore, RAF/MEK/ERK activation appears to generate an early "tightening" of the epithelia, while sustained activation is associated with the loss of barrier function.

The observed early increase in TER is consistent with claudin-2 loss-of-function studies (Hou et al., 2006; Ikari et al., 2011a). The increased junctional incorporation of claudin-1 and -4 may also play a role in the RAF-mediated increase in TER, as they each have barrier-promoting roles (Ikari et al., 2012b; Inai et al., 1999). Therefore, the combined effects of changes in TJ claudin composition are likely to underlie the initial TER increase. As the subsequent decrease in TER does not appear to be due to a reversal in claudin phenotype, alternative mechanisms are likely to be responsible. Sustained activation of the RAF/MEK/ERK pathway is associated with complete disassembly of cell-cell junctions and the complete loss of epithelial barrier function (Chen et al., 2000). At these later time points, gross morphological changes are evident, with cells losing epithelial characteristics and gaining mesenchymal traits. Therefore, it is likely that later decreases in TER are as a result of increased cell movement and the loss of cell-cell contacts required for trans-interactions of TJ components and the formation of a functional paracellular seal. This loss of cell-cell contact may cause the observed internalisation of TJ components and their sequestration in cytoplasm following complete transformation (Chen et al., 2000). More detailed analysis of epithelial permeability with tracers of different molecular weights would be required to determine if this later loss of TER is consistent with an increase in size-selective leak pathway permeability or a more general loss of barrier function due monolayer disruption by cell detachment.

It is currently unclear how these distinct effects of RAF/MEK/ERK signalling are mediated on different timescales. One potential mechanism is the delayed activation of the JNK pathway, which occurs 24 – 48 hours after RAF:ER activation as a result of ERK-mediated secretion of heparin-binding EGF (hbEGF), which acts in an autocrine

fashion (Pritchard et al., 1995). Of note, JNK interacts with Cdc42, which is required for TJ formation and development in airway epithelia (Tanos et al., 2015). Conversely, constitutively active $Cdc42^{V12}$ disrupts the barrier function of confluent MDCKII monolayers, causing a decrease in TER and increase in paracellular flux to large uncharged solutes (Bruewer et al., 2004). Furthermore, HGF leads to TJ disassembly by activating Cdc42 in an ERK-dependent manner (Togawa et al., 2011), linking sustained RAF/MEK/ERK signalling to more wide-ranging effects on the cytoskeleton and TJ disassembly.

What are the biological consequences of RAF/MEK/ERK-mediated TJ remodelling?

As RAF/MEK/ERK pathway activity positively correlates with the degree of epithelial sealing along the renal nephron, the decreased paracellular permeability induced at early time points may reflect a physiologically relevant mechanism for regulating ionic homeostasis in the kidney. Furthermore, relative changes in claudin expression may be involved in renal regeneration and repair. Renal tubules are frequently exposed to hyperosmotic conditions, heavy metals and drugs that damage the epithelium. Injured cells are eliminated from the monolayer, but cell-cell contact must be maintained, or rapidly restored, to maintain a functional barrier. In a similar fashion to specific activation of the RAF/MEK/ERK pathway, hyperosmotic concentrations of NaCl, mannitol or urea each cause the depletion of claudin-2 in MDCKII cells, which increases migratory capacity in an MMP9-dependent manner (Ikari et al., 2011a). Therefore, the rapid downregulation of claudin-2 expression may facilitate renal tubule repair by promoting the migration of adjacent cells into damaged areas.

Subsequent studies have established that hyperosmotic conditions can elicit a delayed upregulation of claudin-4 expression and increase the junctional levels of claudin-1 and -3 (Ikari et al., 2012b). Functionally, this results in increased TER and decreases the migration rate of MDCKII cells (Ikari et al., 2012b). Therefore, hyperosmotic stress appears to generate a biphasic response; initial claudin-2 downregulation serves to promote cell migration and epithelial repair, whereas a delayed increase in cell-cell contact decreases cell migration in an attempt to maintain the integrity of the epithelial barrier.

Although a specific requirement for RAF/MEK/ERK signalling in the hyperosmolarity response has not been demonstrated, EGFR signalling plays a key role in mediating renal epithelial repair; *waved-2* mice, which harbour an EGFR point mutation that reduces RTK activity by >90%, exhibit reduced tissue repair in response to acute

nephrotoxic injury (Wang et al., 2003). EGF is present in high concentrations in the urine, while EGFR expression is confined to the basolateral membrane of epithelial cells in the distal nephron, ureter and bladder (Harris, 1991). Therefore, ligand and receptor are normally segregated by an intact TJ. Additionally, heparin-binding EGF-like growth factor, HB-EGF, is expressed as a membrane-bound precursor, proHB-EGF, which is activated by proteolytic cleavage induced by immune cells in damaged tissues to yield a potent soluble mitogen, sHB-EGF (Singh et al., 2004). Therefore, epithelial damage increases activation of basolateral EGFR through at least two processes: i) increased access of EGF in the urine to basolateral receptors and ii) increased tissue concentrations of sHB-EGF.

The results presented in chapters 3 and 5 indicate that specific activation of the RAF/MEK/ERK pathway can recapitulate many aspects of EGF-mediated changes in TJ composition, with particular respect to claudin expression levels and distribution. Therefore, the EGFR/RAF/MEK/ERK signalling axis may play an important role in mediating the renal tissue damage response by coordinating a complex claudin-based program, which in turn mediates changes in cell migration and barrier function that serve to maintain epithelial integrity. Although ERK was phosphorylated under hyperosmotic conditions, the decrease in claudin-2 protein was not blocked by a MEK inhibitor, suggesting that additional regulatory mechanisms are also involved (Ikari et al., 2011a). Further studies will be required to establish if an EGFR/RAF/MEK/ERK signalling axis mediates the cellular repair in response to other types of renal damage.

Furthermore, in a similar manner to later effects of $BRAF^{V600E}$ expression and ΔCRAF:ER activation, chronic administration of EGF leads to MDCKII dedifferentiation, TJ disassembly and the complete loss of TER (Singh and Harris, 2004; Singh et al., 2004; Singh et al., 2007). Epithelial dedifferentiation is associated with neoplastic transformation, but is also recognised as a necessary step in regeneration following epithelial injury (Singh et al., 2007). Therefore, the more dramatic changes in cell morphology observed at later time points may represent a more rigorous tissue damage response to severe epithelial damage. This is pertinent as tumours are frequently regarded as wounds that fail to heal (Flier et al., 1986). Gene expression data from tissue microarrays have been used to compare gene expression changes in models of renal regeneration and repair (RRR) and renal cell carcinoma (RCC) (Riss et al., 2006). The majority (77%) of genes expressed in RRR and RCC tissues were concordantly regulated, indicating there is an extensive overlap of molecular features and regulatory mechanisms between these two processes. Another study detected increased expression of claudin-1, -3 and -7 and downregulation of claudin-2, in a

model of murine renal ischemia (Kieran et al., 2003). Therefore, there appear to be striking similarities in the claudin response involved in tissue repair, renal carcinoma and some aspects of RAF-driven TJ remodelling. Claudin-based alterations in epithelial permeability and integrity, as well as cell migration, which are normally engaged to induce renal repair, may be co-opted during tumourigenesis to permit uncontrolled growth and invasion.

What are the unique contributions of each TJ protein to the epithelial barrier?

Specific activation of the RAF/MEK/ERK pathway leads to complex changes in TJ composition through the simultaneous yet differential regulation of individual claudin species. Both the downregulation of claudin-2, and the increased junctional expression of claudin-1 or -4, are each independently sufficient to drive the observed increase in TER, making the exact contribution of each species difficult to determine. This could potentially be addressed by studying the effects of RAF/MEK/ERK activation in MDCKI cells, which lack endogenous claudin-2 expression. Although this approach has been used to distinguish biological effects that are dependent on the loss of claudin-2, MDCKI and MDCKII cells are likely to have diverged and have additional differences in addition to claudin-2 expression. For example, a related high-resistance MDCK C7 strain expresses lower levels of claudin-2 and -7, but increased levels of claudin-4 compared to the low-resistance MDCKII strain (Van Itallie et al., 2008). Targeted deletion using TALENs (Tokuda and Furuse, 2015) or Cas9/CRISPR could be used to generate isogenic MDCKII cell lines that differ only in their expression levels of claudin-2. Alternatively, the re-expression of claudin-2 from an exogenous promoter would reveal which aspects of barrier change, for example, the increase in TER or redistribution of claudin-1/-4, could be reversed or blocked through the restoration of claudin-2 protein levels.

The RAF-mediated downregulation of claudin-2 was effectively blocked by the co-treatment with small molecule inhibitors of either MEK or RSK kinases (Doehn et al., 2009). In contrast, the concurrent upregulation of claudin-4 and -7 are independent of RSK function (Doehn et al., 2009). Therefore, the role of claudin-2 downregulation could potentially be addressed by combining the ΔCRAF:ER/4HT approach with specific RSK inhibitors. The activation of ERK, but not RSK, is sufficient to execute the loss of polarity, downstream activation of RSK is required for the weakening of cell to cell contact and increased cellular migration (Čáslavský et al., 2010). Therefore, temporal differences in activation of ERK and RSK could potentially contribute to the dynamic changes in epithelial permeability on different timescales.

How are claudin-claudin interactions dynamically regulated?
Claudin-claudin interactions

The redistribution of claudin-1 and -4 does not represent regulation of the TJ *en masse*, as ZO-1 and occludin do not exhibit the same cytoplasmic staining pattern as claudin-1 and -4. The extensive colocalisation of claudin-1 and -4 along the lateral membrane, at the apical junction and in common cytoplasmic compartments following RAF/MEK/ERK pathway activation, suggests that they may interact at the molecular level. Although claudin-1 and -4 cannot interact in trans (Daugherty et al., 2007), they are thought to interact heteromerically in cis (Koval, 2013). The extent to which claudin-2 can interact in cis with claudin-1 or –4 is currently unclear; reported homo- and heteromeric interactions of claudins expressed in MDCKII cells are summarised in Table 6.1. When two transfected fibroblast populations are co-cultured, claudin 1- or claudin 2-based strands do not laterally associate with each other (Furuse et al., 1999), and are therefore considered to be heterotypically incompatible (Daugherty et al., 2007).

Claudin	1	2	3	4	7
1	Y	(ND)	Y	Y	Y
2		Y	N	(ND)	N
3			Y/N*	Y	N*
4				N*	N*
7					Y

Table 6.1: A summary of homo- and heteromeric claudin interactions. Claudins can interact with each other in a species-specific manner. Cis-interactions have been reported using FRET or Y2H studies. (Y) strong interaction, (N) no interaction, (N*) no interaction by FRET, (Y/N*) interaction by FRET, no interaction by Y2H, (ND) not determined. Table adapted from Koval et al (2013).

Claudin incompatibility may result in the spatial segregation of claudin-2 and claudin-1/-4 under normal conditions. This could potentially be mediated through mutually exclusive protein-protein interactions, for example with ZO-1 or occludin, which are largely confined to the apical junction. Claudin displacement due to incompatibility has been demonstrated where exogenous claudin-8 expression displaces claudin-2 from MDCKII tight junctions (Angelow et al., 2007).

The overall level and distribution of claudin-1, -3, -4 and -7 were not affected in initial claudin-2 knockdown experiments (Ikari et al., 2011b). However, recent studies involving the TALEN-mediated knockout of claudin-2 in MDCKII cells revealed a

subsequent increase in levels of claudin-1, -3, -4 and -7 specifically at the level of the TJ (Tokuda and Furuse, 2015). In contrast, the distribution of ZO-1, occludin, F-actin and myosin was similar between control and claudin-2 knockout cells (Tokuda and Furuse, 2015). Furthermore, the junctional accumulation of these claudins was reversed upon the re-expression of FLAG-claudin-2 (Tokuda and Furuse, 2015). This study suggests that the observed increase in junctional claudin-1 and -4 following ΔCRAF:ER activation is a direct result of claudin-2 depletion. However, the apparent upregulation of claudin-4 expression levels suggests that additional regulatory mechanisms, in addition to claudin-2 suppression, are involved in the ΔCRAF:ER-mediated response. Re-expression of claudin-2 using an exogenous constitutive promoter, similar to the FLAG-claudin-2 construct used in the TALEN claudin-2 knockout study (Tokuda and Furuse, 2015), would determine if claudin-2 depletion is necessary for the junctional accumulation of claudin-1 and -4 following ΔCRAF:ER activation. This claudin-2 expression would not be subject to endogenous transcriptional regulation, so these experiments would also provide further insight into whether RAF/MEK/ERK activity can influence the distribution or trafficking of claudin-2 at the post-transcriptional level.

Claudins that dissociate from ZO-1 migrate diffusely into the lateral membrane (Lee et al., 2008). Claudin-16 normally localises discretely at the TJ with ZO-1, but C-terminal ZO-binding sequence mutants widely distribute along the lateral membrane (Ikari et al., 2004). Furthermore, the overexpression of a claudin-1-myc fusion protein, but not non-epitope tagged claudin-1, induces the aberrant formation of TJ strands along the lateral surface of MDCK cells (McCarthy 2000). Of note, there is no ZO-1 associated with these strands (McCarthy 2000). Therefore, abrogation of the interaction between claudin-1 and ZO-1 through the addition of a C-terminal epitope causes claudin-1 to accumulate along the lateral membrane (McCarthy 2000). RAF/MEK/ERK-mediated claudin-2 depletion could potentially permit the incorporation of claudin-1/-4 into junctional strands through the liberation of previously occupied TJ-associated ZO proteins (Figure 6.1B). Alternatively, differential post-translational modification of C-terminal claudin YV motifs, similar to phosphorylation of claudin-4 caused by EphA2 activity (Tanaka et al., 2005), may influence junctional interactions. Future studies will be required to establish if RAF/MEK/ERK activity dynamically regulates claudin-ZO protein-protein interactions or the phosphorylation state of these TJ proteins.

The junctional claudin repertoire was altered both by $BRAF^{V600E}$ expression and ΔCRAF:ER activation, while ZO-1 and occludin were largely retained at TJ. Claudins bind to ZO protein PDZ domains through a conserved C-terminal YV motif (Itoh et al.,

1999). By contrast, occludin binds to the U5-GUK domain of ZO-1 (Raleigh et al., 2011; Schmidt et al., 2004). Occludin and ZO-1 appear to respond in a similar manner following activation of the RAF/MEK/ERK pathway. Both markers are retained at the apical junction, with a continuous staining pattern encircling each cell. In addition, both occludin and ZO-1 exhibit increased cytoplasmic staining, in a diffuse pattern that is distinct from the discrete punctate compartments that contain both claudin-1 and -4. This raises the possibility that occludin and ZO-1 are regulated together as a complex, while its association with individual claudin species may vary over time. Initially, claudin-2 may bind to ZO-1 via its PDZ domain, generating an occludin:ZO-1:claudin-2 complex (Figure 6.1A). Following RAF/MEK/ERK pathway activation and the depletion of claudin-2, claudin-1 and -4 may bind the ZO-1 PDZ domain, leading to their junctional accumulation (Figure 6.1B). At later time points, further post-translational modification of claudin-1/-4, occludin or ZO-1 may lead to the dissociation of occludin:ZO-1 from claudin-1/-4, leading to distinct distribution of these proteins in the cytoplasm (Figure 6.1C). Coimmunoprecipitation assays involving ZO-1 would reveal any dynamic changes in binding partners over time following stimulation of the RAF/MEK/ERK pathway.

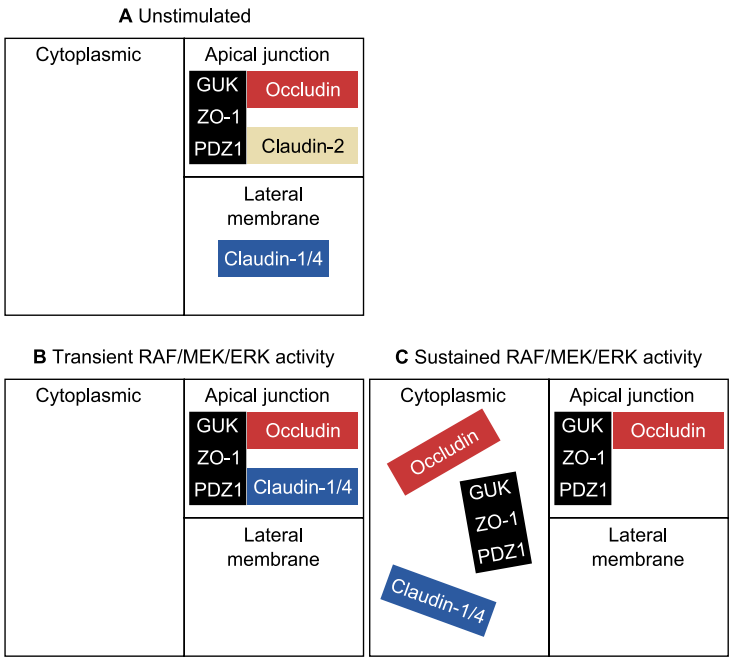

Figure 6.1: A putative model of dynamic changes in protein-protein interactions following RAF/MEK/ERK pathway activation. Under unstimulated conditions, ZO-1, occludin and claudin-2 are all confined to the apical junction, while claudin-1 and -4 are predominantly associated with the lateral membrane. Following RAF/MEK/ERK pathway activation, claudin-2 protein levels are depleted and claudin-1 and -4 accumulate with ZO-1 and occludin at the apical junction. Claudin-1 and -4 are also present in discrete cytoplasmic compartments, independently of ZO-1 and occludin. This may reflect a relatively late disassembly of the junctional complex, potentially due to post-translational modification of constituent proteins that specifically influence interactions between the C-terminal YV claudin motif and the PDZ1 domain of ZO-1.

Subdomain organisation of the tight junction

Lateral, rather than junctional, claudin-1 has been observed in various MDCK strains (Amasheh et al., 2002; Dukes et al., 2011b) and has been associated with adhesion and interaction with cell surface receptors (Günzel and Yu, 2013). This lateral claudin pool may also act as a reserve that allows cells to rapidly alter TJ properties in response to diverse stimuli. However, reports suggest that subapical claudins can form functional TJ stands that contribute to epithelial barrier function. In the inner ear, claudins partition into claudin-14 and claudin-9/-6 subdomains, which are distinguishable as areas with distinct strand morphology (Nunes et al., 2006). Lateral claudin-1/-4 may therefore contribute to TJ permeability under normal conditions. Importantly, lateral claudins have been observed *in vivo* (Rahner et al., 2001) suggesting that this is not an artefact of cultured cell lines. The altered claudin-1/-4 distribution could potentially be accompanied by altered TJ strand architecture, and in turn, permeability, but further work will be required to elucidate any fine changes in TJ fibril architecture that are mediated by RAF/MEK/ERK activity.

Post-translational modification of TJ proteins

The C-terminal tail of claudin-2 is multiply phosphorylated on serine, threonine and tyrosine resides (Van Itallie et al., 2012b). S208 phosphorylation promotes the retention of claudin-2 at areas of cell-cell contact. By contrast, phosphomimetic S208E mutants are targeted less efficiently to the cell surface and accumulate in lysosomal compartments. It appears that S208 phosphorylation may promote retention at, or recycling back to, the plasma membrane, while dephosphorylation is associated with lysosomal trafficking. The amino acids surrounding S208 meet the requirements of a consensus PKCι site, suggesting that PKCι may directly phosphorylate claudin-2 to promote its localisation at the TJ through Rab14-directed trafficking (Lu et al., 2015). These studies directly link claudin-2 phosphorylation and altered trafficking rates. The data presented here indicate that specific activation of the RAF/MEK/ERK pathway causes claudin-2 depletion without affecting endocytic trafficking. As previously discussed, this is in contrast with a reported MEK-dependent increase in claudin-2 internalisation and degradation in response to EGF treatment (Ikari et al., 2011c). Further studies may reveal that differential regulation of claudin-2 phosphorylation and Rab14/PKCι interactions underlie differences between EGFR activation and specific activation of the RAF/MEK/ERK pathway.

Disease-causing WNK mutants have been shown to bind and phosphorylate claudins -1, -2, -3, -4 and -7 on both serine (Tatum et al., 2007) and threonine residues (Ohta et al., 2006). Although hyperphosphorylation of claudin C-terminal domains mediated by

WNK overexpression or mutation is associated with increased paracellular Cl^- permeability, the specific residues and direct consequences of phosphorylation are unknown (Kahle et al., 2004; Ohta et al., 2006; Tatum et al., 2007; Yamauchi et al., 2004). EphA2 phosphorylates claudin-4 in the conserved YV motif that is required for PDZ domain-mediated binding of ZO-1, thereby reducing the junctional incorporation of claudin-4 (Tanaka et al., 2005). It is currently unclear how widely YV motif phosphorylation is conserved as a regulatory mechanism between different claudin species. However, this raises the possibility that claudin-specific kinases and phosphatases mediate differential claudin YV phosphorylation to regulate their interaction with ZO-1 at the apical junction.

Unfortunately, there are few commercially available phosphosite-specific antibodies that target claudins. However, recent studies have utilised phosphate-affinity SDS-PAGE with an acrylamide-pendant "Phos-tag™" reagent (Van Itallie et al., 2012b). Covalent incorporation of this ligand generates a gel matrix, which specifically retards the migration of phosphorylated proteins during electrophoresis (Kinoshita-Kikuta et al., 2007). This approach allows the identification of differentially phosphorylated claudin species under different experimental conditions. Specific phosphorylated residues can be identified by combining Phos-tag™ SDS-PAGE with anti-phosphotyrosine, -phosphoserine or -phosphothreonine antibodies or site-directed mutagenesis. Studies like these may reveal that differential regulation of claudin-1 and/or claudin-4 phosphorylation accompanies their translocation downstream of RAF/MEK/ERK activation.

How are differential responses to common stimuli achieved in specific tissues?

Regulation of TJs and paracellular permeability is essential in various body organs in addition to the kidneys. For example, a functional seal must be maintained in the intestine to provide a barrier against luminal antigens (Dhawan et al., 2011). Defective intestinal epithelial barriers are considered to be an important contributor to intestinal inflammation, inflammatory bowel disease (IBD) and cancer. Therefore, the TJ remodelling reported in this thesis may have relevance to diseases of other tissues, especially given the particularly high incidence of colorectal tumours that exhibit constitutive activation of the RAF/MEK/ERK pathway. For example, 35 – 45% of colorectal cancers have mutations to KRAS (Britten, 2013), up to 20% have mutations to EGFR (Oh et al., 2011) and 5 – 15 % have BRAF mutations (Britten, 2013). However, individual TJ components appear to be differentially regulated by RAF/MEK/ERK signalling in a striking tissue-dependent manner.

While RAF/MEK/ERK activity leads to the loss of claudin-2 in the kidney, it promotes its expression in colorectal tissues (Inai et al., 2013). Furthermore, claudin-2 expression is significantly increased in colorectal cancer and correlates with cancer progression (Dhawan et al., 2011). The resulting increase in paracellular permeability is postulated to increase basolateral access of luminal carcinogens and growth factors to promote tumourigenesis (Dhawan et al., 2011). However, the different biological mechanisms that underlie the tissue-specific regulation of claudin-2 are currently unclear, but the exact repertoire of transcription factors that are expressed is likely to be a contributing factor. Claudin-2 expression is upregulated by transcription factors including Cdx1, Cdx2, HNF-1α and GATA-4 in intestinal cells (Sakaguchi et al., 2002). However, Cdx1/2 expression is confined to the intestine, while HNF-1α is required for claudin-2 expression in liver and intestine, but not in the kidneys (Sakaguchi et al., 2002). Claudin-2 expression is increased by an EGFR/MEK/ERK/c-Fos pathway in lung adenocarcinoma cells (Ikari et al., 2012a). In MDCKII cells, the EGF-mediated downregulation of claudin-2 and upregulation of claudin-4 are both sensitive to inhibition of STAT3 (García-Hernández et al., 2015) and claudin-4 upregulation is also mediated by the transcription factor Sp1 (Ikari et al., 2009), although other transcription factors may be involved. These studies indicate that RAF/MEK/ERK activity regulates claudin-2 expression in a manner dependent on tissue-specific transcription factors. Further work will be required to determine the tissue-specific effects of RAF/MEK/ERK activity on the expression, and subcellular distribution, of other claudin species.

Differential claudin expression has been reported in various cancers (Kwon, 2013). For example, a claudin-low subtype has been identified as particularly aggressive form of triple negative breast cancer, characterised by low expression of luminal markers and high expression of EMT markers, immune response genes and cancer stem cell-like features (Prat et al., 2010). In addition, increased claudin-4 expression has been identified in pancreatic and ovarian cancer (Neesse et al., 2012; Nichols et al., 2004), with reports suggesting it can be either a positive or negative prognostic factor; claudin-4 expression inhibits primary tumour growth (Lin et al., 2013; Shang et al., 2012; Shang et al., 2014) but may promote growth at metastatic sites (Jiwa et al., 2014). Claudin-4 overexpression is therefore a candidate diagnostic biomarker and also a potential target for delivering optical tracers or anticancer drugs conjugated to molecules that specifically bind to claudin-4 (Neesse et al., 2012).

Concluding remarks

In conclusion, regulation of epithelial permeability through TJ remodelling is being increasingly recognised as an important process, in both physiological settings and pathological conditions like inflammatory disease and cancer. The work in this thesis demonstrates that RAF/MEK/ERK activity causes TJ remodelling through surprisingly diverse mechanisms, which has important consequences for understanding how epithelial permeability is dynamically regulated during tissue repair and in tumourigenesis. Future work will be required to address the following key biological questions:

- How do claudins and other proteins interact at the tight junction?
- What are the mechanisms underlying RAF/MEK/ERK-mediated claudin redistribution?
- What are the biological consequences of RAF/MEK/ERK-mediated tight junction remodelling during tissue repair and tumourigenesis?
- How are components of the tight junction dynamically regulated to alter epithelial permeability during tumourigenesis in different tissues?
- Can tissue-dependent claudin signatures be identified that have useful diagnostic, prognostic or therapeutic value?

References

Alexandre, M. D., Lu, Q. and Chen, Y.-H. (2005). Overexpression of claudin-7 decreases the paracellular Cl- conductance and increases the paracellular Na+ conductance in LLC-PK1 cells. *J. Cell Sci.* **118**, 2683–2693.

Amasheh, S., Meiri, N., Gitter, A. H., Schoneberg, T., Mankertz, J., Schulzke, J. D. and Fromm, M. (2002). Claudin-2 expression induces cation-selective channels in tight junctions of epithelial cells. *J. Cell Sci.* **115**, 4969–4976.

Anderson, R. D., Haskell, R. E., Xia, H., Roessler, B. J. and Davidson, B. L. (2000). A simple method for the rapid generation of recombinant adenovirus vectors. *Gene Ther.* **7**, 1034–1038.

Angelow, S., Schneeberger, E. E. and Yu, A. S. L. (2007). Claudin-8 expression in renal epithelial cells augments the paracellular barrier by replacing endogenous claudin-2. *J. Membr. Biol.* **215**, 147–159.

Bagnat, M., Cheung, I. D., Mostov, K. E. and Stainier, D. Y. R. (2007). Genetic control of single lumen formation in the zebrafish gut. *Nat. Cell Biol.* **9**, 954–960.

Bain, J., Plater, L., Elliott, M., Shpiro, N., Hastie, C. J., McLauchlan, H., Klevernic, I., Arthur, J. S. C., Alessi, D. R. and Cohen, P. (2007). The selectivity of protein kinase inhibitors: a further update. *Biochem. J.* **408**, 297–315.

Balda, M. S. and Matter, K. (2008). Tight junctions at a glance. *J. Cell Sci.* **121**, 3677–3682.

Balda, M. S. and Matter, K. (2009). Tight junctions and the regulation of gene expression. *Biochim. Biophys. Acta* **1788**, 761–767.

Balda, M. S., Whitney, J. A., Flores, C., González, S., Cereijido, M. and Matter, K. (1996). Functional dissociation of paracellular permeability and transepithelial electrical resistance and disruption of the apical-basolateral intramembrane diffusion barrier by expression of a mutant tight junction membrane protein. *J. Cell Biol.* **134**, 1031–1049.

Balda, M. S., Garrett, M. D. and Matter, K. (2003). The ZO-1-associated Y-box factor ZONAB regulates epithelial cell proliferation and cell density. *J. Cell Biol.* **160**, 423–432.

Balkovetz, D. F. (2009). Tight junction claudins and the kidney in sickness and in health. *Biochim. Biophys. Acta* **1788**, 858–863.

Basuroy, S., Seth, A., Elias, B., Naren, A. P. and Rao, R. (2006). MAPK interacts with occludin and mediates EGF-induced prevention of tight junction disruption by hydrogen peroxide. *Biochem. J.* **393**, 69–77.

Bauer, H., Zweimueller-Mayer, J., Steinbacher, P., Lametschwandtner, A. and Bauer, H. C. (2010). The dual role of zonula occludens (ZO) proteins. *J. Biomed. Biotechnol.* **2010**, 1–11.

Beck, T. W., Huleihel, M., Gunnell, M., Bonner, T. I. and Rapp, U. R. (1987). The complete coding sequence of the human A-raf-1 oncogene and transforming activity of a human A-raf carrying retrovirus. *Nucleic Acids Res.* **15**, 595–609.

Benezra, M., Greenberg, R. S. and Masur, S. K. (2007). Localization of ZO-1 in the Nucleolus of Corneal Fibroblasts. *Invest. Ophthalmol. Vis. Sci.* **48**, 2043–2049.

Bergeron, S., Lemieux, E., Durand, V., Cagnol, S., Carrier, J. C., Lussier, J. G., Boucher, M.-J. and Rivard, N. (2010). The serine protease inhibitor serpinE2 is a novel target of ERK signaling involved in human colorectal tumorigenesis. *Mol. Cancer* **9**, 1–15.

Bhat, A. A., Sharma, A., Pope, J., Krishnan, M., Washington, M. K., Singh, A. B. and Dhawan, P. (2012). Caudal homeobox protein Cdx-2 cooperates with Wnt pathway to regulate claudin-1 expression in colon cancer cells. *PLoS One* **7**, 1–14.

Bhuin, T. and Roy, J. K. (2014). Rab proteins: The key regulators of intracellular vesicle transport. *Exp. Cell Res.* **8**, 1–19.

Bollig, A., Xu, L., Thakur, A., Wu, J., Kuo, T. H. and Liao, J. D. (2007). Regulation of intracellular calcium release and PP1alpha in a mechanism for 4-hydroxytamoxifen-induced cytotoxicity. *Mol. Cell. Biochem.* **305**, 45–54.

Bonner, T. I., Kerby, S. B., Sutrave, P., Gunnell, M. A., Mark, G. and Rapp, U. R. (1985). Structure and biological activity of human homologs of the raf/mil oncogene. *Mol. Cell. Biol.* **5**, 1400–1407.

Bosch, E., Cherwinski, H., Peterson, D. and McMahon, M. (1997). Mutations of critical amino acids affect the biological and biochemical properties of oncogenic A-Raf and Raf-1. *Oncogene* **15**, 1021–1033.

Boylan, K. L. M., Misemer, B., DeRycke, M. S., Andersen, J. D., Harrington, K. M., Kalloger, S. E., Gilks, C. B., Pambuccian, S. E. and Skubitz, A. P. N. (2011). Claudin 4 is differentially expressed between ovarian cancer subtypes and plays a role in spheroid formation. *Int. J. Mol. Sci.* **12**, 1334–1358.

Britten, C. D. (2013). PI3K and MEK inhibitor combinations: examining the evidence in selected tumor types. *Cancer Chemother. Pharmacol.* **71**, 1395–1409.

Bruewer, M., Hopkins, A. M., Hobert, M. E., Nusrat, A. and Madara, J. L. (2004). RhoA, Rac1, and Cdc42 exert distinct effects on epithelial barrier via selective structural and biochemical modulation of junctional proteins and F-actin. *Am. J. Physiol. Cell Physiol.* **287**, 327–335.

Bruewer, M., Utech, M., Ivanov, A. I., Hopkins, A. M., Parkos, C. A. and Nusrat, A. (2005). Interferon-gamma induces internalization of epithelial tight junction proteins via a macropinocytosis-like process. *FASEB J.* **19**, 923–933.

Brummer, T., Martin, P., Herzog, S., Misawa, Y., Daly, R. J. and Reth, M. (2006). Functional analysis of the regulatory requirements of B-Raf and the B-Raf(V600E) oncoprotein. *Oncogene* **25**, 6262–6276.

Bryant, D. M. and Stow, J. L. (2004). The ins and outs of E-cadherin trafficking. *Trends Cell Biol.* **14**, 427–434.

Butch, E. R. and Guan, K. L. (1996). Characterization of ERK1 activation site mutants and the effect on recognition by MEK1 and MEK2. *J. Biol. Chem.* **271**, 4230–4235.

Cagnol, S. and Rivard, N. (2012). Oncogenic KRAS and BRAF activation of the MEK/ERK signaling pathway promotes expression of dual-specificity phosphatase 4 (DUSP4/MKP2) resulting in nuclear ERK1/2 inhibition. *Oncogene* **32**, 564–576.

Cantwell-Dorris, E. R., O'Leary, J. J. and Sheils, O. M. (2011). BRAFV600E: Implications for Carcinogenesis and Molecular Therapy. *Mol. Cancer Ther.* **10**, 385–394.

Carrozzino, F., Soulie, P., Huber, D., Mensi, N., Orci, L., Cano, A., Feraille, E. and Montesano, R. (2005). Inducible expression of Snail selectively increases paracellular ion permeability and differentially modulates tight junction proteins. *Am. J. Physiol. Cell Physiol.* **289**, 1002–1014.

Čáslavský, J., Klímová, Z. and Vomastek, T. (2010). ERK and RSK regulate distinct steps of a cellular program that induces transition from multicellular epithelium to single cell. *Cell. Signal.* **25**, 2743–2751.

Cassio, D. (2013). Long term culture of MDCK strains alters chromosome content. *BMC Res. Notes* **6**, 1–12.

Caunt, C. J. and Keyse, S. M. (2013). Dual-specificity MAP kinase phosphatases (MKPs): shaping the outcome of MAP kinase signalling. *FEBS J.* **280**, 489–504.

Cereijido, M., González-Mariscal, L. and Borboa, L. (1983). Occluding junctions and paracellular pathways studied in monolayers of MDCK cells. *J. Exp. Biol.* **106**, 205–215.

Cereijido, M., González-Mariscal, L. and Contreras, G. (1989). Tight junction: barrier between higher organisms and environment. *News Physiol. Sci.* **4**, 72–75.

Chalmers, A. D. and Whitley, P. (2012). Continuous endocytic recycling of tight junction proteins : how and why ? *Essays Biochem.* **53**, 41–54.

Chang, T. L., Ito, K., Ko, T. K., Liu, Q., Salto-Tellez, M., Yeoh, K. G., Fukamachi, H. and Ito, Y. (2010). Claudin-1 Has Tumor Suppressive Activity and Is a Direct Target of RUNX3 in Gastric Epithelial Cells. *Gastroenterology* **138**, 255–265.

Chen, Y. H., Lu, Q., Schneeberger, E. E. and Goodenough, D. A. (2000). Restoration of tight junction structure and barrier function by down-regulation of the mitogen-activated protein kinase pathway in ras-transformed Madin-Darby canine kidney cells. *Mol. Biol. Cell* **11**, 849–862.

Chen, J., Xiao, L., Rao, J. N., Zou, T., Liu, L., Bellavance, E., Gorospe, M. and Wang, J.-Y. (2008). JunD Represses Transcription and Translation of the Tight Junction Protein Zona Occludens-1 Modulating Intestinal Epithelial Barrier Function. *Mol. Biol. Cell2* **19**, 3701–3712.

Claude, P. and Goodenough, D. A. (1973). Fracture faces of zonulae occludentes from “tight” and “leaky” epithelia. *J. Cell Biol.* **58**, 390–400.

Cohen, P. and Tcherpakov, M. (2010). Will the ubiquitin system furnish as many drug targets as protein kinases? *Cell* **143**, 686–693.

Cohen, C. D., Klingenhoff, A., Boucherot, A., Nitsche, A., Henger, A., Brunner, B., Schmid, H., Merkle, M., Saleem, M. A., Koller, K.-P., et al. (2006). Comparative promoter analysis allows de novo identification of specialized cell junction-associated proteins. *Proc. Natl. Acad. Sci. U. S. A.* **103**, 5682–5687.

Conibear, E. and Davis, N. G. (2010). Palmitoylation and depalmitoylation dynamics at a glance. *J. Cell Sci.* **123**, 4007–4010.

Corallino, S., Malabarba, M. G., Zobel, M., Di Fiore, P. P. and Scita, G. (2015). Epithelial-to-Mesenchymal Plasticity Harnesses Endocytic Circuitries. *Front. Oncol.* **5**, 1–15.

Coyne, C. B. and Bergelson, J. M. (2005). CAR: a virus receptor within the tight junction. *Adv. Drug Deliv. Rev.* **57**, 869–882.

Darido, C., Buchert, M., Pannequin, J., Bastide, P., Zalzali, H., Mantamadiotis, T., Bourgaux, J. F., Garambois, V., Jay, P., Blache, P., et al. (2008). Defective claudin-7 regulation by Tcf-4 and Sox-9 disrupts the polarity and increases the tumorigenicity of colorectal cancer cells. *Cancer Res.* **68**, 4258–4268.

Daugherty, B. L., Ward, C., Ritzenthaler, J. D., Smith, T. and Koval, M. (2007). Regulation of Heterotypic Claudin Compatibility. *J. Biol. Chem.* **282**, 30005–30013.

Davies, H., Bignell, G. R., Cox, C., Stephens, P., Edkins, S., Clegg, S., Teague, J., Woffendin, H., Garnett, M. J., Bottomley, W., et al. (2002). Mutations of the BRAF gene in human cancer. *Nature* **417**, 949–954.

De Matteis, M. A. and Luini, A. (2008). Exiting the Golgi complex. *Nat. Rev. Mol. Cell Biol.* **9**, 273–284.

Desclozeaux, M., Venturato, J., Wylie, F. G., Kay, J. G., Joseph, S. R., Le, H. T. and Stow, J. L. (2008). Active Rab11 and functional recycling endosome are required for E-cadherin trafficking and lumen formation during epithelial morphogenesis. *Am. J. Physiol. Cell Physiol.* **295**, 545–556.

Dhawan, P., Ahmad, R., Chaturvedi, R., Smith, J. J., Midha, R., Mittal, M., Krishnan, M., Chen, X., Eschrich, S., Yeatman, T. J., et al. (2011). Claudin-2 Expression Increases Tumorigenicity of Colon Cancer Cells: Role of Epidermal Growth Factor Receptor Activation. *Oncogene* **30**, 3234–3247.

Dhomen, N. and Marais, R. (2007). New insight into BRAF mutations in cancer. *Curr. Opin. Genet. Dev.* **17**, 31–39.

Dietze, E. C., Caldwell, L. E., Grupin, S. L., Mancini, M. and Seewaldt, V. L. (2001). Tamoxifen but Not 4-Hydroxytamoxifen Initiates Apoptosis in p53(-) Normal Human Mammary Epithelial Cells by Inducing Mitochondrial Depolarization. *J. Biol. Chem.* **276**, 5384–5394.

Ding, L., Yuguo, Z., Tatum, R. and Chen, Y.-H. (2011). Detection of Tight Junction Barrier Function In Vivo by Biotin. *Methods Mol. Biol.* **762**, 91–100.

Ding, L., Lu, Z., Foreman, O., Tatum, R., Lu, Q., Renegar, R., Cao, J. and Chen, Y.-H. (2012). Inflammation and Disruption of the Mucosal Architecture in Claudin-7 Deficient Mice. *Gastroenterology* **142**, 305–315.

Ding, L., Lu, Z., Lu, Q. and Chen, Y.-H. (2013). The claudin family of proteins in human malignancy: a clinical perspective. *Cancer Manag. Res.* **5**, 367–375.

Doehn, U., Hauge, C., Frank, S. R., Jensen, C. J., Duda, K., Nielsen, J. V, Cohen, M. S., Johansen, J. V, Winther, B. R., Lund, L. R., et al. (2009). RSK is a principal effector of the RAS-ERK pathway for eliciting a coordinate promotile/invasive gene program and phenotype in epithelial cells. *Mol. Cell* **35**, 511–522.

Du, J., Jiang, B., Coffey, R. J. and Barnard, J. (2004). Raf and RhoA cooperate to transform intestinal epithelial cells and induce growth resistance to transforming growth factor beta. *Mol. Cancer Res.* **2**, 233–241.

Dukes, J. D., Whitley, P. and Chalmers, A. D. (2011a). The MDCK variety pack: choosing the right strain. *BMC Cell Biol.* **12**, 1–4.

Dukes, J. D., Fish, L., Richardson, J. D., Blaikley, E., Burns, S., Caunt, C. J., Chalmers, A. D. and Whitley, P. (2011b). Functional ESCRT machinery is required for constitutive recycling of claudin-1 and maintenance of polarity in vertebrate epithelial cells. *Mol. Biol. Cell* **22**, 3192–3205.

Dukes, J. D., Whitley, P. and Chalmers, A. D. (2012). The PIKfyve inhibitor YM201636 blocks the continuous recycling of the tight junction proteins claudin-1 and claudin-2 in MDCK cells. *PLoS One* **7**, 1–10.

Ehrenreiter, K., Piazzolla, D., Velamoor, V., Sobczak, I., Small, J. V., Takeda, J., Leung, T. and Baccarini, M. (2005). Raf-1 regulates Rho signaling and cell migration. *J. Cell Biol.* **168**, 955–964.

Elias, B. C., Suzuki, T., Seth, A., Giorgianni, F., Kale, G., Shan, L., Turner, J. R., Naren, A., Desiderio, D. M. and Rao, R. (2009). Phosphorylation of Tyr-398 and Tyr-402 in occludin prevents Its interaction with ZO-1 and destabilizes Its assembly at the tight junctions. *J. Biol. Chem.* **284**, 1559–1569.

Emuss, V., Garnett, M., Mason, C. and Marais, R. (2005). Mutations of C-RAF are rare in human cancer because C-RAF has a low basal kinase activity compared with B-RAF. *Cancer Res.* **65**, 9719–9726.

Escaffit, F., Boudreau, F. and Beaulieu, J. F. (2005). Differential expression of claudin-2 along the human intestine: Implication of GATA-4 in the maintenance of claudin-2 in differentiating cells. *J. Cell. Physiol.* **203**, 15–26.

Fanning, A. S., Jameson, B. J., Lynne, A., Anderson, J. M., Jesaitis, L. A. and Melvin, J. (1998). The Tight Junction Protein ZO-1 Establishes a Link between the Transmembrane Protein Occludin and the Actin Cytoskeleton The Tight Junction Protein ZO-1 Establishes a Link between the Transmembrane Protein Occludin and the Ac. *J. Biol. Chem.* **273**, 29745–29753.

Farquhar, M. G. and Palade, G. E. (1963). Junctional complexes in various epithelia. *J. Cell Biol.* **17**, 375–412.

Feil, R., Wagner, J., Metzger, D. and Chambon, P. (1997). Regulation of Cre recombinase activity by mutated estrogen receptor ligand-binding domains. *Biochem. Biophys. Res. Commun.* **237**, 752–757.

Flier, J. S., Underhill, L. H. and Dvorak, H. F. (1986). Tumors: Wounds That Do Not Heal. *N. Engl. J. Med.* **315**, 1650–1659.

Flores-Benítez, D., Ruiz-Cabrera, A., Flores-Maldonado, C., Shoshani, L., Cereijido, M. and Contreras, R. G. (2007). Control of tight junctional sealing: role of epidermal growth factor. *Am. J. Physiol. Renal Physiol.* **292**, 828–836.

Forbes, S. A., Beare, D., Gunasekaran, P., Leung, K., Bindal, N., Boutselakis, H., Ding, M., Bamford, S., Cole, C., Ward, S., et al. (2014). COSMIC: exploring the world's knowledge of somatic mutations in human cancer. *Nucleic Acids Res.* **43**, D805–D811.

Fredriksson, K., Van Itallie, C. M., Aponte, A., Gucek, M., Tietgens, A. J. and Anderson, J. M. (2015). Proteomic Analysis of Proteins Surrounding Occludin and Claudin-4 Reveals Their Proximity to Signaling and Trafficking Networks. *PLoS One* **10**, 1–35.

Fujibe, M., Chiba, H., Kojima, T., Soma, T., Wada, T., Yamashita, T. and Sawada, N. (2004). Thr203 of claudin-1, a putative phosphorylation site for MAP kinase, is required to promote the barrier function of tight junctions. *Exp. Cell Res.* **295**, 36–47.

Fuller, S. D. and Simons, K. (1986). Transferrin receptor polarity and recyling accuracy in "tight" and "leaky" strains of Madin-Darby canine kidney cells. *J. Cell Biol.* **103**, 1767–1779.

Furuse, M., Hirase, T., Itoh, M., Nagafuchi, A., Yonemura, S., Tsukita, S. and Tsukita, S. (1993). Occludin: A novel integral membrane protein localizing at tight junctions. *J. Cell Biol.* **123**, 1777–1788.

Furuse, M., Sasaki, H., Fujimoto, K. and Tsukita, S. (1998a). A single gene product, claudin-1 or -2, reconstitutes tight junction strands and recruits occludin in fibroblasts. *J. Cell Biol.* **143**, 391–401.

Furuse, M., Fujita, K., Hiiragi, T., Fujimoto, K. and Tsukita, S. (1998b). Claudin-1 and -2: novel integral membrane proteins localizing at tight junctions with no sequence similarity to occludin. *J. Cell Biol.* **141**, 1539–1550.

Furuse, M., Sasaki, H. and Tsukita, S. (1999). Manner of interaction of heterogeneous claudin species within and between tight junction strands. *J. Cell Biol.* **147**, 891–903.

Furuse, M., Furuse, K., Sasaki, H. and Tsukita, S. (2001). Conversion of zonulae occludentes from tight to leaky strand type by introducing claudin-2 into Madin-Darby canine kidney I cells. *J. Cell Biol.* **153**, 263–272.

Furuse, M., Hata, M., Furuse, K., Yoshida, Y., Haratake, A., Sugitani, Y., Noda, T., Kubo, A. and Tsukita, S. (2002). Claudin-based tight junctions are crucial for the mammalian epidermal barrier: a lesson from claudin-1-deficient mice. *J. Cell Biol.* **156**, 1099–1111.

Gálvez-Santisteban, M., Rodriguez-Fraticelli, A. E., Bryant, D. M., Vergarajauregui, S., Yasuda, T., Bañón-Rodríguez, I., Bernascone, I., Datta, A., Spivak, N., Young, K., et al. (2012). Synaptotagmin-like proteins control the formation of a single apical membrane domain in epithelial cells. *Nat. Cell Biol.* **14**, 838–849.

García-Hernández, V., Flores-Maldonado, C., Rincon-Heredia, R., Verdejo-Torres, O., Bonilla-Delgado, J., Meneses-Morales, I., Gariglio, P. and Contreras, R. G. (2015). EGF regulates claudin-2 and -4 expression through Src and STAT3 in MDCK cells. *J. Cell. Physiol.* **230**, 105–115.

Gottardi, C. J., Arpin, M., Fanning, A. S. and Louvard, D. (1996). The junction-associated protein, zonula occludens-1, localizes to the nucleus before the maturation and during the remodeling of cell-cell contacts. *Proc. Natl. Acad. Sci. U. S. A.* **93**, 10779–10784.

Green, K. J., Getsios, S., Troyanovsky, S. and Godsel, L. M. (2010). Intercellular junction assembly, dynamics, and homeostasis. *Cold Spring Harb. Perspect. Biol.* **2**, 1–22.

Greulich, H. and Erikson, R. L. (1998). An Analysis of Mek1 Signaling in Cell Proliferation and Transformation An Analysis of Mek1 Signaling in Cell Proliferation and Transformation. *J. Biol. Chem.* **273**, 13280–13288.

Guasch, R. M., Scambler, P., Jones, G. E. and Ridley, A. J. (1998). RhoE Regulates Actin Cytoskeleton Organization and Cell Migration RhoE Regulates Actin Cytoskeleton Organization and Cell Migration. *Mol. Cell. Biol.* **18**, 4761–4471.

Guillemot, L., Spadaro, D. and Citi, S. (2013). The junctional proteins cingulin and paracingulin modulate the expression of tight junction protein genes through GATA-4. *PLoS One* **8**, 1–8.

Günzel, D. and Fromm, M. (2012). Claudins and other tight junction proteins. *Compr. Physiol.* **2**, 1819–1852.

Günzel, D. and Yu, A. S. L. (2013). *Claudins and the modulation of tight junction permeability.*

Hansen, S. H., Zegers, M. M., Woodrow, M., Rodriguez-Viciana, P., Chardin, P., Mostov, K. E. and McMahon, M. (2000). Induced expression of Rnd3 is associated with transformation of polarized epithelial cells by the Raf-MEK-extracellular signal-regulated kinase pathway. *Mol. Cell. Biol.* **20**, 9364–9375.

Harris, R. C. (1991). Potential physiologic roles for epidermal growth factor in the kidney. *Am. J. Kidney Dis.* **17**, 627–630.

Heidorn, S. J., Milagre, C., Whittaker, S., Nourry, A., Niculescu-Duvas, I., Dhomen, N., Hussain, J., Reis-Filho, J. S., Springer, C. J., Pritchard, C., et al. (2010). Kinase-dead BRAF and oncogenic RAS cooperate to drive tumor progression through CRAF. *Cell* **140**, 209–221.

Hindley, A. and Kolch, W. (2002). Extracellular signal regulated kinase (ERK)/ mitogen activated protein kinase (MAPK) -independent functions of Raf kinases. *J. Cell Sci.* **115**, 15757–15781.

Hirano, S., Nose, A., Hatta, K., Kawakami, A. and Takeichi, M. (1987). Calcium-dependent cell-cell adhesion molecules (cadherins): Subclass specificities and possible involvement of actin bundles. *J. Cell Biol.* **105**, 2501–2510.

Honda, H., Pazin, M. J., Ji, H., Wernyj, R. P. and Morin, P. J. (2006). Crucial roles of Sp1 and epigenetic modifications in the regulation of the cldn4 promoter in ovarian cancer cells. *J. Biol. Chem.* **281**, 21433–21444.

Hou, J., Gomes, A. S., Paul, D. L. and Goodenough, D. a (2006). Study of claudin function by RNA interference. *J. Biol. Chem.* **281**, 36117–36123.

Hou, J., Rajagopal, M. and Yu, A. S. L. (2013). Claudins and the Kidney Volume 75: Annual Review of Physiology. *Annu. Rev. Physiol.* **75**, 479–501.

Hu, J., Stites, E. C., Yu, H., Germino, E. A., Meharena, H. S., Stork, P. J. S., Kornev, A. P., Taylor, S. S. and Shaw, A. S. (2013). Allosteric Activation of Functionally Asymmetric RAF Kinase Dimers. *Cell* **154**, 1036–1046.

Huang, R. Y.-J., Guilford, P. and Thiery, J. P. (2012). Early events in cell adhesion and polarity during epithelial-mesenchymal transition. *J. Cell Sci.* **125**, 4417–4422.

Ikari, A., Hirai, N., Shiroma, M., Harada, H., Sakai, H., Hayashi, H., Suzuki, Y., Degawa, M. and Takagi, K. (2004). Association of paracellin-1 with ZO-1 augments the reabsorption of divalent cations in renal epithelial cells. *J. Biol. Chem.* **279**, 54826–54832.

Ikari, A., Atomi, K., Takiguchi, A., Yamazaki, Y., Miwa, M. and Sugatani, J. (2009). Epidermal growth factor increases claudin-4 expression mediated by Sp1 elevation in MDCK cells. *Biochem. Biophys. Res. Commun.* **384**, 306–310.

Ikari, A., Sato, T., Takiguchi, A., Atomi, K., Yamazaki, Y. and Sugatani, J. (2011a). Claudin-2 knockdown decreases matrix metalloproteinase-9 activity and cell migration via suppression of nuclear Sp1 in A549 cells. *Life Sci.* **88**, 628–633.

Ikari, A., Takiguchi, A., Atomi, K., Sato, T. and Sugatani, J. (2011b). Decrease in claudin-2 expression enhances cell migration in renal epithelial Madin-Darby canine kidney cells. *J. Cell. Physiol.* **226**, 1471–1478.

Ikari, A., Takiguchi, A., Atomi, K. and Sugatani, J. (2011c). Epidermal growth factor increases clathrin-dependent endocytosis and degradation of claudin-2 protein in MDCK II cells. *J. Cell. Physiol.* **226**, 2448–2456.

Ikari, A., Sato, T., Watanabe, R., Yamazaki, Y. and Sugatani, J. (2012a). Increase in claudin-2 expression by an EGFR/MEK/ERK/c-Fos pathway in lung adenocarcinoma A549 cells. *Biochim. Biophys. Acta - Mol. Cell Res.* **1823**, 1110–1118.

Ikari, A., Atomi, K., Takiguchi, A., Yamazaki, Y., Hayashi, H., Hirakawa, J. and Sugatani, J. (2012b). Enhancement of cell-cell contact by claudin-4 in renal epithelial Madin-Darby canine kidney cells. *J. Cell. Biochem.* **113**, 499–507.

Ikawa, S., Fukui, M., Ueyama, Y., Tamaoki, N., Yamamoto, T. and Toyoshima, K. (1988). B-raf, a new member of the raf family, is activated by DNA rearrangement. *Mol. Cell. Biol.* **8**, 2651–2654.

Ikenouchi, J., Matsuda, M., Furuse, M. and Tsukita, S. (2003). Regulation of tight junctions during the epithelium-mesenchyme transition: direct repression of the gene expression of claudins/occludin by Snail. *J. Cell Sci.* **116**, 1959–1967.

Ikenouchi, J., Furuse, M., Furuse, K., Sasaki, H., Tsukita, S. and Tsukita, S. (2005). Tricellulin constitutes a novel barrier at tricellular contacts of epithelial cells. *J. Cell Biol.* **171**, 939–945.

Ikenouchi, J., Sasaki, H., Tsukita, S., Furuse, M. and Tsukita, S. (2008). Loss of Occludin Affects Tricellular Localization of Tricellulin. *Mol. Biol. Cell* **19**, 4687–4693.

Inai, T., Kobayashi, J. and Shibata, Y. (1999). Claudin-1 contributes to the epithelial barrier function in MDCK cells. *Eur. J. cell Biol. J. Cell Biol.* **78**, 849–855.

Inai, T., Kitagawa, N., Hatakeyama, Y., Ikebe, T., Iida, H. and Fujita, M. (2013). Inhibition of extracellular signal-regulated kinase downregulates claudin-2 expression and alters paracellular permeability in mouse rectum CMT93-II cells. *Tissue Cell* **2**, 1–8.

Itoh, M., Furuse, M., Morita, K., Kubota, K., Saitou, M. and Tsukita, S. (1999). Direct binding of three tight junction-associated MAGUKs, ZO-1, ZO-2, and ZO-3, with the COOH termini of claudins. *J. Cell Biol.* **147**, 1351–1363.

Ivanov, A. I., Nusrat, A. and Parkos, C. A. (2004). Endocytosis of Epithelial Apical Junctional Proteins by a Clathrin-mediated Pathway into a Unique Storage Compartment. *Mol. Biol. Cell* **15**, 176–188.

Jan, C. R., Cheng, J. S., Chou, K. J., Wang, S. P., Lee, K. C., Tang, K. Y., Tseng, L. L. and Chiang, H. T. (2000). Dual effect of tamoxifen, an anti-breast-cancer drug, on intracellular Ca(2+) and cytotoxicity in intact cells. *Toxicol. Appl. Pharmacol.* **168**, 58–63.

Janda, E., Nevolo, M., Lehmann, K., Downward, J., Beug, H. and Grieco, M. (2006). Raf plus TGFbeta-dependent EMT is initiated by endocytosis and lysosomal degradation of E-cadherin. *Oncogene* **25**, 7117–7130.

Jesaitis, L. A. and Goodenough, D. A. (1994). Molecular characterization and tissue distribution of ZO-2, a tight junction protein homologous to ZO-1 and the Drosophila discs-large tumor suppressor protein. *J. Cell Biol.* **124**, 949–961.

Jiwa, L. S., Diest, P. J. Van, Hoefnagel, L. D., Wesseling, J., Wesseling, P. and Moelans, C. B. (2014). Upregulation of Claudin-4 , CAIX and GLUT-1 in distant breast cancer metastases. *BMC Cancer* **14**, 1–6.

Kahle, K. T., Macgregor, G. G., Wilson, F. H., Van Hoek, A. N., Brown, D., Ardito, T., Kashgarian, M., Giebisch, G., Hebert, S. C., Boulpaep, E. L., et al. (2004). Paracellular Cl- permeability is regulated by WNK4 kinase: insight into normal physiology and hypertension. *Proc. Natl. Acad. Sci. U. S. A.* **101**, 14877–14882.

Kalluri, R. and Weinberg, R. A. (2009). The basics of epithelial-mesenchymal transition. *J. Clin. Invest.* **119**, 1420–1428.

Kamata, T. and Pritchard, C. (2011). Mechanisms of aneuploidy induction by RAS and RAF oncogenes. *Am. J. Cancer Res.* **1**, 955–971.

Kamata, T., Hussain, J., Giblett, S., Hayward, R., Marais, R. and Pritchard, C. (2010). BRAF inactivation drives aneuploidy by deregulating CRAF. *Cancer Res.* **70**, 8475–8486.

Kang, J. H., Choi, H. J., Cho, H. Y., Lee, J. H., Ha, I. S., Cheong, H. Il and Choi, Y. (2005). Familial hypomagnesemia with hypercalciuria and nephrocalcinosis associated with CLDN16 mutations. *Pediatr. Nephrol.* **20**, 1490–1493.

Katsuno, T., Umeda, K., Matsui, T., Hata, M., Tamura, A., Itoh, M., Takeuchi, K., Fujimori, T., Nabeshima, Y., Noda, T., et al. (2008). Deficiency of Zonula Occludens-1 Causes Embryonic Lethal Phenotype Associated with Defected Yolk Sac Angiogenesis and Apoptosis of Embryonic Cells. *Mol. Biol. Cell* **19**, 2465–2475.

Keon, B. H., Schäfer, S., Kuhn, C., Grund, C. and Franke, W. W. (1996). Symplekin, a novel type of tight junction plaque protein. *J. Cell Biol.* **134**, 1003–1018.

Khoo, S., Griffen, S. C., Xia, Y., Baer, R. J., German, M. S. and Cobb, M. H. (2003). Regulation of insulin gene transcription by ERK1 and ERK2 in pancreatic beta cells. *J. Biol. Chem.* **278**, 32969–32977.

Kieran, N. E., Doran, P. P., Connolly, S. B., Greenan, M. C., Higgins, D. F., Leonard, M., Godson, C., Taylor, C. T., Henger, A., Kretzler, M., et al. (2003). Modification of the transcriptomic response to renal ischemia/reperfusion injury by lipoxin analog. *Kidney Int.* **64**, 480–492.

Kimura, T., Sakisaka, T., Baba, T., Yamada, T. and Takai, Y. (2006). Involvement of the Ras-Ras-activated Rab5 guanine nucleotide exchange factor RIN2-Rab5 pathway in the hepatocyte growth factor-induced endocytosis of E-cadherin. *J. Biol. Chem.* **281**, 10598–10609.

Kinoshita-Kikuta, E., Aoki, Y., Kinoshita, E. and Koike, T. (2007). Label-free kinase profiling using phosphate affinity polyacrylamide gel electrophoresis. *Mol. Cell. proteomics MCP* **6**, 356–366.

Kitt, K. N., Hernández-Deviez, D., Ballantyne, S. D., Spiliotis, E. T., Casanova, J. E. and Wilson, J. M. (2008). Rab14 Regulates Apical Targeting in Polarized Epithelial Cells. *Traffic* **9**, 1218–1231.

Ko, K. S., Arora, P. D., Bhide, V., Chen, A. and McCulloch, C. A. (2001). Cell-cell adhesion in human fibroblasts requires calcium signaling. *J. Cell Sci.* **114**, 1155–1167.

Köhler, K. and Zahraoui, A. (2005). Tight junction: a co-ordinator of cell signalling and membrane trafficking. *Biol. cell* **97**, 659–665.

Kohno, Y., Okamoto, T., Ishibe, T., Nagayama, S., Shima, Y., Nishijo, K., Shibata, K. R., Fukiage, K., Otsuka, S., Uejima, D., et al. (2006). Expression of claudin7 is tightly

associated with epithelial structures in synovial sarcomas and regulated by an Ets family transcription factor, ELF3. *J. Biol. Chem.* **281**, 38941–38950.

Koval, M. (2013). Differential pathways of claudin oligomerization and integration into tight junctions. *Tissue barriers* **1**, 1–7.

Krause, G., Winkler, L., Mueller, S. L., Haseloff, R. F., Piontek, J. and Blasig, I. E. (2008). Structure and function of claudins. *Biochim. Biophys. Acta* **1778**, 631–645.

Krishnan, M., Lapierre, L. A., Knowles, B. C. and Goldenring, J. R. (2013). Rab25 regulates integrin expression in polarized colonic epithelial cells. *Mol. Biol. Cell* **24**, 818–831.

Kwon, M. J. (2013). Emerging roles of claudins in human cancer. *Int. J. Mol. Sci.* **14**, 18148–18180.

Laemmli, U. K. (1970). Cleavage of structural proteins during the assembly of the head of bacteriophage T4. *Nature* **227**, 680–685.

Lan, M., Kojima, T., Osanai, M., Chiba, H. and Sawada, N. (2004). Oncogenic Raf-1 regulates epithelial to mesenchymal transition via distinct signal transduction pathways in an immortalized mouse hepatic cell line. *Carcinogenesis* **25**, 2385–2395.

Laprise, P., Langlois, M. J., Boucher, M. J., Jobin, C. and Rivard, N. (2004). Down-Regulation of MEK/ERK Signaling by E-Cadherin-Dependent PI3K/Akt Pathway in Differentiating Intestinal Epithelial Cells. *J. Cell. Physiol.* **199**, 32–39.

Larre, I., Lazaro, A., Contreras, R. G., Balda, M. S., Matter, K., Flores-Maldonado, C., Ponce, A., Flores-Benitez, D., Rincon-Heredia, R., Padilla-Benavides, T., et al. (2010). Ouabain modulates epithelial cell tight junction. *Proc. Natl. Acad. Sci. U. S. A.* **107**, 11387–11392.

Le Moellic, C., Boulkroun, S., González-Nunez, D., Dublineau, I., Cluzeaud, F., Fay, M., Blot-Chabaud, M. and Farman, N. (2005). Aldosterone and tight junctions: modulation of claudin-4 phosphorylation in renal collecting duct cells. *Am. J. Physiol. Cell Physiol.* **289**, 1513–1521.

Lee, D. B. N., Jamgotchian, N., Allen, S. G., Abeles, M. B. and Ward, H. J. (2008). A lipid-protein hybrid model for tight junction. *Am. J. Physiol. Renal Physiol.* **295**, 1601–1612.

Lehmann, K., Janda, E., Pierreux, C. E., Ryto, M., Schulze, A., Mcmahon, M., Hill, C. S., Beug, H. and Downward, J. (2000). Raf induces TGFbeta production while blocking its apoptotic but not invasive responses : a mechanism leading to increased malignancy in epithelial cells. *Genes Dev.* **14**, 2610–2622.

Lemieux, E., Bergeron, S., Durand, V., Asselin, C., Saucier, C. and Rivard, N. (2009). Constitutively active MEK1 is sufficient to induce epithelial-to-mesenchymal transition in intestinal epithelial cells and to promote tumor invasion and metastasis. *Int. J. Cancer* **125**, 1575–1586.

Lemieux, E., Boucher, M.-J., Mongrain, S., Boudreau, F., Asselin, C. and Rivard, N. (2011). Constitutive activation of the MEK/ERK pathway inhibits intestinal epithelial cell differentiation. *Am. J. Physiol. Gastrointest. Liver Physiol.* **301**, 719–730.

Lenormand, P., Sardet, C., Pagès, G., L'Allemain, G., Brunet, A. and Pouysségur, J. (1993). Growth factors induce nuclear translocation of MAP kinases (p42mapk and p44mapk) but not of their activator MAP kinase kinase (p45mapkk) in fibroblasts. *J. Cell Biol.* **122**, 1079–1088.

Li, D. and Mrsny, R. J. (2000). Oncogenic Raf-1 disrupts epithelial tight junctions via downregulation of occludin. *J. Cell Biol.* **148**, 791–800.

Li, S., Gerrard, E. R. and Balkovetz, D. F. (2004). Evidence for ERK1/2 phosphorylation controlling contact inhibition of proliferation in Madin-Darby canine kidney epithelial cells. *Am. J. Physiol. Cell Physiol.* **287**, 432–439.

Li, J., Zhuo, M., Pei, L. and Yu, A. S. L. (2013). Conserved aromatic residue confers cation selectivity in claudin-2 and claudin-10b. *J. Biol. Chem.* **288**, 22790–22797.

Lin, X., Shang, X., Manorek, G. and Howell, S. B. (2013). Regulation of the Epithelial-Mesenchymal Transition by Claudin-3 and Claudin-4. *PLoS One* **8**, 1–13.

Lippincott-Schwartz, J., Altan-Bonnet, N. and Patterson, G. H. (2003). Photobleaching and photoactivation: following protein dynamics in living cells. *Nat. Cell Biol.* **5**, S7–S14.

Lipschutz, J. H., Li, S., Arisco, A. and Balkovetz, D. F. (2005). Extracellular signal-regulated kinases 1/2 control claudin-2 expression in Madin-Darby canine kidney strain I and II cells. *J. Biol. Chem.* **280**, 3780–3788.

Liu, J., Suresh Kumar, K. G., Yu, D., Molton, S. A., McMahon, M., Herlyn, M., Thomas-Tikhonenko, A. and Fuchs, S. Y. (2007). Oncogenic BRAF regulates β-Trcp expression and NF-κB actviity in human melanoma cells. *Oncogene* **26**, 1954–1958.

Lock, J. G. and Stow, J. L. (2005). Rab11 in Recycling Endosomes Regulates the Sorting and Basolateral Transport of E-Cadherin. *Mol. Biol. Cell* **16**, 1744–1755.

Lopez-Bayghen, E., Jaramillo, B. E., Huerta, M., Betanzos, A. and González-Mariscal, L. (2006). TJ Proteins That Make Round Trips to the Nucleus. In *Tight Junctions*, pp. 76–100.

Lu, R., Johnson, D. L., Stewart, L., Waite, K., Elliott, D. and Wilson, J. M. (2014). Rab14 regulation of claudin-2 trafficking modulates epithelial permeability and lumen morphogenesis. *Mol. Biol. Cell* **25**, 1744–1754.

Lu, R., Dalgalan, D., Mandell, E. K., Parker, S. S., Ghosh, S. and Wilson, J. M. (2015). PKCι interacts with Rab14 and modulates epithelial barrier function through regulation of claudin-2 levels. *Mol. Biol. Cell* **Feb**,.

Luissint, A. C., Nusrat, A. and Parkos, C. A. (2014). JAM-related proteins in mucosal homeostasis and inflammation. *Semin. Immunopathol.* **36**, 211–226.

Mankertz, J., Tavalali, S., Schmitz, H., Mankertz, A., Riecken, E. O., Fromm, M. and Schulzke, J. D. (2000). Expression from the human occludin promoter is affected by tumor necrosis factor alpha and interferon gamma. *J. Cell Sci.* **113**, 2085–2090.

Mankertz, J., Hillenbrand, B., Tavalali, S., Huber, O., Fromm, M. and Schulzke, J.-D. (2004). Functional crosstalk between Wnt signaling and Cdx-related transcriptional activation in the regulation of the claudin-2 promoter activity. *Biochem. Biophys. Res. Commun.* **314**, 1001–1007.

Mansour, S. J., Matten, W. T., Hermann, A. S., Candia, J. M., Rong, S., Fukasawa, K., Vande Woude, G. F. and Ahn, N. G. (1994). Transformation of mammalian cells by constitutively active MAP kinase kinase. *Science (80-.).* **265**, 966–970.

Marais, R., Light, Y., Paterson, H. F., Mason, C. S. and Marshall, C. J. (1997). Differential regulation of Raf-1, A-Raf, and B-Raf by oncogenic Ras and tyrosine kinases. *J. Biol. Chem.* **272**, 4378–4383.

Markov, A. G., Aschenbach, J. R. and Amasheh, S. (2015). Claudin clusters as determinants of epithelial barrier function. *IUBMB Life* **January**, 1–7.

Martínez-Estrada, O. M., Cullerés, A., Soriano, F. X., Peinado, H., Bolós, V., Martínez, F. O., Reina, M., Cano, A., Fabre, M. and Vilaró, S. (2006). The transcription factors Slug and Snail act as repressors of Claudin-1 expression in epithelial cells. *Biochem. J.* **394**, 449–457.

Martìn-Padura, I., Lostaglio, S., Schneemann, M., Williams, L., Romano, M., Fruscella, P., Panzeri, C., Stoppacciaro, A., Ruco, L., Villa, A., et al. (1998). Junctional adhesion

molecule, a novel member of the immunoglobulin superfamily that distributes at intercellular junctions and modulates monocyte transmigration. *J. Cell Biol.* **142**, 117–127.

Masaki, T., Stambe, C., Hill, P. A., Dowling, J., Atkins, R. C. and Nikolic-Paterson, D. J. (2004). Activation of the extracellular-signal regulated protein kinase pathway in human glomerulopathies. *J. Am. Soc. Nephrol.* **15**, 1835–1843.

Mason, C. S., Springer, C. J., Cooper, R. G., Superti-Furga, G., Marshall, C. J. and Marais, R. (1999). Serine and tyrosine phosphorylations cooperate in Raf-1, but not B-Raf activation. *EMBO J.* **18**, 2137–2148.

Matallanas, D., Birtwistle, M., Romano, D., Zebisch, A., Rauch, J., von Kriegsheim, A. and Kolch, W. (2011). Raf family kinases: old dogs have learned new tricks. *Genes Cancer* **2**, 232–260.

Matter, K. and Balda, M. S. (2003). Signalling to and from tight junctions. *Nat. Rev. Mol. Cell Biol.* **4**, 225–236.

McCarter, S. D., Johnson, D. L., Kitt, K. N., Donohue, C., Adams, A. and Wilson, J. M. (2010). Regulation of tight junction assembly and epithelial polarity by a resident protein of apical endosomes. *Traffic* **11**, 856–866.

McCarthy, K. M., Skare, I. B., Stankewich, M. C., Furuse, M., Tsukita, S., Rogers, R. A., Lynch, R. D. and Schneeberger, E. E. (1996). Occludin is a functional component of the tight junction. *J. Cell Sci.* **109**, 2287–2298.

McCrea, P. D., Gu, D. and Balda, M. S. (2009). Junctional music that the nucleus hears: cell-cell contact signaling and the modulation of gene activity. *Cold Spring Harb. Perspect. Biol.* **1**, 1–29.

McMahon, M. (2001). Steroid Receptor Fusion Proteins for Conditional Activation of Raf-MEK-ERK Signaling Pathway. *Methods Enzymol.* **332**, 401–417.

Mellman, I. and Yarden, Y. (2013). Endocytosis and cancer. *Cold Spring Harb. Perspect. Biol.* **5**, 1–24.

Meşe, G., Richard, G. and White, T. W. (2007). Gap junctions: basic structure and function. *J. Invest. Dermatol.* **127**, 2516–2524.

Milatz, S., Krug, S. M., Rosenthal, R., Günzel, D., Müller, D., Schulzke, J.-D., Amasheh, S. and Fromm, M. (2010). Claudin-3 acts as a sealing component of the tight junction for ions of either charge and uncharged solutes. *Biochim. Biophys. Acta* **1798**, 2048–2057.

Miranda, K. C., Khromykh, T., Christy, P., Le, T. L., Gottardi, C. J., Yap, A. S., Stow, J. L. and Teasdale, R. D. (2001). A Dileucine Motif Targets E-cadherin to the Basolateral Cell Surface in Madin-Darby Canine Kidney and LLC-PK1 Epithelial Cells. *J. Biol. Chem.* **276**, 22565–22572.

Montesano, R., Soriano, J. V, Hosseini, G., Pepper, M. S. and Schramek, H. (1999). Constitutively active mitogen-activated protein kinase kinase MEK1 disrupts morphogenesis and induces an invasive phenotype in Madin-Darby canine kidney epithelial cells. *Cell growth Differ.* **10**, 317–332.

Morimoto, S., Nishimura, N., Terai, T., Manabe, S., Yamamoto, Y., Shinahara, W., Miyake, H., Tashiro, S., Shimada, M. and Sasaki, T. (2005). Rab13 mediates the continuous endocytic recycling of occludin to the cell surface. *J. Biol. Chem.* **280**, 2220–2228.

Mostov, K. E., Su, T., Beest, M. and ter Beest, M. (2003). Polarized epithelial membrane traffic: conservation and plasticity. *Nat. Cell Biol.* **5**, 287–293.

Mullin, J. M., Leatherman, J. M., Valenzano, M. C., Huerta, E. R., Verrechio, J., Smith, D. M., Snetselaar, K., Liu, M., Francis, M. K. and Sell, C. (2005). Ras Mutation Impairs Epithelial Barrier Function to a Wide Range of Nonelectrolytes. *Mol. Biol. Cell* **16**, 5538–5550.

Muto, S., Hata, M., Taniguchi, J., Tsuruoka, S., Moriwaki, K. and Saitou, M. (2010). Claudin-2 – deficient mice are defective in the leaky and cation-selective paracellular permeability properties of renal proximal tubules. *Proc. Natl. Acad. Sci. U. S. A.* **107**, 8011–8016.

Nakayama, F., Semba, S., Usami, Y., Chiba, H., Sawada, N. and Yokozaki, H. (2008). Hypermethylation-modulated downregulation of claudin-7 expression promotes the progression of colorectal carcinoma. *Pathobiology* **75**, 177–185.

Neesse, A., Griesmann, H., Gress, T. M. and Michl, P. (2012). Claudin-4 as therapeutic target in cancer. *Arch. Biochem. Biophys.* **524**, 64–70.

Nichols, L. S., Ashfaq, R. and Iacobuzio-Donahue, C. a (2004). Claudin 4 protein expression in primary and metastatic pancreatic cancer: support for use as a therapeutic target. *Am. J. Clin. Pathol.* **121**, 226–230.

Nishimura, N. and Sasaki, T. (2008). Cell-Surface Biotinylation to Study Endocytosis and Recycling of Occludin. *Methods Mol. Biol.* **440**, 89–96.

Nunes, F. D., Lopez, L. N., Lin, H. W., Davies, C., Azevedo, R. B., Gow, A. and Kachar, B. (2006). Distinct subdomain organization and molecular composition of a tight junction with adherens junction features. *J. Cell Sci.* **119**, 4819–4827.

Nusrat, A., Giry, M., Turner, J. R., Colgan, S. P., Parkos, C. A., Carnes, D., Lemichez, E., Boquet, P. and Madara, J. L. (1995). Rho protein regulates tight junctions and perijunctional actin organization in polarized epithelia. *Proc. Natl. Acad. Sci. U. S. A.* **92**, 10629–10633.

Nusrat, A., Parkos, C. A., Verkade, P., Foley, C. S., Liang, T. W., Innis-Whitehouse, W., Eastburn, K. K. and Madara, J. L. (2000). Tight junctions are membrane microdomains. *J. Cell Sci.* **113**, 1771–1781.

O'Neill, E. and Kolch, W. (2004). Conferring specificity on the ubiquitous Raf/MEK signalling pathway. *Br. J. Cancer* **90**, 283–288.

Oh, B.-Y., Lee, R.-A., Chung, S.-S. and Kim, K. H. (2011). Epidermal growth factor receptor mutations in colorectal cancer patients. *J. Korean Soc. Coloproctol.* **27**, 127–132.

Ohta, A., Yang, S. S., Rai, T., Chiga, M., Sasaki, S. and Uchida, S. (2006). Overexpression of human WNK1 increases paracellular chloride permeability and phosphorylation of claudin-4 in MDCKII cells. *Biochem. Biophys. Res. Commun.* **349**, 804–808.

Palacios, F., Price, L., Schweitzer, J., Collard, J. G., D'Souza-Schorey, C. and Souza-Schorey, C. D. (2001). An essential role for ARF6-regulated membrane traffic in adherens junction turnover and epithelial cell migration. *EMBO J.* **20**, 4973–4986.

Palacios, F., Tushir, J. S., Fujita, Y. and Souza-Schorey, C. D. (2005). Lysosomal Targeting of E-Cadherin: a Unique Mechanism for the Down-Regulation of Cell-Cell Adhesion during Epithelial to Mesenchymal Transitions Lysosomal Targeting of E-Cadherin : a Unique Mechanism for the Down-Regulation of Cell-Cell Adhesion during E. *Mol. Cell. Biol.* **25**, 389–402.

Patton, E. E., Widlund, H. R., Kutok, J. L., R, K. K., Amatruda, J. F., Murphey, R. D., Berghmans, S., Mayhall, E. A., Traver, D., Fletcher, C. D. M., et al. (5AD). BRAF Mutations Are Sufficient to Promote Nevi Formation and Cooperate with p53 in the Genesis of Melanoma. *Curr. Biol.* **15**, 249–254.

Pfaffl, M. W. (2001). A new mathematical model for relative quantification in real-time RT-PCR. *Nucleic Acids Res.* **29**, 1–6.

Plath, T., Detjen, K., Welzel, M., von Marschall, Z., Murphy, D., Schirner, M., Wiedenmann, B. and Rosewicz, S. (2000). A novel function for the tumor suppressor p16(INK4a): induction of anoikis via upregulation of the alpha(5)beta(1) fibronectin receptor. *J. Cell Biol.* **150**, 1467–1478.

Poulikakos, P. I. and Solit, D. B. (2011). Resistance to MEK inhibitors: should we co-target upstream? *Sci. Signal.* **4**, 1–3.

Pouysségur, J., Volmat, V. and Lenormand, P. (2002). Fidelity and spatio-temporal control in MAP kinase (ERKs) signalling. *Biochem. Pharmacol.* **64**, 755–763.

Prat, A., Parker, J. S., Karginova, O., Fan, C., Livasy, C., Herschkowitz, J. I., He, X. and Perou, C. M. (2010). Phenotypic and molecular characterization of the claudin-low intrinsic subtype of breast cancer. *Breast Cancer Res.* **12**, 1–18.

Pratilas, C. A. and Solit, D. B. (2010). Targeting the mitogen-activated protein kinase pathway: physiological feedback and drug response. *Clin. Cancer Res.* **16**, 3329–3334.

Pratilas, C. A., Taylor, B. S., Ye, Q., Viale, A., Sander, C., Solit, D. B. and Rosen, N. (2009). (V600E)BRAF is associated with disabled feedback inhibition of RAF-MEK signaling and elevated transcriptional output of the pathway. *Proc. Natl. Acad. Sci. U. S. A.* **106**, 4519–4524.

Pritchard, C., Samuels, M. L., Bosch, E., Mcmahon, M. and Mahon, M. M. C. (1995). Conditionally oncogenic forms of the A-Raf and B-Raf protein kinases display different biological and biochemical properties in NIH Conditionally Oncogenic Forms of the A-Raf and B-Raf Protein Kinases Display Different Biological and Biochemical Propertie. *Mol. Cell. Biol.* **15**, 6430–6442.

Qin, W., Ren, Q., Liu, T., Huang, Y. and Wang, J. (2013). MicroRNA-155 is a novel suppressor of ovarian cancer-initiating cells that targets CLDN1. *FEBS Lett.* **587**, 1434–1439.

Rahner, C., Mitic, L. L. and Anderson, J. M. (2001). Heterogeneity in expression and subcellular localization of claudins 2, 3, 4, and 5 in the rat liver, pancreas, and gut. *Gastroenterology* **120**, 411–422.

Raleigh, D. R., Marchiando, A. M., Zhang, Y., Shen, L., Sasaki, H., Wang, Y., Long, M. and Turner, J. R. (2010). Tight Junction – associated MARVEL Proteins MarvelD3, Tricellulin, and Occludin Have Distinct but Overlapping Functions. *Mol. Biol. Cell* **21**, 1200–1213.

Raleigh, D. R., Boe, D. M., Yu, D., Weber, C. R., Marchiando, A. M., Bradford, E. M., Wang, Y., Wu, L., Schneeberger, E. E., Shen, L., et al. (2011). Occludin S408 phosphorylation regulates tight junction protein interactions and barrier function. *J. Cell Biol.* **193**, 565–582.

Rian, H., Krens, S. F. G., Spaink, H. P. and Snaar-Jagalska, B. E. (2013). Generation of Constitutive Active ERK Mutants as Tools for Cancer Research in Zebrafish. *ISRN Cell Biol.* 1–11.

Rincon-Heredia, R., Flores-Benitez, D., Flores-Maldonado, C., Bonilla-Delgado, J., García-Hernández, V., Verdejo-Torres, O., Castillo, A. M., Larré, I., Poot-Hernández, A. C., Franco, M., et al. (2014). Ouabain induces endocytosis and degradation of tight junction proteins through ERK1/2-dependent pathways. *Exp. Cell Res.* **320**, 108–118.

Riss, J., Khanna, C., Koo, S., Chandramouli, G. V. R., Yang, H. H., Hu, Y., Kleiner, D. E., Rosenwald, A., Schaefer, C. F., Ben-Sasson, S. A., et al. (2006). Cancers as wounds that do not heal: Differences and similarities between renal regeneration/repair and renal cell carcinoma. *Cancer Res.* **66**, 7216–7224.

Ritt, D. A., Monson, D. M., Specht, S. I. and Morrison, D. K. (2010). Impact of feedback phosphorylation and Raf heterodimerization on normal and mutant B-Raf signaling. *Mol. Cell. Biol.* **30**, 806–819.

Roberts, P. J. and Der, C. J. (2007). Targeting the Raf-MEK-ERK mitogen-activated protein kinase cascade for the treatment of cancer. *Oncogene* **26**, 3291–3310.

Robertson, S. E., Rao, S., Setty, G., Sitaram, A., Marks, M. S., Lewis, R. E. and Chou, M. M. (2006). Extracellular signal-regulated kinase regulates clathrin-independent endosomal trafficking. *Mol. Biol. Cell* **17**, 645–657.

Röring, M., Herr, R., Fiala, G. J., Heilmann, K., Braun, S., Eisenhardt, A. E., Halbach, S., Capper, D., von Deimling, A., Schamel, W. W., et al. (2012). Distinct requirement for an intact dimer interface in wild-type, V600E and kinase-dead B-Raf signalling. *EMBO J.* **31**, 2629–2647.

Roskoski, R. (2012). MEK1/2 dual-specificity protein kinases: structure and regulation. *Biochem. Biophys. Res. Commun.* **417**, 5–10.

Royer, C. and Lu, X. (2011). Epithelial cell polarity: a major gatekeeper against cancer? *Cell Death Differ.* **95**, 1470–1477.

Rushworth, L. K., Kidger, A. M., Delavaine, L., Stewart, G., van Schelven, S., Davidson, J., Bryant, C. J., Caddye, E., East, P., Caunt, C. J., et al. (2014). Dual-specificity phosphatase 5 regulates nuclear ERK activity and suppresses skin cancer by inhibiting mutant Harvey-Ras (HRasQ61L)-driven SerpinB2 expression. *Proc. Natl. Acad. Sci. U. S. A.* **111**, 18267–18272.

Saitou, M., Fujimoto, K., Doi, Y., Itoh, M., Fujimoto, T., Furuse, M., Takano, H., Noda, T. and Tsukita, S. (1998). Occludin-deficient embryonic stem cells can differentiate into polarized epithelial cells bearing tight junctions. *J. Cell Biol.* **141**, 397–408.

Saitou, M., Furuse, M., Sasaki, H., Schulzke, J. D., Fromm, M., Takano, H., Noda, T. and Tsukita, S. (2000). Complex phenotype of mice lacking occludin, a component of tight junction strands. *Mol. Biol. Cell* **11**, 4131–4142.

Sakaguchi, T., Gu, X., Golden, H. M., Suh, E., Rhoads, D. B. and Reinecker, H.-C. (2002). Cloning of the human claudin-2 5'-flanking region revealed a TATA-less promoter with conserved binding sites in mouse and human for caudal-related homeodomain proteins and hepatocyte nuclear factor-1alpha. *J. Biol. Chem.* **277**, 21361–21370.

Samuels, M. L., Weber, M. J., Bishop, J. M. and Mcmahon, M. (1993). Conditional transformation of cells and rapid activation of the mitogen-activated protein kinase cascade by an estradiol-dependent human raf-1 protein kinase. *Mol. Cell. Biol.* **13**, 6241–6252.

Santarpia, L., Lippman, S. M. and El-Naggar, A. K. (2012). Targeting the MAPK-RAS-RAF signaling pathway in cancer therapy. *Expert Opin. Ther. Targets* 103–119.

Sasaki, H., Matsui, C., Furuse, K., Mimori-Kiyosue, Y., Furuse, M. and Tsukita, S. (2003). Dynamic behavior of paired claudin strands within apposing plasma membranes. *Proc. Natl. Acad. Sci. U. S. A.* **100**, 3971–3976.

Savagner, P. (2010). The epithelial-mesenchymal transition (EMT) phenomenon. *Ann. Oncol.* **21**, 89–92.

Schmidt, A., Utepbergenov, D. I., Mueller, S. L., Beyermann, M., Schneider-Mergener, J., Krause, G. and Blasig, I. E. (2004). Occludin binds to the SH3-hinge-GuK unit of zonula occludens protein 1: Potential mechanism of tight junction regulation. *Cell. Mol. Life Sci.* **61**, 1354–1365.

Schoenenberger, C. A., Zuk, A., Kendall, D. and Matlin, K. S. (1991). Multilayering and loss of apical polarity in MDCK cells transformed with viral K-ras. *J. Cell Biol.* **112**, 873–889.

Shang, X., Lin, X., Alvarez, E., Manorek, G. and Howell, S. B. (2012). Tight junction proteins claudin-3 and claudin-4 control tumor growth and metastases. *Neoplasia* **14**, 974–985.

Shang, X., Lin, X. and Howell, S. B. (2014). Claudin-4 controls the receptor tyrosine kinase EphA2 pro-oncogenic switch through β-catenin. *Cell Commun. Signal.* **12**, 1–15.

Shaul, Y. D. and Seger, R. (2007). The MEK/ERK cascade: from signaling specificity to diverse functions. *Biochim. Biophys. Acta* **1773**, 1213–1226.

Shen, L. and Turner, J. R. (2005). Actin Depolymerization Disrupts Tight Junctions via Caveolae-mediated Endocytosis. *Mol. Biol. Cell* **16**, 3919–3936.

Shen, L., Weber, C. R. and Turner, J. R. (2008). The tight junction protein complex undergoes rapid and continuous molecular remodeling at steady state. *J. Cell Biol.* **181**, 683–695.

Shen, L., Weber, C. R., Raleigh, D. R., Yu, D. and Turner, J. R. (2011). Tight junction pore and leak pathways: a dynamic duo. *Annu. Rev. Physiol.* **73**, 283–309.

Shin, K., Fogg, V. C. and Margolis, B. (2006). Tight junctions and cell polarity. *Annu. Rev. Cell Dev. Biol.* **22**, 207–235.

Singh, A. B. and Harris, R. C. (2004). Epidermal growth factor receptor activation differentially regulates claudin expression and enhances transepithelial resistance in Madin-Darby canine kidney cells. *J. Biol. Chem.* **279**, 3543–3552.

Singh, A. B., Tsukada, T., Zent, R. and Harris, R. C. (2004). Membrane-associated HB-EGF modulates HGF-induced cellular responses in MDCK cells. *J. Cell Sci.* **117**, 1365–1379.

Singh, A. B., Sugimoto, K., Dhawan, P. and Harris, R. C. (2007). Juxtacrine activation of EGFR regulates claudin expression and increases transepithelial resistance. *Am. J. Physiol. Cell Physiol.* **293**, 1660–1668.

St Johnston, D. and Ahringer, J. (2010). Cell polarity in eggs and epithelia: parallels and diversity. *Cell* **141**, 757–774.

Stanton, V. P., Nichols, D. W., Laudano, A. P. and Cooper, G. M. (1989). Definition of the Human raf Amino-Terminal Regulatory Region by Deletion Mutagenesis. *Mol. Cell. Biol.* **9**, 639–647.

Steed, E., Rodrigues, N. T. L., Balda, M. S. and Matter, K. (2009). Identification of MarvelD3 as a tight junction-associated transmembrane protein of the occludin family. *BMC Cell Biol.* **10**, 1–14.

Steed, E., Balda, M. S. and Matter, K. (2010). Dynamics and functions of tight junctions. *Trends Cell Biol.* **20**, 142–149.

Stevenson, B. R., Siliciano, J. D., Mooseker, M. S. and Goodenough, D. A. (1986). Identification of ZO-1: A high molecular weight polypeptide associated with the tight junction (Zonula Occludens) in a variety of epithelia. *J. Cell Biol.* **103**, 755–766.

Sturm, O. E., Orton, R., Grindlay, J., Birtwistle, M., Vyshemirsky, V., Gilbert, D., Calder, M., Pitt, A., Kholodenko, B. and Kolch, W. (2010). The mammalian MAPK/ERK pathway exhibits properties of a negative feedback amplifier. *Sci. Signal.* **3**, 1–7.

Suzuki, A., Ishiyama, C., Hashiba, K., Shimizu, M., Ebnet, K. and Ohno, S. (2002). aPKC kinase activity is required for the asymmetric differentiation of the premature junctional complex during epithelial cell polarization. *J. Cell Sci.* **115**, 3565–3573.

Suzuki, T., Elias, B. C., Seth, A., Shen, L., Turner, J. R., Giorgianni, F., Desiderio, D., Guntaka, R. and Rao, R. (2009). PKC eta regulates occludin phosphorylation and epithelial tight junction integrity. *Proc. Natl. Acad. Sci. U. S. A.* **106**, 61–66.

Suzuki, H., Nishizawa, T., Tani, K., Yamazaki, Y., Tamura, A., Ishitani, R., Dohmae, N., Tsukita, S., Nureki, O. and Fujiyoshi, Y. (2014). Crystal Structure of a Claudin Provides Insight into the Architecture of Tight Junctions. *Science (80-.).* **344**, 304–307.

Takahashi, S., Iwamoto, N., Sasaki, H., Ohashi, M., Oda, Y., Tsukita, S. and Furuse, M. (2009). The E3 ubiquitin ligase LNX1p80 promotes the removal of claudins from tight junctions in MDCK cells. *J. Cell Sci.* **122**, 985–994.

Tanaka, M., Kamata, R. and Sakai, R. (2005). EphA2 phosphorylates the cytoplasmic tail of claudin-4 and mediates paracellular permeability. *J. Biol. Chem.* **280**, 42375–42382.

Tanami, H., Imoto, I., Hirasawa, A., Yuki, Y., Sonoda, I., Inoue, J., Yasui, K., Misawa-Furihata, A., Kawakami, Y. and Inazawa, J. (2004). Involvement of overexpressed wild-type BRAF in the growth of malignant melanoma cell lines. *Oncogene* **23**, 8796–8804.

Tanos, B. E., Bay, A. P.-, Salvarezza, S., Vivanco, I., Mellinghoff, I., Osman, M., Sacks, D. B. and Rodriguez-, E. (2015). IQGAP1 Controls Tight Junction Formation Through Differential Regulation Of Claudin Recruitment. *J. Cell Sci.* **January**,.

Tatum, R., Zhang, Y., Lu, Q., Kim, K., Jeansonne, B. G. and Chen, Y. H. (2007). WNK4 phosphorylates ser206 of claudin-7 and promotes paracellular Cl- permeability. *FEBS Lett.* **581**, 3887–3891.

Tatum, R., Zhang, Y., Salleng, K., Lu, Z., Lin, J.-J., Lu, Q., Jeansonne, B. G., Ding, L. and Chen, Y.-H. (2010). Renal salt wasting and chronic dehydration in claudin-7-deficient mice. *Am. J. Physiol. Renal Physiol.* **298**, 24–34.

Thompson, N. and Lyons, J. (2005). Recent progress in targeting the Raf/MEK/ERK pathway with inhibitors in cancer drug discovery. *Curr. Opin. Pharmacol.* **5**, 350–356.

Togawa, A., Sfakianosa, J., Ishibe, S., Suzuki, S., Fujigakib, Y., Kitagawac, M., Mellman, I., Cantley, L. G., Sfakianos, J., Suzuki, S., et al. (2011). Hepatocyte Growth Factor stimulated cell scattering requires ERK and Cdc42-dependent tight junction disassembly. *Biochem. Biophys. Res. Commun.* **400**, 271–277.

Tokuda, S. and Furuse, M. (2015). Claudin-2 Knockout by TALEN-Mediated Gene Targeting in MDCK Cells: Claudin-2 Independently Determines the Leaky Property of Tight Junctions in MDCK Cells. *PLoS One* **10**, 1–22.

Tokuda, S., Higashi, T. and Furuse, M. (2014). ZO-1 Knockout by TALEN-Mediated Gene Targeting in MDCK Cells: Involvement of ZO-1 in the Regulation of Cytoskeleton and Cell Shape. *PLoS One* **9**, 1–16.

Traweger, A., Fang, D., Liu, Y. C., Stelzhammer, W., Krizbai, I. A., Fresser, F., Bauer, H. C. and Bauer, H. (2002). The tight junction-specific protein occludin is a functional target of the E3 ubiquitin-protein ligase itch. *J. Biol. Chem.* **277**, 10201–10208.

Traweger, A., Toepfer, S., Zweimueller-Mayer, J., Lehner, C., Tempfer, H., Bauer, H. H.-C., Wagner, R. N., Gehwolf, R., Krizbai, I. and Wilhelm, I. (2013). Beyond cell-cell adhesion: Emerging roles of the tight junction scaffold ZO-2. *Tissue barriers* **1**, 1–8.

Tsao, H., Chin, L., Garraway, L. A. and Fisher, D. E. (2012). Melanoma: From mutations to medicine. *Genes Dev.* **26**, 1131–1155.

Tsukita, S., Furuse, M. and Itoh, M. (2001). Multifunctional strands in tight junctions. *Nat. Rev. Mol. Cell Biol.* **2**, 285–293.

Tsukita, S., Yamazaki, Y., Katsuno, T. and Tamura, A. (2008). Tight junction-based epithelial microenvironment and cell proliferation. *Oncogene* **27**, 6930–6938.

Tsukita, S., Katsuno, T., Yamazaki, Y., Umeda, K., Tamura, A. and Tsukita, S. (2009). Roles of ZO-1 and ZO-2 in establishment of the belt-like adherens and tight junctions with paracellular permselective barrier function. *Ann. N. Y. Acad. Sci.* **1165**, 44–52.

Turksen, K. and Troy, T.-C. (2011). Junctions gone bad: claudins and loss of the barrier in cancer. *Biochim. Biophys. Acta* **1816**, 73–79.

Turner, J. R., Buschmann, M. M., Sailer, A., Calvo, I. R. and Shen, L. (2014). The role of molecular remodeling in differential regulation of tight junction permeability. *Semin. Cell Dev. Biol.* 1–9.

Umeda, K., Ikenouchi, J., Katahira-Tayama, S., Furuse, K., Sasaki, H., Nakayama, M., Matsui, T., Tsukita, S., Furuse, M. and Tsukita, S. (2006). ZO-1 and ZO-2 independently determine where claudins are polymerized in tight-junction strand formation. *Cell* **126**, 741–754.

Van Itallie, C. M. and Anderson, J. M. (1997). Occludin confers adhesiveness when expressed in fibroblasts. *J. Cell Sci.* **110**, 1113–1121.

Van Itallie, C. M. and Anderson, J. M. (2014). Architecture of tight junctions and principles of molecular composition. *Semin. Cell Dev. Biol.* 1–9.

Van Itallie, C., Rahner, C. and Anderson, J. M. (2001). Regulated expression of claudin-4 decreases paracellular conductance through a selective decrease in sodium permeability. *J. Clin. Invest.* **107**, 1319–1327.

Van Itallie, C. M., Colegio, O. R. and Anderson, J. M. (2004). The Cytoplasmic Tails of Claudins Can Influence Tight Junction Barrier Properties through Effects on Protein Stability. *J. Membr. Biol.* **199**, 29–38.

Van Itallie, C. M., Gambling, T. M., Carson, J. L. and Anderson, J. M. (2005). Palmitoylation of claudins is required for efficient tight-junction localization. *J. Cell Sci.* **118**, 1427–1436.

Van Itallie, C. M., Holmes, J., Bridges, A., Gookin, J. L., Coccaro, M. R., Proctor, W., Colegio, O. R. and Anderson, J. M. (2008). The density of small tight junction pores varies among cell types and is increased by expression of claudin-2. *J. Cell Sci.* **121**, 298–305.

Van Itallie, C. M., Mitic, L. L. and Anderson, J. M. (2012a). SUMOylation of claudin-2. *Ann. N. Y. Acad. Sci.* **1258**, 60–64.

Van Itallie, C. M., Tietgens, A. J., LoGrande, K., Aponte, A., Gucek, M. and Anderson, J. M. (2012b). Phosphorylation of claudin-2 on serine 208 promotes membrane retention and reduces trafficking to lysosomes. *J. Cell Sci.* **125**, 4902–4912.

Van Itallie, C. M., Aponte, A., Tietgens, A. J., Gucek, M., Fredriksson, K. and Anderson, J. M. (2013). The N and C termini of ZO-1 are surrounded by distinct proteins and functional protein networks. *J. Biol. Chem.* **288**, 13775–13788.

Van Itallie, C. M., Tietgens, A. J., Aponte, A., Fredriksson, K., Fanning, A. S., Gucek, M. and Anderson, J. M. (2014). Biotin ligase tagging identifies proteins proximal to E-cadherin, including lipoma preferred partner, a regulator of epithelial cell-cell and cell-substrate adhesion. *J. Cell Sci.* **127**, 885–895.

Vereecke, L., Beyaert, R. and van Loo, G. (2011). Enterocyte death and intestinal barrier maintenance in homeostasis and disease. *Trends Mol. Med.* **17**, 584–593.

Vermeer, P. D., Einwalter, L. A., Moninger, T. O., Rokhlina, T., Kern, J. A., Zabner, J. and Welsh, M. J. (2003). Segregation of receptor and ligand regulates activation of epithelial growth factor receptor. *Nature* **422**, 322–326.

Wang, Z., Chen, J.-K., Wang, S.-W., Moeckel, G. and Harris, R. C. (2003). Importance of functional EGF receptors in recovery from acute nephrotoxic injury. *J. Am. Soc. Nephrol.* **14**, 3147–3154.

Wang, Z., Wade, P., Mandell, K. J., Akyildiz, A., Parkos, C. A., Mrsny, R. J. and Nusrat, A. (2007). Raf 1 represses expression of the tight junction protein occludin via activation of the zinc-finger transcription factor slug. *Oncogene* **26**, 1222–1230.

Weber, C. R. (2012). Dynamic properties of the tight junction barrier. *Ann. N. Y. Acad. Sci.* **1257**, 77–84.

Wickenden, J. A., Jin, H., Johnson, M., Gillings, A. S., Newson, C., Austin, M., Chell, S. D., Balmanno, K., Pritchard, C. A. and Cook, S. J. (2008). Colorectal cancer cells with the BRAF(V600E) mutation are addicted to the ERK1/2 pathway for growth factor-independent survival and repression of BIM. *Oncogene* **27**, 7150–7161.

Wilcox, E. R., Burton, Q. L., Naz, S., Riazuddin, S., Smith, T. N., Ploplis, B., Belyantseva, I., Ben-Yosef, T., Liburd, N. A., Morell, R. J., et al. (2001). Mutations in the gene encoding tight junction claudin-14 cause autosomal recessive deafness DFNB29. *Cell* **104**, 165–172.

Wortzel, I. and Seger, R. (2011). The ERK Cascade: Distinct Functions within Various Subcellular Organelles. *Genes Cancer* **2**, 195–209.

Xu, J., Kausalya, P. J., Phua, D. C. Y., Ali, S. M., Hossain, Z. and Hunziker, W. (2008). Early Embryonic Lethality of Mice Lacking ZO-2, but Not ZO-3, Reveals Critical and Nonredundant Roles for Individual Zonula Occludens Proteins in Mammalian Development. *Mol. Cell. Biol.* **28**, 1669–1678.

Yamamura, R., Nishimura, N., Nakatsuji, H., Arase, S. and Sasaki, T. (2008). The Interaction of JRAB / MICAL-L2 with Rab8 and Rab13 Coordinates the Assembly of Tight Junctions and Adherens Junctions. *Mol. Biol. Cell* **19**, 971–983.

Yamauchi, K., Rai, T., Kobayashi, K., Sohara, E., Suzuki, T., Itoh, T., Suda, S., Hayama, A., Sasaki, S. and Uchida, S. (2004). Disease-causing mutant WNK4 increases paracellular chloride permeability and phosphorylates claudins. *Proc. Natl. Acad. Sci. U. S. A.* **101**, 4690–4694.

Yoon, S. and Seger, R. (2006). The extracellular signal-regulated kinase: multiple substrates regulate diverse cellular functions. *Growth factors* **24**, 21–44.

Yu, A. S. L., McCarthy, K. M., Francis, S. A., McCormack, J. M., Lai, J., Rogers, R. A., Lynch, R. D. and Schneeberger, E. E. (2005). Knockdown of occludin expression leads

to diverse phenotypic alterations in epithelial cells. *Am. J. Physiol. Cell Physiol.* **288**, 1231–1241.

Yu, A. S. L., Cheng, M. H., Angelow, S., Günzel, D., Kanzawa, S. A., Schneeberger, E. E., Fromm, M. and Coalson, R. D. (2009). Molecular basis for cation selectivity in claudin-2-based paracellular pores: identification of an electrostatic interaction site. *J. Gen. Physiol.* **133**, 111–127.

Yu, D., Marchiando, A. M., Weber, C. R., Raleigh, D. R., Wang, Y., Shen, L. and Turner, J. R. (2010). MLCK-dependent exchange and actin binding region-dependent anchoring of ZO-1 regulate tight junction barrier function. *Proc. Natl. Acad. Sci. U. S. A.* **107**, 8237–8241.

Zahraoui, A., Louvard, D. and Galli, T. (2000). Tight Junction, Platform for Trafficking Signaling Protein Complexes. *J. Cell Biol.* **151**, 31–36.

Zihni, C. and Terry, S. (2015). RhoGTPase signalling at epithelial tight junctions: Bridging the GAP between polarity and cancer. *Int. J. Biochem. Cell Biol.* 1–6.

Appendix

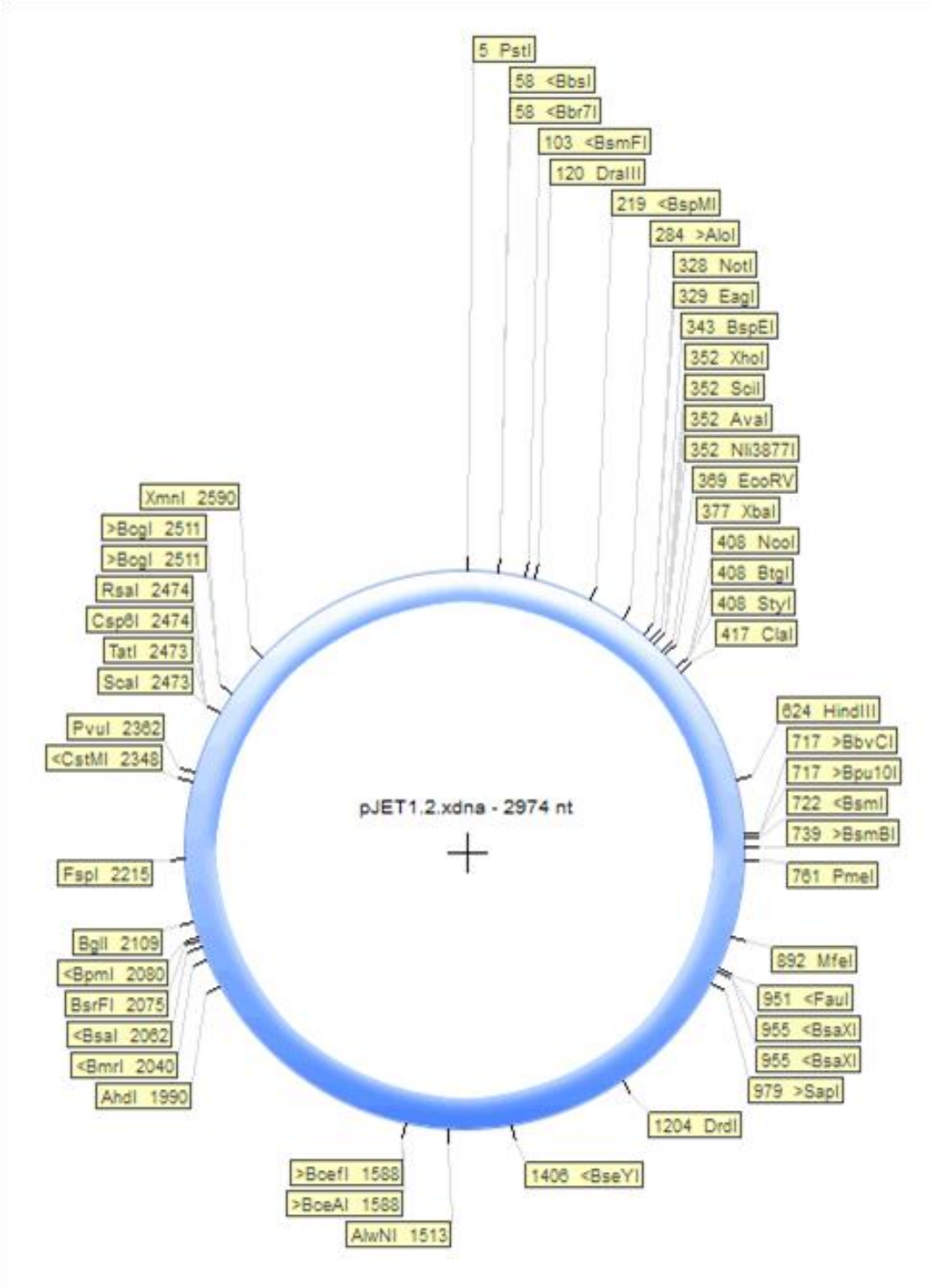

Figure A1: Plasmid map of pJET1.2. pJET1.2 is provided as a blunt cloning vector with the CloneJET PCR Cloning Kit (Thermo Scientific). Blunt-ended PCR products can be directly ligated into this intermediate vector for use in subsequent cloning projects.

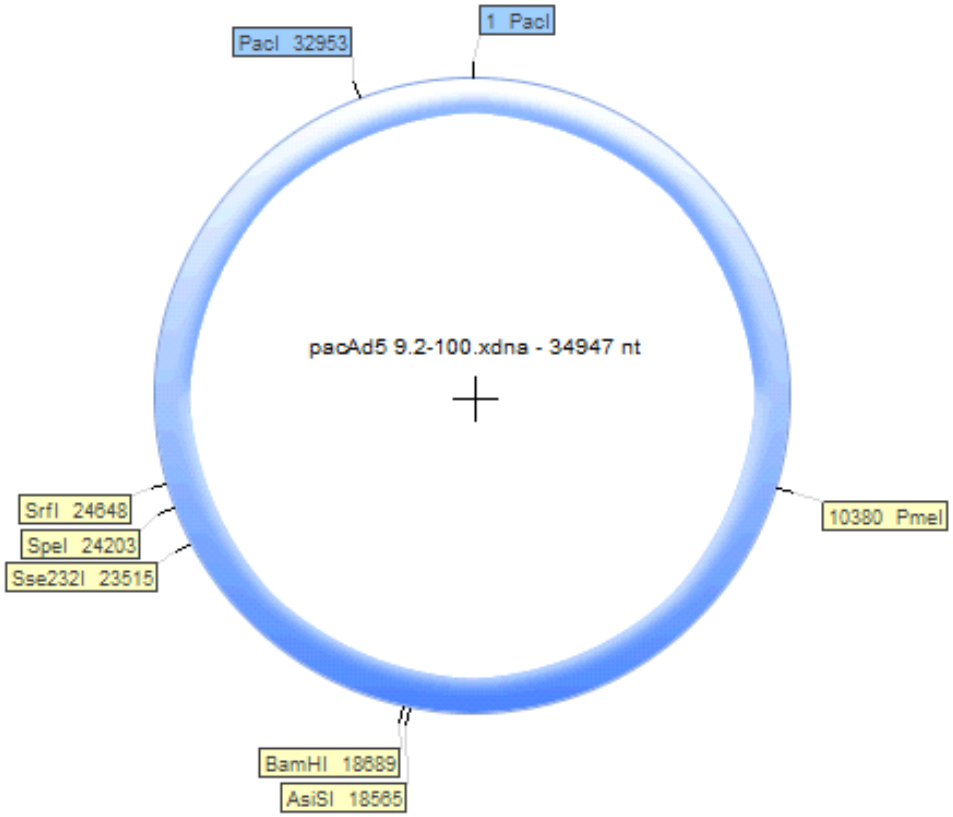

Figure A2: Plasmid map of pacAd5 9.2 – 100 sub 360. This is the adenoviral shuttle vector. After PacI digestion, this vector is cotransfected with the required shuttle vector into HEK293 cells. Recombination leads to the generation of adenovirus, which is subsequently harvested and purified.

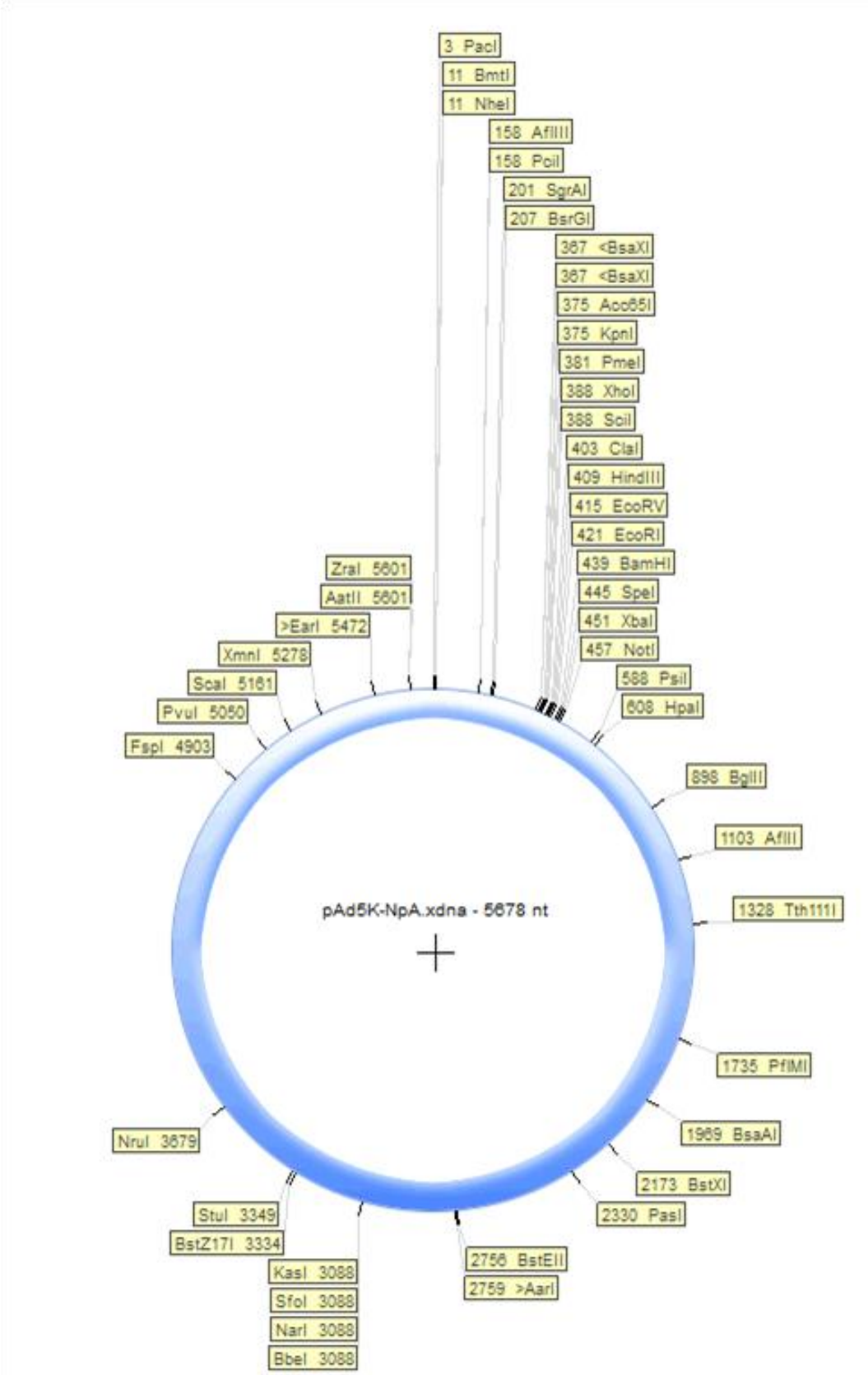

Figure A3: Plasmid map of pAd5 K-NpA. pAd5 K-Npa is an adenoviral shuttle vector. For the generation of recombinant adenovirus, the transgene of interest must be subcloned into the multiple cloning site of this vector. Subsequent digestion with PacI and cotransfection with the pacAd5 9.2 – 100 sub360 adenoviral backbone vector is required for recombination in an E1-proficient cell line, for example HEK293.

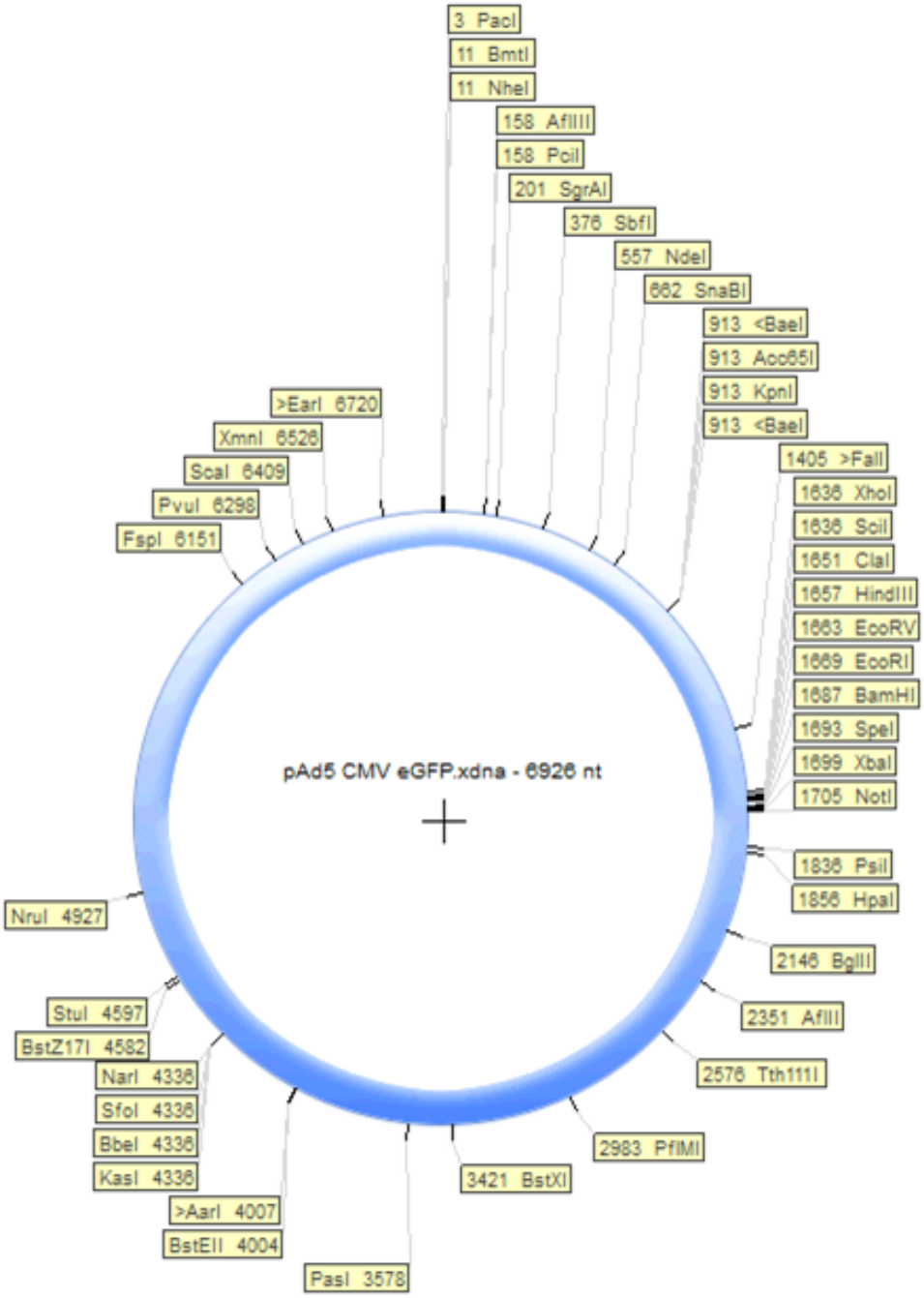

Figure A4: Plasmid map of pAd5CMVeGFP. The cytomegalovirus (CMV) promoter and eGFP were ligated in to the pAd5 K-NpA shuttle vector for the generation of the control GFP adenovirus. pAd5CMVeGFP cloning and adenovirus production were carried out by Dr. Jim Caunt and Dr. Paul Whitley.

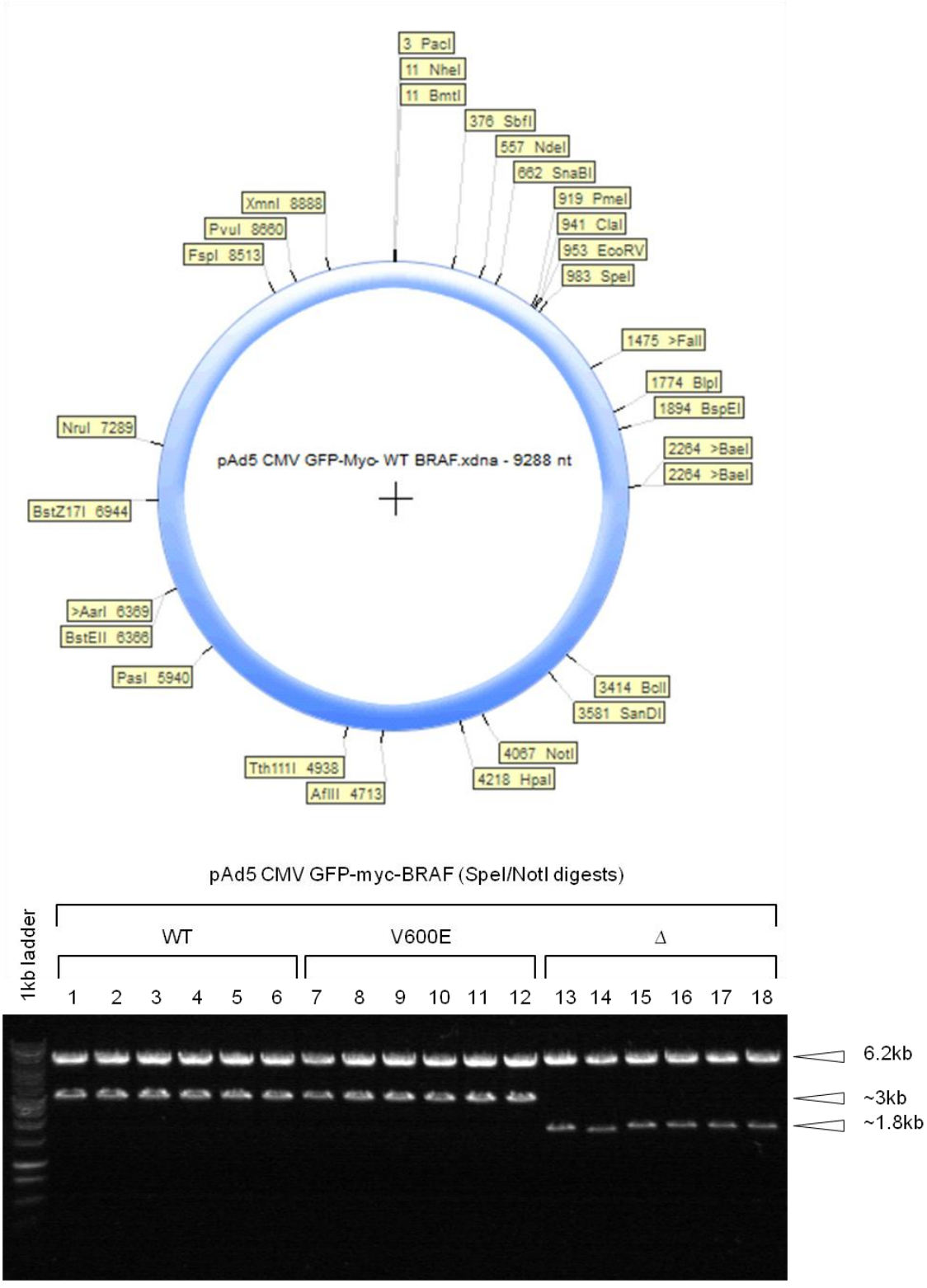

Figure A5: Plasmid map of pAd5CMV GFP-myc-BRAF. GFP- and myc-tagged $BRAF^{WT}$ and $BRAF^{V600E}$ were cloned between the SpeI and NotI sites of pAd5CMV K-NpA. An analytical SpeI/NotI digest produces the predicted bands of 6.2kb (pAd5 CMV vector) and ~3kb (GFP-myc-BRAF) for $BRAF^{WT}$ (clones 1 – 6) and $BRAF^{V600E}$ (clones 7 – 12). An N-terminally truncated ΔBRAF construct was also produced and a SpeI/NotI digest generated bands of 6.2kb and ~1.8kb, corresponding to truncated ΔBRAF. The ΔBRAF construct was not used for experiments in this thesis.

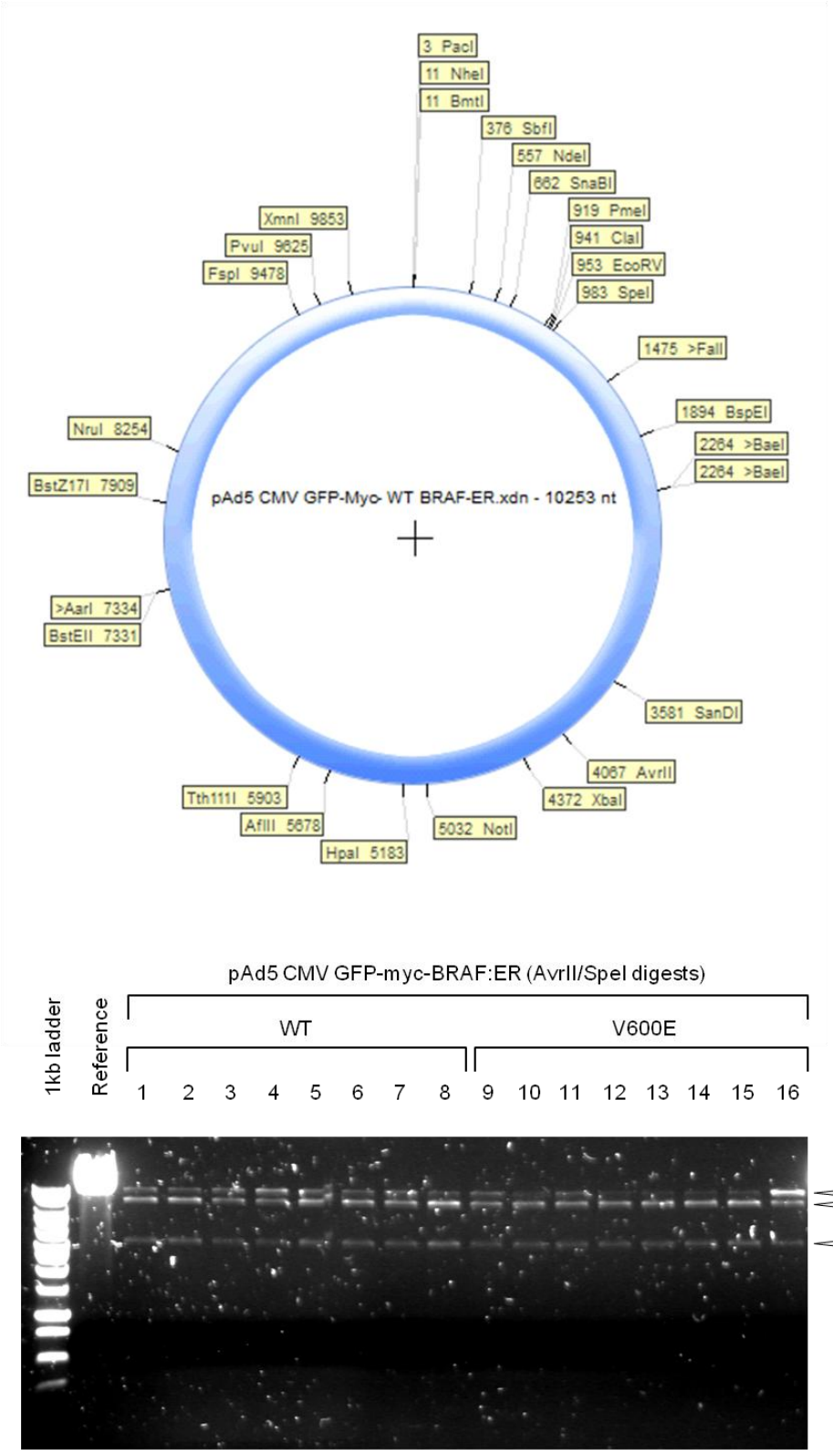

Figure A6: Plasmid map of pAd5CMV GFP-myc-BRAF:ER. Sequences encoding $BRAF^{WT}$ and $BRAF^{V600E}$ ER fusion proteins were cloned between the BspEI and NotI sites of the existing pAd5CMV GFP-myc-BRAF vectors (Figure A5). An analytical AvrII/SpeI digest produces the predicted bands of 7.2kb (pAd5 CMV vector) and ~3.1kb for $BRAF^{WT}$:ER (clones 1 – 8) and $BRAF^{V600E}$:ER (clones 9 – 16). The reference lane represents the parent pAd5CMV GFP-myc-$BRAF^{WT}$ vector digested with AvrII/SpeI. The parent vector lacks the AvrII restriction site and generates a band corresponding to the SpeI-linearised ~9.3kb vector. The larger molecular weight band for each clone corresponds to undigested/partially digested vector.

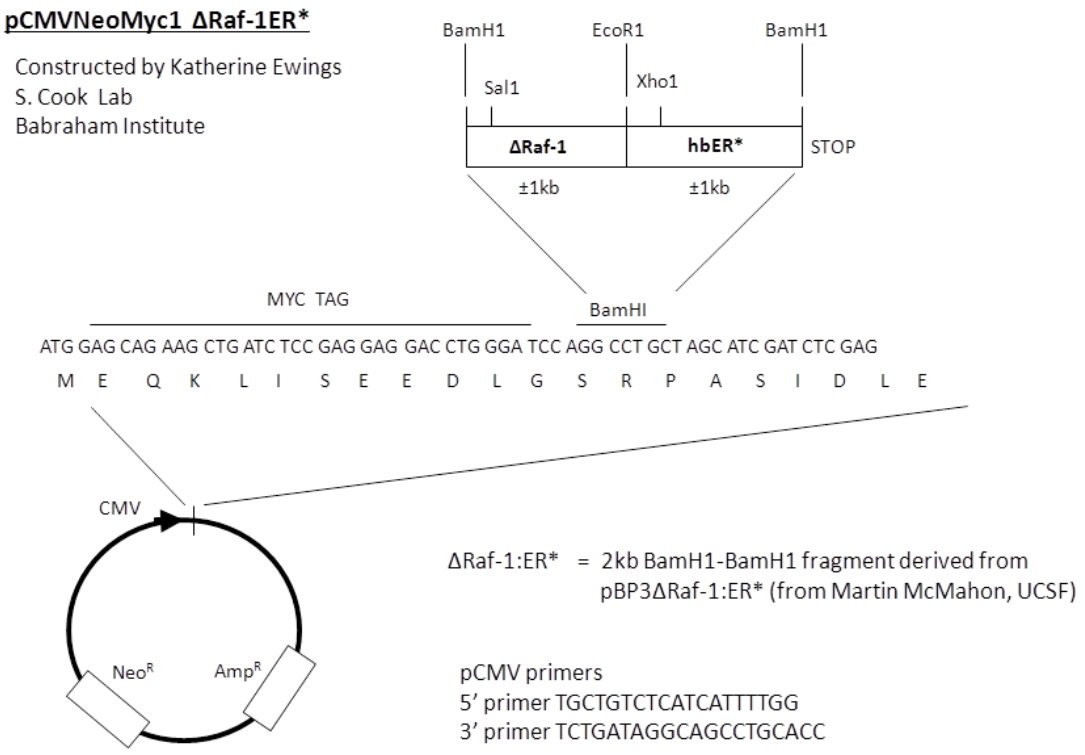

Figure A7: Details of the pCMVNeoMyc1ΔRaf-1:ER* vector. This vector was a kind gift from Dr. Simon Cook (Babraham Institute, Cambridge, UK) and was used for cloning pAd5CMVeGFPΔCRAF:ER, pAd5CMVmycΔCRAF:ER and pAd5CMVHAΔCRAF:ER.

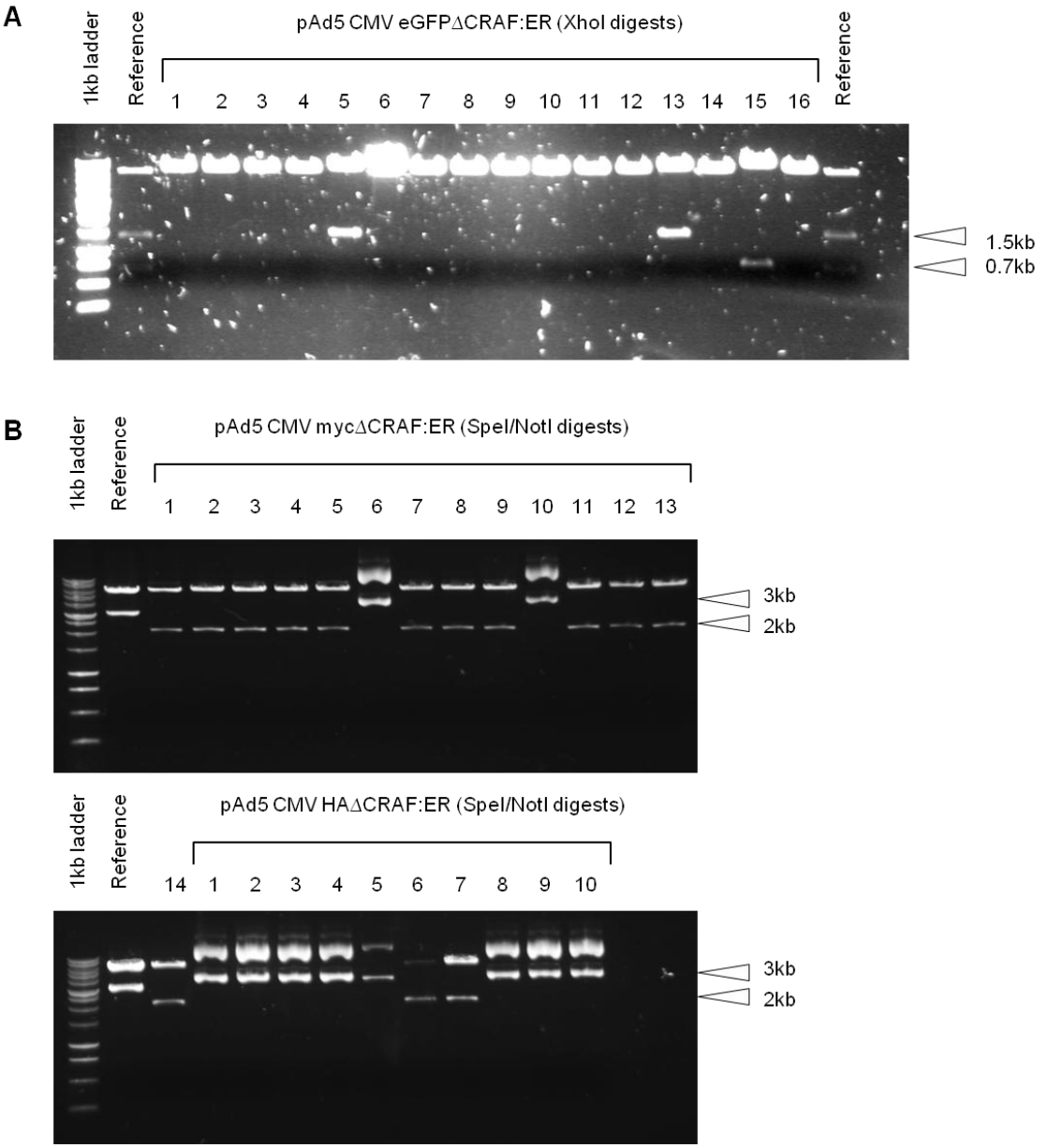

Figure A8: Analytical digests of pAd5CMVΔCRAF:ER constructs. (A) ΔCRAF:ER was subcloned from the parent pCMVNeoMyc1ΔRaf-1:ER* vector into pAd5CMVeGFP using a single BamHI restriction digest. A XhoI digest was used to screen clones. The reference lane represents the parent pCMVNeoMyc1ΔRaf-1:ER* vector digested with BamHI and XhoI. This generates three bands: a large molecular weight vector and two were molecular bands of ~1.5kb and 0.7kb (see Figure A7). A single XhoI digest reveals the orientation of ΔCRAF:ER cloning. The correctly orientated ΔCRAF:ER generates a band of 1.5kb (clones 5 and 13), while the reverse orientation produces a band of 0.7kb (clone 15). The remaining clones do not contain a valid insert. Clone 5 was subsequently sequenced and used for adenovirus generation. (B) Both myc- and HA-tagged ΔCRAF:ER products were generate by PCR and subcloned between the SpeI and NotI sites of pAd5CMV GFP-myc-BRAF^{WT}. An analytical SpeI/NotI digest generated a predicted band of ~2kb for mycΔCRAF:ER (all clones except clone 6 and 10) and HAΔCRAF:ER (clones 6 and 7). The reference lane shows the parent pAd52.CMV GFP-myc-BRAF^{WT} digested with SpeI/NotI, which generates a 3kb fragment.

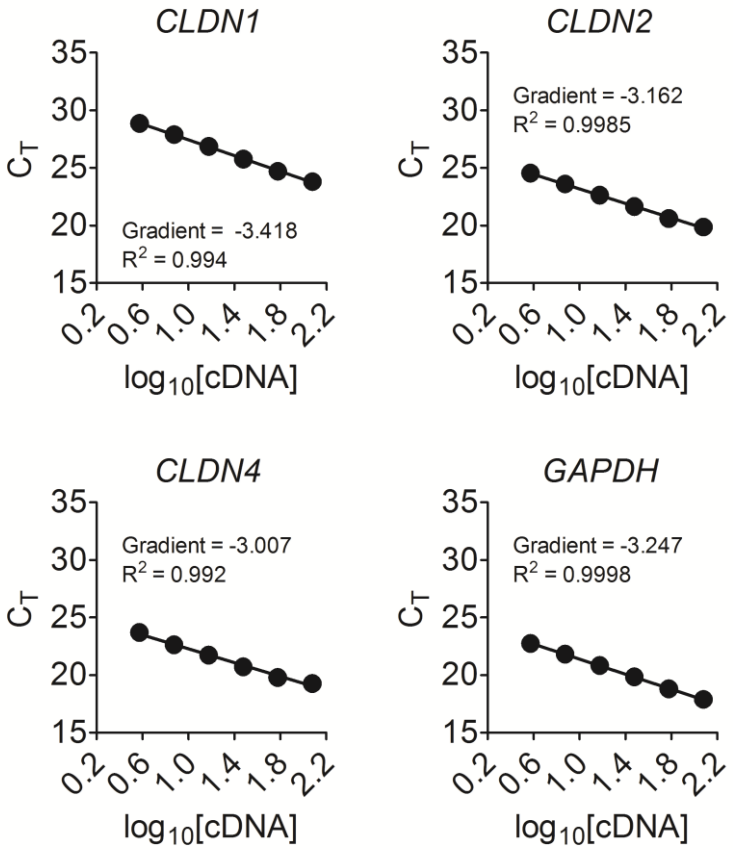

Figure A9: Validation of primers used in RT-qPCR. Primer pairs targeting *CLDN1, CLDN2, CLDN4* and *GAPDH* were validated by performing PCR reactions with serial dilutions of template cDNA. Each primer pair generated a linear standard curve of threshold cycle (C_T) plotted against $\log_{10}$[cDNA]. R^2 values are displayed on each plot. Amplification efficiency (E) was calculated from the gradient of each standard curve using the formula: $E = 10^{-1/slope}$. Amplification was not detected within 35 cycles for control "no reverse transcriptase" PCR reactions, indicating successful removal of genomic DNA contaminants. Melt curve analysis revealed a single PCR product was generated by each primer pair.